LUMINESCENCE STUDY OF
ION-IMPLANTED GALLIUM NITRIDE

DISSERTATION

Eric Silkowski, Captain, USAF

AFIT/DS/ENP/96-09

DEPARTMENT OF THE AIR FORCE
AIR UNIVERSITY
AIR FORCE INSTITUTE OF TECHNOLOGY

DTIC QUALITY INSPECTED 8

Wright-Patterson Air Force Base, Ohio

AFIT/DS/ENP/96-09

LUMINESCENCE STUDY OF
ION-IMPLANTED GALLIUM NITRIDE

DISSERTATION

Eric Silkowski, Captain, USAF

AFIT/DS/ENP/96-09

19970519 025

Approved for public release: distribution unlimited

AFIT/DS/ENP/96-09

LUMINESCENCE STUDY OF ION-IMPLANTED GALLIUM NITRIDE

DISSERTATION

Presented to the Faculty of the Graduate School of Engineering

of the Air Force Institute of Technology

Air University

In Partial Fulfillment of the

Requirements for the Degree of

Doctor of Philosophy

Eric Silkowski, B.A, M.S.

Captain, USAF

November 1996

Approved for public release: distribution unlimited

LUMINESCENCE STUDY OF ION-IMPLANTED GALLIUM NITRIDE

Eric Silkowski, B.A., M.S.
Captain, USAF

Approved:

_____   15 Nov. 96
Yung Kee Yeo
Professor of Physics
Chairman, Advisory Committee

_____   15 Nov 96
Robert L. Hengehold
Professor of Physics
Member, Advisory Committee

_____   15 Nov 96
Mark E. Oxley
Professor of Mathematics and Statistics
Member, Advisory Committee

_____   15 Nov 96
Milton E. Franke
Professor of Aeronautics and Astronautics
Dean's Representative

Accepted:

_____
Robert A. Calico, Jr.
Dean, Graduate School of Engineering

Acknowledgments

I am indebted to my dissertation advisor, Dr. Yung Kee Yeo. His steady encouragement and frequent reminder "you must work harder" kept me going through the most difficult periods of this work. I must also acknowledge the assistance of several colleagues. M. Asif Khan of APA Optics, Barbara Goldenberg of Honeywell, and Ting Lei of Wright Laboratories provided the GaN samples necessary for this work. Dr. Charles Cerney and Mr. John Hoelsher of Wright Laboratories performed several of the ion implantations. I also want to thank my fellow students for the many enlightening discussions and occasional distractions we shared over these past few years. Also, Dr. Paul Thee's help in teaching me the nuances of using much of the laboratory equipment was greatly appreciated. Finally, the tireless assistance of Mr. Greg Smith and Ms. Belinda Johnson made my experimental work run smoothly.

Most of all, I must thank my wife, Christina Dobrowolski, to whom this document is dedicated, for her great love and understanding. Through the many months I spent in the laboratory and at my computer she gave me unending support and encouragement. Her skills as an editor helped make this document more readable. Heartfelt thanks go to my children, Alexander and Kathleen, for the joy they've brought into my life.

Eric Silkowski

Table of Contents

List of Figures

vii

xi

List of Tables

List of Notation

Å	Angstroms
AES	Auger Electron Spectroscopy
Al	Aluminum
AlN	Aluminum Nitride
Ar	Argon
As	Arsenic
Au	Gold
Be	Beryllium
C	Carbon
CB	Conduction Band
Cd	Cadmium
CL	Cathodoluminescence
cm	Centemeter
CVD	Chemical Vapor Deposition
D-A	Donor-Acceptor
E_g	Energy Gap
Er	Erbium
eV	Electron Volt
FA	Furnace Anneal
F-B	Free-to-Bound
FReD	Frequency Doubled
FWHM	Full Width at Half Maximum
Ga	Gallium
GaAs	Gallium Arsenide
GaN	Gallium Nitride
Ga_N	Gallium Antisite Defect
Ge	Germanium
He	Helium
Hg	Mercury
InN	Indium Nitride
IR	Infrared
K	Kelvins
KV	Kilo Volts
LO	Longitudinal Optical Phonon
LP	Long Pass
MBE	Molecular Beam Epitaxy
meV	Milli Electron Volt
Mg	Magnesium
MOCVD	Metal-Organic Chemical Vapor Deposition

MOVPE	Metal-Organic Vapor Phase Epitaxy
MOMBE	Metal-Organic Molecular Beam Epitaxy
mW	Milli Watt
N	Nitrogen
nA	Nano Ampere
Nd	Neodymium
nm	Nanometer
N_{Ga}	Nitrogen antisite defect
N_N	Nitrogen on a nitrogen site
O	Oxygen
OD	Optical Density
OF	Open Face Annealing
P	Phosphorous
PC	Personal Computer
PCA	Proximity Cap Annealing
PL	Photoluminescence
PLE	Photoluminescence Excitation Spectroscopy
PMT	PhotoMultiplier Tube
RE	Rare Earth
RTA	Rapid Thermal Anneal
s	Seconds
Si	Silicon
SiC	Silcon Carbide
SIMS	Secondary Ion Mass Spectrometry
UV	Ultraviolet
V	Volt
VB	Valence Band
V_{GA}	Gallium Vacancy
V_N	Nitrogen Vacancy
VPE	Vapor Phase Epitaxy
WL/ELR	Wright Laboratories, Solid State Electronics Directorate
WZ	Wurtzite
X	Exciton
ZB	Zincblende
Zn	Zinc

AFIT/DS/ENP/96-09

Abstract

Luminescence and absorption measurements were used to demonstrate the efficacy of ion implantation for introducing various classes of dopants into GaN. A wide range of implantation and annealing studies were performed with several dopant species (Ar, Zn, C, O, Si, Be, Mg, Nd, Er). Room temperature ion implantation was performed on MOCVD- and MBE-grown GaN samples at energies between 100 and 1150 keV with doses ranging from 1×10^{13} to 1×10^{15} cm^{-2}. Conventional furnace annealing in flowing NH$_3$ or N$_2$ gas resulted in good implantation damage recovery at an annealing temperature of 1000 °C for 90 min. Annealing temperature was found to be the determining factor in implantation damage recovery. It was discovered that surface degradation occurred for annealing in an NH$_3$ environment at temperatures above 1000 °C. An optimal annealing temperature of 1000 °C and an optimal annealing gas environment of NH$_3$ were found for the optical activation of Zn, Mg, Er, and Nd. Several new luminescence features were observed for the various dopants. Zn-implanted GaN was found to have a strong luminescence peak in the blue at 2.86 eV. The energetic location and width of this luminescence peak was insensitive to temperature changes and excitation intensity changes. These properties suggested that an internal Zn center transition was responsible. A unique photoluminescence peak was observed for Mg-implanted GaN at 3.426 eV, and may have resulted from a Mg-bound exciton transition.

Nd was implanted into GaN for the first time. A rich luminescence spectrum was observed originating from three manifolds, the $^4F_{3/2} \rightarrow {}^4I_{13/2}$, $^4F_{3/2} \rightarrow {}^4I_{11/2}$, and $^4F_{3/2} \rightarrow {}^4I_{9/2}$, of the Nd^{3+} center. The $^4F_{3/2} \rightarrow {}^4I_{11/2}$ emissions were found to persist to room temperature with no shift in energetic location. Strong evidence was obtained for the existence of only one non-cubic Nd^{3+} center. An energy level model was proposed which accounted for all of the observed transitions. Oxygen co-implantation was found to result in no enhancement in Nd luminescence and no changes in the annealing properties or peak locations. Er- implanted GaN was found to be strongly luminescent on the $^4I_{13/2} \rightarrow {}^4I_{15/2}$ transitions. The $^4I_{11/2} \rightarrow {}^4I_{15/2}$ transitions were observed in GaN:Er for the first time. The $^4I_{13/2} \rightarrow {}^4I_{15/2}$ manifold was found to lose only one-half of its integrated intensity as temperature was increased from 2 to 300 K. Numerous 'hot' lines were discovered. The large number of observed peaks indicated multiple, non-cubic Er luminescence centers. An energy level model requiring at least two luminescence centers was proposed which predicted the majority of the observed luminescence peaks. Oxygen co-implantation was found to enhance the $^4I_{13/2} \rightarrow {}^4I_{15/2}$ peaks, and lower the optimal annealing temperature from 1000 to 800 °C. The formation of Er-O complexes was thought to be responsible. Together, this work's success in optically activating several species demonstrated the viability of post growth ion implantation as a means of introducing optically active dopants in GaN. Furthermore, the optical properties of implanted dopants in GaN proved to hold many properties of interest for future device makers.

LUMINESCENCE STUDY OF ION-IMPLANTED GALLIUM NITRIDE

I. Introduction

Optoelectronic devices have become common in today's Air Force weapon systems. Air Force applications would be greatly benefited by the development of semiconductor optoelectronic devices functioning in the blue and ultraviolet (UV). Applications would range from full color flat screen displays to high density data storage. A class of semiconductors having optical emissions in the blue and near-UV regions of the spectrum is the so-called wide bandgap semiconductors. Two advances envisioned with wide bandgap materials are in the creation of secure Earth-satellite links, and detectors which are blind to solar radiation. Also, since green and red diodes are currently available, the development of blue diodes allows the creation of high-brightness, three-color, flat screen displays. Probably the single most anticipated application of a blue or UV laser would be its use in high density optical data storage.

In addition, the increasingly harsh environments in which Air Force weapons systems must operate require new advances in semiconductor science. According to a recent Air Force Office of Scientific Research study (Morkoc *et al.,* 1993) "due to the increasing need for device operation in adverse thermal environments and large power amplification, new materials with high thermal stability must be sought and developed."

The wide-bandgap semiconductors hold the promise of operation at temperatures significantly higher than the 150 °C upper limit of current military specifications. For example, high temperature operation will allow more direct control over important systems such as aircraft engines. By placing semiconductor devices directly in the engine compartment, they will be better able to directly monitor the combustion process. One semiconductor which is very promising for both optical and electrical applications is gallium nitride (GaN).

GaN is a semiconducting material with a bandgap of 3.5 eV, which is much larger than the 1~1.5 eV bandgaps of most semiconductors in use today. And, unlike the indirect bandgap semiconductors such as silicon carbide (SiC), GaN is a direct bandgap material which has been shown to lase in the UV (Yang *et al.*, 1995). Furthermore, GaN along with indium nitride (InN) and aluminum nitride (AlN) form a system of alloys with bandgaps tunable from 1.8 to 6.2 eV (Strite and Morkoc, 1992). Thus, a very wide optical range is available with this material system. Alloys and heterostructures of these compounds are already being employed in commercially sold blue diodes (Morkoc and Mohammad, 1995) proving the value of this material system. GaN also has applications for high temperature electronics. For conventional semiconductors, electrons can be promoted by intrinsic thermal processes at elevated temperatures making them unstable and unsuitable for high temperature operation. A large bandgap insures that only small numbers of charge carriers will be promoted to the conduction band from the valence band by thermal processes. Therefore, with high quality material, only intentionally

introduced dopants will contribute to the conductivity at high temperatures, and controllable devices may be fabricated. Furthermore, GaN is nearly as hard as diamond, and is thermally stable up to high temperatures. With its large bandgap and thermal stability, devices made from GaN should be able to operate in the harsh environments envisioned for future Air Force Systems.

In order to create devices from any semiconductor material, effective means of doping must be found and well understood. Doping during growth can be used to create layered devices; however, post-growth doping methods are also needed. Diffusion has proved to be too slow for practical use in GaN even at elevated temperatures (Wilson *et al*, 1995). However, ion implantation is a proven doping method in silicon (Si) and gallium arsenide (GaAs) technology which offers numerous advantages including the ability to implant almost any dopant at any desired dose. However, ion implantation produces damage to the crystal, and therefore requires annealing to activate the dopant species. Before predictable and reliable implantation doping becomes a reality for GaN, the complexities of the implantation and annealing processes must be understood.

This study undertook three goals: to achieve successful optical activation of ion implanted dopants in GaN, to systematically study the annealing conditions for optimal dopant optical activation, and to study the optical properties of ion implanted dopants. This research will provide a key element towards the ultimate goal of fabricating GaN based optoelectronic devices. Thus, before optoelectronic devices can be fabricated by ion-implantation, a firm understanding of the implantation and annealing processes must

be developed. Furthermore, the various optically active species must be well characterized in order to allow the design of optoelectronic devices.

In order to achieve these goals, the dopants magnesium (Mg), zinc (Zn), carbon (C), and beryllium (Be) were chosen since they are potential p-type dopants. Zn has been the most studied dopant in GaN; however, there is no consensus as to the nature of the Zn deep level and associated blue luminescence transition. Furthermore, although blue luminescence from ion-implanted Zn has been demonstrated, optimal implantation and annealing conditions have not been determined. Mg is a known p-type dopant in GaN; however, the conditions under which Mg activates are not well understood. C is a possible p-type dopant and a well-known contaminant in GaN. Again, little is known about the conditions under which C doping is successful. Despite being a potential p-type dopant, almost no reports of Be doping of GaN can be found in the literature. Si was implanted since it is a known n-type dopant, and little is known about its optical activity in GaN. Also, no extensive implantation studies have been reported for Si. Another common impurity in GaN is oxygen (O); therefore, its effects on the properties of GaN are of great interest as it may be partially responsible for the high background n-type conductivity found in nominally undoped GaN. Finally, the rare-earth elements erbium (Er) and neodymium (Nd) were chosen for their sharp, temperature independent optical transitions, and the fact that their expected optical transitions occur at wavelengths far away from the GaN bandedge and deep luminescence peaks. Together, the study of

several implanted species in GaN was expected to provide greater insight into implantation damage effects and annealing processes than any one implant alone.

This document is organized as follows. Chapter II includes the background material necessary for understanding the ion implantation considerations employed in this work, the annealing process, and the basic types of luminescence transitions anticipated. Furthermore, previous work with GaN will be reviewed with special emphasis on dopants. Chapter III will cover the samples used in this study, and the implantation and annealing parameters used. A detailed description of the experimental equipment and procedures used for photoluminescence (PL), cathodoluminescence (CL), and absorption measurements will be given in Chapter IV. Ion implantation and annealing results will be presented in Chapter V. The first section of Chapter V will provide a baseline to understanding GaN luminescence spectra. The low temperature PL spectra of metal-organic chemical vapor deposition (MOCVD) as-grown GaN will be discussed, as well as the CL results for molecular beam epitaxy (MBE) as-grown samples characterized in support of Wright Laboratory's (WL/ELR) growth efforts. This will be followed by the results of annealing studies performed on as-grown GaN. Since all ion-implanted samples require annealing, an understanding of the effects of high temperature annealing was necessary in order to separate annealing effects from implantation damage. Next in Chapter V follows a study of argon (Ar) implantation in GaN. Argon is an inert species, and this allowed an assessment of the effects of implantation damage and the subsequent recovery upon annealing. Next, a number of sections will discuss the individual species

implanted including zinc, carbon, oxygen, silicon, beryllium, magnesium, neodymium, and erbium. Chapter VI will close the document with a summary of contributions and recommendations for further study.

II. Background

This chapter introduces the concepts of ion implantation, annealing, and luminescence as necessary for understanding the results of this work. Also, relevant physical properties of GaN are discussed, and a comprehensive review of previous work relating to GaN doping, defects, and annealing will be given.

Ion Implantation

Ion implantation is a technique wherein dopant species are driven into a solid at high energy. This post-growth doping technique offers several advantages over other doping methods such as diffusion. For example, ion implantation is not limited to any particular type of ion; however, some ions are more difficult to implant than others. Also, very accurate control of the depth and distribution with a minimal lateral spread of the dopant is possible. Another advantage of ion implantation is that it is not an equilibrium process, thus ions can be injected in concentrations exceeding the thermal equilibrium concentration. However, this does not insure 100% electrical activation (Wilson and Brewer, 1979:290). Furthermore, ion implantation is performed in a very clean high vacuum environment which helps to prevent unwanted contamination. A particular need for ion implantation of wide bandgap semiconductors exists in that diffusion has been found to be a very slow process in these materials (Wilson *et al.*, 1995).

Ion implantation allows the experimenter to set the energy with which ions are implanted. This ability allows the experimenter to control the depth of the peak concentration. One can also regulate the amount of ions implanted, and this quantity is called the dose. The researcher is thus able to control the concentration level of the implanted species. Finally, the researcher can control the temperature of the substrate during implantation and the rate of implantation. These four parameters can have a great influence on the type and extent of the damage experienced by the host lattice.

Implanted ions eventually must be stopped by interaction with the atoms of the host material. The interaction is generally classified as either electronic stopping or nuclear stopping (Gibbons, 1968). The rate of energy loss with distance, dE/dx, in the material is called the stopping power, $S = dE/dx$. The total rate of energy loss of the moving ion, which is thus the sum of the nuclear, $S_n(E)$, and electronic, $S_e(E)$, stopping powers, is given by

$$\frac{dE}{dx} = S_n(E) + S_e(E).$$
(2-1)

To find the total distance an ion will travel, called the range, R, one must perform the integration

$$R = \int_0^R dx = \int_0^{E_0} \frac{dE}{dE/dx} = \int_0^{E_0} \frac{dE}{S_n(E) + S_e(E)}.$$
(2-2)

2-2

Nuclear stopping dominates at low ion kinetic energies while electronic stopping dominates at high ion kinetic energies. Therefore, if an ion enters the solid at high enough energy, it will initially lose energy to electronic processes resulting in few lattice atoms being displaced from their lattice sites through direct collisions. However, as the ions lose energy, the nuclear interaction will dominate. Thus many of the ions will lose their remaining energy in creating Frenkel pairs. That is, a lattice atom will be knocked off its lattice site leaving behind a vacancy, and it will become an interstitial. Many such pairs can be created by each energetic ion as well as secondary pairs created by the dislodged host atoms as they lose energy.

The stopping of ions is a statistical process, and the final distribution of ions, n(x), in the host is usually well described by a Gaussian distribution (Ryssel and Ruge, 1986:14) as given by

$$n(x) = \frac{\phi}{\sqrt{2\pi}\,\Delta R_p} e^{\left[-\frac{\left(x - R_p\right)^2}{2\Delta R_p^2} \right]}, \qquad (2\text{-}3)$$

where ϕ is an ion dose, x is the depth below the surface, R_p is the projected range on x, and ΔR_p is the projected straggle or standard deviation of the projected range. The peak concentration is given by the coefficient in above equation, and occurs at a depth R_p.

Annealing

Ion-implantation damage and the steps necessary to repair it are a major downside of ion implantation. "It is presently acknowledged that damage to a crystalline lattice during ion implantation is a complex and not completely understood phenomenon." (Wilson & Brewer, 1979:312) Consequently, experimental examination of each ion species and substrate are necessary to determine effective implantation and annealing conditions.

Ion implantation is known to cause many types of damage to the crystalline lattice of semiconductor materials. The implanted ion species can eventually go into a substitutional site in the lattice, can lodge at an interstitial site, or can form clusters or precipitation centers. The energetic ion also imparts significant energy to the atoms in the crystal thereby causing substantial damage to the lattice. Lattice atoms can be knocked off their lattice sites to form vacancies and interstitials. Figure 2-1 shows a schematic illustration of the simplest types of defects seen in an implanted binary compound, AB. The native point defects and the location of dopants on lattice or interstitial sites are shown. In GaN, if a gallium (Ga) lattice site is left empty, it is called a Ga vacancy, V_{Ga}. Similarly, if a nitrogen (N) site is left vacant, it is called a N vacancy, V_N. In a binary compound like GaN, a Ga atom can be knocked onto a N site to form the so-called Ga antisite, Ga_N. Similarly, a N can lodge on a Ga site forming the N antisite, N_{Ga}. These four types of defects (V_{Ga}, V_N, Ga_N, N_{Ga}) are known as native defects since they occur naturally in ideally pure GaN. When the implanted species is at or above its
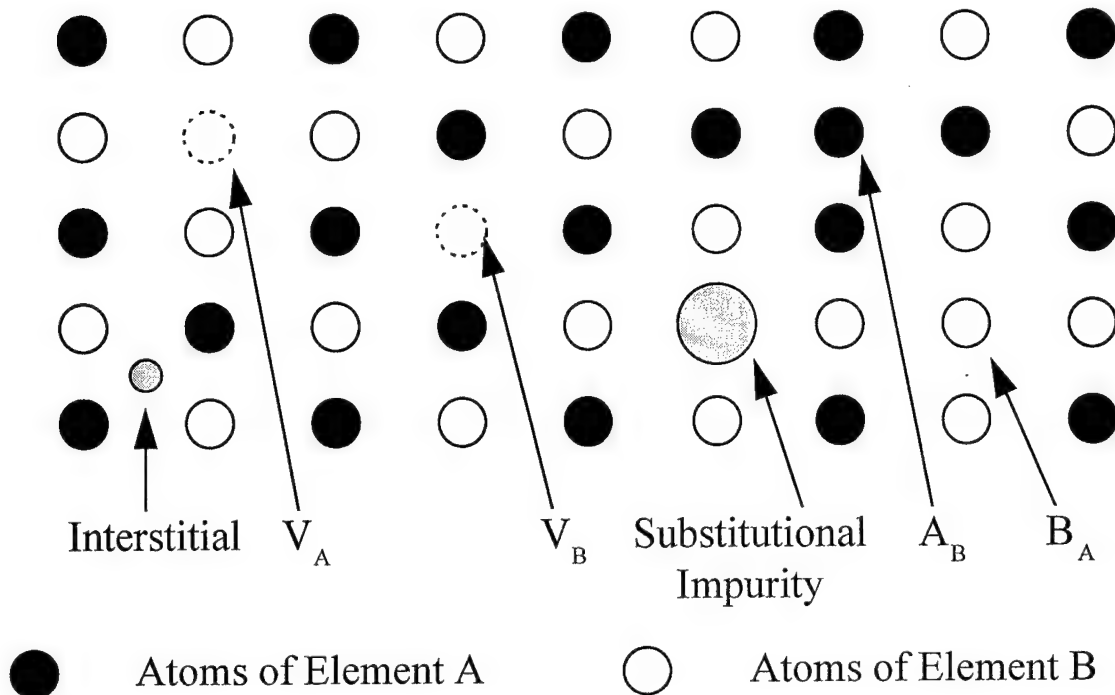
Figure 2-1. Schematic illustration of native defects and impurities.

solubility limit in the host lattice, clusters and precipitation centers can form causing substantial changes in the implant's doping behavior. Other extended defects such as dislocation loops are also possible.

The various types of damage and defects caused by ion implantation can have a wide range of effects on semiconductor properties. Generally, the creation of defects is detrimental to the semiconductor through the reduction of the minority carrier lifetime and the reduction of mobility. For instance, Si and GaAs implanted at doses of 10^{13} to 10^{14} cm^{-2} have mobilities reduced to only 1 cm^2/Vs (Ryssel and Ruge, 1986:41). The

carrier concentration after implantation can also be low since carriers can become trapped at defect sites. The optical properties of implanted layers are also affected. For instance, a material's index of refraction can be increased by implantation, and this technique is currently used in the production of waveguide channels in opto-electronic components (Hunsperger, 1991:54). Also, damage can create non-radiative pathways resulting in poor luminescence. The lifetime of an excited state which has two pathways of radiative, τ_r, and non-radiative, τ_{nr}, decays is given by

$$\frac{1}{\tau} = \frac{1}{\tau_r} + \frac{1}{\tau_{nr}} \, . \tag{2-4}$$

A decrease in the non-radiative lifetime results in a decrease in the overall lifetime, and thus less radiative transitions can be expected.

The concentration of defects present in a semiconductor in excess of their thermodynamic equilibrium values can be reduced in many cases by thermodynamic driving forces. Annealing is the process of removing these defects, usually by heating the material in question. The excess defects can be reduced in number of ways: 1) by migration and subsequent recombination with their counterpart, e.g., a vacancy with an interstitial, 2) by migration and complex formation, 3) by migration and capture at a sink such as a surface or grain boundary, or 4) by dissociation if they are complexes. Figure 2-2 is a graphical depiction of the activation energies for several annealing processes. All such processes can be characterized by an activation energy (Bourgoin and Lannoo,
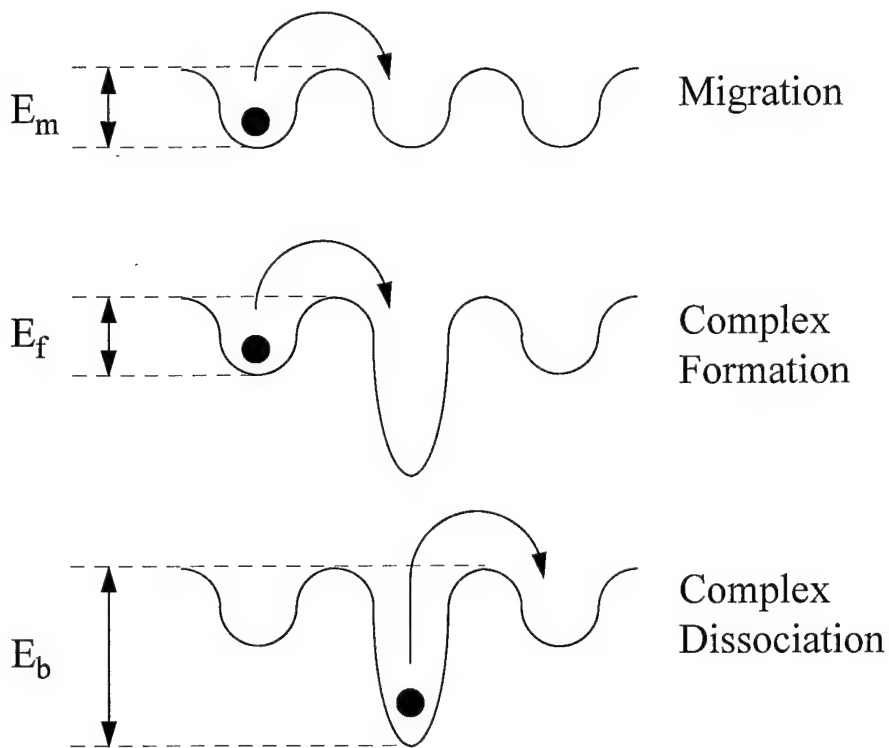
Figure 2-2. Activation energy barrier for defect migration, complex formation, and complex dissociation (after Bourgoin and Lannoo, 1983: 247).

1983:247). This activation energy is commonly thought of as the energy barrier which must be overcome for the annealing process to occur.

The kinetics of defect recombination can be modeled by noting that the rate of change of the concentration of defects, N, is given by

$$\frac{dN}{dt} = -KN^{n},$$ (2-5)

where K is the reaction constant, and n is the order of the reaction. This equation simply reflects the idea that the rate of decrease in the number of defect centers is proportional to the nth power of the concentration of defects. For n=1, we have a simple dependence on concentration. Situations of n=2 arise in the case of recombination of two defect centers. For instance, production of vacancies and interstitials by irradiation are in equal densities $(n_v = n_i)$, therefore, the rate must be proportional to the concentration of each defect, and thus

$$\frac{dn_v}{dt} = \frac{dn_i}{dt} = -Kn_v n_i = -Kn_v^2 \ .$$

(2-6)

In many cases, however, the direct measurement of the defect concentration is difficult, and some material property related to defect concentration can be measured. In such cases, a property, P, will be measured. This property can follow the kinetics described by the above equation. If we assume that there is an energy barrier to overcome for defect recombination, the reaction constant takes the form

$$K = -A \exp\left(\frac{E}{kT}\right) ,$$

(2-7)

where A is a constant, E is the activation energy, k is Boltzmann's constant, and T is the temperature.

An experimental way of determining activation energies of annealing processes is possible using isochronal annealing. A given property, P, is measured for identical samples annealed at two different temperatures, T_1 and T_2, for an identical length of time, t. Integrating Equation 2-7 with respect to time gives

$$P(t) = -A \exp\left(\frac{E}{kT}\right) \int_0^t P^n(t) dt.$$

(2-8)

Taking the natural logarithm of the ratio for the two anneals results in

$$\ln\left|\frac{P_1(t)}{P_2(t)}\right| = \frac{E}{k}\left(\frac{1}{T_2} - \frac{1}{T_1}\right).$$

(2-9)

Thus, a plot of ln(P) as a function of 1/kT has a slope -E, and the activation energy, E, is determined.

Luminescence

Luminescence is the term used to describe the process of light emission, either visible or invisible, occurring when an electron makes a transition from a state of higher energy to one of lower energy states. The primary condition necessary for luminescence

to occur is that the electron be in a non-equilibrium state (Pankove, 1971:107). Consequently, by examining the conditions under which luminescence occurs or does not occur, one can gain valuable information about the upper and lower states involved in the transition.

In order to create electrons in non-equilibrium states, some means must be employed to excite the semiconductor sample. Excitation by means of light (usually a laser) is called photoluminescence (PL). Excitation by means of an electron beam is called cathodoluminescence (CL). For semiconductor samples, the excitation must provide large numbers of electrons promoted from states in the valence band (VB) to states in the conduction band (CB). Therefore, for PL, the laser must generate photons with energy greater than the bandgap (E_g) of the material. In CL, the electrons are generally accelerated with energies well in excess of E_g.

Many different de-excitation pathways are possible. First, the electrons can lose energy non-radiatively in processes that eventually result in heating of the sample. Non-radiative pathways are not directly detected by PL or CL because they result in no light output. Second, electrons can lose energy in radiative transitions resulting in luminescence, as illustrated in Figure 2-3. Typically, the electrons excited above E_g will decay non-radiatively to the bottom of the conduction band. From there, they can make a transition all the way to the valence band, the so-called band-to-band (B-B) radiation. Another possibility is that an electron at the bottom of the conduction band can make a transition radiatively to an acceptor level within the band gap, a so-called free-to-bound
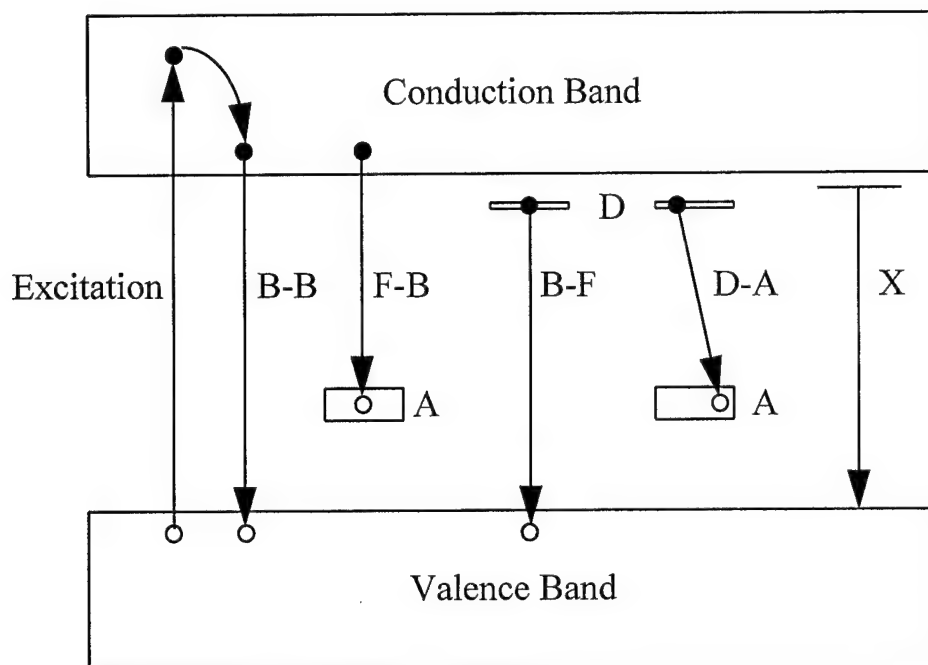
Figure 2-3. Common luminescence transitions in semiconductors.

(F-B) transition. Similarly, a hole in the valence band can make a transition radiatively to the donor level, which is also called a free-to-bound (F-B) transition. Transitions between donors and acceptors (D-A) are also commonly seen. Other excited states with energies less than E_g such as excitons (X) can also result in strong luminescence. Furthermore, phonons can be emitted during many optical transitions, resulting in so-called phonon replicas of peaks.

The ability to observe the above transitions makes optical methods particularly well suited to the identification of electrically active dopant species in semiconductors (Dean, 1982:102). Determining the concentration of these dopants is difficult by optical

means alone. However, some insight can be obtained from spatial linewidths, energy shifts, and intensity ratios between spectral components involving different species (Dean, 1982:102). Thus, for the study of implanted semiconductors, there are a myriad of details which can be learned from PL and CL. To gain the full measure of information available, low cryogenic temperatures are necessary (Dean, 1982:89). Since spectral lines are broadened by thermal energy, low temperatures allow the narrowest spectral lines, and thus offer the best opportunity for the identification of dopant centers. Low temperatures may also enhance the ratio of radiative to non-radiative transitions. Furthermore, valuable diagnostic information about the radiative centers can be found through studies of the temperature dependence of luminescence peaks.

Basic Properties of GaN

Many of the basic physical properties of GaN have been studied and values for some of the more important properties are available in the literature. Table II-1 gives a comparison of physical properties of GaN with those of several other wide bandgap materials such as InN, AlN, SiC, and the more familiar GaAs. However, it should be noted that many of the values reported in the literature were obtained with GaN grown under widely varying conditions and thus with widely varying crystal quality and doping. Therefore, caution should be exercised before accepting the values for GaN produced under different conditions.

Table II-1. Selected properties of wide bandgap semiconductors.

	GaAs	InN	GaN	AlN	6H-SiC
Crystal Structure	ZB*	WZ	WZ	WZ	6H
Direct/Indirect	Direct	Direct	Direct	Direct	Indirect
Bandgap (eV) $T \approx 0$ K	1.5191^f		3.5^b	6.28^b	3.023^f
$T \approx 300$ K	1.424^f	1.89^b	3.39^b	6.2^b	2.86^f
Lattice Constants: (Å) $a =$	5.6533^f	3.548^b	3.189^b	3.112^b	3.0806^f
$c =$	-----	5.760^b	5.185^b	4.982^b	15.117^f
Density (g/cm^3)	5.316^a	6.81^f	6.10^a	3.255^f	3.211^f
Mobility: (cm^2/Vs) electrons	9200^f	250^f	440^f		500^f
holes	400^f		400^c	14^c	40^f
Electron Effective Mass	0.067^f	0.11^b	0.2^b		$1.5_{\parallel}^f$ $0.25_{\perp}^f$
Hole Effective Mass	0.082^f		0.8^f		1.0^f
Thermal Conductivity (W/cm K @ 300 K)	0.46^d		1.3^b	2^b	4.2^f
Index of Refraction	3.4^e	$2.85\text{-}3.05^b$	$2.33\text{-}2.67^b$	2.15^b	$2.66\text{-}2.78^f$
Dielectric Constant	13.1^d	9.3^f	9.5^f	9.14^f	
Melting Point (K)	1513^f	1373^f	1500^a	3273^f	

[*] ZB stands for zincblende, WZ stands for wurtzite
[a] Chemical Rubber Company, 1994
[b] Strite and Morkoc, 1992
[c] Frederikse, 1989
[d] Sze, 1981
[e] Pankove, 1971
[f] Madelung, 1991

The low temperature bandgap (E_g) of GaN is close to 3.5 eV (Strite and Morkoc, 1992 and references therein). The optical transitions observed from high quality GaN at low temperatures do not originate from band-to-band recombination. However, exciton

transitions to the three split levels of the valence band maxima at the Brilliouin Zone center are much more likely.

Grimmeiss and Monemar (1970) used PL on powder samples of GaN, and found emissions at 3.476 eV (4.2 K). They found that the peak occurred in all samples at the same energy independent of doping, the half-width of the emissions was several meV independent of temperature and excitation density, and the emissions were still observed at temperatures above 300 K. On this basis, they concluded that these emissions were due to free exciton recombination. Table II-2 is a listing of the free exciton energetic location as reported by various researchers. The table lists the temperature the observation was made at as well as the GaN growth method. Dingle *et al.* (1971) did absorption, reflection, and luminescence measurements on vapor phase epitaxy (VPE)

Table II-2. Free excitons in GaN.

Free X (eV)	Temp (K)	Growth	Reference
3.476	4.2	Powder	Grimmeiss & Monemar (1970)
3.474 ± 0.002	2	VPE	Dingle et al. (1971)
3.475	90	Bulk	Pikhtin et al. (1974)
3.4751 ± 0.0005 A	1.6	VPE	Monemar (1974)
3.4815 ± 0.001 B	1.6	VPE	Monemar (1974)
3.493 ± 0.005 C	1.6	VPE	Monemar (1974)
3.4770 ± 0.0006 A	4.2	Powder	Ogino & Aoki (1980)
3.4823 ± 0.0006 B	4.2	Powder	Ogino & Aoki (1980)
3.4886 ± 0.0006 C	4.2	Powder	Ogino & Aoki (1980)
3.494 ± 0.002 L	5	VPE	Dai et al. (1982)
3.479 ± 0.002 T	5	VPE	Dai et al. (1982)
3.518 A		MOCVD	Shan et al. (1994a)
3.493 B		MOCVD	Shan et al. (1994a)
3.485 C		MOCVD	Shan et al. (1994a)

grown GaN, and concluded that the free exciton transition occurs at 3.474±0.002 eV at 2 K. They also reported weak structure at 3.38 eV, which is believed to be a 90 meV longitudinal optical (LO) phonon replica that exhibited the same polarized reflectance behavior as the exciton line. The photo luminescence excitation (PLE) study by Monemar (1974) revealed energy values for the three free excitons associated with the splitting of the valence band at the Γ point. These are the A exciton ($\Gamma^c_7 \rightarrow \Gamma^v_9$), the B exciton ($\Gamma^c_7 \rightarrow \Gamma^v_7$), and the C exciton ($\Gamma^c_7 \rightarrow \Gamma^v_7$), and the measured values are found in Table II-2. Ogino and Aoki (1980) also used PLE on powder samples and needle crystals to determine very similar values for the excitons. Later work by Dai *et al.* (1982) disputes the earlier findings, and proposes that the free exciton actually lies as high as 3.494 eV. They also observed a peak at 3.476 eV, but it had the following properties. The line shifted in energy from sample to sample, had a strong temperature dependence indicating a low activation energy, had strong intensity, and had a nonlinear intensity change and shift with excitation intensity. Since these features are not characteristic of a free exciton emission, they suggested that the emission was associated with an exciton bound to a shallow localized energy level.

Shan *et al.* (1995a) measured the low temperature exciton transitions of MOCVD GaN grown by Honeywell. The results of PL spectra measured at 15 K are shown in Figure 2-4. There are three transitions possible for free excitons but only the two lower energy transitions were observed in luminescence. A strong transition from the donor bound exciton to the A band was also observed at low temperature.
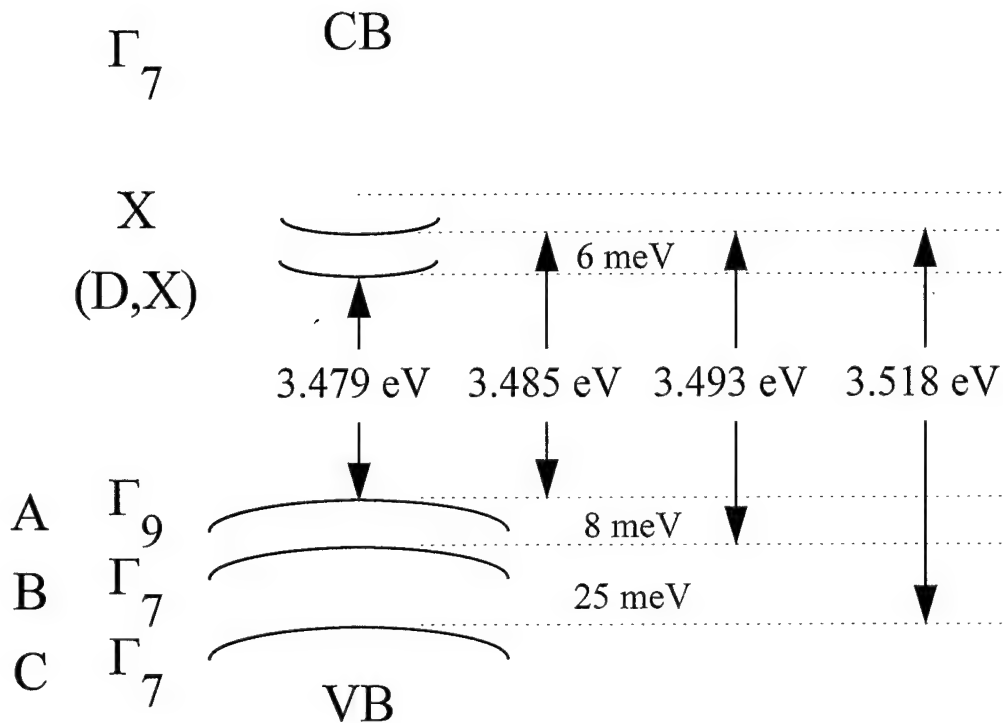
Figure 2-4. GaN bandstructure (after Shan *et al.* 1995a).

Bound exciton emissions had been reported by many researchers at energies lower than free exciton energies. Table II-3 lists the energetic positions of bound excitons reported in the literature. The table lists the temperature the observation was made at as well as the GaN growth method. MOVPE stands for metal-organic vapor phase epitaxy. Dingle *et al.* (1971) observed substantial absorption in VPE grown GaN on sapphire at energies 6-20 meV below the free exciton level. They concluded that bound excitons

Table II-3. Bound excitons in GaN

X Bound To:	(eV)	Temp (K)	Growth	Reference
Neutral Donor	3.467	2	VPE	Dingle *et al.* (1971)
Neutral Donor	3.4716	<30	Needle	Matsumoto & Aoki (1974b)
Neutral Donor	3.469 ± 0.001	4.2	VPE	Lagerstedt & Monemar (1974)
Neutral Donor	3.472	4.2	Powder	Ogino & Aoki (1979)
Neutral Donor	3.4719 ± 0.0004	4.2	Powder	Ogino & Aoki (1980)
Neutral Donor	3.49	4.2	MOVPE	Amano *et al.* (1990)
Neutral Donor	3.465	4.2	VPE	Ilegems & Dingle (1973)
Neutral Donor	3.472	1.6	VPE	Vavilov *et al.* (1979)
Neutral Donor	3.4685	1.6	VPE	Marasina *et al.* (1976)
Neutral Donor	3.479		MOCVD	Shan *et al.* (1995)
Neutral Acceptor	3.455	2	VPE	Dingle *et al.* (1971)
Neutral Acceptor	3.455	4.2	VPE	Ilegems & Dingle (1973)
Neutral Acceptor	3.455	4.2	Bulk	Pikhtin *et al.* (1974)
Neutral Acceptor	3.455	1.6	VPE	Vavilov *et al.* (1979)
Neutral Cd	3.454 ± 0.001	4.2	VPE	Lagerstedt & Monemar (1974)
Neutral Cd	3.4553 ± 0.0002	4.2	VPE	Ilegems *et al.* (1972)
not assigned	3.476	5	VPE	Dai *et al.* (1982)
not assigned	3.472	4.2	VPE	Matsumoto & Aoki (1974a)
not assigned	3.472	4.2	VPE	Matsumoto *et al.* (1974)

could be responsible. Also, Dingle *et al.* (1971) concluded that the luminescence suggested that annihilation of excitons bound to neutral donors could occur at 3.466-3.468 eV, and exciton decay occurred at a neutral acceptor at 3.455 eV. Also, the authors suggested that features found at 3.38 and 3.29 eV are the one 90 meV LO phonon replica and the two 90 meV LO phonon replica of the neutral donor bound exciton emission. Ilegems *et al.* (1972) observed a luminescence peak at 3.4553±0.0002 eV which they attributed to an exciton decaying at a neutral cadmium (Cd) acceptor on a Ga site. They also observed a strong phonon replica at 3.364 eV due to the 90 meV LO phonon. Matsumoto and Aoki (1974b) attributed a PL peak at 3.4716 eV (<30 K) in undoped GaN

needle crystals to an exciton bound to a neutral donor. They determined an activationenergy of 10±1 meV, and no shift in peak position was observed below 30 K. Above 30 K but below 150 K, they found the temperature dependence of the peak to be $dE/dT = -3.5 \times 10^{-4}$ eV/K, and for temperatures between 150 and 300 K, $dE/dT = -6.0 \times 10^{-4}$ eV/K. In addition, peaks at 3.46 eV and 3.42 eV were observed but no conclusions as to their origins were offered. Numerous near gap peaks were observed by Lagerstedt and Monemar (1974) for GaN:Cd. The dominant peak was attributed to an exciton bound to a neutral donor at 3.469±0.001 eV having an LO phonon replica at 3.377±0.002 eV. Also seen was a 3.454±0.001 eV peak which was attributed to an exciton bound to an acceptor, presumably Cd.

Shan *et al.* (1995b) performed pressure dependence studies of the luminescence of Honeywell MOCVD grown GaN. They found that the yellow band showed a strong sublinear dependence on pressure as compared to the exciton emissions. This data was consistent with the attribution of the yellow band to deep defect states.

Many researchers have observed luminescence features in the energy range of approximately 3.0 to 3.3 eV, which have been attributed to donor-acceptor transitions. Table II-4 is a listing of the D-A energetic location as reported by various researchers. The table lists the energetic locations of LO phonon replicas, the temperature the observation was made at, and the GaN growth method. Grimmeiss and Monemar (1970) observed a set of features at 3.27, 3.18, 3.09, and 3.00 eV. These peaks were spaced at 90 meV intervals suggesting phonon replicas of the highest energy peak. The constant

Table II-4. Donor-acceptor transitions in GaN.

D-A (eV)	+1LO	+2LO	Temp (K)	Growth	Reference
3.27	3.18	3.09	4.2	Powder	Grimeiss & Monemar (1970)
3.2571	3.1672	3.0768	1.6	VPE	Dingle & Ilegems (1971)
3.27	3.18	3.09	77	VPE	Cunningham et al. (1972)
3.268			4.2	VPE	Ilegems et al. (1972)
3.264	3.174	3.08	4.2	VPE	Ilegems & Dingle (1973)
3.27	3.18		4.2	VPE	Matsumoto & Aoki (1974a)
3.27			4.2	Needle	Matsumoto & Aoki (1974b)
3.268	3.187	3.097	4.2	VPE	Matsumoto et al. (1974)
3.263 ± 0.003			4.2	VPE	Lagerstedt & Monemar (1974)
3.311 ± 0.002			10	VPE	Dai et al. (1982)

relative intensity of the peaks provides supporting evidence for this conclusion. Dingle and Ilegems (1971) gave convincing evidence of the D-A transition. Both VPE layers on sapphire and free-single-crystal hexagonal needles were studied in the energy range from 3.26 to 2.99 eV. They also observed the regular spacing of 90±1 meV between the 3.2571, 3.1672, and 3.0768 eV emissions, and found identical radiative lifetimes for these three lines. Although a value was not specified, the lifetimes were reported to be orders of magnitude faster than other spectral features. Time resolved spectra also showed that the peaks narrowed and shifted to lower energy as the time delay after the pulse was increased, which is the result expected from more distantly spaced D-A pair recombinations. Thus, they concluded this was a D-A transition. Temperature dependent studies showed that at higher temperatures, a new band appeared with a thermal activation energy of 30±5 meV. This new feature was considered likely to be a free-electron bound-hole transition.

Cunningham *et al.* (1972) observed D-A peaks in single-crystals of GaN at 3.27 eV with subpeaks at 3.18 and 3.09 eV (77 K). They noted that the emissions in this band became relatively more intense for samples with lower carrier concentration, but could not determine if this was due to an increase in the number of luminescence centers involved or a decrease in the number and efficiency of alternate recombination modes.

Matsumoto and Aoki (1974b) measured the temperature dependence of the D-A peak at 3.27 eV in needle crystals. They found an energy shift of the D-A band given by dE/dT= $+1.2 \times 10^{-4}$ eV/K for 20 K<T<110 K, and dE/dT= -0.7×10^{-4} eV/K for 110 K<T<220 K. To interpret these shifts, they postulated a high-energy band located 30 meV above the D-A band. This higher energy band was due to free-electron bound-hole transitions, and was used to explain the positive temperature coefficient at lower temperatures. At higher temperatures, the reduction of the band gap offset the positive shifts. The bandgap reduction was 50 meV between 110 K and 220 K while the higher energy band was only 30 meV above the D-A band. Using their model, an acceptor binding energy of 160±20 meV and donor binding energy of approximately 80 meV were calculated.

Another report of D-A peaks in GaN comes from Lagerstedt and Monemar (1974). They observed the main peaks at 3.263±0.003 eV (4 K) in undoped and Cd-doped GaN. Several 91.5 meV replicas were observed as well as a high energy band which overlapped the main D-A peak at temperatures of 25-100 K. The D-A peaks showed a broad hump at 25 meV below the peak and a 60 meV long tail. Both structures

were reproduced in all phonon replicas and had the same temperature dependence, indicating an intimate relationship between these structures and the D-A peak.

Dai *et al.* (1982) observed the 3.27 eV emissions which have been attributed to D-A pair recombination. However, they also attributed emissions at 3.311±0.002 eV to D-A transitions in VPE grown GaN on sapphire. These emissions did not change in energy from sample to sample. The emissions also shifted to higher energy at higher excitation intensity.

Previous Work with Doped GaN

Zinc Numerous groups have observed luminescence related to Zn in GaN. The predominant luminescence band of Zn has a peak in the range from 2.85 to 2.91 eV. Ilegems *et al.* (1972) observed strong emissions in this band at 4.2 K from chemical vapor deposition (CVD) grown GaN:Zn having Zn concentrations estimated at $5x10^{18}$ to $4x10^{20}$ cm^{-3}. Pankove *et al.* (1974) reported this peak at 2.86 eV, and found a full width at half maximum (FWHM) of 350 meV (78K). The peak location varied between samples by as much as 20 meV.

Ejder and Grimmeiss (1974) also reported that GaN:Zn grown on sapphire exhibited a PL peak at 2.85 eV. Monemar *et al.* (1980a) noted that the 2.87 eV emissions observed by his group could be shifted by as much as 30 meV between different crystals. More recently, M.R.H. Khan *et al.* (1992) studied GaN grown by hydride VPE with Zn concentrations less than 10^{19} cm^{-3}. They observed the band at 2.89 eV (4.2 K) with a

FWHM of 200 meV. In addition to the slight variations in peak location between samples, researchers have reported differing accounts on shifts of this band with temperature, intensity, and pressure.

Differing results have been reported for the shift of the blue peak position with temperature, and several values have been reported for the temperature quenching of this peak. Ilegems *et al.* (1972) reported that the peak shifted from 2.85 eV at 100 K to a higher energy of 2.9 eV at 300 K. They observed that the temperature quenching of this peak had an activation energy 330±15 meV in the 200-400 K temperature range. Pankove *et al.* (1974) found a non-substantial shift of the peak with temperature over a range of 78 to 286 K, and that the FWHM remained constant at 350 meV. They also reported that the PL signal dropped rapidly above 160 K with activation of 180 to 490 meV. Edjer and Grimmeiss (1974) found that the temperature dependence of the Zn peak showed a shift to higher energy with increasing temperature in the range 78 of 190 K, and moved to lower energy above 190 K. In the higher temperature region, the shift followed E_g, and they concluded that this level may be pinned to the valence band. Boulou *et al.* (1979) reported that the temperature quenching of the 2.85 eV peak (300 K) gave an activation energy of 300±70 meV. They found the FWHM to follow the temperature dependent form given by

$$W(T) = W(0) \left[\coth\left(\frac{h\nu_q}{2kT}\right) \right]^{\frac{1}{2}},$$

(2-10)

where w(0) is the FWHM at 0 K and hv_q, the phonon energy, has a value of 45 meV. Monemar *et al.* (1980a) found that the 2.87 eV peak shifted to lower energy by about 15± 3 meV between 220 and 295 K (no shift up from 4 K to 220 K); this shift was greater than the shift in the bandgap over this range. They also found that the samples fell into two groups with respect to temperature quenching. One group quenched rapidly above 100 K, the other has luminescence which persisted to room temperature. MRH Khan *et al.* (1992) found that the peak decreased in energy as the temperature changed from 4.2 to 300 K, but the shift did not exceed 20 meV. This shift was much less than was expected for E_g. Teisseyre *et al.* (1995) reported that neither the shape nor the position of the 2.9 eV line changed (within 20-30 meV) for temperatures between 80 and 300 K; however, for higher temperatures, dramatic changes took place. A new line at 2.3 eV begins to dominate the spectrum as the 2.9 eV line decreases in intensity at temperatures up to 500 K. They concluded that since this new peak was similar to that seen in undoped GaN, it must not be Zn related. In summary, these various reports indicated at most a 50 meV shift in the peak position with temperature. The reports conflicted as to the direction of the shift. The values given for the activation energy of the non-radiative quenching centers were in fair agreement ranging from 180 meV to 490 meV. The variation amongst different groups in the activation energy was understandable since the presence of non-radiative centers was highly dependent on growth/processing conditions.

Pankove *et al.* (1974) studied the intensity dependence of the blue luminescence, and found that intensity was proportional to excitation intensity over four orders of

magnitude, but the peak shifted to higher energy with increased excitation. The shift in energetic location was about 60 meV from 2.795 to 2.855 eV (78 K). The peak shift dependence with excitation intensity followed an approximately exponential dependence given by $\exp(h\upsilon/E)$ where $E\sim5$ meV, suggesting a tailing of states in the CB. In contrast, MRH Khan *et al.* (1992) observed no shift with excitation intensity.

Teisseyre *et al.* (1995) studied the pressure dependence of GaN:Zn grown by a high pressure crystal growth bulk method. The Zn concentration was reported to be about 10^{19} cm^{-3}. The Zn peak at 2.9 eV had a similar shift as the bandgap, shifting from 2.89 eV to over 3.05 eV at 5 GPa, thus arguing against an internal transition at a complex center.

Several researchers have examined the luminescence decay characteristics of the blue peak. Ilegems *et al.* (1972) reported a decay time which stayed constant at 0.4 µs over a wide range of Zn doping. Pankove *et al.* (1974) found the luminescence to be slow with a 10 µs rise time at 78 K and a 5 µs rise time at 300 K. The decay was found to be half as long. Malinovskii *et al.* (1980) measured a significantly shorter 0.015 µs decay time. Bergman *et al.* (1987) found the decay to be exponential with a time constant of 0.3 µs in GaN:Zn that had a Zn concentration of $\sim10^{18}$ cm^{-3}. The peak was attributed to a free-to-bound transition, and the Zn_{Ga} acceptor binding energy was 340 meV. A slower tail was also found and thought to be due to distant D-A pairs. MRH Khan *et al.* (1992) studied GaN with Zn concentrations of less than 10^{19} cm^{-3} finding that the decay time has two characteristic times, 0.5 and 2.3 µs. For low Zn concentrations, the blue

band split into a lower energy component having the fast decay time and a higher energy component having the slower decay time. The higher energy peak behaved like a D-A transition. The lower energy peak behaved like a D-A at faster times, and a self-activated pair at slower times.

Other types of measurements performed on GaN:Zn include photoconductivity and optical quenching. Ejder and Fagerstrom (1975) performed photoconductivity measurements which showed that the photoconductivity increased markedly at 3.2 eV with a further increase at 3.4 eV. They concluded that Zn acted as an acceptor located 3.12 eV (4 K) below the CB. Furthermore, they reported that this level was pinned to the VB since the acceptor level and energy gap showed a similar temperature dependence as the calculated shift. Photoconductivity measurements by Pankove & Berkeyheiser (1974) confirmed the presence of an Urbach tail below the bandedge.

Ejder and Grimmeiss (1974) performed infrared quenching experiments which showed a threshold energy of 0.48 eV for Zn. They also found photoluminescence excitation thresholds of 3.1 eV for Zn. The threshold energies had the same temperature dependence as E_g, which was not expected for an internal transition or complex. These results could indicate that there was a significant lattice relaxation process occurring since the total energy for Zn was 3.1+0.48=3.58 eV which was larger than the bandgap. They also noted a low energy tail in the conduction band.

Using the data available, several models for the blue Zn center in GaN have been formulated. Ilegems et al. (1972) did not come to a conclusion as to the structure of the

center involved, but did state that Zn acted as an acceptor. They also noted that the results obtained were consistent with a strongly lattice coupled single electronic transition. The no-phonon line for such a transition would be in the range of 3.1 to 3.2 eV and Zn would have a binding energy of ~190 meV.

Pankove *et al.* (1974) concluded that the responsible transition was a tunneling assisted radiative transition from a CB tail to Zn acceptor levels. This would explain several features of the luminescence observed by his group. The peak shifted with higher energy as excitation increased which suggested an exponential distribution of states either in the CB or impurity band. The near-gap emissions were absent, since all holes were trapped at Zn centers (non-radiative capture). The slow process (5 μs at 30 K) supported the idea of a tunneling mechanism. They were unable to induce VB-acceptor transitions by infrared pumping, since the Zn levels were filled. And finally, the peak did not shift with the bandgap as temperature was changed from 78 to 286 K since the transition was from the quasi Fermi level.

Monemar *et al.* (1980a) found what they believed were phonon replicas spaced 74 ±2 meV apart on the 2.87 eV peak. They took this as proof of a phonon-assisted envelope rather than a broadened electronic level in contradiction to Pankove *et al.* (1974). They estimated a binding energy of 0.37±0.04 eV. They also used measurements of optical cross sections as well as absorption experiments to estimate the binding energy to be 0.34 ±0.04 eV at 4.2 K (Monemar *et al.*, 1980b). The absorption and emission peaks overlapped at 3.16 eV (4.2 K). This suggested a no-phonon line at 3.16 eV giving 3.5-

3.16=0.34 eV. They concluded that a simple linear model of phonon coupling can give good agreement in explaining the lattice relaxation phenomena observed; however, the addition of several "unobserved" phonon modes were necessary to achieve the best fit.

MRH Khan et al. (1992) concluded, as did Pankove et al. (1974), that the Zn deep level was an acceptor, and that the electron which makes a transition to this deep level comes from the quasi-Fermi level in the tail of states of the conduction band. They also concluded that there was a contribution from a $Zn-V_N$ complex as well. Teisseyre et al. (1995) concluded that a localized donor (not a hydrogenic, effective mass donor) to acceptor transition was responsible for the 2.9 eV GaN:Zn luminescence.

Clearly, the exact nature of the Zn center responsible for the 2.89 eV blue luminescence is under active debate due to the conflicting data seen by different researchers. Variations in material quality between different researchers using differing growth methods no doubt played a role in this situation. Despite of the aforementioned conflicts, some reasonably certain results are that Zn in low concentration acts as a deep acceptor level, the 2.87 eV peak is not the result of an internal transition at a complex center, and that Zn_{Ga} is responsible for the 2.87 eV peak.

One of the parameters which differed among the various researchers was the Zn concentration. Vast changes in the observed luminescence peaks resulted from increasing Zn concentration. Ilegems et al. (1972) reported that the Zn blue peak location showed a definite shift to lower energy by 100 meV as doping level increased from 5×10^{18} to 4×10^{20} cm^{-3}. They noted that the lowest doped sample showed the narrowest blue band

with the highest peak energy (2.91 eV), and the D-A bands seen in nominally undoped GaN were still present. At higher concentrations, the D-A band disappeared as did the acceptor bound exciton band at 3.455 eV.

Matsumoto *et al.* (1974) observed a Zn-related peak in PL at much lower energy than the blue peak. The peak was seen at 2.4 eV and was attributed to a D-A transition. The peak shifted by 40 meV to higher energy with a ten-fold increase in excitation, which would be characteristic of a D-A transition. Furthermore, GaN:Zn showed an absorption band in the range 3.00-3.46 eV (300 K) whereas undoped GaN did not. This absorption band was attributed to the same donor as would be involved in the Zn related D-A transition at 2.4 eV. On the other hand, as Zn doping increased, the 2.4 eV peak shifted to higher energy. To explain this in the context of a D-A transition, they postulated that Zn formed complexes instead of simple acceptor levels. Since Zn concentration was not uniform, the peak would be broadened by the above mechanism. Also, since Zn formed a deep level, strong phonon coupling could also have broadened the peak.

Jacob *et al.* (1977) found Zn related bands at 2.85, 2.5, 2.2, and 1.9 eV (300 K) as Zn concentration was increased. The same group continued to study these centers and noticed that in the concentration range of 10^{18} to 10^{20} cm^{-3}, the blue band was seen at 2.85 eV (300 K) with an external quantum efficiency of 1% (Boulou *et al.* ,1979). However, for Zn levels greater than 5×10^{19} cm^{-3}, green (2.5 eV), yellow (2.2 eV), and red (1.9 eV) bands appeared in succession as Zn concentration was increased. The intensity of each band was closely related to the Zn concentration. From temperature quenching

measurements, activation energies of 0.30±0.07 eV, 0.8±0.1 eV, and over 1 eV were found for the blue, green, and yellow bands, respectively. They interpreted these results as being consistent with D-A pair transitions, which were presumed to be between V_N and $Zn\text{-}V_N$ complexes with strong phonon coupling.

Monemar $et\ al.$ (1980a) found four different Zn emission centers in VPE grown GaN on sapphire. The main peak occurred at 2.87 eV for $Zn < 10^{19}$ cm^{-3}, but peaks at 2.6, 2.2, and 1.8 eV were observed at progressively higher Zn doping levels. Unfortunately, due to the high doping levels required, the detailed nature of these four Zn related centers could not be determined. However the authors explained that the simplest model would be that the 2.87 eV peak was due to Zn_{Ga} while the other centers are the three possible valence states of Zn_N. They also estimated binding energies of 0.37±0.04 eV, 0.65±0.08 eV, 1.02±0.05 eV, and 1.43±0.08 eV. Monemar $et\ al.$ (1980b) used optical cross section and absorption experiments to estimate the binding energies of the four Zn related centers, finding similar values of 0.34±0.04 eV, 0.65±0.08 eV, 1.02±0.05 eV, and 1.42± 0.08 eV (4.2 K).

Near edge luminescence was often quenched in GaN:Zn. However, at lower doping levels, some peaks were observed. Ilegems $et\ al.$ (1972) found an acceptor bound exciton line at 3.455 eV at low temperature in the highest doped samples. Pankove $et\ al.$ (1974) reported that the samples with the highest n-type conductivity showed near-gap emissions at 3.44 eV. The near-gap emissions were quenched in the highest doped

samples which were completely compensated. Monemar *et al.* (1980a) noted that Zn levels of 10^{19} cm^{-3} and above cause the donor bound exciton and D-A band to disappear.

The electrical activity of Zn in GaN has been studied to a lesser extent than the optical properties. By virtue of Zn's position in the periodic table, it was expected that Zn_{Ga} would behave as an acceptor, and thus Zn was of considerable interest for producing p-type material. Ilegems *et al.* (1972) performed Hall measurements on GaN:Zn with estimated Zn concentrations of between 5×10^{18} and 4×10^{20} cm^{-3}. The results indicated that the Zn layers were still n-type with a carrier concentration between $1\text{-}6\times10^{19}$ cm^{-3} and mobility of 30 to 80 cm^2/Vs. Pankove and Berkeyheiser (1974) did photoconductivity studies which showed a sharp change in electrical behavior when the during growth the Zn temperature was above 430 °C. They attributed this to preferential filling of Zn on Ga sites at lower concentration, and preferential filling of Zn on N sites at higher concentration. At these higher concentrations, the GaN:Zn showed little photoconductivity below the bandedge, and was highly insulating.

Pankove *et al.* (1974) reported that the intensity of the blue emission increased until the point at which compensation occurred (78K). Jacob *et al.* (1977) also noted that as Zn levels increased, so did resistivity, and the luminescence peaks seemed to be closely related to the resistivity. As the resistivity increased, the blue band disappeared, and the other bands began to appear in succession.

Amano *et al.* (1988a) noticed that the blue luminescence from Zn doped (10^{19}-10^{20} cm^{-3}) GaN grown with an AlN buffer layer on sapphire by MOVPE increased

irreversibly after application of low energy electron beam irradiation (LEEBI). The irradiation for approximately 300 sec with a 9-30 kV, 16-300 nA electron beam caused the Zn doped samples to show an increase in CL intensity of the peak at 430 nm, while undoped samples showed no such change. PL measurements confirmed that the effects were irreversible, thus showing that the luminescence centers were somehow changed by irradiation. They also annealed the samples at 1030 °C for 25-60 min in a mixture of N_2 and NH_3, and found blue luminescence decreased with annealing. They attributed this decrease to the dissociation of Zn and/or N.

Jacob *et al.* (1977) also performed an annealing experiment with GaN:Zn. They annealed their highest resistivity samples (which showed the 2.2 eV peak) in a mixture of N_2 and NH_3 at 950 °C, and after 30 min the green band appeared. After 50 minutes, the green band dominated the spectrum, and the blue band was present. After 95 hours of annealing, only the blue peak remained, and the layer had become more n-type conducting. The authors offered no explanation for this behavior.

Amano *et al.* (1988b) observed that the densities of non-radiative centers increased as Zn concentration increased. PL and EL studies suggested that Zn atoms can form non-radiative complex centers with native defects such as V_N.

Two studies of Zn implantation of GaN have been reported by Pankove and Hutchby (1974, 1976). First (1974), they implanted several concentrations of Zn into n-type GaN. They found luminescence at 2.87 eV similar to that seen in VPE-grown GaN:Zn, as well as the quenching of near edge luminescence as Zn concentration

increased. The implants were quite shallow with a flat profile between 60 and 320 Å below the surface. The samples were all annealed at 1050 °C for 60 min in NH_3. The luminescence efficiency was found to be inversely proportional to the log of the concentration from 1×10^{18} to 2×10^{19} cm^{-3}. The later study (1976) reported the Zn-related peak at 2.88 eV. They also noted that the samples showed emissions at 1.75 eV and at 2.15 eV which were thought to be implantation related.

Magnesium Magnesium has proven to be the most successful p-type dopant in GaN to date, although it has not been without difficulties. Early attempts to dope with Mg were met with frustration since only compensated material seemed to result. However, since the important role of hydrogen was discovered, new techniques have been developed to circumvent these limitations leading to the growth of controllable p-type GaN:Mg. Ion implanted Mg has received only limited attention. Reports of the luminescence observed from GaN:Mg have varied widely. The location of the dominant, broad Mg-related peak has been observed to shift from 3.2 to 2.95 eV as the Mg concentration increases.

Ilegems and Dingle (1973) reported Mg-related peaks from VPE-grown GaN. Lightly doped samples had a luminescence peak at 3.455 eV, which was attributed to an acceptor bound exciton. An LO phonon replica of this peak was present at 3.362 eV. Upon higher Mg doping, a broad peak first appeared at 3.15 eV, and continued to shift to lower energy ultimately stopping at 2.95 eV as Mg content was increased further.

A series of papers appeared in the early 1970's which dealt with m-i-n luminescent diodes fabricated using Mg-doped insulating layers (Maruska *et al.*, 1972; Maruska *et al.*, 1973, Maruska and Stevenson, 1974). High resistivity layers of Mg-doped GaN were grown on sapphire using VPE. Under forward bias, a violet-Mg related EL peak of 400 meV wide was observed to peak at energies in the range 2.86 and 2.92 eV. In reverse bias, a 750 meV wide peak was observed in the green at 2.5 eV. It was found that light was generated at discrete spots within the Mg doped layer just below the cathode. Since the threshold voltage was larger than the bandgap, and high field strengths were present in the depletion region, the authors suggested an impact ionization mechanism was responsible for generating the blue luminescence.

Mg peaks have been observed using CL on VPE-grown GaN:Mg. Liu *et al.* (1977) found that as Mg concentration was increased, the peak shifted from the near-gap value of 3.30 to 2.95 eV. The peak also broadened to a width of 600 meV at the highest Mg concentration. The CL intensity fell as Mg concentration was increased, abruptly falling to zero as full compensation was achieved. The Mg was found to be nonuniformly distributed within the GaN layer having higher concentration at low-angle grain boundaries.

Amano *et al.* (1989a) examined the effects of low energy electron beam irradiation (LEEBI) on MOVPE grown GaN:Mg. The films had improved crystalline quality since they were grown using a 50 nm AlN buffer layer. The samples doped with 4×10^{19} to 1×10^{20} cm^{-3} were subjected to a 10 keV, 60 μA electron beam. Although no

change in the properties of undoped films was observed, an order of magnitude increase in PL intensity, at 300 K, was observed for the 2.78 eV peak. Similarly grown GaN:Mg films (Amano et al., 1989b) were confirmed to become p-type after LEEBI treatment.

In further study, Amano et al. (1990) found that at low Mg concentration, the 3.27 eV D-A peak dominated at 4 K. As Mg concentration was increased above 5×10^{19} cm^{-3}, a blue band centered at 2.95 eV dominated at 4 K. At room temperature, this peak shifted to 2.7 eV, and a broad green feature was present. However, if Mg concentration was increased above 2×10^{20} cm^{-3}, only the green band centered at 2.25 eV remained at 300 K. From the above data, they concluded that the Mg acceptor level had an activation energy of 190 meV. Based on the temperature dependence of the D-A peak at low Mg concentration, Akasaki et al. (1991) concluded that the Mg acceptor had a somewhat lower activation energy of 155-165 meV. This determination assumed that Mg was the acceptor involved in the D-A transition. Later work achieved p-type GaN with carrier a concentration of 1.4×10^{17} cm^{-3} at 300 K from LEEBI treated GaN:Mg (Akasaki et al., 1993).

Nakamura et al. (1991) showed that GaN:Mg p-type films could be produced without the need for LEEBI treatment. They grew films by MOCVD with GaN buffer layers which showed p-type conductivity from as-grown GaN. The Mg was shown to be uniformly distributed in the GaN layer. Post-growth LEEBI increased the PL intensity of 2.76 eV Mg emissions by a factor of five at 300 K and the hole concentration increased to 3×10^{18} cm^{-3}. Nakamura et al. (1992a) also showed that p-type films could be created

from high resistivity GaN:Mg by post-growth thermal annealing. The resistivity dropped sharply upon annealing above 400 °C in N_2, and reached its lowest value around 700 °C. The resistivity then remained constant up to 1000 °C. The relative PL intensity of the 2.76 eV emissions was maximum at 700 °C, and decreased at higher temperatures while the resistivity remained constant. The PL intensity was therefore not directly related to the p-type conductivity. Vacuum annealing showed identical results. Further study (Nakamura *et al.*, 1992b) showed that the presence of H during NH_3 annealing at temperatures above 400 °C resulted in an increase in the resistivity reversing the N_2 annealing. Thus, they were able to show that H causes a neutralization of the Mg acceptor levels probably through Mg-H complexing.

Wang and Davis (1993) also reported p-type GaN without the need for subsequent LEEBI or thermal annealing treatment. The key to their success was growth by MBE with an AlN buffer layer. They achieved hole concentrations of up to 10^{18} cm^{-3}. No optical results were reported for these films.

To study the role of hydrogen in p-type conductivity, Brandt *et al.* (1994) purposely hydrogenated MBE grown GaN:Mg. The material was p-type without post-growth treatment and had a hole concentration of up to 10^{19} cm^{-3}. Upon hydrogenation, the hole concentration dropped by an order of magnitude offering confirmation that H passivates the Mg acceptor. Furthermore, a new PL line at 3.35 eV was observed at 4 K in addition to the Mg-related 3.25 eV peak. The authors postulated the formation of a hydrogen-related donor level to explain this new PL peak.

Zavada *et al.* (1994) studied the incorporation and stability of hydrogen in GaN. They exposed GaN films to a deuterium plasma or implanted deuterium at 40 keV to a dose of 5×10^{15} cm^{-2}. They also annealed the samples at temperatures up to 900 °C in flowing N_2 for 20 min using a proximity cap. Secondary ion mass spectrometry (SIMS) was used to determine the depth profile of the deuterium. There was a high concentration of deuterium near the surface which they believed was most likely in molecular form. Below this, they found a plateau in the profile which probably resulted from deuterium trapped at impurities or native defects. They did not observe any redistribution of the deuterium at annealing temperatures up to 800 °C. However, annealing at 900 °C resulted in 99% of the deuterium being lost from the plasma treated samples, and 84% lost from the implanted samples. Furthermore, the deuterium retained the shape of the original profile in the case of the implanted samples. This indicated that the deuterium was decorating the implantation damage. The authors concluded that implantation induced damage is stable at least up to 900 °C, but hydrogen could be removed.

Ohba and Hatano (1994) also examined hydrogen incorporation in GaN:Mg. During MOCVD growth, the hydrogen concentration was found to increase linearly with Mg concentration, which suggested the formation of Mg-H complexes. Hydrogen concentration was also found to decrease after thermal annealing at 800 °C for 30 min in Ar gas.

There are only a few reports of Mg-implanted GaN to date. Pankove and Hutchby (1976) found a broad PL peak at 3.21 eV which was unique to the Mg implanted sample.

The sample had been annealed at 1050 °C for 60 min in NH_3. The samples were implanted with a flat profile of peak concentration of 5×10^{18} cm^{-3} between a depth of 60 and 320 Å. A broad luminescence peak at 2.15 eV was observed in Mg implanted GaN as well as all other ion implanted samples, and was thus attributed to implantation damage. Rubin *et al.* (1994) reported the creation of p-type GaN by implantation at 40-60 keV with a Mg dose of 2.02×10^{14} cm^{-2}. Higher energy implantation at 80-100 keV did not result in p-type material due to high strain and defect levels which did not anneal out after 30 min in N_2 at 800 °C. No luminescence results were reported for the implanted GaN, and only a limited range of annealing parameters was explored.

In summary, Mg p-type doping can be accomplished during growth, although, depending on conditions, post-growth processing may be required for activation. However, only very recently have there been reports of ion implanted p-type GaN:Mg. Results seem to indicate that implantation of Mg results in heavy lattice damage which was stable even after annealing. Luminescence associated with Mg ranges from the D-A band at lower Mg concentrations to a deeper band at 2.9 eV at higher Mg concentrations. The relationship between the optical centers and electrical activation is as of yet uncertain.

Silicon Recently, as GaN crystal quality has improved and the background n-type carrier concentration has been reduced, the use of controlled n-type doping has become

necessary. Silicon has become the dopant of choice for this purpose. Despite silicon's widespread use, its role in the optical properties of GaN is still under active debate.

One of the first intentional dopings of GaN with Si was performed by Pankove and Hutchby (1976), who observed only broad luminescence at 2.16 eV. Since this same luminescence was observed from all samples implanted with other species, the luminescence was attributed to implantation damage. Thus, no Si related luminescence was observed.

MRH Khan *et al.* (1986) has concluded that unintentional Si doping during growth was responsible for the D-A band in GaN. They showed a correlation between the Si level measured in their samples by X-ray microprobe analysis and Auger electron spectroscopy with the intensity of the D-A band in undoped and Zn-doped hydride VPE-grown GaN. They found a sub-linear relationship between D-A intensity and Si concentration in the range of 10^{16} to 10^{18} cm^{-3} which was given by the relationship $I=[Si]^{0.66}$. If each Si atom was participating in the D-A transition, then an exponent of one would be expected. Thus, there was some unknown activation factor involved. From the sharp thermal quenching of the D-A band above 200 K, they concluded that Si at higher temperatures could act as an acceptor level.

Koide *et al.* (1991) reported successful m-i-n blue diodes using Si-doped GaN grown by MOVPE as the n-type layer. Smooth, crack-free Si-doped layers could be grown while adjusting the free electron concentration from the undoped values of less than 10^{16} to as high as 2×10^{18} cm^{-3}. All films grown with Si were n-type, suggesting that

Si resided on a Ga site and acted as a donor. Also, the room temperature ionization ratio increased with Si doping. This behavior suggested that Si formed an impurity band at the higher concentrations, subsequently lowering the ionization energy, which was characteristic of such bands. The electron mobility decreased with higher doping levels at room temperature probably due to increased ionized impurity scattering. No photoluminescence was reported for the Si layer.

Nakamura *et al.* (1992c) obtained smooth, mirror-like GaN:Si films by MOCVD growth with n-type carrier concentrations up to 2×10^{19} cm^{-3}. Room temperature PL spectra of the GaN:Si films showed both a strong band at 3.26 eV (D-A related) and a bright deep level luminescence in the yellow at 2.2 eV. However, they could not correlate changes in the intensities of these bands with carrier concentration. They also observed Fabry-Perot interference fringes in the PL data, which was indicative of the film's smoothness. The intensity of the UV emissions increased when the crystalline quality of the Si-doped layers was poor.

Hall effect and deep level transient spectroscopy (DLTS) data have provided some information which may lead to a better understanding of Si centers in GaN. Hacke *et al.* (1994) performed Hall effect measurements on GaN:Si grown by MOVPE with SiH$_4$. They found that below a carrier concentration of 1×10^{17} cm^{-3} measured at 300 K, the layer exhibited carrier freeze out over a large range of temperature with an activation energy of 28.0 ± 0.5 meV. Above concentrations of 10^{17} cm^{-3}, the films exhibited metallic impurity band conduction. DLTS showed only a negligible amount of deep levels from

native defects or unintentionally introduced dopants indicating that Si was the shallow donor responsible for the Hall results. Room temperature PL showed that the Si doped GaN had 20 times as intense a yellow peak as the undoped material, and that the UV peak only appeared in the highest doped samples. The yellow peak was less intense in the highly doped GaN compared to the intermediate doping level. DLTS was performed on GaN:Si with a n-type carrier concentration of 1.86×10^{17} cm^{-3} at room temperature by Gotz et al. (1994). They found two deep levels at concentrations well below the donor density. The first had an activation energy of 0.49 eV and a concentration of about 6×10^{14} cm^{-3}, and the second had an activation energy of 0.18 eV with a concentration of about 7×10^{13} cm^{-3}. No determination was made on the nature of these centers.

In summary, reliable n-type doping with Si has been achieved using several GaN growth methods, and high quality GaN:Si films can be obtained. Near bandgap UV luminescence seems to be quenched by Si doping. Yellow deep level luminescence may be enhanced by Si doping. D-A luminescence can also be seen in some Si doped samples, and may be enhanced over undoped levels. Si can clearly act as a donor in GaN but the exact nature of Si centers and the connection to the luminescence properties of GaN remains uncertain.

Oxygen Oxygen is a common contaminant in GaN. Therefore, its optical and electrical behavior are of great interest. However, because of the difficulty in eliminating unwanted oxygen during GaN growth or processing, it has proved difficult to isolate its effects.

Pankove and Hutchby (1976) give one of the first reports of intentional oxygen incorporation in GaN. After implanting O, they found only weak 2.15 eV luminescence which they attributed to implantation damage. Thus, no oxygen related luminescence was found.

Chung and Gershenzon (1992) did extensive studies on the influence of oxygen on the electrical and optical properties of MOVPE-grown GaN. They introduced water into the growth process by bubbling H_2 through ultra-pure de-ionized water. Electron Probe Micro Analysis was used to determine impurity levels. The detectability limit of Si was about 0.7% and none was detected in any of the samples. Only films grown at low temperatures of 500 and 600 °C with intentional oxygen incorporation showed carbon, and the C levels were 1.7 and 0.62%, respectively, in these two samples. For oxygen, the detectability limit was 0.4% and thus only the films grown at low temperature of 500 and 600 °C showed enough oxygen to measure at 4.8 and 2.8 %, respectively. Thus the major impurity in these samples was oxygen.

Growth experiments showed that oxygen was also incorporated unintentionally during growth, the source being the NH_3 used in the growth process. Upon purifying the NH_3 gas, the carrier concentration of the samples grown dropped by over an order of magnitude. When oxygen was then intentionally introduced, the carrier concentration returned to the previous higher value. Whenever water was introduced into the growth process, the carrier concentration exceeded 10^{20} cm^{-3}. Thus the introduction of oxygen was responsible for the high n-type carrier concentration.

When oxygen was introduced during the growth of Zn-doped layers, higher Zn concentrations were necessary to achieve compensation. However, the presence of oxygen did not influence incorporation in the films. The authors suggested that the formation of ZnO may be responsible for this compensation effect.

The observed optical transitions showed anomalous behavior with oxygen content. Oxygen introduced a tail in the conduction band detected by optical absorption measurements. Absorption in the violet imparted a yellow tint to the samples. Furthermore, the sharp bandedge luminescence was broadened with heavy oxygen doping. Chung and Gershenzon proposed a model based on impurity band formation, and concluded that oxygen formed a 'shallow' deep donor in GaN about 78 meV (measured at 4 K) below the CB. As doping increased, the impurity band merged with the CB to form the absorption tail.

They observed an 80 meV wide PL peak at 3.470 eV in GaN grown without purification. When purified, the band remained at the same position but the FWHM decreased to 28 meV. When water was intentionally introduced, the FWHM increased in proportion to the amount of water. Furthermore, with high oxygen doping, another peak at 3.424 eV appeared, and eventually overpowered the 3.470 eV peak.

Chung and Gershenzon also implanted as-grown material with oxygen and annealed it in NH_3. The lowest dose implantations of 10^{15} cm^{-2} resulted in band-to-band luminescence. At a dose of 10^{16} cm^{-2}, the recovery of the 3.47 eV near-edge peak was

observed. At the still higher doses of 10^{17} cm^{-2} the 3.424 eV peak appeared. They proposed that the 3.424 eV peak may be the result of an oxygen donor to VB transition.

In summary, major work on oxygen in GaN due to Chung and Gershenzon suggests that oxygen acts as a 'shallow' donor in GaN. In higher concentration, oxygen may lead to the formation of an impurity band which eventually merges with the conduction band. Furthermore, a PL peak at 3.424 eV has been attributed to oxygen..

Carbon Carbon is a common contaminant in GaN, and it has been suggested that it may be responsible for the yellow band observed in luminescence. Carbon is also expected to act as an acceptor in GaN generating recent interest in carbon as a p-type dopant. An early report of carbon in GaN did not find any carbon related luminescence peaks.

Pankove and Hutchby (1976) implanted C with a dose of 5×10^{18} cm^{-3} into GaN reporting a broad peak at 2.17 eV. The peak intensity was high, but most of the other species implanted showed this same peak so they attributed it to implantation damage.

Ogino and Aoki (1980) studied carbon doping of needle-like crystals of GaN grown by the sublimation-recrystallization of GaN powder, and microcrystals synthesized by direct reaction of molten Ga and NH_3. The introduction of SiO into the growth showed no influence on the yellow band nor did growth using Ga_2O_3. However, doping with C always emphasized the yellow band. The peak position dependence on the excitation-intensity and temperature indicated that the source of the D-A pair for the yellow band involved the V_N at 25 meV below the CB and a deep carbon-related acceptor

at 860 ± 40 meV above the VB. They interpreted their results in terms of a configuration coordinate model. The deep acceptor was thought to be a complex consisting of a V_{Ga}-C where the carbon atom was substitutional on the Ga nearest neighbor site.

Abernathy *et al.* (1995) recently claimed p-type conductivity with GaN:C grown by metal-organic molecular beam epitaxy (MOMBE) on semi-insulating GaAs. They noted that the growth rate decreased with the CCl_4 flow rate while the p-type carrier concentration increased. They did not report any PL data or data on the crystalline quality of their films. The limited available data indicates that carbon acts as an acceptor in GaN. Furthermore C may be responsible for the broad yellow D-A peak centered at about 2.2 eV.

Beryllium Beryllium is a possible p-type dopant in GaN which has received little attention to date. Ilegems and Dingle (1973) gave one of the earliest reports of GaN:Be which they grew by VPE. Be doping caused the films to be highly resistive, and have a dull pale-yellow appearance. In the lowest doped samples, only the exciton and D-A luminescence were observed. With higher doping, the yellow-green band appeared between 2.07 and 2.36 eV. While the amount of Be in the films was estimated based on growth parameters, the true amount was not experimentally determined.

Pankove *et al.* (1973) also reported that the addition of Be to VPE-grown GaN resulted in highly insulating material. Only a broad peak at 2.16 ± 0.04 eV was observed in PL at a sample temperature of 77 K. No D-A or near-gap emissions were observed.

Pankove and Hutchby (1976) implanted Be with a dose of 10^{20} cm^{-3} into GaN. After annealing for 60 min in NH$_3$, they found only the broad peak at 2.16 eV.

In summary, little work has been done on Be doping of GaN. No Be related luminescence have been reported, and p-type doping with Be has not been achieved.

Erbium and Neodymium There are few reports of rare-earth (RE) doped GaN in the literature. The most extensive work has been done with Er-implanted GaN. The first report of Er in GaN showed the characteristic 1.54 µm Er emissions from Er-implanted MBE-grown GaN on sapphire (Wilson *et al.,* 1994). They implanted GaN at 300 keV with a dose of 2×10^{14} cm^{-2}, achieving a peak Er concentration of ~8×10^{18} cm^{-3} at about 50 Å below the surface. However, they only observed RE luminescence from samples co-implanted with oxygen at 40 keV with a dose of 1×10^{15} cm^{-2}. Annealing was performed at temperatures ranging from 600 to 800 °C. The intensity was best for the 700 °C anneal, and dropped with the 800 °C anneal. They did not report the annealing times or the gas environment used. The samples were excited with the 457.9 nm line of an Ar ion laser at a power level of about 200 mW. They reported well-defined emissions due to the Er $^4I_{13/2}\rightarrow\,^4I_{15/2}$ transitions at 6, 77, and 300 K, noting that the number of lines increased with temperature while the total intensity remained about constant.

RE emissions from Er-implanted GaN were observed using CL by Qui *et al.* (1995). These samples were VPE- or MOCVD-grown GaN implanted with Er at a dose of 1×10^{14} or 1×10^{15} cm^{-2} at 400 keV, and were co-implanted with oxygen at 80 keV with a dose of 1×10^{16} cm^{-2}. The samples were annealed at 900 °C for 30-60 min in flowing

ammonia at 10-20 torr pressure. No luminescence was observed without annealing, and oxygen appeared necessary to activate the RE. The CL was performed with a 10-20 μA electron beam accelerated to 6-20 kV. They only observed one peak at 0.81 eV which they attributed to Er. The integrated peak intensity stayed constant between 6 and 300 K but the FWHM increased by about 10% at 300 K versus 6 K.

Other Implanted Dopants Nitrogen was implanted into undoped GaN to see if V_N could be filled and thereby reduce the high n-type carrier concentration (Saxena *et al.,* 1975). Hall effect measurements were not performed due to the relatively thin implanted layers because implantation was done at 60 keV. Therefore, to determine the effect of the implantation, a chromium contact was made to either the implanted or unimplanted GaN. The unimplanted GaN showed ohmic behavior because of the high n-type carrier concentration. However, the implanted layer showed rectifying behavior. This result was taken to be consistent with the concept that the implanted nitrogen replaced nitrogen vacancies lowering the number of donors. However, it should be noted that the samples were not annealed, and so any lattice damage would not have been repaired. Since implantation damage almost always results in insulating material, the resulting metal-insulator-semiconductor structure could also be consistent with rectifying contact behavior.

Pankove and Hutchby (1976) implanted thirty-five elements into GaN. The most characteristic luminescence was found for phosphorus at 2.88 eV, zinc at 2.88 eV, magnesium at 3.2 eV, cadmium at 2.70 eV, arsenic at 2.58 eV, calcium at 2.50 eV,

mercury at 2.43 eV, silver at 1.52 eV, and beryllium at 2.16 eV. All samples showed emissions at 1.75 eV, and almost all showed emissions at 2.15 eV. Both emissions were thought to be implantation related. Annealing of most samples was performed at 1050 °C for 60 min. in flowing NH_3.

Very broad CL peaks were observed for phosphorus (P) and arsenic (As) implants in GaN by Metcalfe et al. (1978). Before implantation, the as-grown samples had n-type carrier concentrations of 4×10^{19} cm^{-3}, and showed very broad CL emissions. Implantation was performed at 40 keV for P and 82 keV for As, thus the implanted depths were rather shallow. Calculated peak dopant concentrations for both dopants were approximately 10^{18}, 10^{19}, and 10^{20} cm^{-3}. The implantation quenched the luminescence, and thus the samples were annealed in NH_3 at temperatures between 600 and 930 °C. P was found to have a broad feature at 2.85 eV, which was insensitive to temperature between 77 and 294 K, while As showed a broad peak, which shifted from 2.58 eV at 73 K to 2.53 eV at 295 K. The As peak is similar to that observed by Pankove and Hutchby (1976). Also observed in all implanted and annealed samples was a CL peak centered at 2.2 eV, somewhat higher in energy than the 2.15 eV peak observed by Pankove and Hutchby (1976), and was thought to be damage related. In summary, Metcalfe et al. (1978) observed no sharp CL peaks from the P and As implants in GaN and, given the very broad CL spectra of the as-grown material, this was not surprising.

Khan et al. (1983a) implanted Be and N into GaN to achieve compensation levels of 10^{15}-10^{17} cm^{-3} necessary to form chromium/gold Schottky barriers. They also

observed compensation to 10^{16}-10^{17} cm^{-3} in Al$_x$Ga$_{1-x}$N, where x ranged from 0 to 0.22 (Khan *et al.* 1983b). Optical results were not reported.

SIMS profiles of several species implanted into mixed phase (WZ and ZB) GaN grown on GaAs by Wilson *et al.* (1995) showed little or no redistribution of the implanted species after capless annealing at temperatures up to 900 °C. beryllium, carbon, magnesium, silicon, zinc, germanium, and selenium showed no diffusion at temperatures up to 700 °C. Sulfur showed a small redistribution for temperatures above 600 °C. Although the authors reported that zinc and selenium showed a small redistribution above 800 °C, they did not show what changes occurred in the profile nor did they specify the gas environment used during annealing.

Summary: Dopants in GaN Much of the data on the luminescence of dopants in GaN is unclear. Many details regarding the energetic location of luminescence peaks and the underlying mechanisms responsible have not been conclusively determined for intentionally doped GaN. Furthermore, the causes of the common luminescence peaks observed for nominally undoped GaN are in dispute. The donor(s) and acceptor(s) responsible for the D-A peaks have not been conclusively identified. The center responsible for the broad yellow peak commonly seen in undoped and doped GaN has also not been conclusively determined.

Defects in GaN

Bu *et al.* (1995) grew Ga rich GaN. Low temperature PL from these samples showed greatly enhanced yellow emissions as compared to material grown with a 1:1 Ga:N ratio. Based on this piece of evidence, they concluded that the yellow band was related to the Ga_N anti-site double-acceptor.

Recently, the dislocation densities of high brightness nitride based double heterostructure blue LEDs were examined (Lester *et al.,* 1995). The devices which were grown by MOCVD on sapphire showed extremely high surface dislocation densities on the order of 10^{10} cm^{-2}. This was six orders of magnitude larger than the dislocation densities at which GaAs:Si LEDs will not operate. Thus, the authors concluded that dislocations in GaN are much less efficient non-radiative centers than in GaAs. They attributed this behavior to the more ionic nature of bonding in GaN, and the fact that Fermi level pinning does not occur in GaN.

Thermal Stability and Annealing of GaN

Knowledge of GaN's thermal stability is necessary before high temperature devices can be fabricated or high temperature processing steps such as annealing can be used effectively. However, much of the data on GaN's thermal stability has been collected in conjunction with the development of high temperature growth techniques. Only limited data is currently available on annealing processes in GaN. Of the few implantation studies, none aimed at understanding the annealing process. Furthermore,

as will become evident from the information that follows, many of the reports differ in their observations.

One of the earliest studies was done by Schoonmaker et $al.$ (1965), who found that fine powdered GaN began to dissociate at temperatures around 900 °C. They also found that liquid Ga metal can act as a catalyst for the decomposition of GaN. That is, as the GaN decomposes and N_2 gas was released, the remaining Ga metal will act as a catalyst to further speed the decomposition process. Thurmond and Logan (1972) studied the equilibrium pressure of N_2 over VPE grown GaN. They concluded that at temperatures above 800 °C, the equilibrium pressure of N_2 over GaN was greater than one atmosphere. Thus, above 800 °C, decomposition of GaN would occur at atmospheric pressure by the reaction $GaN \rightarrow Ga + 1/2 \, N_2$.

Ilegems and Montgomery (1973) examined whether changes in native defect concentration would occur at temperatures up to 1025 °C in a controlled H_2:NH_3 atmosphere. Electrical measurements showed that conductance decreased after higher temperature annealing and after annealing with lower NH_3 content. This result could not be attributed to a decrease in the concentration of V_N. V_N are expected to act as donors and one would therefore expect the highest NH_3 concentration during annealing to produce the lowest conductance via the reaction $NH_3 + V_N \rightarrow N_N + 3/2 \, H_2$. They concluded that the most likely cause for the observed decrease in conductance was material loss. They attributed this to a reaction with the residual oxygen in the system.

They concluded that there were no significant stoichiometry changes at anneal times on the order of one hour and temperatures up to 1025 °C.

Morimoto (1974) examined the thermal decomposition of VPE GaN in air, N_2, and H_2 atmospheres. Samples annealed in air or N_2 showed no weight loss nor was the surface changed at temperatures up to 1000 °C. In H_2, however, weight loss began at 400 °C, and the surface began to show damage at 600 °C. By 800 °C, the surface became rough and annealing above 900 °C resulted in Ga separation at the surface. The author postulated that the reaction GaN $+3/2H_2 \rightarrow Ga+NH_3$ was leading to the decomposition.

Pankove and Hutchby (1976) annealed several as-grown GaN samples in conjunction with their search for luminescence centers using ion implantation. One sample was annealed successively for 60 minute periods in NH_3 at 925, 950, 975, and 1000 °C. The sample showed only near-edge luminescence after annealing at temperatures up to 975 °C. After annealing at 1000 °C, the efficiency of the near-edge peak dropped by a factor of two, and a new peak was observed at 1.75 eV. The 1.75 eV peak was also seen in the implanted samples annealed at 1000 °C. Another sample annealed at 1050 °C showed the D-A band as well as the other peaks.

Another group (Karpinski *et al.,* 1984) measured the vapor pressure of N_2 over GaN at high temperatures and pressures. Based on this data, they formulated a kinetic model to predict the decomposition rate of GaN in N_2 (Karpinski and Porowski, 1984). They concluded that the decomposition of GaN in N_2 at temperatures below 1100 °C proceeded very slowly.

Lin *et al.* (1993) cite the need to understand the high temperature stability of GaN for device operation as the motivation for their study of the annealing behavior of electron cyclotron resonance molecular beam epitaxy (ECR-MBE) grown GaN on 6H-SiC. On the highest quality undoped material, annealing in N_2 at 700 °C increased the near-edge PL signal. However, annealing at 900 °C for 30 minutes decreased the near-edge PL signal. At the same temperatures, rapid thermal anneal (RTA) for 30 seconds and furnace anneal (FA) with a Si_3N_4 cap showed results similar to the capless results. They concluded that the PL signal decreased for reasons other than N decomposition. They suggested that increases in the surface recombination rate or changes in carrier diffusion length may have been responsible. For low quality samples, which were partially amorphous, the PL intensity increased after FA at 700 °C, and was even more improved after the 900 °C anneal. This result suggested that solid phase epitaxy was taking place in these lower quality samples. They also note the appearance of the 2.2 eV yellow peak after annealing at 900 °C. They attributed the yellow band's formation to an increase in point defects and antisites caused by annealing.

Wickenden *et al.* (1994) studied annealing-related effects in GaN buffer layers in an effort to understand the changes experienced by these layers during subsequent GaN film growth. Buffer layers are also called nucleation layers because they consist of numerous individual crystals which have formed on the substrate material. As they grew larger, they coalesced into a single film covering the substrate. The GaN grown in this manner usually contained amorphous regions. Since these layers were not single

crystalline and have high defect and dislocation densities, annealing can result in significant changes. However, it should be noted that buffer layers are significantly different from implanted layers or high quality GaN layers. Thus, annealing induced changes may differ in these cases. They annealed the films by linearly ramping the temperature to a value between 870 and 1050 °C at 30 °C/min to simulate the temperature environment typically used in GaN film growth. Absorbance data showed a maximum slope in the range 360-365 nm corresponding to the fundamental band gap. Upon annealing, the slope at the absorption edge increased with annealing temperature. Taking the gradient of the absorbance spectrum resulted in a peak at the band edge. These maximum gradients were subjected to an Arrhenius analysis. The apparent energy for the crystallization of GaN was found by this analysis to be 0.9 eV. It was noted that since the anneals were not isothermal (temperature was not held constant), the conditions necessary for an Arrhenius analysis were not rigorously met. However, the authors noted that the value obtained was similar to other alloys. They suggested that possible recrystallization mechanisms were movement of vacancies or dislocations, self- diffusion within the bulk material, creep, and grain boundary diffusion. They also observed from x-ray diffraction data that the crystallinity increased after annealing, and tensile strain was reduced. Some samples were ramped to 1015 °C, and annealed for periods up to 120 minutes. They found that most of the change in absorption occurred during the initial temperature ramp. Furthermore, the x-ray data showed that after 20 min at 1015 °C the crystalline quality began to deteriorate.

The thermal stability of GaN on two orientations of sapphire and 6H-SiC was studied by Sun *et al.* (1994). They annealed samples in N_2 or H_2 at 900 or 1000 °C in one hour increments. They found that the MOCVD films grown on (0001) sapphire showed improved crystal quality after annealing at 900 °C in N_2 for four hours. However, for samples annealed in H_2, there was severe surface decomposition. Furthermore, the n-type carrier concentration remained constant during N_2 annealing, but H_2 annealing resulted in an increase in carrier concentration and drop in mobility. They attributed the surface decomposition in H_2 ambients to the reaction $GaN + 3/2\ H_2 \rightarrow Ga + NH_3$.

Overall, there seems to be general agreement that the GaN surface is less damaged by annealing in an N_2 atmosphere than either NH_3 or H_2. There is, however, no clear consensus as to the temperature at which decomposition becomes noticeable. Based on all the evidence, a temperature of 900 to 1000 °C can be expected to show a noticeable level of surface degradation in NH_3. One can also expect the near-edge PL intensity to drop and deep levels to become evident. Some evidence suggests that NH_3 annealing may not cause stoichiometry changes in the GaN thin films.

Annealing low quality samples in N_2 at temperatures of 900 to 1000 °C should not result in such high surface degradation, and may in fact improve the crystalline quality. However, high quality material annealed at these temperatures in N_2 may show decreased near-edge luminescence. The reason may be less related to nitrogen decomposition than to an increase in the surface recombination rate or a change in the carrier diffusion length. As with NH_3 annealing, deep levels may be formed during N_2 annealing.

III. Samples and Sample Preparation

This chapter will begin by providing background information about the as-grown GaN samples used in this study and their processing prior to implantation. Next, the parameters used for implantation of each ion species will be given. Then, the annealing process will be described. Lastly, a discussion of the possible native defects and contaminants present in the samples and introduced through processing will be given.

Samples Used

The as-grown GaN samples used in this study were obtained from three different sources. Both APA Optics and Honeywell supplied metal-organic chemical vapor deposition (MOCVD) grown GaN, and the Solid State Electronics Directorate of Wright Laboratories (WL/ELR) supplied molecular beam epitaxy (MBE) grown GaN. All of the GaN films used in this study were grown on sapphire substrates. Nearly all of the substrate was c-plane sapphire, however, a few r-plane substrate samples were available from WL/ELR. A list of the as-grown samples used in this study is given in Table III-1. The grower, method of growth, sample identification number, and orientation of the substrate are provided.

The samples supplied by APA Optics were grown on ½" square sapphire substrates. Honeywell provided 2" diameter wafers. The samples supplied by WL/ELR were irregular in shape when received, having been previously cut from larger wafers. In

order to have sufficient quantities of samples for direct comparison of different annealing conditions on identically implanted GaN, the samples were cut into sizes ranging from about 6 mm × 6 mm down to 3 mm × 3 mm. Cutting was accomplished by scoring the GaN side of the sample with a diamond tipped scriber and breaking along the scratch. The goal was to create square samples; however, since the samples did not always break along the scribe mark, many samples were somewhat irregular in shape

Table III-1. List of as-grown GaN samples on sapphire substrates showing source, growth method, and sapphire substrate orientation.

Source	Growth Method	ID #	Substrate
APA Optics	MOCVD	246.3	c-plane
APA Optics	MOCVD	248.3	c-plane
APA Optics	MOCVD	292.3	c-plane
APA Optics	MOCVD	701.3	c-plane
APA Optics	MOCVD	873.3	c-plane
APA Optics	MOCVD	890.3	c-plane
APA Optics	MOCVD	946.1	c-plane
APA Optics	MOCVD	1342.1	c-plane
APA Optics	MOCVD	1349.1	c-plane
APA Optics	MOCVD	1462.1	c-plane
APA Optics	MOCVD	1548.1	c-plane
APA Optics	MOCVD	1551.1	c-plane
Honeywell	MOCVD	E02388	c-plane
Honeywell	MOCVD	E02524	c-plane
Honeywell	MOCVD	E02525	c-plane
WL/ELR	MBE	282 008	c-plane
WL/ELR	MBE	282 008	r-plane
WL/ELR	MBE	283 009	c-plane
WL/ELR	MBE	283 009	r-plane

Before implantation, annealing, or optical studies, the samples were typically degreased using acetone and methanol. The residual degreasing agents were blown off using dry N_2 gas.

Implantation

For each element implanted, a set of specific doses and energies were chosen, and these are shown in Table III-2. The projected range (R_p), standard deviation (ΔR_p, also called straggling), and peak concentration of the ions were calculated using the PROFILE code (Implant Sciences, Danvars, MA). The input parameters were the density of GaN, the ion species, implantation energy, and dose. The resulting implantation profiles as calculated are shown in Figures 3-1 through 3-7.

Physical factors as well as hardware limitations were important considerations in choosing the energy with which to implant a given species. The implantation hardware used by UES, Inc. and WL/ELR to perform the implantations imposed an upper limit on the energy of implantation for the given ions. With the exception of the rare earth's (Er and Nd), all implantations were performed on machines with an upper limit of 400 keV. The most important physical consideration was that the ions be implanted as deeply as possible in order to ameliorate any possible effects of the surface. Since the ion energy governs the depth of the implant, the highest energies possible were chosen in most cases. In some instances, such as for Be and Mg, lower energies were imposed by the implantation apparatus. Since only a relatively small ion beam current was obtained with

Table III-2. Ion implantation parameters and calculated doping profiles.

Ion	At. #	At. Wt.	Energy (keV)	Dose (cm^{-2})	R_p (Å)	ΔR_p (Å)	Peak Concentration (cm^{-3})
Be	4	9	200	5×10^{13}	4270	1284	1.5×10^{18}
C	6	12	390	1×10^{14}	4990	1280	3.1×10^{18}
N	7	14	-----	-----	-----	-----	-----
O	8	16	135	5×10^{14}	1657	702	2.8×10^{19}
			390	1×10^{14}	4203	1207	3.3×10^{18}
Mg	12	24	100	5×10^{13}	958	492	4.1×10^{18}
			300	2.2×10^{14}	3035	1187	7.4×10^{18}
			300	8.2×10^{14}	3035	1189	2.7×10^{19}
Si	14	28	390	5×10^{14}	3339	1227	1.6×10^{19}
Ar	18	40	390	5×10^{14}	2211	765	2.6×10^{19}
Zn	30	64	390	1×10^{13}	1419	519	7.7×10^{17}
			390	1×10^{14}	1419	519	7.7×10^{18}
			390	2.25×10^{14}	1419	519	1.7×10^{19}
Ga	31	69	-----	-----	-----	-----	-----
Nd	60	144	910	1×10^{13}	1623	450	8.9×10^{17}
			910	5×10^{13}	1623	450	4.4×10^{18}
Er	68	166	1150	1×10^{13}	1644	406	9.8×10^{17}
			1150	5×10^{13}	1644	406	4.9×10^{18}

Be and Mg and the beam current diminished with acceleration, these implants were done at somewhat lower energies. Nd and Er were both implanted on a higher energy machine at UES, Inc. so as to achieve reasonable depths with these extremely heavy ions.

The dose in each case was chosen to achieve a desired minimum concentration over a range of at least several thousand Angstroms. Since optimal concentration levels
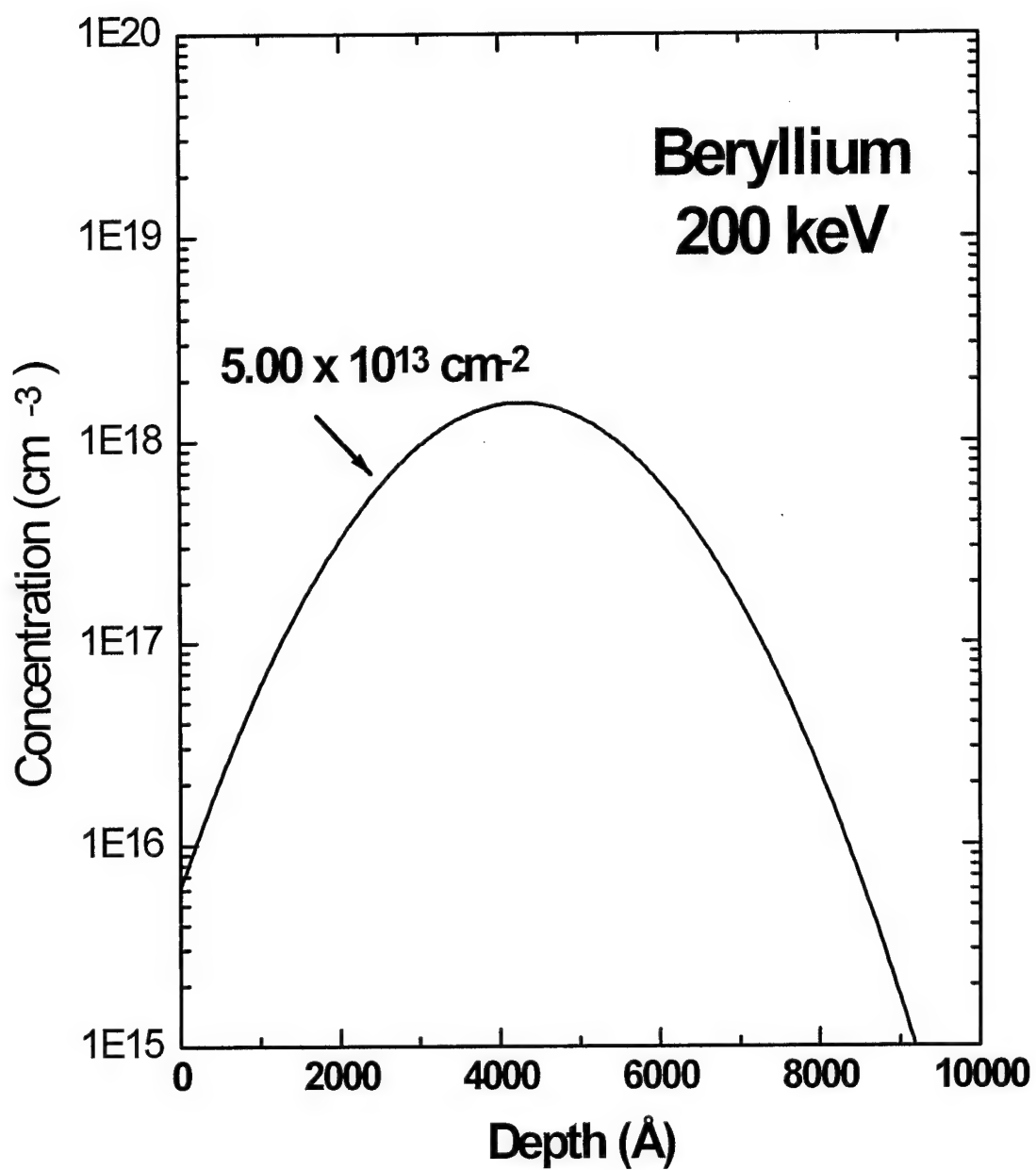
Figure 3-1. Ion implantation depth profile calculated for beryllium-implanted GaN.
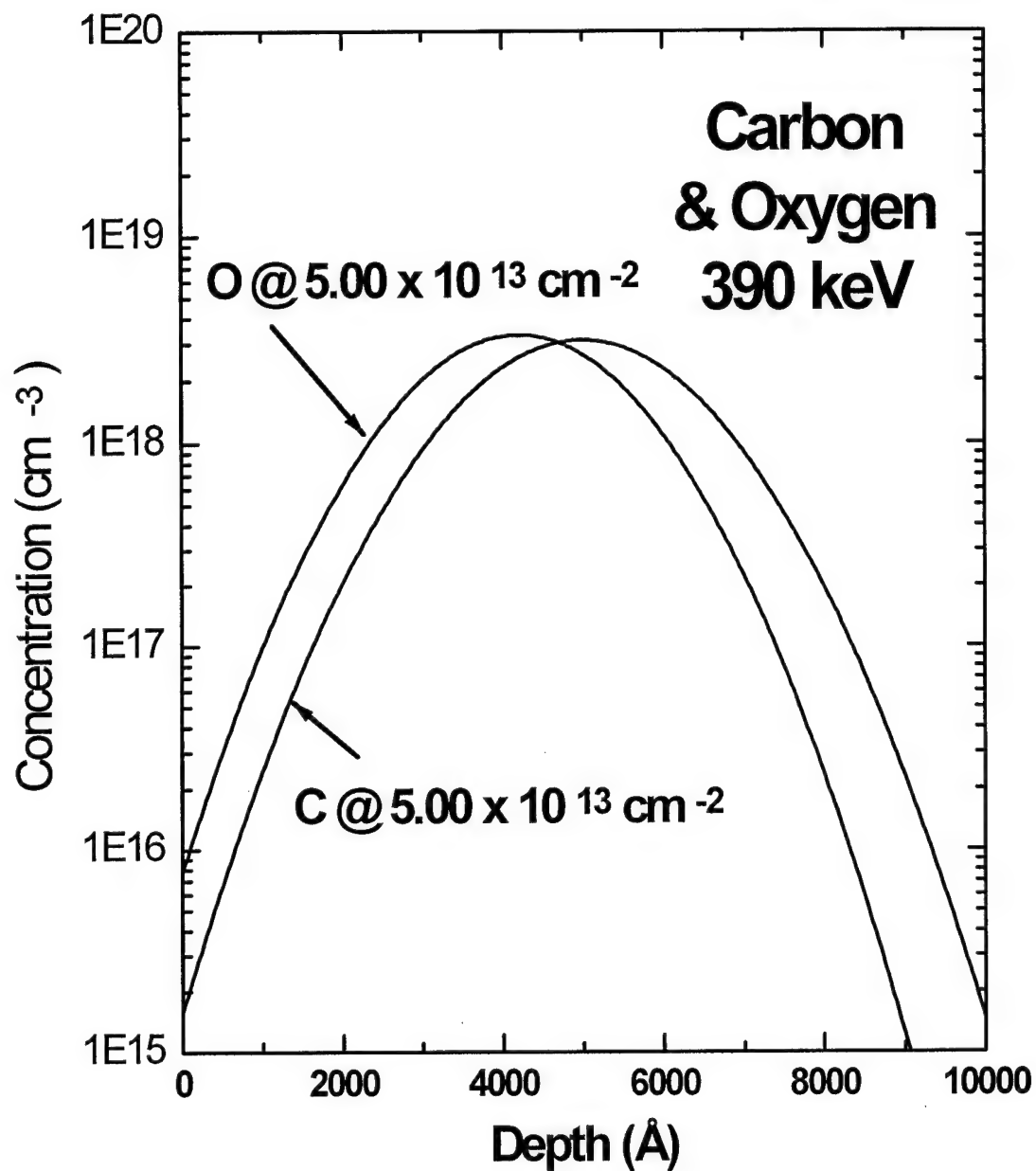
Figure 3-2. Ion implantation depth profile calculated for carbon- and oxygen-implanted GaN.
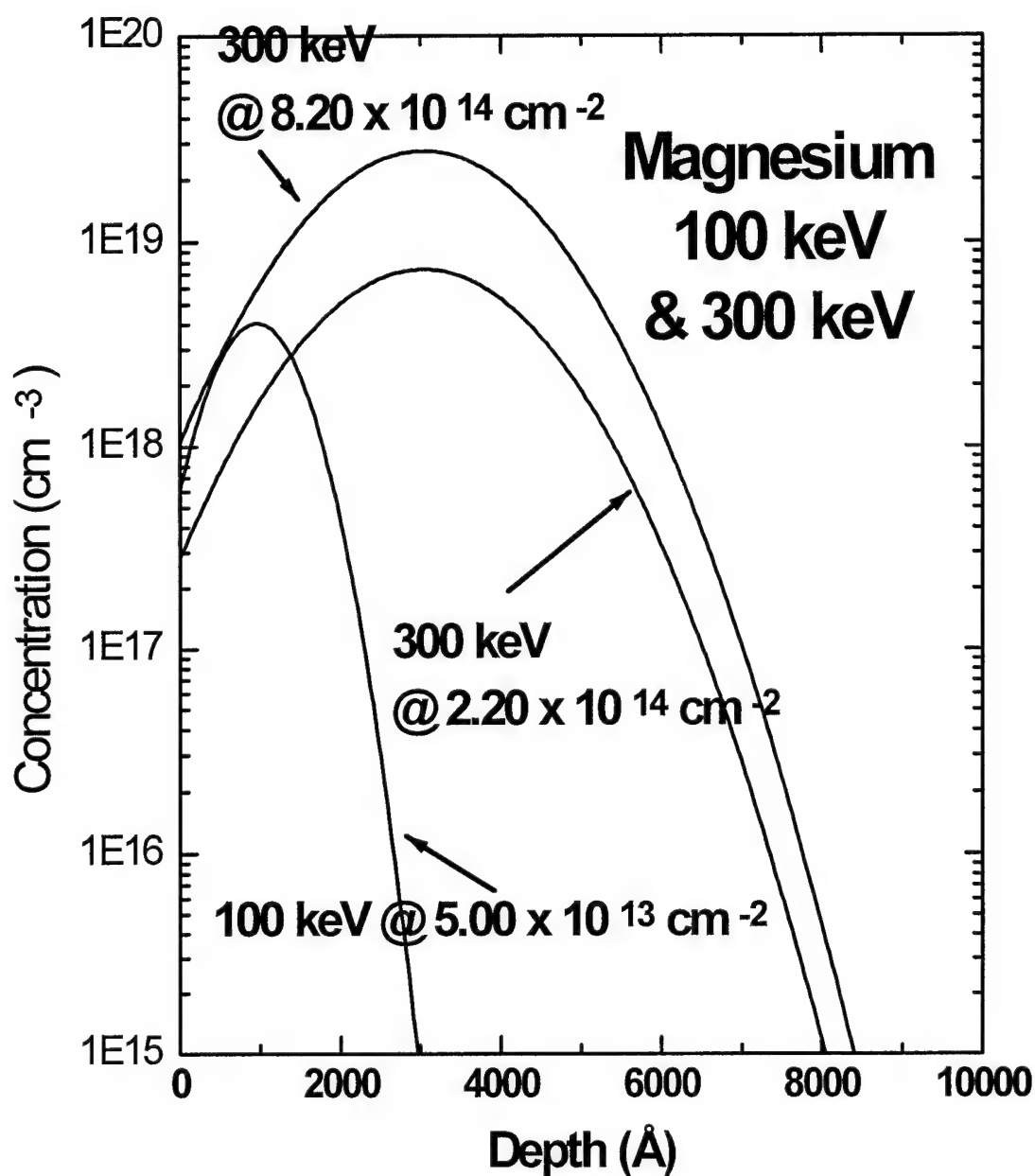
Figure 3-3. Ion implantation depth profiles calculated for magnesium-implanted GaN.
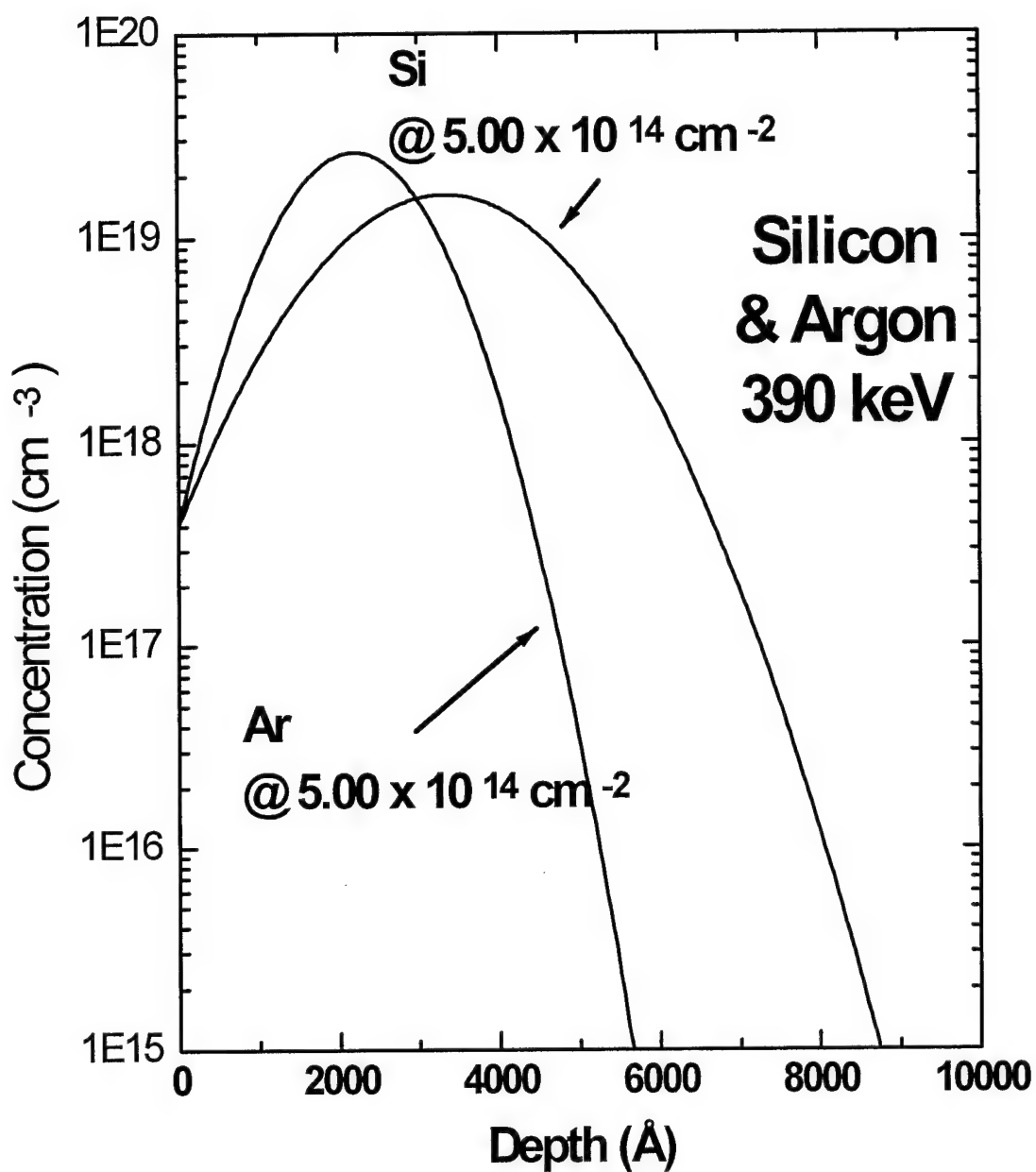
Figure 3-4. Ion implantation depth profile calculated for silicon- and argon-implanted GaN.
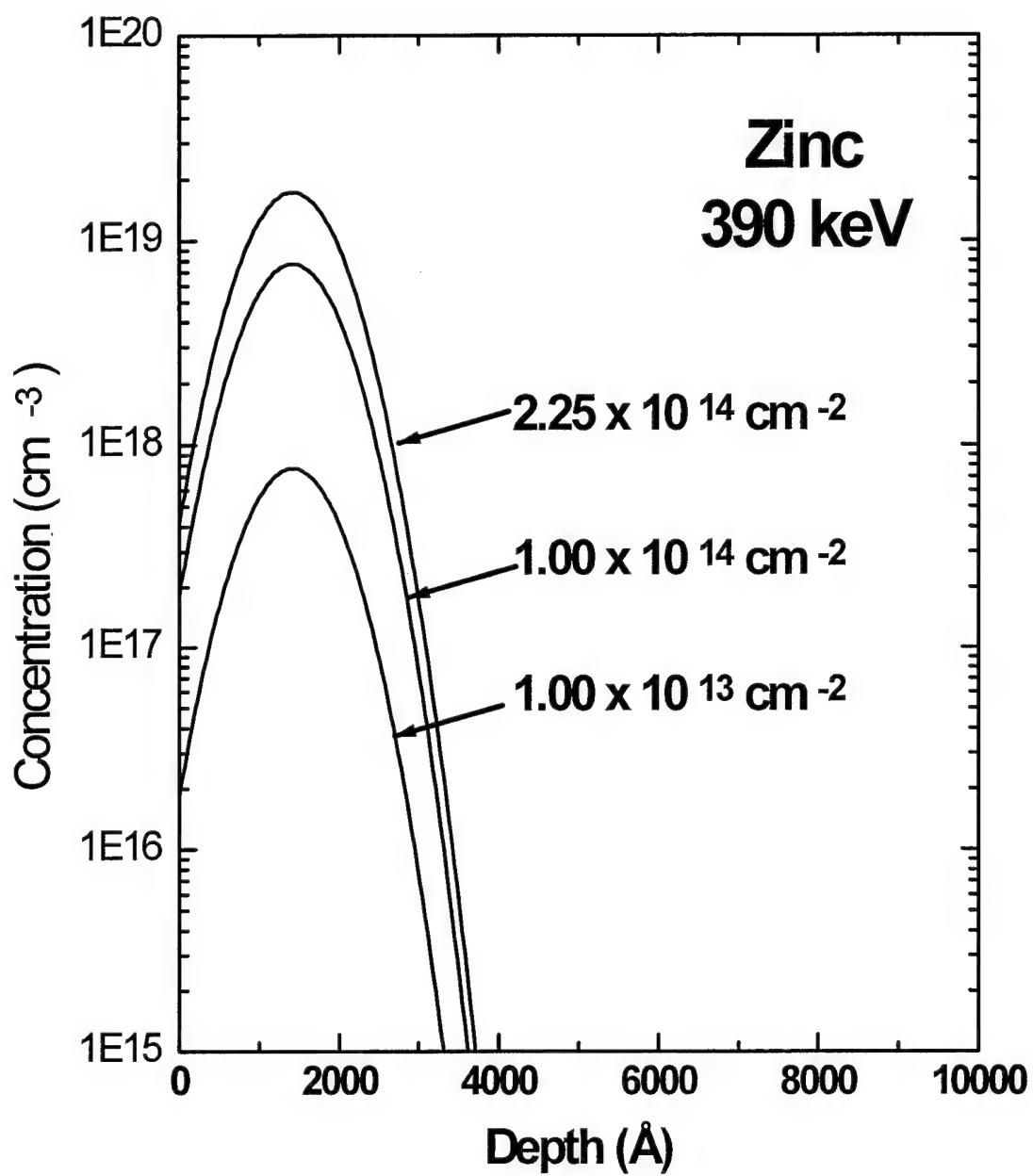
Figure 3-5. Ion implantation depth profile calculated for zinc-implanted GaN.
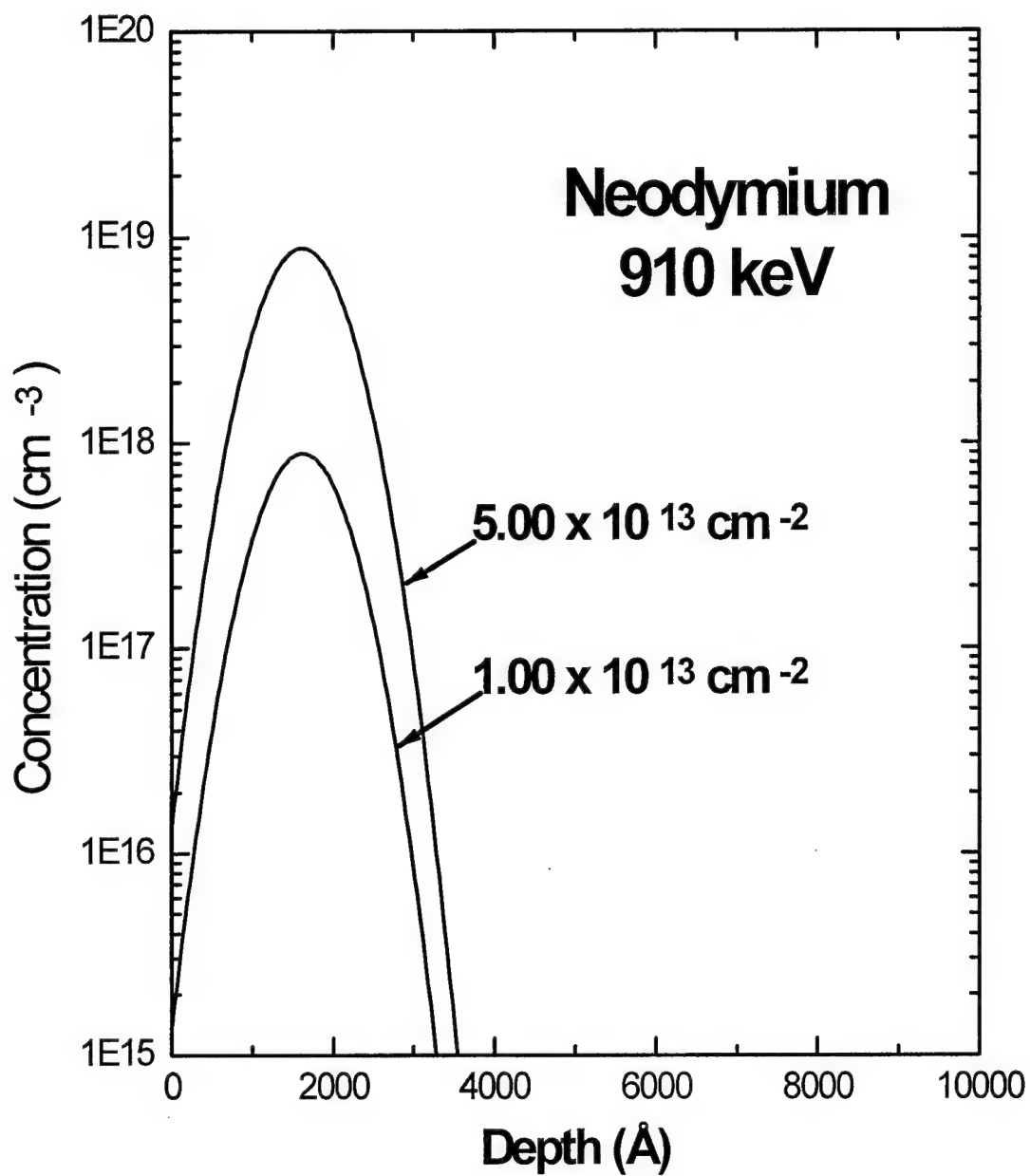
Figure 3-6. Ion implantation depth profile calculated for neodymium-implanted GaN.
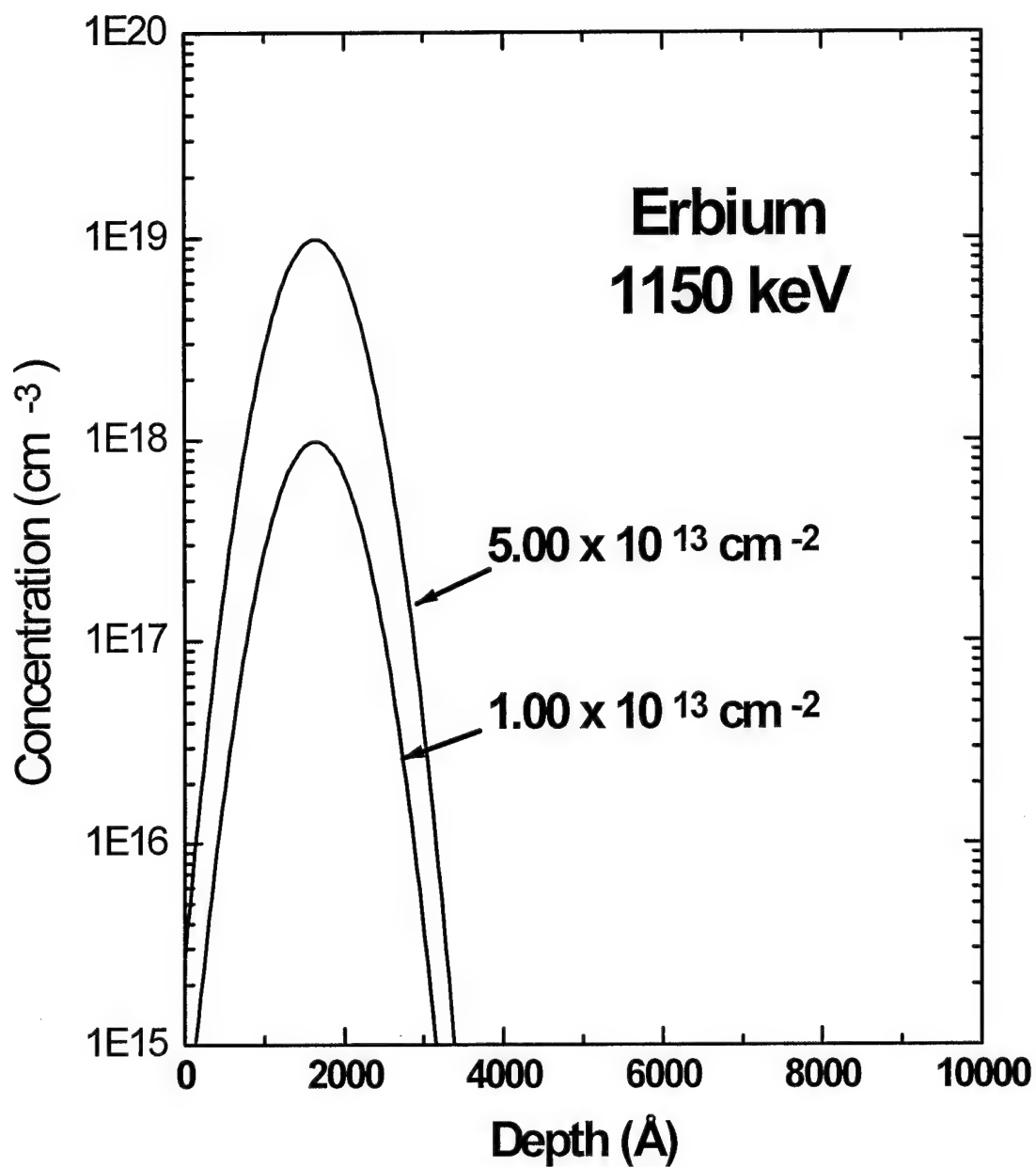
Figure 3-7. Ion implantation depth profiles calculated for erbium-implanted GaN.

to achieve optical or electrical activation were unknown for GaN, some judgment was necessary in selecting the desired dose. The dose also has a role in determining the amount of damage the crystal endures during implantation. Since the role of damage in optical and electrical activation in GaN was also unknown, judgment was again called for. Whenever possible, several doses were implanted in order to study the dose dependence of activation. Unfortunately, in most cases, not enough identical GaN samples were available to study at all dose levels. A major consideration was the ability to detect the implant optically. Since the implant profile is shallow compared to the total thickness of GaN, a concentration high enough to be detected above the as-grown GaN signal was necessary. In most cases, a limitation on the beam current achieved by the implanter caused the maximum doses available to be lower than desired.

For implantation, the sapphire side of the samples was glued to a Si wafer which was then mounted inside the implantation chamber. The sample holder was maintained at room temperature during implantation. To achieve a homogenous implantation across the wafer, the sample holder was rastered in the horizontal direction and rocked about 10° in the vertical direction. For each horizontal sweep, the sample was rocked 35.7 times, and this insured a uniform coverage.

The sources used in generating the implant species were CO_2 gas for both C and O, Ar gas, Er and Nd oxides, and metallic Mg and Zn. The highest ion beam currents typically used by the implanter for implants below 400 keV were 400 μA for C and O, 60 μA for Ar, 50 μA for Mg, and 1.2 μA for Zn.

Annealing

Furnace annealing (FA) was the primary annealing method used. The samples were placed inside a clean quartz tube on a quartz sample holder as shown in Figure 3-8. Either anhydrous ammonia (NH_3) or dry nitrogen (N_2) gas flowed over the samples during annealing. The entire tube assembly was placed inside the tube furnace and heated at temperatures up to 1100 °C. The temperature was monitored using a calibrated thermocouple.
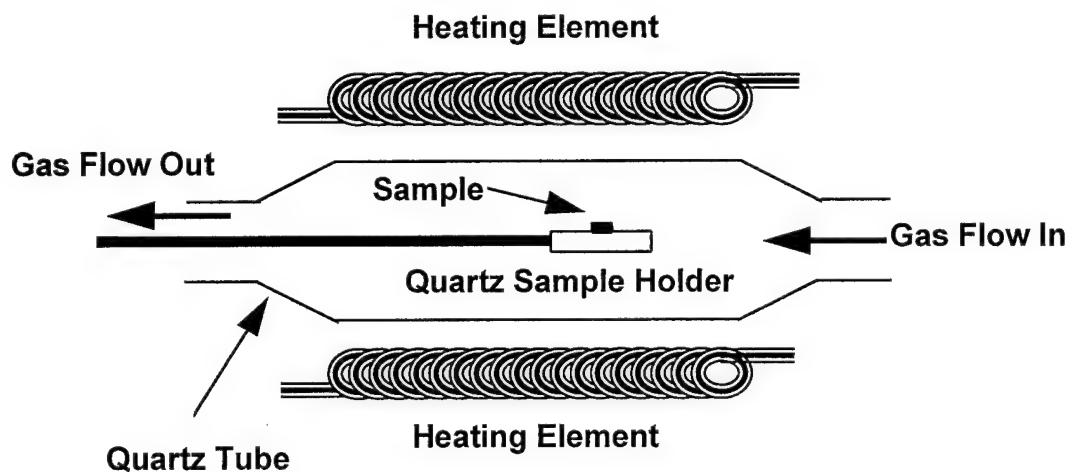
Figure 3-8. Schematic diagram of annealing furnace.

Many of the samples were annealed with the GaN face exposed to the clean gas environment to avoid possible contamination from direct contact with the sample holder. However, to determine optimal annealing conditions, the proximity annealing technique (PA) was also used. In this method, two GaN samples are placed face-to-face during

annealing. This method uses the intimate contact of the two GaN surfaces to prevent the outgassing of the more volatile atom, in this case nitrogen.

A small number of samples were annealed using the rapid thermal anneal (RTA) technique. This technique is often used to prevent the redistribution and possible separation of the dopant species by out diffusion. The short annealing time used does not allow enough time for redistribution of the implanted species to occur. RTA was performed in a vacuum environment using a high temperature lamp. Due to the rapid temperature increase and the potentially great temperature difference between the sample and the sensor located at different distances from the lamp, temperature measurement with the RTA method is very difficult. For this study, the estimated sample temperature was 1000 °C and annealing was performed for 30 to 90 s.

Native Defects and Unintentional Contaminants

Since GaN growth technology is still in its infancy compared to Si or GaAs, there are still serious contamination issues which are only now being explored. The unintentional contamination levels of the samples used in this study are unknown. However, some general conclusions can be drawn from the existing literature and the experience of the growers. For example, the MOCVD growth method used by both APA Optics and Honeywell uses triethylgallium and ammonia (NH_3). Both of these materials contain small amounts of unintended impurities such as carbon and oxygen.

Material from APA Optics that was cleaned by a procedure similar to that used here was subjected to Auger electron spectroscopy (AES) by Khan *et al.* (1993). The AES revealed peaks due to carbon and oxygen with magnitudes about 25% of that of nitrogen. After a special high temperature cleaning procedure where Ga was deposited and evaporated off in an ultra-high vacuum, the carbon peak was reduced to 2% of the nitrogen peak value while the oxygen peak was near the detectivity limit of AES. Thus, the carbon and oxygen contamination can be very high at the surface after exposure to the environment and degreasing. They reported that the C and O levels in the bulk of the material can possibly be as high as parts per hundred. The samples APA Optics provided for this study were grown under nearly identical conditions, and are thus presumed to be similarly contaminated.

WL/ELR used a solid Ga source and NH_3 for MBE growth of the GaN used in this study. X-ray analysis showed a 100 arcsec FWHM for GaN grown on c-plane sapphire and a 150 arcsec FWHM for GaN grown on r-plane sapphire (Lei *et al.*, 1995). The impurities levels have not been experimentally determined for these samples.

Based on the existing body of knowledge of GaN growth, it is safe to assume that the films used in this study have a high dislocation and defect density, have significant quantities of unintentional dopants, and may not be perfect crystalline.

IV. Characterization Techniques

This chapter will describe in detail the experimental apparatus and techniques most extensively used during the course of this work. First, photoluminescence (PL) will be described since this was the characterization technique most used. Then, the very similar technique of cathodoluminescence (CL) will be discussed, followed by a comparison of the relative strengths of each. Next, a short discussion of the error analysis common to PL and CL will be given. Optical absorption, a characterization technique used to complement the luminescence measurements, will be described in the final section.

Photoluminescence

Figure 4-1 is a schematic diagram illustrating the low temperature photoluminescence setups used. A low temperature capable PL setup includes a monochromatic excitation source, a sample chamber with cryostat, optics for the collection and focusing of the luminescence, a spectrometer to disperse the light into its component wavelengths, a photon detector, and a data collection system. Several different detectors, lasers, and laser beam conditioning arrangements were used during the course of this work as will be described below.
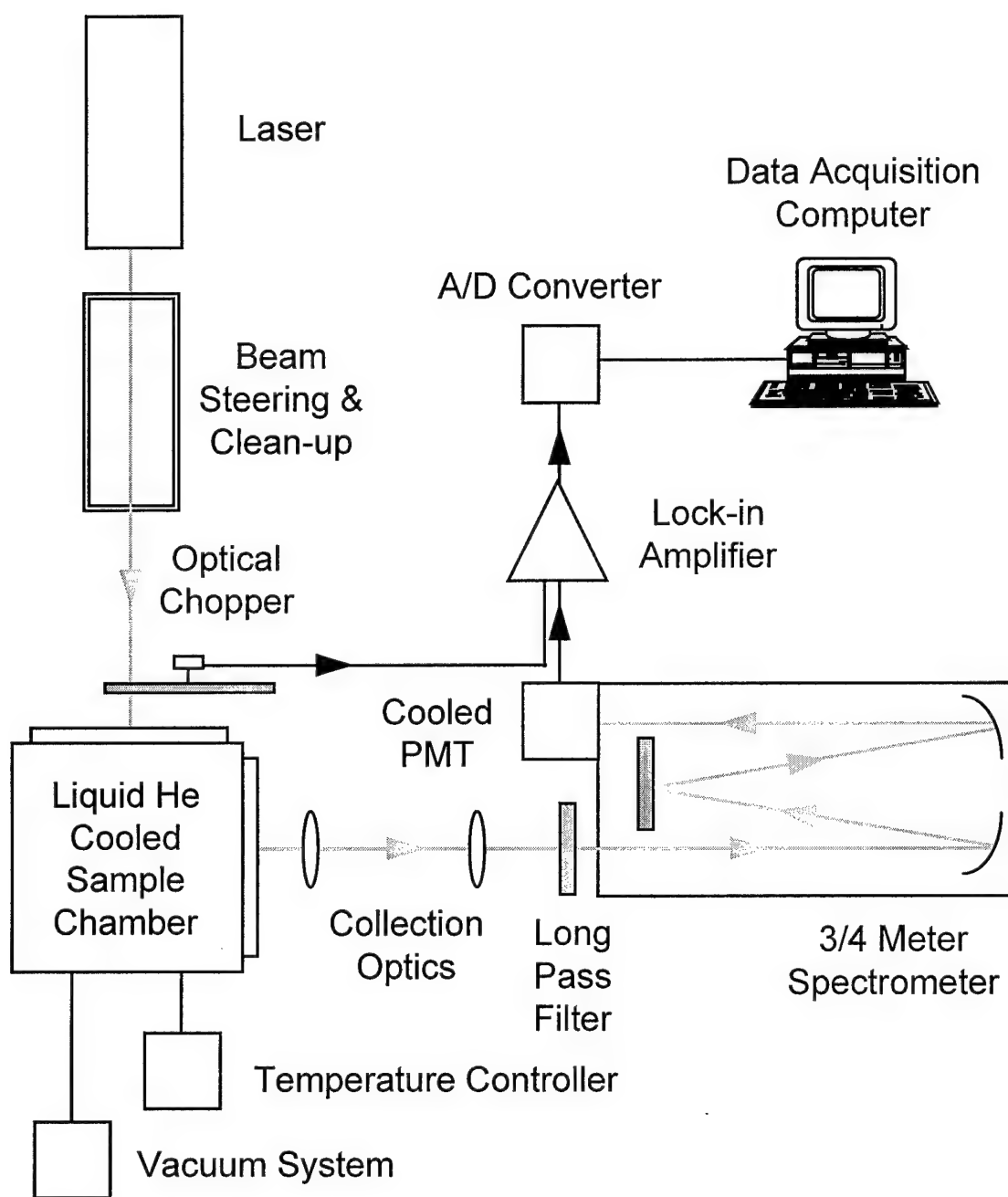
Figure 4-1. Experimental setup for low temperature photoluminescence.

Two different laser excitation sources were used. First, a Spectra Physics 2085 argon-ion laser was operated multi-line from 275.4 nm (4.502 eV) to 305.5 nm (4.058 eV) in the UV. This laser was capable of generating up to 200 mW of laser output when run with a 60 A plasma tube current. However, due to limitations in the electrical service, the laser was more typically run at 50 A plasma tube current, and typically produced 50 mW of laser output in the UV. This same laser was also operated on numerous single lines in the visible for excitation of the rare earth implanted samples.

The second laser source used was a Coherent Innova 300 Series FReD laser. This laser contains an Argon-ion plasma tube, however, there is also an intra-cavity β-Barium Borate nonlinear optical crystal used to frequency double (FReD) the visible wavelength Argon laser radiation to wavelengths in the UV. This laser was operated such that the 488 nm Argon line was doubled to 257.2 nm (4.821 eV) in the UV with up to 200 mW of power.

Since UV light is readily absorbed by most optical glass, special UV grade fused silica right angle prisms (Oriel 46160) were necessary to steer the laser beam onto the samples. The laser entered and exited the prisms at normal incidence for minimal refection loss and was reflected at forty-five degrees by total internal reflection off the larger prism surface. This technique resulted in losses of about 10% of the incident laser power per prism. The prisms were mounted on a periscope allowing easy steering of the laser beam onto the sample.

To achieve good signal-to-noise, it was necessary to remove unwanted spectral features from the laser output. Different methods were necessary for the different lasers used, thus Figure 4-1 displays a generic box for "beam steering and cleanup." In the case of the Ar-ion laser operating in the UV, so-called plasma tube lines resulting from atomic transitions within the excited Ar gas were prevalent in the blue region of the spectrum. These lines were often on the same order of intensity as the emissions from the implanted samples and were in the same spectral region of interest. In order to remove these lines, several techniques were used. First, an Oriel 66217 UV dichroic mirror was used. At a forty-five degree angle of incidence, this mirror reflected UV radiation at about 95% efficiency in the range of 260 nm to 320 nm while allowing visible radiation with wavelengths above 350 nm to pass through the filter with 85% transmittance. Thus, when used as one of the beam steering elements, this mirror greatly reduced the amount of plasma tube radiation incident on the sample. However, the small amount of plasma tube intensity which was reflected by the dichroic mirror was sufficient to interfere with PL measurements on some samples. A second measure employed was the use of a 270 nm bandpass filter. This filter cut down the plasma tube line intensity by several orders of magnitude, but also decreased the UV laser intensity by 82-90%. A final measure to prevent unwanted laser emissions from reaching the sample was the use of an adjustable iris. The iris was used to limit the laser beam diameter at the laser output. The plasma tube emissions do not result from stimulated emission, and are therefore divergent, exiting the laser in a wider cone of light than the UV laser lines. Therefore, the iris

effectively eliminated a sizable percentage of the unwanted blue emissions before they were focused onto the sample by the fused silica optics. Finally, the laser light was focused onto the sample using one of the UV grade fused silica lenses.

Plasma tube lines were not present in the output of the FReD laser; however, the green 488 nm line was. To eliminate this unwanted laser line, an Oriel 46160 UV grade fused silica prism was used as a dispersive element. This prism gave a sufficient linear separation between the UV line and the green line such that, at a distance of about 30 cm, the UV could be allowed to pass through an iris while the green was completely blocked. Since this effectively eliminated all wavelengths other than the UV, the 270 nm bandpass filter was no longer used. Consequently, more laser power was available to excite the sample when using the FReD laser.

The samples were glued to a stainless steel or copper cold finger with rubber cement. The cold finger was inserted into a Janis 10DT liquid He variable temperature cryostat. The cryostat contained a reservoir for liquid He which remained at a temperature of 4.2 K. The liquid He was isolated from the environment by means of an outer reservoir of liquid nitrogen which remained at a temperature of 77 K. The liquid level in the reservoir was monitored using an American Magnetics 110A liquid He level meter. The reservoirs were isolated from one another and the room by means of a vacuum jacket. The vacuum jacket was pumped to a pressure of 1-10 mm Hg by either an Alcatel 5081 turbomolecular pump with an Alcatel 2012A mechanical backing pump or an Alcatel Drytel 31 pump. The flow of liquid He to the sample chamber was

regulated by a needle valve and the sample chamber could be completely flooded with liquid He if desired. To attain temperatures below 4.2 K, the sample chamber was pumped with a high flow rate (500 l/min) Sargent-Welch Duo-Seal 1397 mechanical vacuum pump. By pumping the pooled liquid He in the sample chamber, helium vapor at temperatures down to 1.4 K could flow across the face of the samples.

For operation above 4.2 K and up to 300 K, the sample holder was equipped with a resistive heating element. The temperature was controlled by a Lakeshore DRC82C or Lakeshore 805 temperature controller to within ± 1 K, and was monitored using a calibrated Si temperature probe.

Samples could be illuminated in one of three configurations as shown in Figure 4-2. The GaN sample could be attached to the sample holder with the GaN face up or face down. In the face up configuration the laser could be focused to enter into the GaN surface or to enter the sample from the edge. In both cases, the luminescence was collected from the face of the sample. The sample could also be attached to the cold finger with its GaN face down in which case the laser would enter the sample from the sapphire side. The luminescence would then be collected after exiting the sapphire substrate.

Light from the sample was collected and focused onto the spectrometer slit by means of two lenses. The SPEX 750M spectrometer used had an f/# of f/6.0, and for the optimal light gathering and resolution, the lens used to focus the luminescence onto the spectrometer slit was chosen to be as close as possible in an off-the-shelf item. A Melles

FACE
Illumination

BACK
Illumination

Damaged
Layer

GaN

Sapphire

EDGE
Illumination

Laser
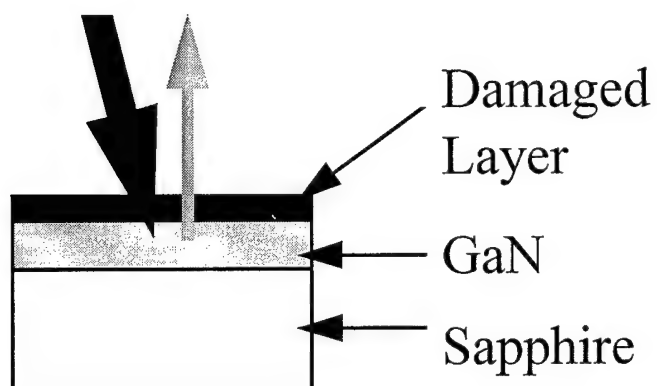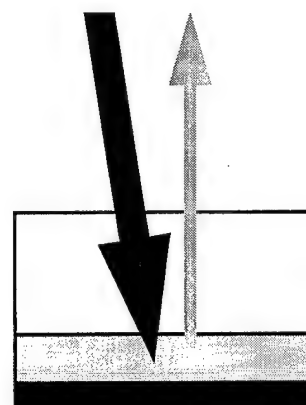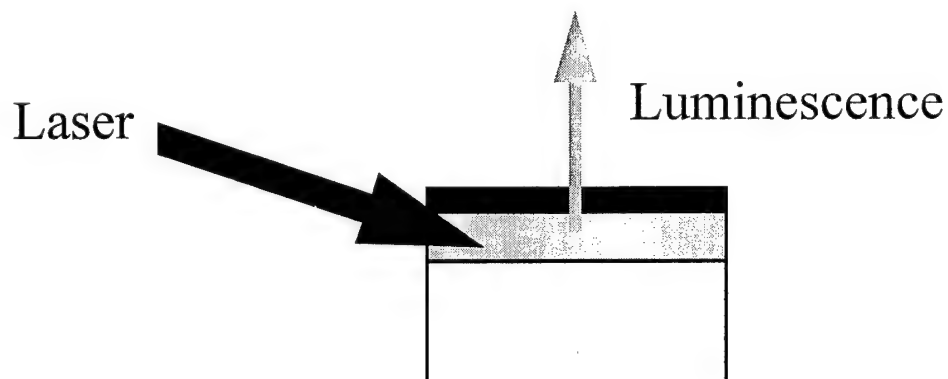
Luminescence

Figure 4-2. Three configurations used for illumination of samples in photoluminescence.

Griot 01LQD025 UV grade fused silica lens with a focal length of 300 mm and a diameter of 50 mm was chosen since it has an f/# of exactly f/6.0. The collection lens used was a Melles Griot 01LQD013 UV grade fused silica with a 100 mm focal length and a 50 mm diameter. The diameter was chosen to match that of the focusing lens for minimal light loss. The focal length was convenient since it allowed the sample to be placed at the focus of the lens but still gave sufficient space between the lens and cryostat housing for adjusting alignment.

Before light entered the spectrometer, a 345 nm long pass (LP) filter was often used for UV/visible measurements or an 850 nm or 1000 nm LP filter was used for IR measurements. This filter insured that no emissions from the laser entered the spectrometer by allowing only light with wavelengths longer than the LP wavelength to pass. Laser radiation can result in damage to the sensitive detectors used. Damage can occur even when the spectrometer is not tuned to the laser wavelength because higher order diffractions of the laser lines will appear at integer multiples of the primary wavelength. These higher order diffractions also have the undesirable effect of masking the true spectrum. For example, if the 345 nm LP filter were not used with the FReD laser, an intense second order feature would occur at 514.4 nm.

To disperse the luminescence signal from the samples, a SPEX 750M spectrometer was used. This spectrometer contained a 1200 gr/mm grating blazed for optimal signal at 500 nm when used for UV/visible luminescence detection and a grating

blazed for 1200 nm for IR detection. The focal length of this instrument is 0.750 m, and a resolution of 0.2 Å at 7000 Å was possible. The spectrometer was controlled by the SPEX MSD2 and SPEX DM3000. The entire setup was controlled by a personal computer (PC). The entrance and exit slit widths were adjustable using the micrometers provided from a minimum of 3 μm to a maximum of 3 mm. Typical operating widths were 100-1000 μm. The entrance slit height was also adjustable to the following settings "open", "2", "1", "0.2", "lowest dot", "middle dot", and "highest dot". The typical settings used were "0.2", "lowest dot", or fully open.

A Burle C31034A GaAs photomultiplier tube (PMT) was used to collect the light output from the spectrometer exit slit for UV/visible detection. This tube was chosen because of its near constant responsivity over the wide wavelength range of 300 nm to 850 nm. The typical operating bias used was −1400 V and was provided by the DM3000 unit. A Products for Research TE176TSRF Refrigerated Chamber PMT housing and power supply were used to keep the tube cool and reduce the dark current to a low value. Temperature control was accomplished by opening a valve from a pressurized liquid nitrogen dewar allowing the cold liquid to flow to the PMT housing. Typical operating temperatures were -20 to -40 °C.

The PMT signal was a current generated at the anode of the device. This current was then either input into the DM3000 directly using the DM303 current acquisition module or input into a lock-in amplifier. In the latter case, the voltage output of the lock-in amplifier was then input into the DM300 with the DM303M voltage acquisition

module. The use of a lock-in amplifier afforded the ability to chop the laser excitation source with a Stanford Research SR540 chopper and controller. Chopping the excitation and using a Stanford Research SR530 or SR830 lock-in amplifier allowed for the rejection of background signal such as that due to room lights. One drawback of using the lock-in amplifier was the limited dynamic range of the output. The lock-in used produced a 0-10 V output, however the DM3000 did not have this limitation. The DM3000 could register outputs from 1 cps up to 1.4×10^6 cps.

For PL measurements in the IR, from 0.8 to 1.7 μm, an Allied Detector Corp. 403 series germanium (Ge) detector was used in place of the PMT. This was powered by a North Coast Scientific Bias Supply model 823A. Since these detectors are susceptible to muon radiation due to cosmic rays, a North Coast Scientific Muon Filter model 829B was also used.

Since the luminescence originating at the laser spot differed from that originating at points away from the laser spot (as will be discussed below), great care was taken to insure only luminescence originating at the laser spot on the sample was recorded. The image of the sample was observed on the entrance port of the spectrometer to insure the alignment of this spot was achieved. Furthermore, the slit width and height were selected so as to insure that no stray light entered the spectrometer.

Calibration of the spectrometers was accomplished through the use of gas discharge calibration lamps with known spectral lines. Typically, a neon lamp was used since this offered convenient, narrow spectral lines in the near-UV. A krypton lamp was

used for IR calibration. Linear regression was found to adequately represent the shift in spectrometer peak reading compared to the actual peak positions. Once the spectrometer was calibrated, it was found that the calibration remained virtually unchanged (± 0.5 Å) unless the system was modified. Calibrations were taken on an occasional basis to verify their accuracy.

For the purposes of this study, determining the absolute magnitude of spectral features was not necessary. However, relative comparisons of spectral intensity for a given spectral feature were necessary. In this case, accurate comparisons at a given wavelength were possible with careful experimental procedure. To compare relative intensities of different peaks at different wavelengths within a given spectrum, the system response function must be considered. First, the response of the C31034 PMT was tested as a function of input signal intensity. This was done by setting the spectrometer to 7000 Å and recording the signal strength from a blackbody source at 1000 °C. A series of neutral density filters were used to reduce the amount of signal reaching the detector by a known amount. The PMT showed a near linear response over three orders of magnitude in intensity as shown in Figure 4-3. The line shown is a fit to the data which was forced to go through zero as there was zero recorded dark count from the PMT.

Next, spectra were taken with an Electro-Optical Industries WS143 simulated blackbody powered by a 215B controller. The blackbody was specified to have an emissivity of 0.99 ± 0.01 and was operated at its maximum temperature of 1273 K (1000

°C). The photon spectral radiance for a perfect blackbody was calculated using the Planck radiation law (Boyd, 1983:55)

$$L_p(\lambda, T) = \frac{2c}{\lambda^4} \left(\frac{1}{\exp\left(\frac{hc}{kT\lambda}\right) - 1} \right) , \qquad (4\text{-}1)$$

where L_p is the photon spectral radiance in photons/s/m^2/sr/m, λ is the wavelength, T is the temperature in K, c is the speed of light, h is Planck's constant, and k is Boltzmann's
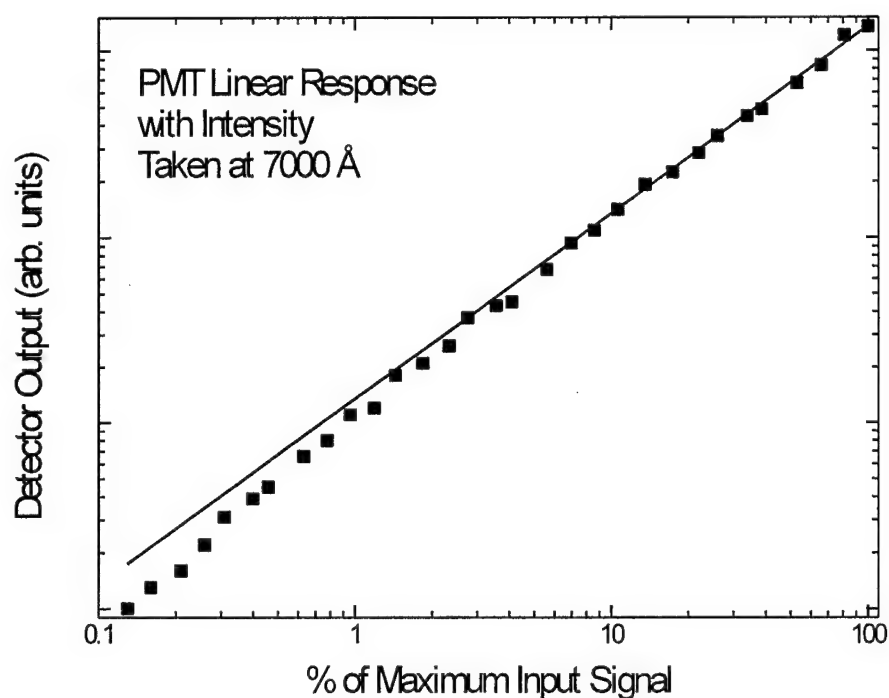
Figure 4-3. Photomultiplier tube response as a function of input light intensity for light of 7000 Å wavelength.

constant. Since only the relative response within the range of interest, 350-700 nm, was important, the theoretical curve was normalized for fitting as shown in Figure 4-4. The measured spectrum showed a steep roll off above 850 nm where the PMT response was poor. At the low wavelength end of the spectrum, the PMT signal approached a constant value which does not follow the blackbody spectrum. The relative system response is a function which can be used to multiply a measured signal at each wavelength to give a
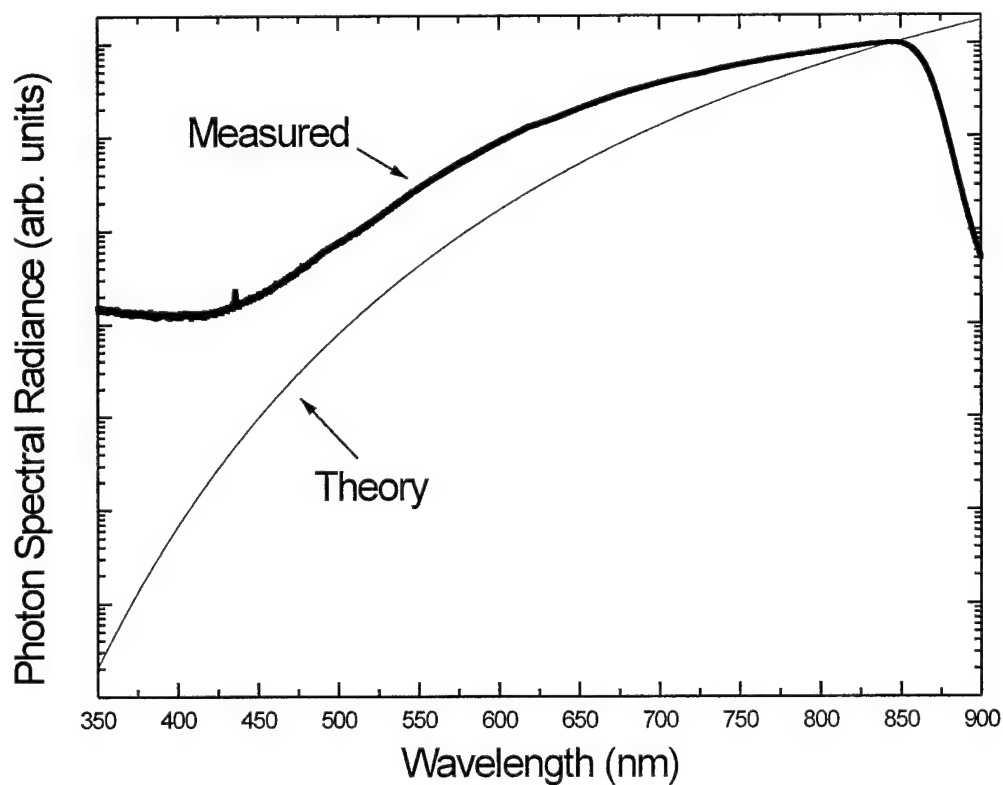
Figure 4-4. Measured blackbody spectrum for photoluminescence setup with photomultiplier tube.

SYSTEM RESPONSE CURVE
Measured with Black Body at 1273 K

Measured Response
Assuming a Perfect Blackbody

Log-Linear Fit to Response Function
in Region of Interest (350 - 700 nm)

(y-axis) System Response Function (arb. units)

(x-axis) Wavelength (nm)
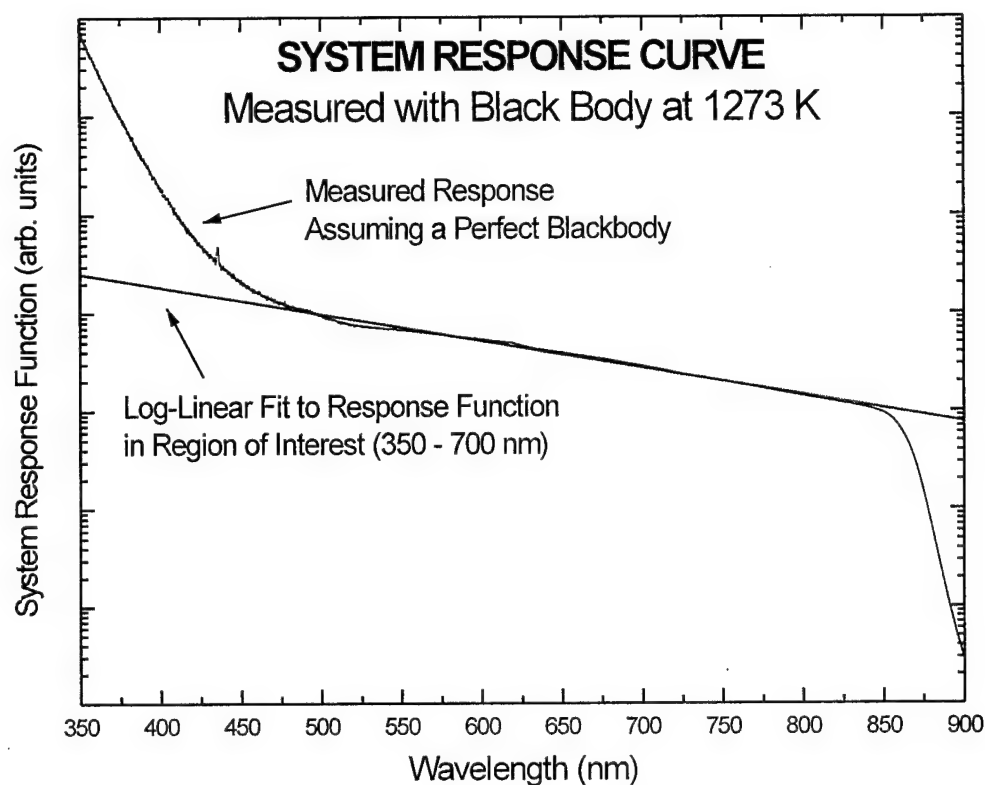
Figure 4-5. Calculated relative system response for photoluminescence setup with photomultiplier tube.

corrected signal. Thus to calculate the relative system response, the measured curve was divided by the normalized blackbody curve point-by-point. The relative system response calculated by this method is shown in Figure 4-5. The result is very similar to the specifications for the PMT response except at shorter wavelengths where the result suggests that the system response is several orders of magnitude larger at 350 nm than at 500 nm. However, since the simulated blackbody was not designed to operate at these short wavelengths, it is a near certainty that the simulated blackbody is not following Planck's law in this region. Therefore, since the system was expected to much more

4-14

closely follow the PMT response, the log-linear trend of the curve at 500 nm was taken to be the true system response. A log-linear fit was performed on the data so that the relative system response over the desired spectral region of 350 - 700 nm could be extracted. The measured result in arbitrary units was

$$R(\lambda) = 10^{-2.757 \times 10^6 \lambda}.$$

(4-2)

where R is the system response, and λ is the wavelength.

Some measurements required the attenuation of either the laser beam or the sample luminescence. For this purpose, a set of UV neutral density filters was used. These filters ranged from optical density (OD) 0.1 to 3.0 in increments of 0.1 OD. Before use, they were characterized in a spectrophotometer, and were found to be nearly constant in OD except for a slight dip in the UV. The measured OD curve was used whenever data obtained using the filters was analyzed.

Cathodoluminescence

The only major difference between the CL system and the PL were the sample chamber and excitation source. In order to propagate an electron beam to a sample, a vacuum environment is necessary. A large vacuum chamber was used for this purpose. The CL system setup is illustrated in Figure 4-6. The chamber contained ports on which
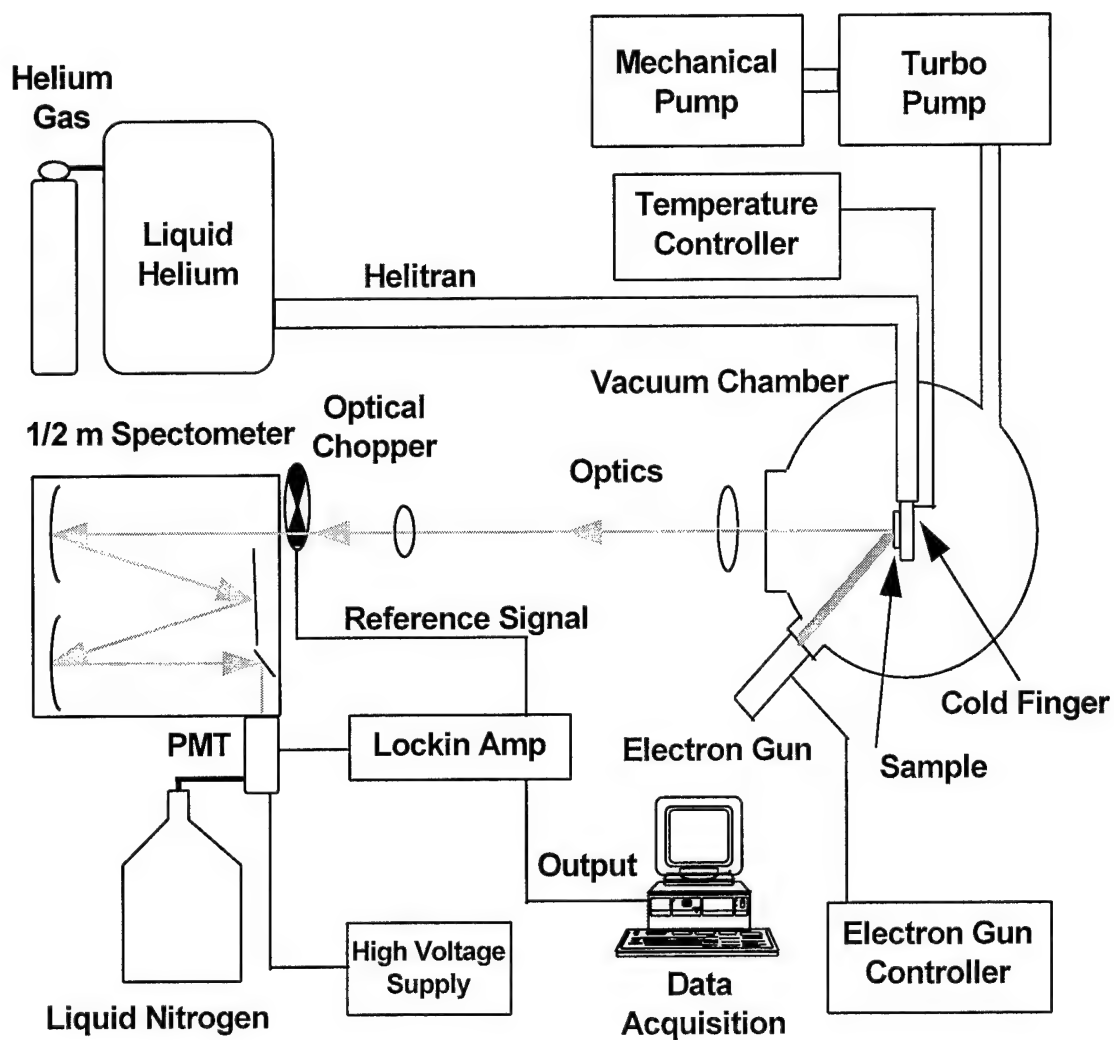
Figure 4-6. Low temperature cathodoluminescence setup.

were mounted the electron guns, a thermocouple vacuum gauge, and an ionization

vacuum gauge. The chamber contained a glass window through which the luminescence

was collected. The vacuum was provided by an Alcatel 5150 turbomolecular pump

backed by a 500 l/m Sargent-Welch Duo-Seal 1397 mechanical pump. After

approximately five hours, these pumps were able to attain the 10^{-7} torr vacuum necessary

for operation of the electron guns. The vacuum was monitored with a Teledyne-

Hastings-Raydist DV-6M thermocouple vacuum gauge, a Huntington IK-100 ionization

gauge, and JC Controls IG 4400 ionization gauge

Two electron guns were used during the course of this work. The first was a VG

Microtech LEG72 electron gun with power supply capable of up to a 2000 μA beam

current and 5 keV beam acceleration. The spot size was rated at a minimum of 60 μm at

5 keV and 1 μA. The second gun was a Kimball Physics EMG-14 electron gun with a

EGPS-14B power supply. This gun was capable of 10 nA to 100 μA beam current and

100 eV to 10 keV acceleration with a spot size of 1 mm to 25 mm. The Kimball Physics

gun also offered the advantage of a beam blanking feature allowing operation similar to

the effect of optically chopping a laser. To chop the beam, the gun synchronously steered

the beam into an internal beam dump by ramping a voltage across a set of internal

steering plates. The ramp signal and frequency were provided by a Wavetek model 23 12

MHz synthesized function generator. The output from the signal generator was used by

the Stanford SR830 DSP lock-in amplifier as the reference frequency. The lock-in was

then able to subtract the cathode glow and other background from the signal.

The sample holder for the system fit into the top port of the vacuum chamber, and

provided space for about four typical samples. However, at higher beam energies, the

limited steering ability of the electron beam often restricted the useful area of the sample

holder to one sample on the front and one on the back. Temperature was monitored with

a calibrated Si diode mounted on the front side of the sample holder within a centimeter of the actual sample position. Care was necessary in steering the electron beam so as not to damage this sensor. The sample holder also had a resistive heating element for temperature control above 10 K up to 300 K. A Lakeshore 330 temperature controller was used to read the output of the sensor and control the heater. Cooling power for the sample was provided by a helitran. The helitran flowed liquid helium (He) from a dewar onto the top of the cold finger (without entering the vacuum space). The helitran was capable of cooling the sample to about 10 K.

When the VG Microtech electron gun (which did not offer a beam blanking option) was used, in some cases, it was necessary to subtract from the data the signal due to the glow of the hot cathode. The hot cathode glow resembled the luminescence of an incandescent light bulb, and was very bright in the visible. In order to subtract this signal, it was necessary to take a second spectrum with the high voltage turned off and subtract this spectrum from the data. The data collection was nearly identical to that used for PL except that the spectrometer used was a 0.5 m SPEX 500M instead of a 0.75 m.

Relative Merits of PL and CL

Although the data obtained was quite similar in appearance, each technique offered certain advantages and disadvantages. The PL system used in this study could attain lower temperatures than the CL system (1.4 K vs. 10 K). In some materials, this could result in observing new peaks only discernible at the lowest temperatures.

Furthermore, the PL system's sample holder could accommodate more samples than the CL system's, and they could be changed out more quickly. PL also offered the ability to chop the optical excitation source with a mechanical chopper allowing the use of a lock-in amplifier for background noise subtraction. When the VG Microtech electron gun was used in the CL system, the only means to remove background signal (especially, that due to cathode glow) was by taking a spectrum with the high voltage turned off and subtracting it from the data. This technique was effective, however, it required twice the number of spectra. For these reasons, PL was used to characterize the majority of the samples.

One of the disadvantages of PL was the difficulties caused by plasma tube lines when the Ar ion laser was used in the UV. These lines could not be removed with optical chopping since they originated from the excitation source. Extensive measures were necessary to reduce the plasma tube emissions to a manageable level. However, these measures reduced the overall UV laser intensity significantly. Thus, the total excitation power available with PL was less than that available with CL. The CL system was capable of putting over 1 W of power directly on the sample, whereas PL power levels at the sample were typically in the 10's of mW with the Ar laser and 100 mW with the FReD laser.

A final consideration in choosing PL or CL is the physical difference in excitation mechanisms. PL involves absorption of photons, and CL involves the energy loss mechanisms of energetic electrons passing into the material. Photon absorption typically

manifests itself as an exponentially decreasing intensity as the beam passes into the solid. The penetration depth is determined by the material properties themselves, and the user can only control the total number of photons on the target (for a given fixed wavelength laser). In CL, however, the electrons lose energy by elastic and inelastic scattering events. Most of the energy loss for a monoenergetic beam occurred inside a pear-shaped excitation volume within the material (Yacobi and Holt, 1990:59). Thus, by controlling the accelerating voltage of the electron beam, the user can exercise a certain amount of penetration depth control. This ability can be important for looking at layered structures. Finally, the two absorption mechanisms may lead to different luminescence. That is, the absorption of a photon may lead to a different excited state within the sample than the excited state created by excitation due to electrons, the result of which could be different luminescence signals.

Damage due to the excitation must always be considered. In the case of photoluminescence, damage is minimal unless the laser beam is tightly focused. Although electron energies of up to 100 keV can often be used without inducing atomic displacement damage (Yacobi and Holt, 1990:55), CL can still cause damage which can be significant if the beam is focused on one spot for too long at too high an energy. The differential heating of the sample can cause physical changes such as localized annealing or even melting. In fact, low energy electron beam irradiation (LEEBI) was the first method discovered for obtaining p-type GaN:Mg (Amano *et al.* 1989b).

The measurement uncertainty in wavelength is mainly governed by the spectrometer and data collection systems. The diffraction grating has a resolution which is determined by the total number of rulings, N, the wavelength being diffracted, λ, and the order of the diffraction, m. Even a perfectly monochromatic source will be measured to have a linewidth given by (see for example Hecht, 1987:428)

$$\Delta\lambda_g = \frac{\lambda}{mN}.$$

(4-3)

Typically, the grating linewidth is small compared to the linewidth broadening caused by the slits. Above a certain minimum slit size (typically under 10 µm) at a given wavelength, an increased slit width will result in a better signal-to-noise ratio but will cause broadening of any spectral features. This slit linewidth is given by

$$\Delta\lambda_s = \frac{bd\cos\theta}{mfP},$$

(4-4)

where b is the slit width, d is the ruling spacing on the grating, θ is the diffraction angle, f is the focal length, and P = 1.002 is the plate factor which depends on the geometry of the

instrument (Instruments SA, 1988). The total instrument linewidth is the sum of these two contributions

$$\Delta\lambda_t = \Delta\lambda_g + \Delta\lambda_s. \tag{4-5}$$

Calculated values of instrument linewidth are shown in Figure 4-7 for several representative values of slit width for the SPEX 750M spectrometer with 500 nm blazed grating. To determine the actual instrument linewidth as a function of slit width, a neon gas discharge lamp was used. The FWHM of the 3447.7 Å line of neon was examined as a function of slit width. The results showed excellent agreement with the calculated values as shown in Figure 4-8. The 3447.7 Å line was chosen because it is relatively strong, and occurred in the spectral region in which the sharpest GaN lines are found.

The data collection software used allowed for the selection of the data point spacing. For most measurements, a data point spacing of between 0.2 and 1.0 Å was used. Therefore, the data sampling spacing placed an upper limit on the accuracy of determination of peak locations of this same size. Since the total instrument linewidth exceeded these values by a factor of from 2 to 50, this data spacing was deemed quite sufficient. The background dark count was kept to under a few hundred counts per second when using the PMT in the DM3000's photon counting mode by cooling the detector. However, electronic instrument noise was evident in all the spectra. To achieve the

necessary signal-to-noise ratio to clearly discern weak luminescence signals from the

implanted samples, the slit width was usually kept open to a standard 1 mm.
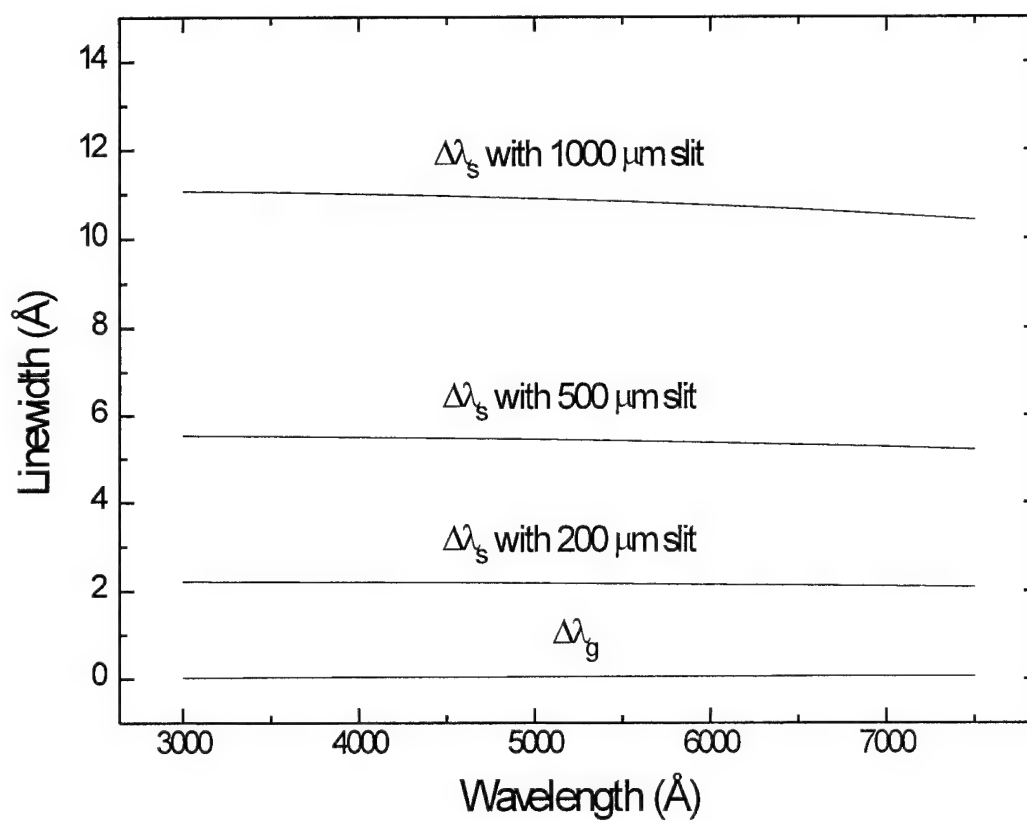
Figure 4-7. Calculated instrument broadening linewidths for the SPEX 750M spectrometer.
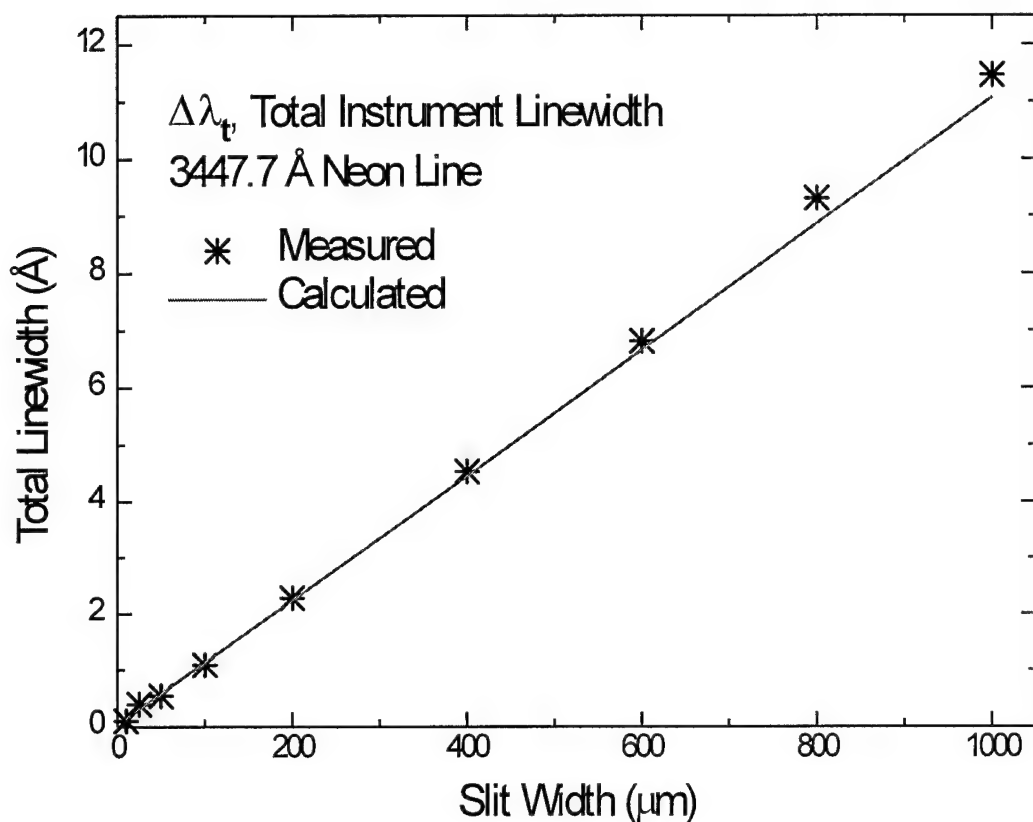
Figure 4-8. Total instrument linewidth for the SPEX 750M spectrometer with 500 nm blazed grating measured and calculated for the 3447.7 Å line of neon.

Optical Absorption

A Perkin-Elmer LAMBDA 19 UV/VIS spectrometer was used for optical absorption measurements. The spectrometer is a self-contained, PC controlled unit capable of scanning a range of 180-900 nm. The unit uses a double-beam, double-monochrometer to perform measurements along two optical paths and ratio them. Since

one path is ratioed against the other, a convenient background subtraction can be performed. The spectrometer uses a Deuterium lamp for UV measurements and a Tungsten-Halogen lamp for the visible. The internal detector is a side-window PMT. All measurements using this instrument were performed at room temperature.

The quantity measured by the spectrophotometer is transmittance, the ratio of transmitted intensity to incident intensity, $T = I_t/I_i$. Figure 4-9 shows a schematic illustration of light incident on a sample. Of the incident light that strikes the sample with intensity I_i, an intensity I_A is absorbed, an intensity I_S is scattered, and an intensity I_T is

$$I_a = I_A + I_S + I_R$$
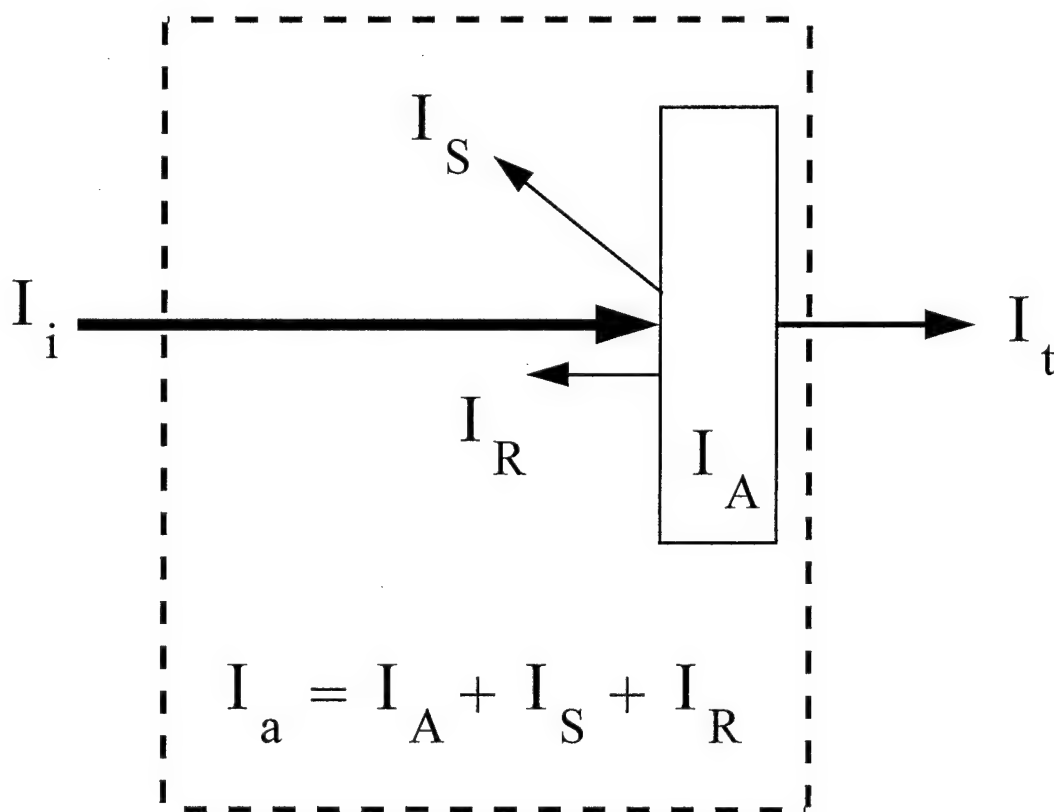
Figure 4-9. Optical absorption schematic showing light of intensity I_i incident on a sample, with intensities I_S scattered, I_A absorbed, I_R reflected, and I_t transmitted.

4-25

transmitted. The total quantity lost at the sample is I_a and the ratio $A = I_a/I_i$ is called absorptance. However, the quantity of most interest is the absorption coefficient of the material. The absorption coefficient, α, follows the well known relationship

$$I_t = I_i \exp(-\alpha L),\qquad(4\text{-}6)$$

where L is the physical pathlength through the absorbing layer. This equation assumes that the absorption coefficient is uniform throughout the depth of the sample. This relation can be rewritten with the substitution $T = I_t/I_i$ to give

$$\alpha L = \ln\left(\frac{1}{T}\right).\qquad(4\text{-}7)$$

Since the actual pathlength through the sample was difficult to measure, the implanted samples were not uniform in depth, and for the purposes of this study, only relative changes in absorption were required, no attempt was made to determine the numerical value of the absorption coefficient. Instead, the quantity αL measured in arbitrary units was used. This quantity has the benefit that it is directly measurable, and is related to the properties of the absorbing centers through a constant factor.

V. Results and Discussion

This chapter will present the experimental results. First, low temperature photoluminescence data will be presented for the as-grown GaN. Since this same material will be ion implanted, the as-grown data will provide a baseline for future comparison. In order to study the effects of annealing alone, as-grown GaN was annealed under conditions identical to the conditions used for ion-implanted GaN. This data will serve as a baseline for separating the effects of annealing for implantation. Another important consideration to ion-implantation of semiconductors is the effects of damage. The inert element argon was implanted to study the annealing of ion-implantation damage in GaN by observing the recovery of the original GaN properties. Next, the results for the various implanted species will be presented. Zinc-, carbon-, oxygen-, silicon-, beryllium-, magnesium-, neodymium-, and erbium-implanted GaN results will follow in sequence.

As-Grown GaN

The GaN samples implanted during the course of this study were obtained from three sources. MOCVD GaN grown on c-plane sapphire substrates were obtained from both APA Optics and Honeywell. Wright Laboratories provided MBE GaN grown on both c- and r-plane sapphire substrates. Each as-grown GaN host was characterized by low temperature PL or CL prior to implantation. This section will describe the results of those studies, and will serve as a baseline for comparison with the implantation studies to

follow. Since considerable low temperature luminescence studies have been performed in the past to explore the origin of the native GaN luminescence peaks, and this was not the focus of this work, detailed studies were not performed.

All samples were nominally undoped, although all exhibited varying degrees of n-type conductivity. Each GaN host exhibited slightly different PL spectra; however, in all cases, a familiar set of native GaN luminescence peaks was present. The most substantial differences did not occur within a sample set obtained from a given supplier, but between the sample sets obtained from different suppliers.

Figure 5-1 shows typical low temperature PL spectra of MOCVD grown GaN from APA Optics. The spectra of five different GaN samples are compared. All substrates showed a strong peak located at energies between 3.473 and 3.478 eV. The FWHM of this peak varied from 7 to 13 meV over the sample set. This peak has been attributed to the recombination of an exciton bound to a native donor (Dingle et al., 1971b). The identity of the donor remains uncertain; however, the nitrogen vacancy is the most likely candidate (Strite and Morkoc, 1992). Also present in these samples was a series of usually three distinct peaks having an approximately 90 meV energy spacing. The peak occurring at the highest energy, 3.27 eV, was also the most intense. These peaks have been identified as radiative transitions between shallow donors and shallow acceptors (Grimmeiss and Monemar, 1970). The shallow donor is usually assumed to be the same native donor responsible for the donor bound exciton peak. No consensus exists as to the origin of the shallow acceptor. The two distinct peaks at lower energy are the
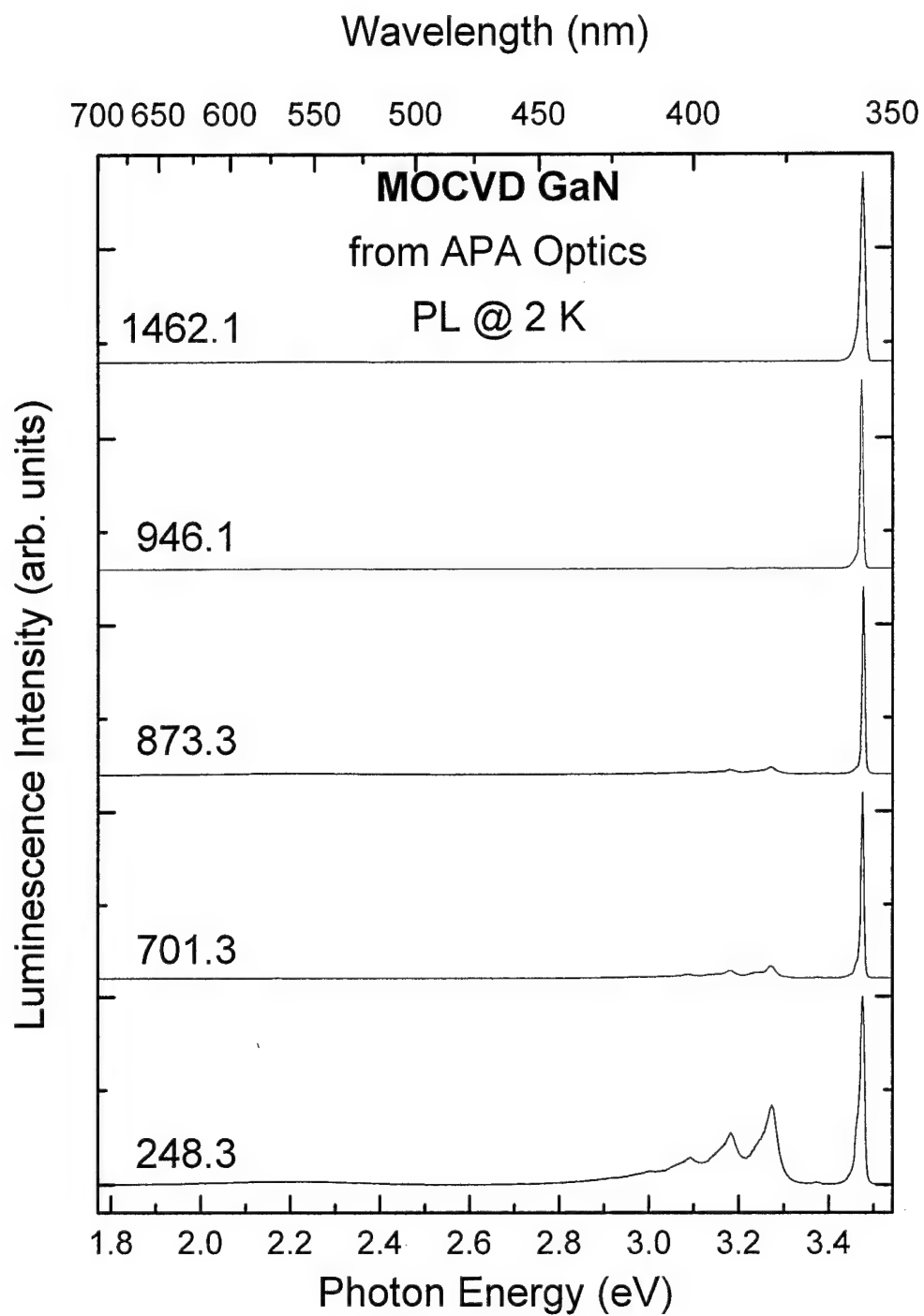
Figure 5-1. Photoluminescence taken at 2 K for several as-grown MOCVD GaN samples obtained from APA Optics.

one LO and two LO phonon replicas of the zero phonon line. Finally, a broad yellow peak centered at about 2.2 eV was always observed in MOCVD GaN from APA Optics. The FWHM of this peak was approximately 250 meV. This yellow peak has been attributed to carbon contamination during growth (Ogino and Aoki, 1980), deep defect levels (Shan *et al.*, 1995b), or a transition between a deep donor and shallow acceptor (Glaser *et al.*, 1995).

The relative intensities of these native GaN luminescence peaks varied considerably among the different samples. This result probably arose from varying amounts of native defects present in the samples due to slight differences in the grown environment. In all cases, the UV peak dominated the luminescence spectra. The D-A peak was of greater intensity than the yellow peak in several samples; however, the reverse was true in others.

The MOCVD grown GaN samples from Honeywell, although similar to the APA samples, showed some interesting differences. Figure 5-2 shows the low temperature PL spectra of one representative sample. The exciton peak was higher in energy than the peak observed for APA Optics samples, and was located at 3.493 eV. The average difference in energy between the UV peaks in Honeywell and APA Optics samples was 17 meV. This energy difference was substantially larger than the distribution in peak position observed within the APA Optics and Honeywell sample sets. The exciton peaks in each sample set were clearly of a different origin. The peak in the Honeywell samples has been identified as a radiative transition resulting from the recombination of a free
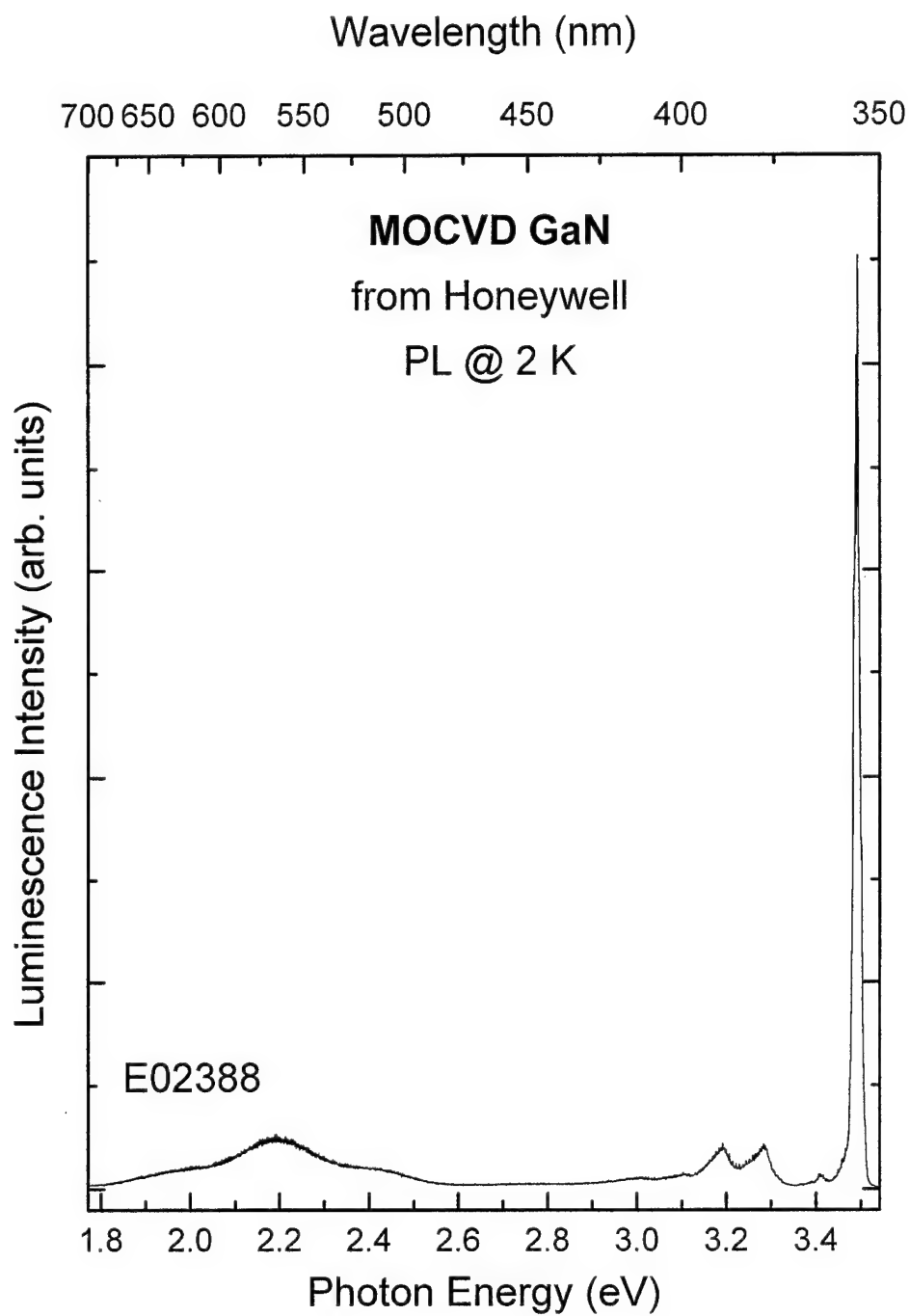
Figure 5-2. Photoluminescence taken at 2 K of a representative as-grown MOCVD GaN sample obtained from Honeywell.

exciton with the hole located in the upper Γ_7 valence band (Shan *et al.*, 1995a) as depicted in Figure 2-4. This peak was asymmetric, and showed evidence of a low energy shoulder. The shoulder was not resolvable from the main peak. Similar samples from Honeywell were reported to exhibit a free exciton to Γ_9 transition at 3.485 eV in photoreflectance (Shan *et al.*, 1995a). The shoulder observed in these samples was consistent with the occurrence of the free exciton to Γ_9 transition at 3.485 eV. An LO phonon replica of the exciton peak occurred at 3.410 eV. The difference between the exciton peak energy and LO replica energy was 83 meV. Thus, the 3.410 eV peak may be an LO replica of the free exciton to Γ_9 valence band transition at 3.485 eV since 3.485 - 0.091 = 3.410 eV.

The D-A peaks in the Honeywell samples also occurred at a slightly higher energy than observed in the APA Optics samples. The zero phonon D-A peak of the Honeywell samples was found at 3.28 eV. The one LO phonon replica of the D-A peak occurred at 3.192 eV, which made the energy spacing 91 meV. The yellow peak was similar to that observed in MOCVD GaN grown by APA Optics. The maximum occurred at about 2.19 eV, and the FWHM was approximately 250 meV. The relative intensities of the various peaks were also similar to those encountered in MOCVD GaN grown by APA Optics. The exciton peak always dominated the spectrum of the as-grown samples from Honeywell.

The gas-source MBE grown GaN samples obtained from Wright Laboratories exhibited significant differences as compared to both sets of MOCVD grown samples. Since these samples were grown by a unique gas-source MBE process, a more substantial

effort was made to supply the growers with information to aid in the development of the growth process. Unfortunately, due to a series of equipment failures at Wright Laboratories, only a few GaN samples became available for study. GaN samples grown on both c- and r-plane substrates were studied. Figure 5-3 shows the low temperature CL spectra of two GaN hosts grown on c-plane sapphire. The GaN labeled 009 x283 was grown at approximately twice the rate as the sample labeled 008 x282. Figure 5-4 shows the low temperature CL spectra of GaN grown on r-plane substrates. The sample numbers refer to the growth run, and since these samples were grown at the same time as the c-plane material, they have the same identifier. All MBE samples showed a deep yellow peak centered at about 2.15 eV with a FWHM of about 250 meV. This peak was very similar to the deep yellow peaks observed in MOCVD grown GaN except that it was centered at a slightly lower energy.

The UV peaks of these gas source MBE grown samples were significantly different from those recorded for MOCVD grown GaN. The peak locations and FWHM values measured at a sample temperature of 6 and 300 K are given in Table V-1. The peak at 3.424 eV was most likely oxygen related (Chung and Gershenzon, 1992). These samples were known to have significant oxygen present in the grown environment due to unintentional H_2O contamination in the NH_3 gas source.
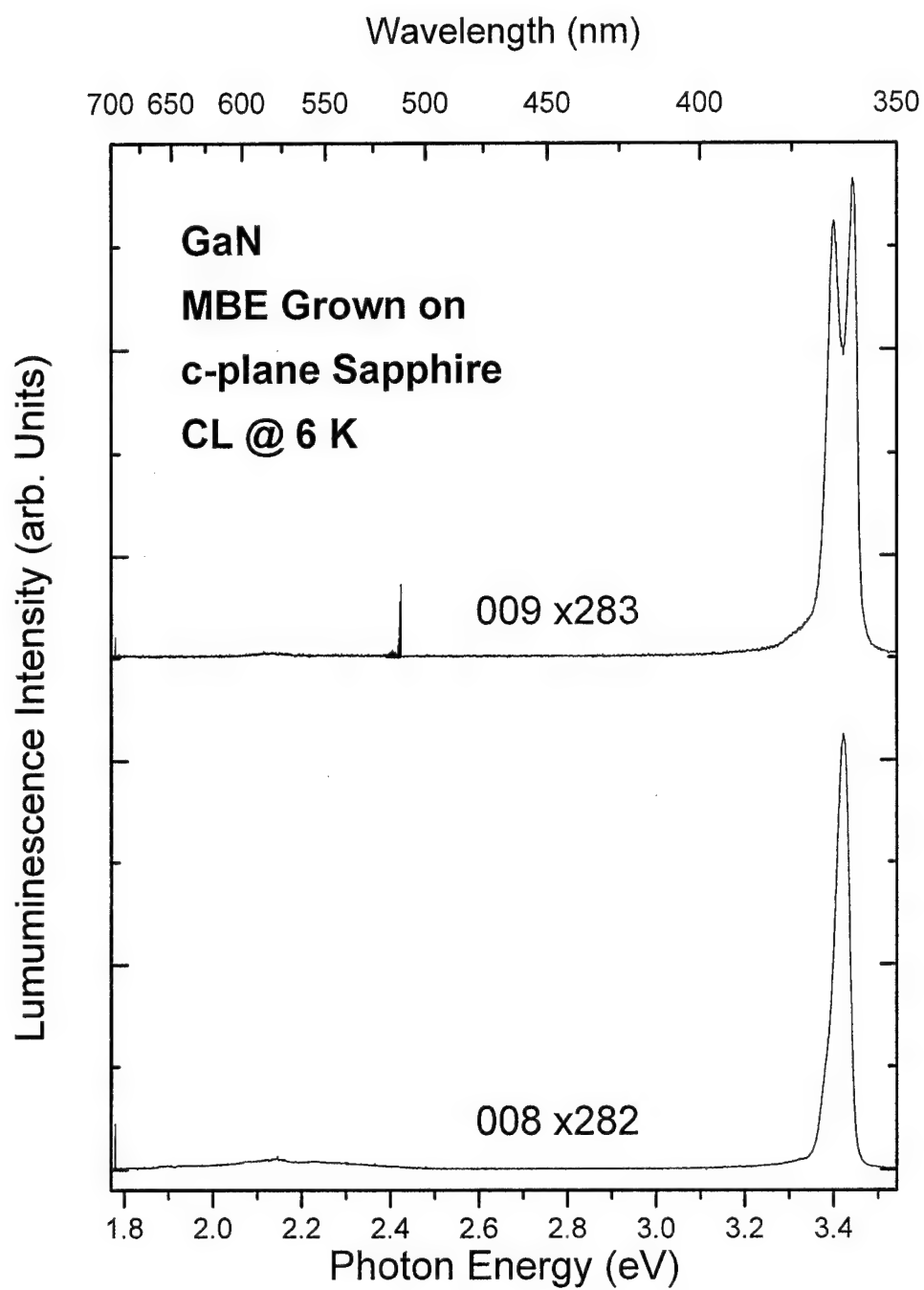
Figure 5-3. Cathodoluminescence taken at 6 K for two GaN samples grown by MBE on c-plane sapphire.
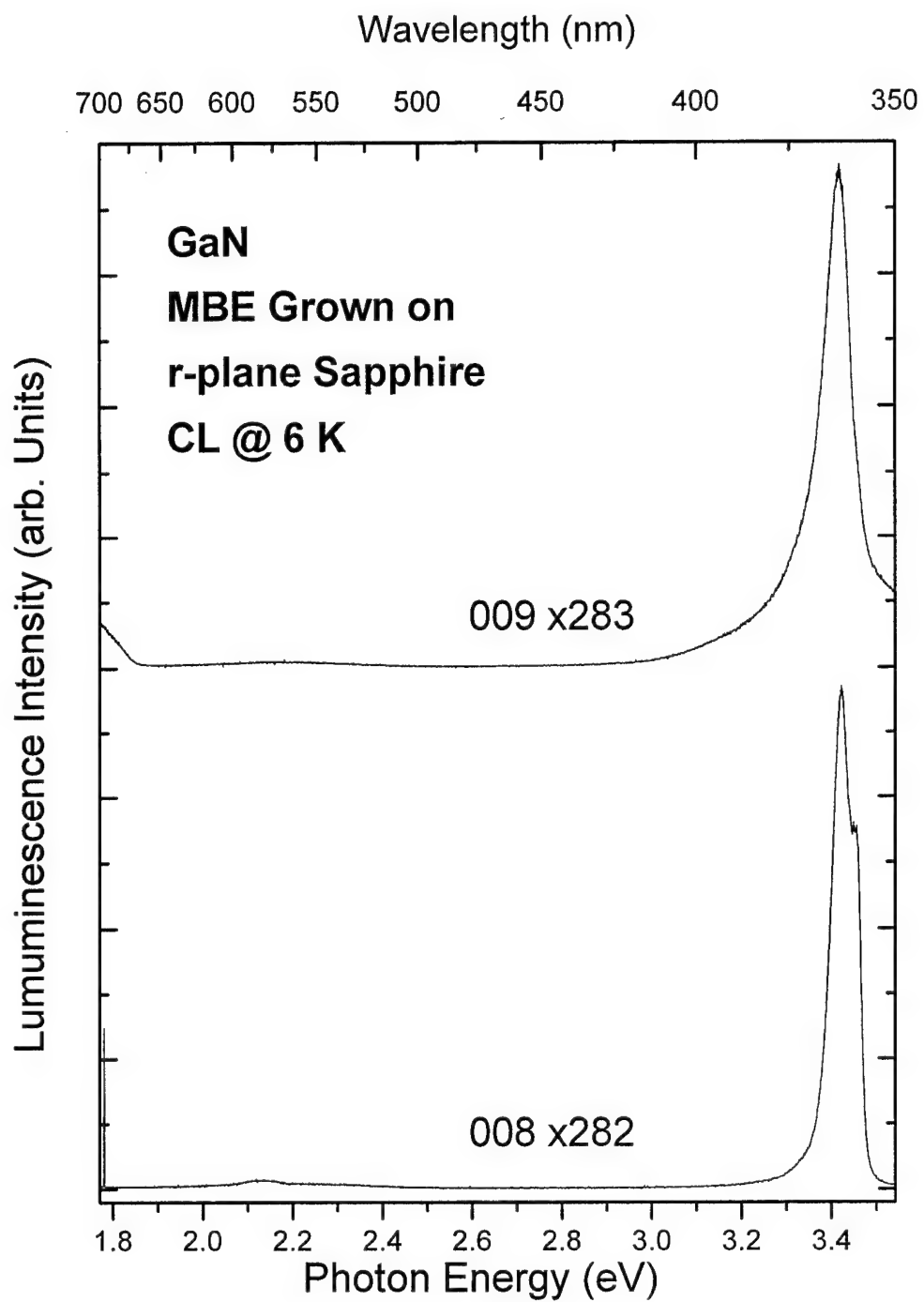
Figure 5-4. Cathodoluminescence taken at 6 K for two GaN samples grown by MBE on r-plane sapphire.

Table V-1. UV Peak Locations for MBE Grown GaN.

Sample ID	6 K		300 K	
	Energy (eV)	FWHM (meV)	Energy (eV)	FWHM (meV)
008 x282 c-plane	3.424	38	3.374	105
008 x282 r-plane	3.423	68	3.391	118
009 x283 c-plane	3.448 / 3.402	76 (= 38 + 38)	3.379	92
009 x283 r-plane	3.417	77	3.374	241

CL spectra were also taken at a sample temperature of 300 K. The results are shown in Figures 5-5 and 5-6. A comparison of the CL spectra collected at sample temperatures of 6 and 300 K showed a red shift as was expected. The shift was 50, 32, 69/23, and 43 meV for the c-plane 008 x282, c-plane 009 x283, r-plane 008 x282, and r-plane 009 x283 samples, respectively. These shifts were less than the expected shift of the bandgap over this temperature range which should have been approximately 110 meV. The peaks also broadened considerably and decreased in intensity. The low temperature CL double peak found for the c-plane GaN 009 x283 sample was replaced by a single peak at room temperature. A temperature dependent study was performed on the r-plane 009 x283 GaN sample. The spectra shown in Figure 5-7 revealed a decrease in the overall intensity of the peaks as temperature was increased. Furthermore, the lower energy peak gained in relative intensity as compared to the higher energy peak as temperature was increased. Finally, the peaks merged to become a single broad luminescence feature. The broad nature of these peaks and the likely high concentration
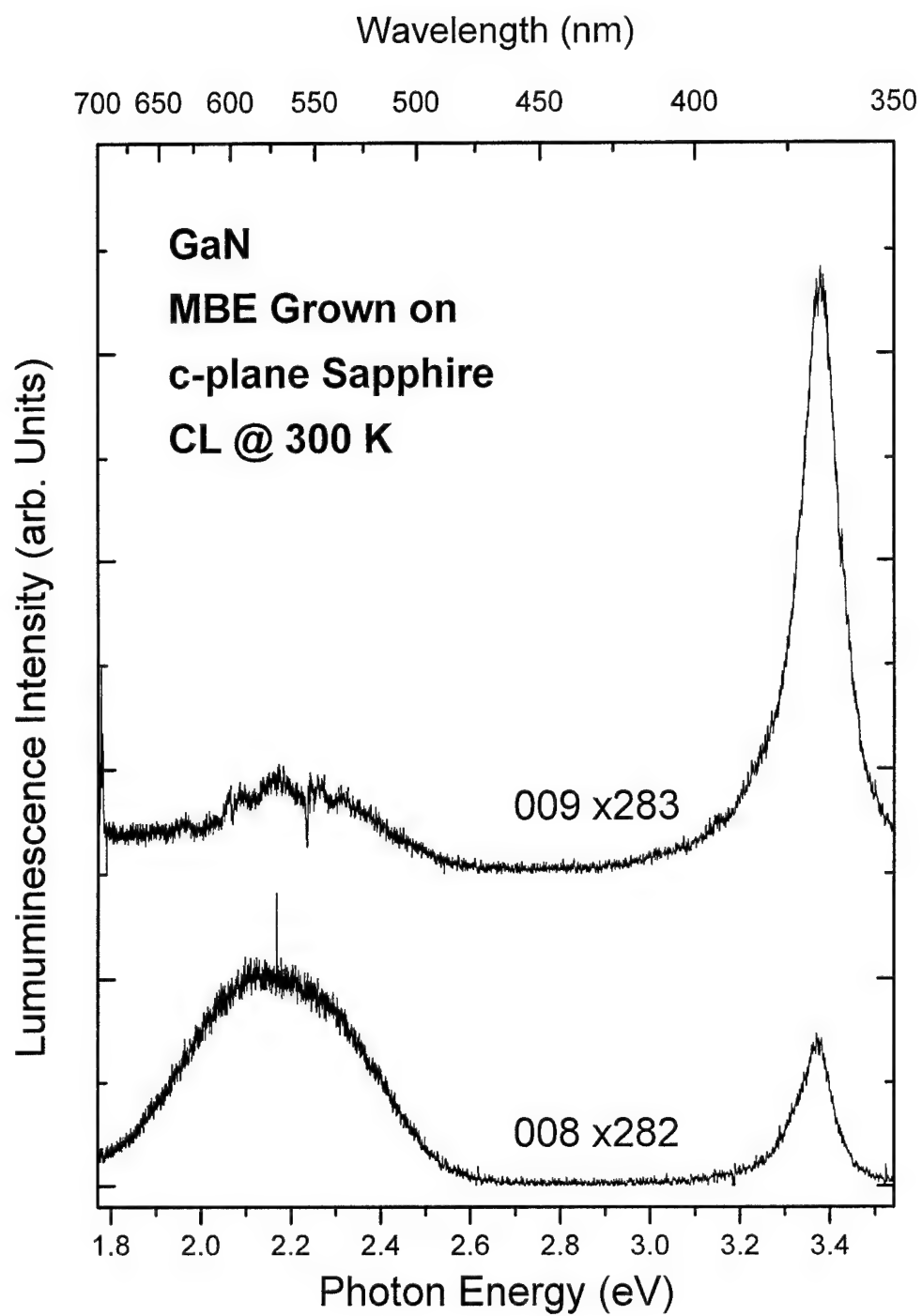
Figure 5-5. Cathodoluminescence taken at 300 K for two GaN samples grown by MBE on c-plane sapphire.
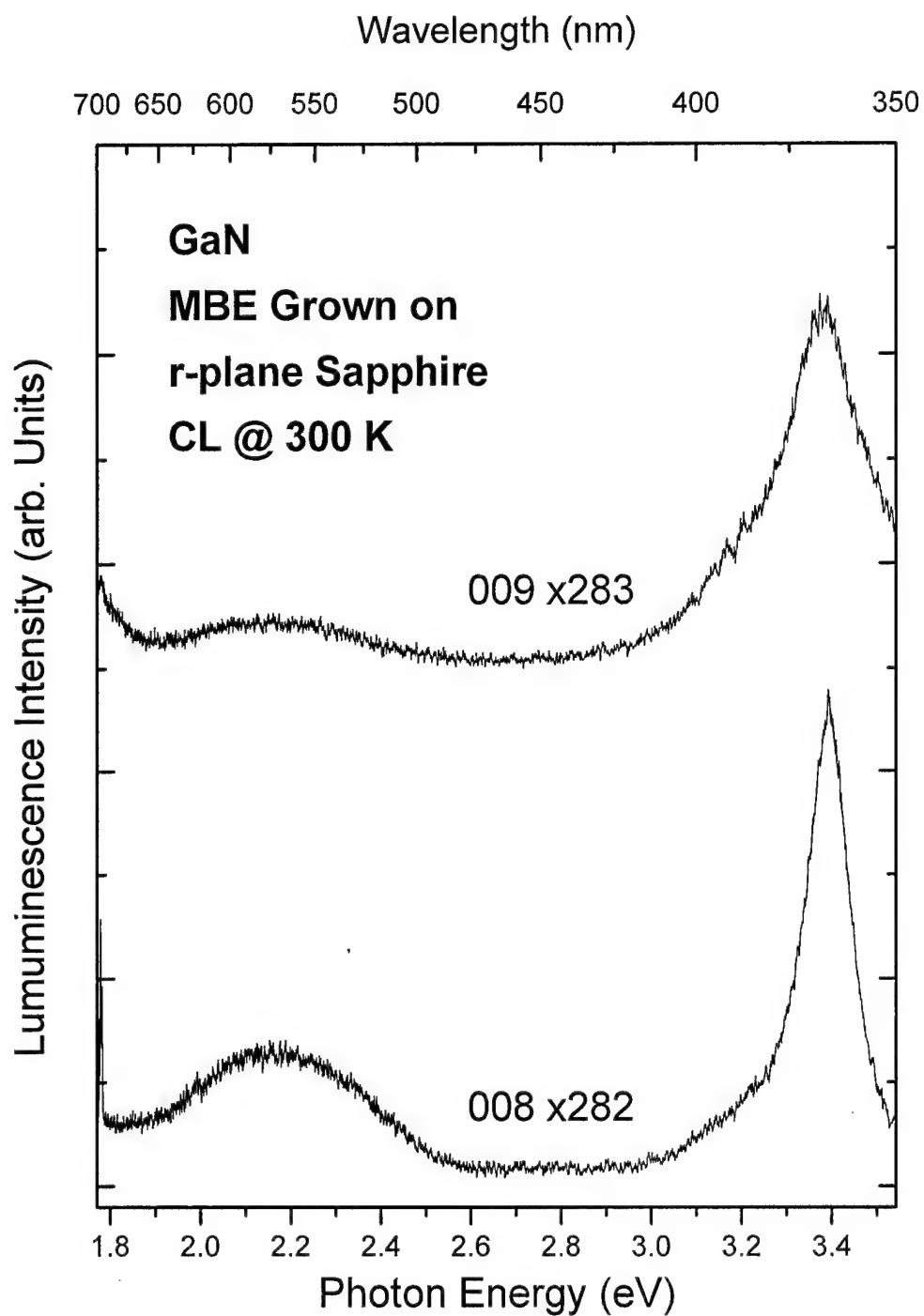
Figure 5-6. Cathodoluminescence taken at 300 K for two GaN samples grown by MBE on r-plane sapphire.
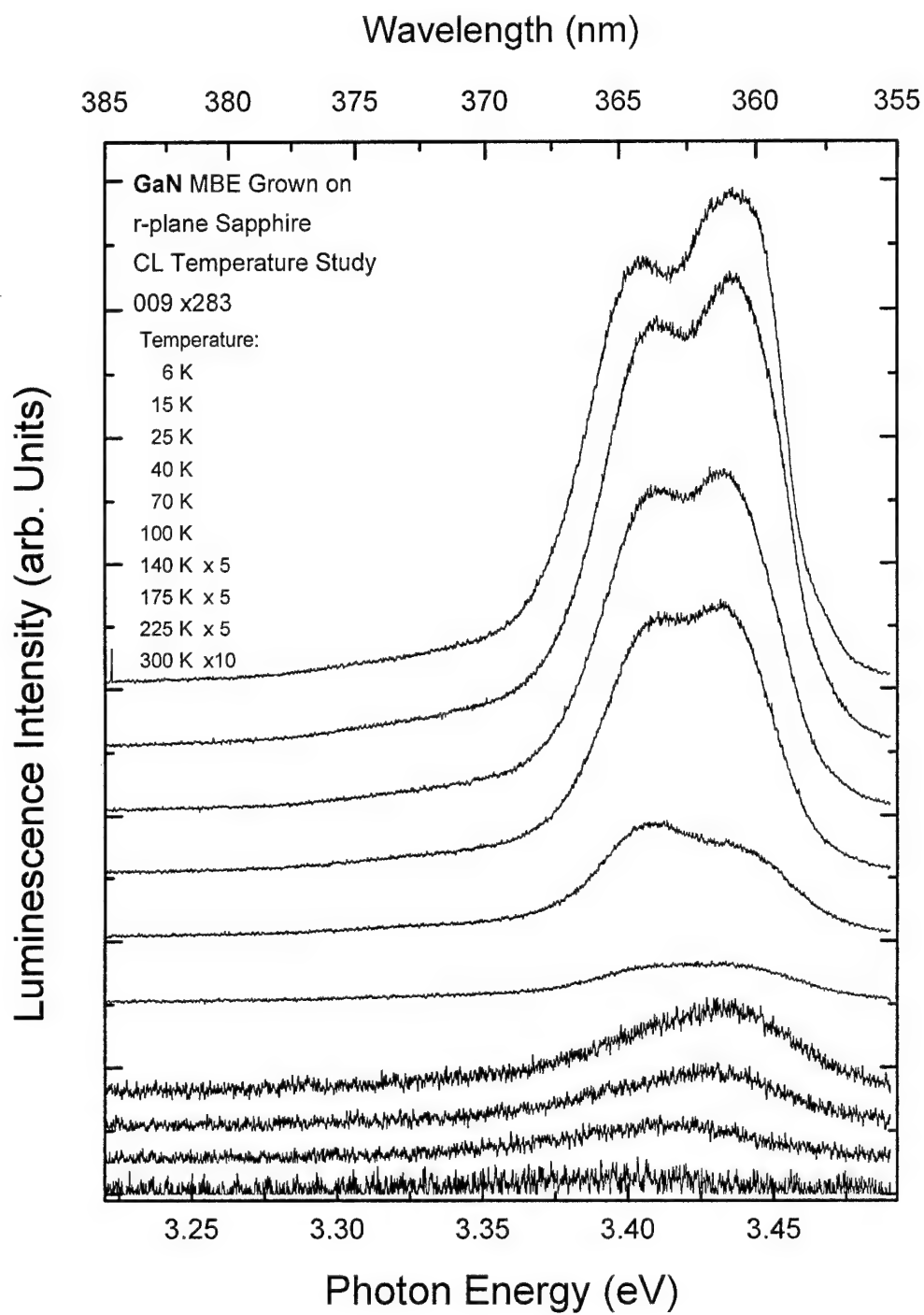
Figure 5-7. Photoluminescence taken at various temperatures for MBE GaN sample 009 x283 grown on r-plane sapphire.

of oxygen, which is a known donor in GaN, suggested the formation of a donor band. As temperature was increased, the impurity band merged with the conduction band resulting in the broad single peak. The D-A band was not present as a distinct spectral feature in the MBE grown samples. The D-A band may have been quenched by the formation of the donor impurity band.

In summary, three different sources of wurtzite phase GaN were characterized. The MOCVD grown samples obtained from APA Optics and Honeywell showed many similarities. The yellow band and D-A band were present, and quite similar in energetic locations and FWHMs in both sample sets. The UV peaks showed the only real differences between these sample sets. The UV peak of the Honeywell samples was identified as resulting from the recombination of an exciton bound to a native donor, whereas the UV peak of the APA Optics samples was identified as resulting from the recombination of a free exciton with the hole located in the upper Γ_7 valence band. This difference indicated a slightly higher level of native defects in the APA Optics samples. The MBE grown samples obtained from Wright Laboratories were significantly different from both sets of MOCVD grown samples. These samples had no discernible D-A peaks and the yellow band occurred at lower energy. The UV peaks occurred at lower energy and with larger FWHM than those observed for the MOCVD grown samples. The UV peaks in the MBE grown GaN were identified as oxygen related. The presence of high contamination levels in these samples can be expected to interfere with the activation of implanted species.

In order to understand the effects caused by annealing alone, a series of un-implanted samples were annealed under conditions identical to those used for implanted samples. One set of samples was furnace annealed in flowing NH_3 gas, and another set was annealed in flowing N_2 gas. Both absorption and PL measurements were performed on these samples. Since these samples were never implanted, all changes observed were the direct result of thermal annealing.

PL was performed by illuminating the samples from the GaN surface with the FReD laser operating at a power level of 150 mW. Slit widths were kept at 1 mm and the '0.2' slit height setting was used. Although narrower slit widths could have been used, these settings were selected to be identical to those used with the implanted samples, thus allowing direct comparisons of the spectra. Since the signal strength was large, well characterized neutral density filters were necessary for most spectra.

The PL studies of these un-implanted, annealed samples were performed by aligning the samples in a vertical arraignment on the sample holder. To examine a different sample, the sample holder could be moved either up or down without rotation. This arrangement allowed only minimal adjustment of the optics to maximize the PL signal on the exciton line. The signal was always maximized on the exciton line to insure that errors due to misalignment would not compromise relative intensity comparisons.

First, the NH_3 anneals will be examined. The spectra displayed in Figure 5-8 showed no shifts in peak locations nor any new luminescence peaks, but did show

Figure 5-8. Photoluminescence spectra taken at 2 K for as-grown GaN annealed at various temperatures in an NH₃ Environment.

dramatic changes in relative peak heights. The D-A band showed the most dramatic, systematic change. This band increased in intensity with annealing temperature until the 1050 °C anneal.

Figure 5-9 shows the ratio of the individual peak intensity for each peak of the NH_3 annealed samples divided by against the intensity of the corresponding peak in the un-annealed sample. The un-annealed sample's exciton peak intensity ranged from 1.3 to 3.3 times greater than that of each annealed sample's exciton peaks. Although the exciton peak intensity of all annealed samples was lower than that of the un-annealed sample's peak intensity, there was a slight upward trend in peak intensity with annealing temperature. Again, the 1050 °C anneal showed a drop in intensity as compared to the 1000 °C anneal.

The yellow band varied in intensity from 0.96 to 1.46 times the intensity of the un-annealed sample's yellow peak intensity. A weakly increasing trend may have been present as annealing temperature was increased. Furthermore, a curious change in the etalon interference fringes of the yellow peak was observed for the 1000 and 1050 °C anneals. Below an annealing temperature of 900 °C, the yellow peak has widely spaced etalon peaks. The 1000 and 1050 °C anneals have much more closely spaced peaks. The spacing of the etalon peaks should be inversely proportional to the index of refraction. As damage was created within the surface layer during annealing of the 1000 and 1050 °C annealed samples, the index of refraction was likely to have increased (see
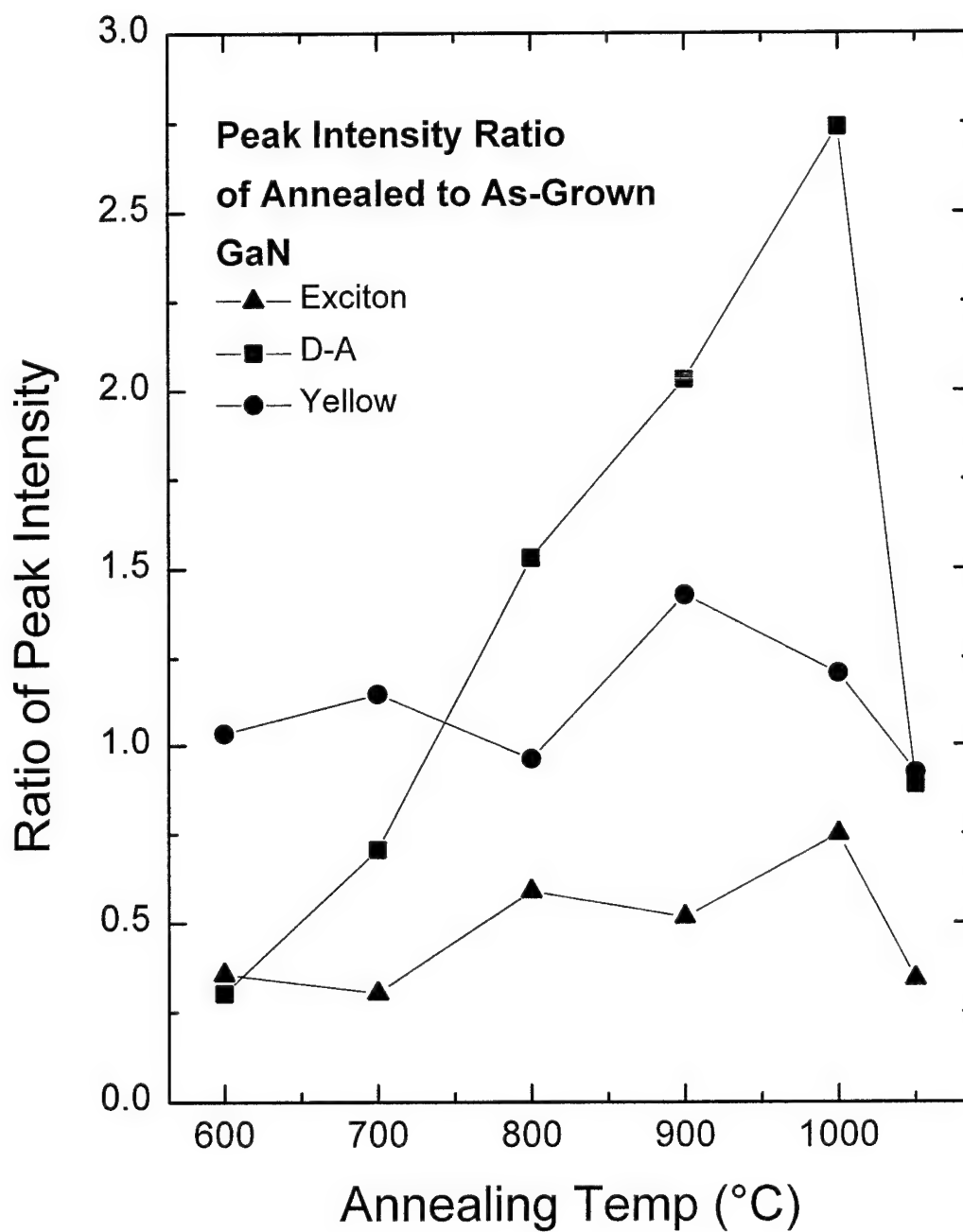
Figure 5-9. NH$_3$ annealed, as-grown GaN peak intensity changes with annealing temperature normalized against as-grown values.

Hunsperger, 1991:54 for reference to this effect in other semiconductors) and thus the spacing of the etalon peaks decreased.

The overall intensity of the 1050 °C anneal was low and there was evident surface degradation. The surface of this sample no longer had a clear, mirror like face as was observed for all samples annealed below 1050 °C, but instead had a milky white appearance. Since the 1050 °C anneal showed visible surface damage, the decrease in overall luminescence intensity can be attributed to increased laser energy absorption at the surface with subsequent non-radiative decay within the damaged layer.

Room temperature absorption measurements were taken below the bandedge to examine the effects of implantation and annealing. No distinct absorption features were found below the bandedge of as-grown or implanted samples. Figure 5-10 shows the full spectra plotted as $Ln(\alpha L)$, where α is the absorption coefficient and L is the sample thickness. The spectra have been displaced vertically for clarity. The repeating structure of peaks resulted from an etalon effect occurring between the smooth mirrorlike faces of the GaN/sapphire wafer. The spectra had a steep, nearly linear portion closest to the bandgap which tapered off to a nearly constant baseline well below the bandgap. The steep portion nearest the bandgap was indicative of bandtailing. At the lower energies, additional absorption phenomena may be occurring.

Below bandgap absorption can indicate perturbations of the bandedge caused by the random perturbations of defects. Figure 5-11 is a plot of the natural log of absorption as a function of photon energy near the bandedge for the NH_3 annealed samples. The as-
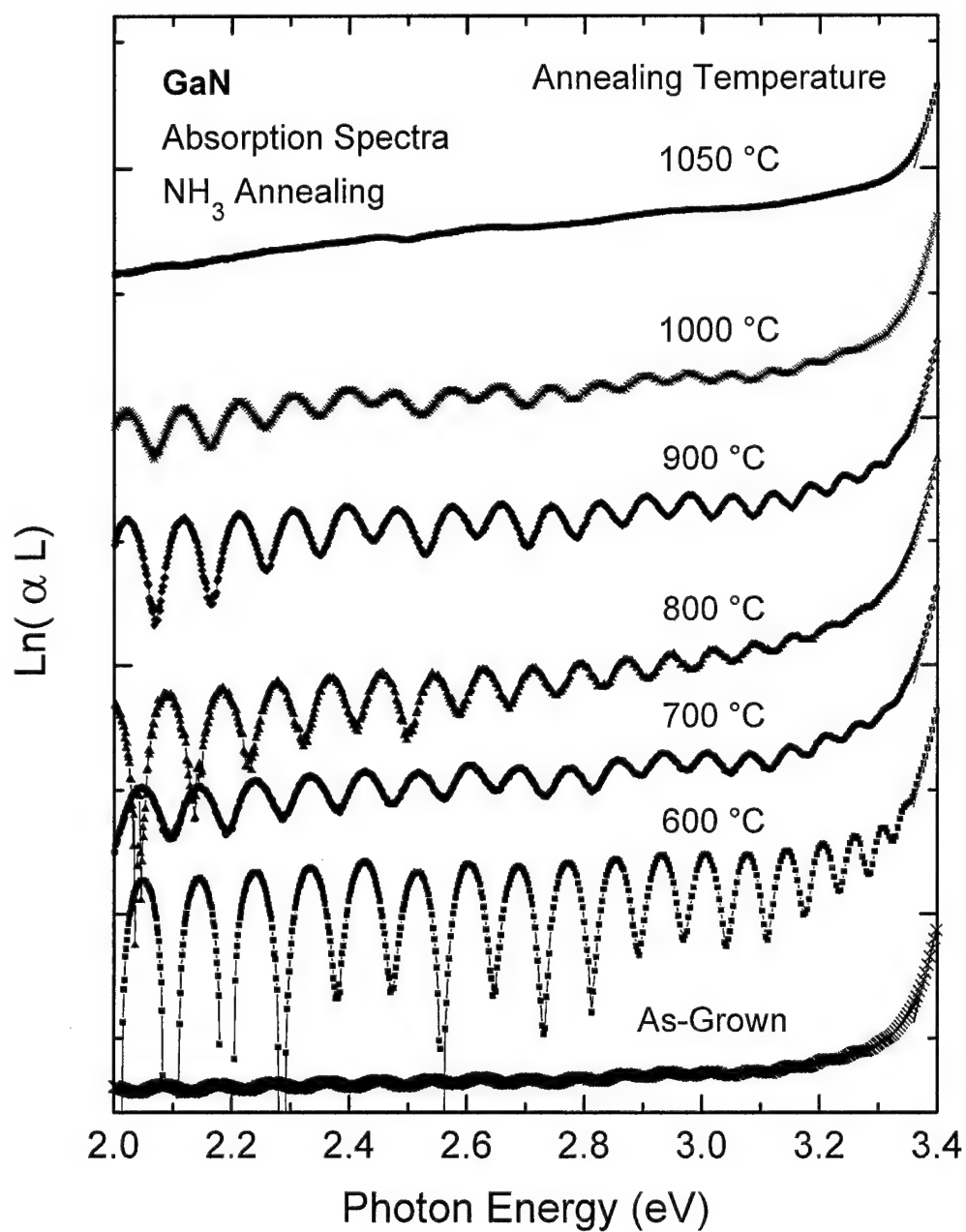
Figure 5-10. Room temperature absorption spectra of as-grown GaN annealed at various temperatures in NH_3.
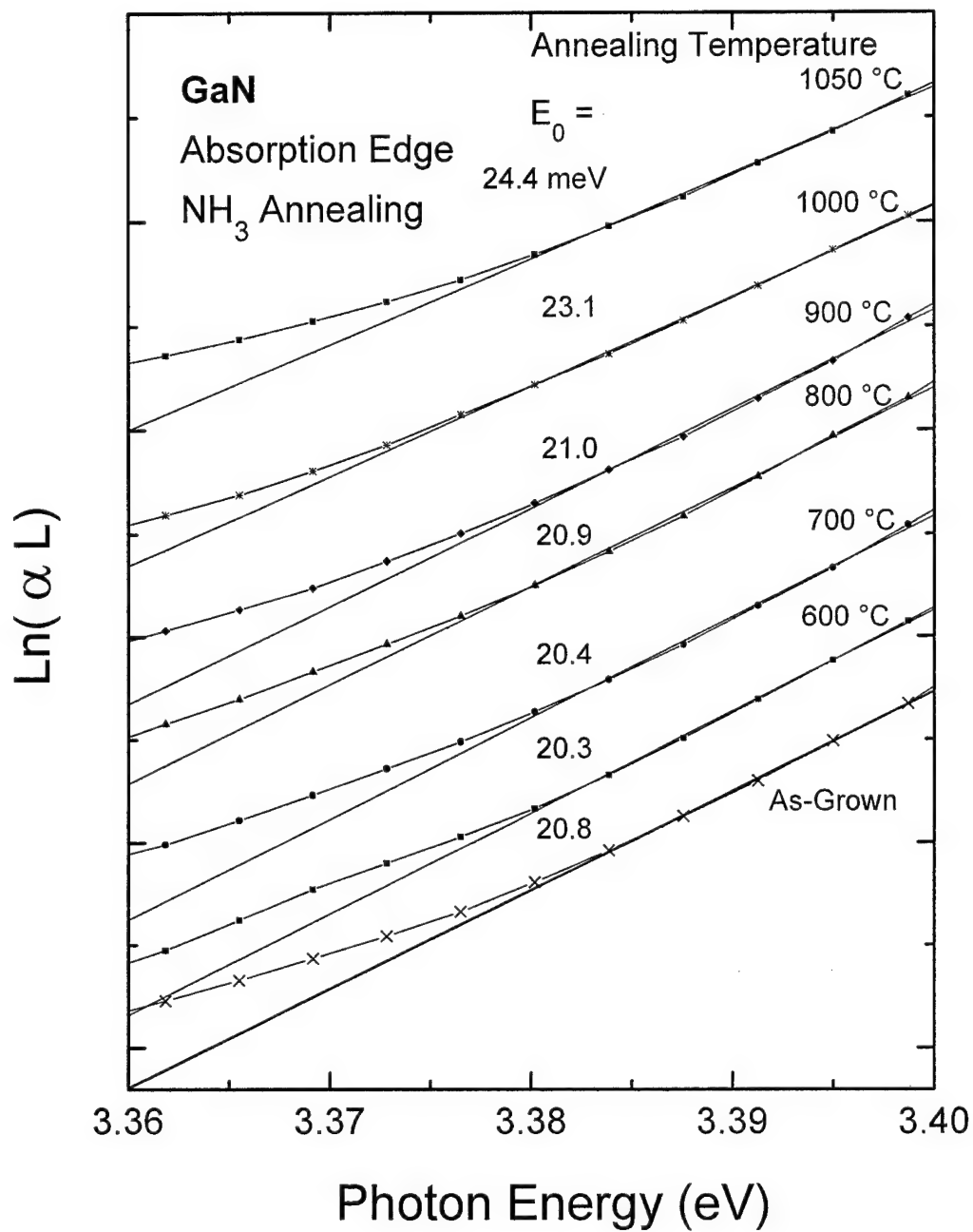
Figure 5-11. Room temperature absorption edge of as-grown GaN annealed at various temperatures in NH_3.

grown, un-implanted sample's room temperature absorption data showed slight absorption below the bandedge. A nearly linear relationship between $\ln \alpha L$ and photon energy just below E_g was found. The inverse slope of a linear fit gave an energy, E_0, of 20.8 meV. Following Pankove's treatment (1965), this value represents the 'length' of the exponential tail of states at the bandedge. A shallow tail in the density of states near the bandedge was expected at room temperature. This so-called Urbach tail (1953) has length $1/kT = 25$ meV at 300 K. Thus, this low value for E_0 demonstrated the high quality of the GaN used. Absorption measurements taken at the bandedge on the annealed samples show values of E_0 between 20 and 25 meV as seen if Figure 5-11. If the bandedges had tails due to perturbations, then an Urbach type thermal contribution would be expected. The observed values indicated that little band tailing other than the thermal contribution existed in the as-grown annealed samples. There was a slight upward trend in E_0 which may be an indication of a slight increase in band tailing resulting from higher temperature annealing.

A set of samples similar to the set annealed in NH_3 was prepared for the N_2 annealing study. Figure 5-12 shows low temperature photoluminescence spectra of an as-grown GaN sample and a sample from the same GaN wafer annealed at 800 °C for 120 min in N_2. Great care was taken to insure that the relative intensities of these spectra were directly comparable. As was the case for NH_3 annealing, samples of the same substrate annealed in N_2 also showed no shifts in peak locations nor any new PL peaks and a decrease in exciton peak intensity was observed. In this case, a factor of five drop
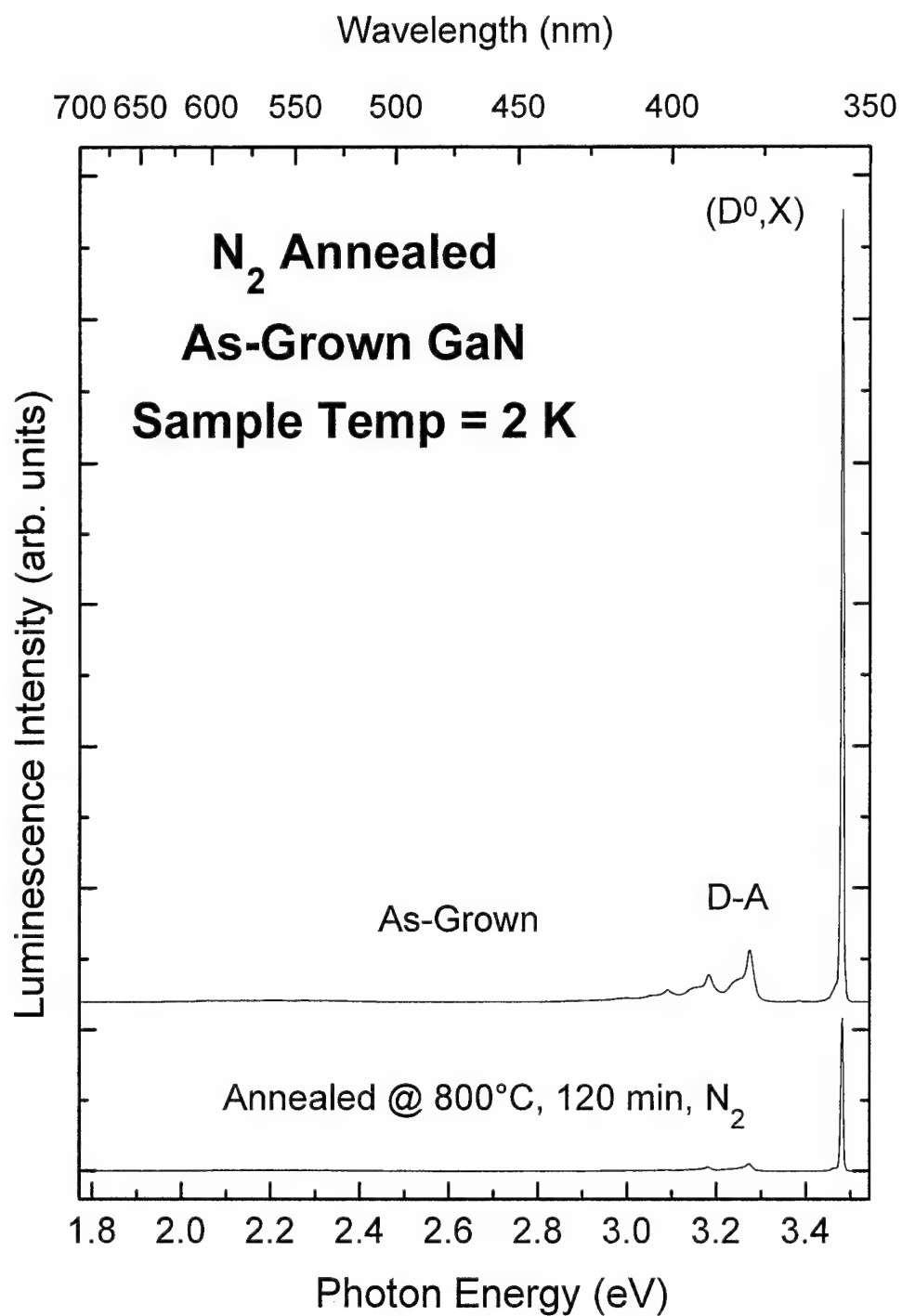
Figure 5-12. Photoluminescence spectra taken at 2 K for as-grown GaN and GaN annealed at 800 °C for 120 min in a N_2 environment.

in luminescence was observed. The exciton peak dominated the spectrum in all luminescence measurements of as-grown GaN annealed in N_2 at temperatures ranging from 700 to 1000 °C. Difficulty was encountered in measuring the absolute intensities of the exciton peaks for these samples due to unstable laser intensity during the measurements. However, all samples showed no new peaks and showed only minor shifts in relative peak intensity. Figure 5-13 shows the spectra which have been normalized on exciton peak intensity. Clearly, the D-A luminescence did not show any increase with annealing temperature in contrast to the case of NH_3 annealing.

The fact that there were no luminescence peak shifts for either NH_3 or N_2 annealing indicated that there were no new types of radiative centers being formed by annealing in NH_3 or N_2. However, since the relative intensity of the D-A peak was enhanced after high temperature NH_3 annealing, it is likely that the concentration of radiative centers involved in the D-A emissions has increased. Since no increase in D-A emissions was observed for N_2 annealing, this contrasting result must be related to the chemistry of the NH_3 gas at the GaN surface at elevated temperatures. It is known that NH_3 gas begins to dissociate at elevated temperatures, releasing H_2 gas. In the present study, H_2 gas was observed to be present during annealing by its characteristic burning when mixed with air upon opening the furnace tube. GaN decomposition attributed to the reaction $GaN + 3/2H_2 \rightarrow Ga + NH_3$ has been observed by other researchers to occur at temperatures as low as 400 °C when H_2 was present (Morimoto, 1974; Sun et al., 1994). Since excess Ga would be left at the surface as the H_2 gas escaped, an increase in V_N at

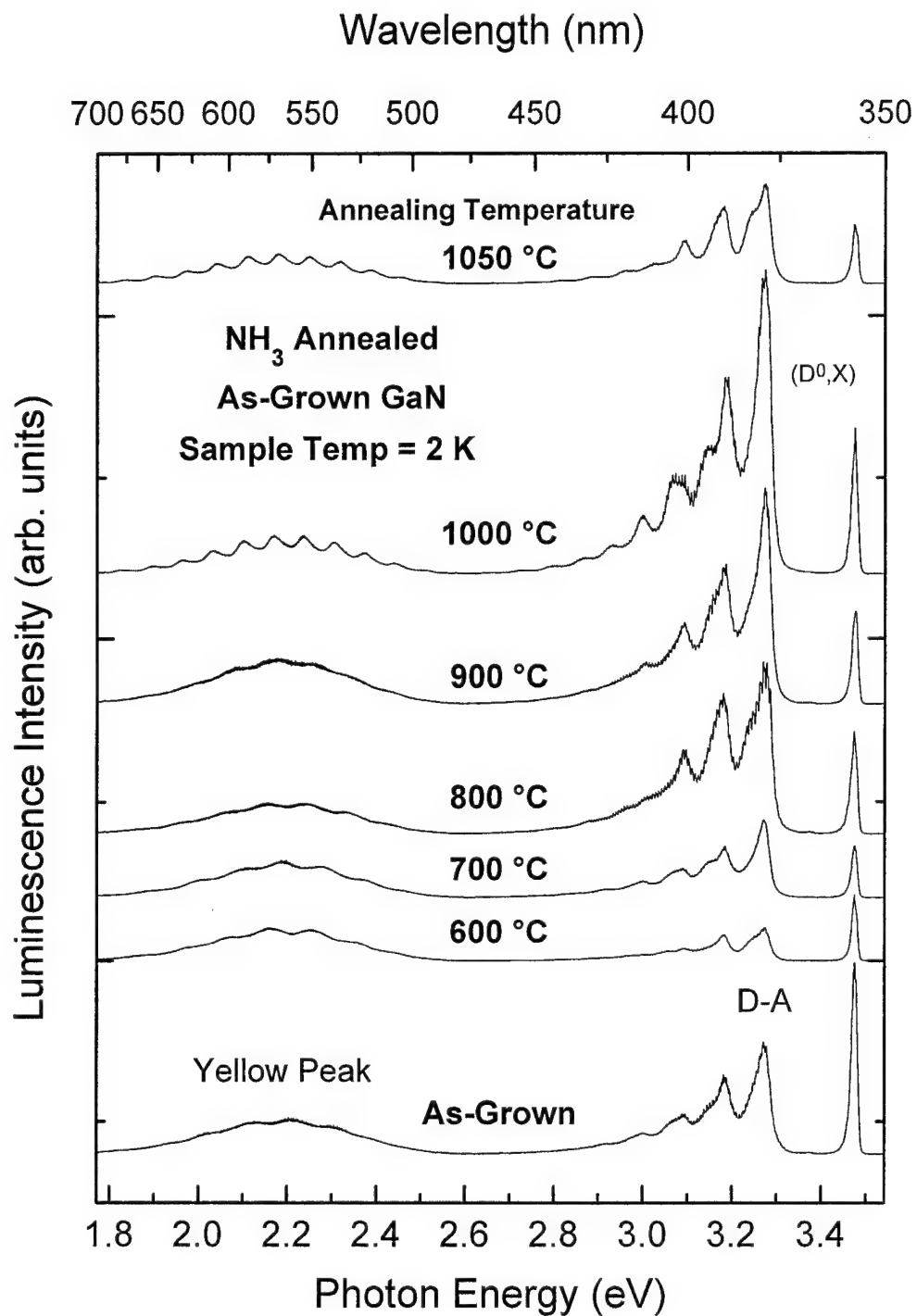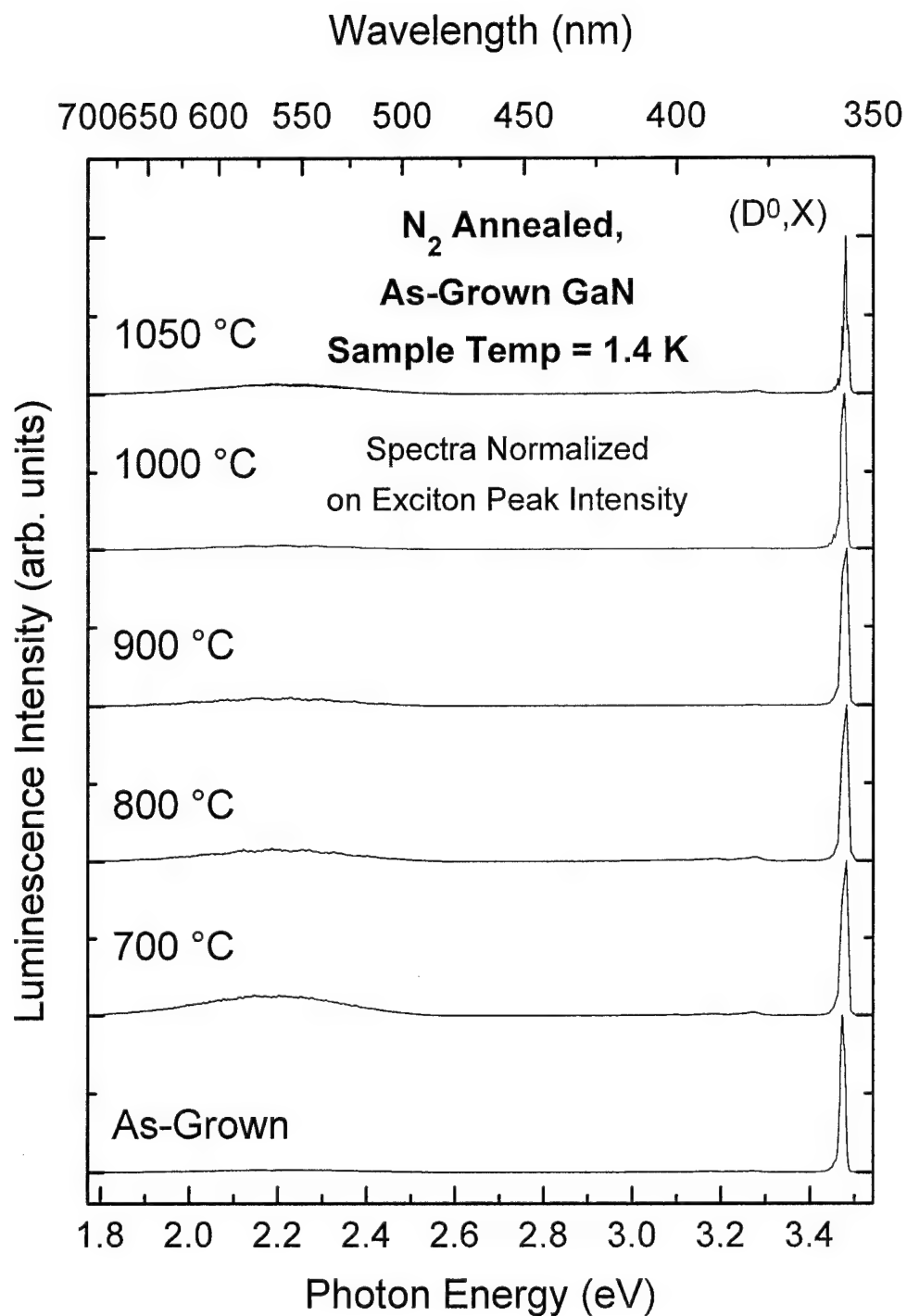**Figure 5-13**. Photoluminescence spectra taken at 2 K for as-grown GaN annealed at various temperatures in a N_2 environment.

the surface would occur. Thus, it is probable that the H_2 gas present in the NH_3 annealing gas environment led to deterioration of the GaN surface due to the reaction described above. This deterioration resulted in increased V_N which was responsible for increased D-A luminescence. The results of the absorption measurements which showed an increasing trend in E_0 with annealing temperature in an NH_3 environment were also consistent with the formation of additional damage centers at the GaN surface.

Decomposition of GaN in an N_2 atmosphere is thought to proceed slowly at temperatures below 1000 °C (Morimoto, 1974; Karpinski and Porowski, 1984; Sun *et al.*, 1994). Thus, since N does not leave the GaN, additional V_N are not created in large numbers, and the D-A band does not increase in intensity with annealing temperature in an N_2 environment. Furthermore, the results of absorption measurements at the bandedge as shown in Figure 5-14 do not show an increasing trend with annealing temperature as was the case for NH_3 annealing. This is consistent with a finding of no substantial increase in V_N below a 1000 °C annealing temperature.

Another possible mechanism for increased DA emissions after annealing at higher temperatures in an NH_3 environment could be due to contamination during annealing. In one study, silicon was linked to D-A emissions (MRH Khan *et al.*, 1986). The possibility exists that the quartz annealing furnace tube could be a source of Si contamination. However, Si contamination should result in a D-A increase for annealing in N_2 as well as annealing in NH_3. Since no increase was observed for N_2 annealing, Si contamination
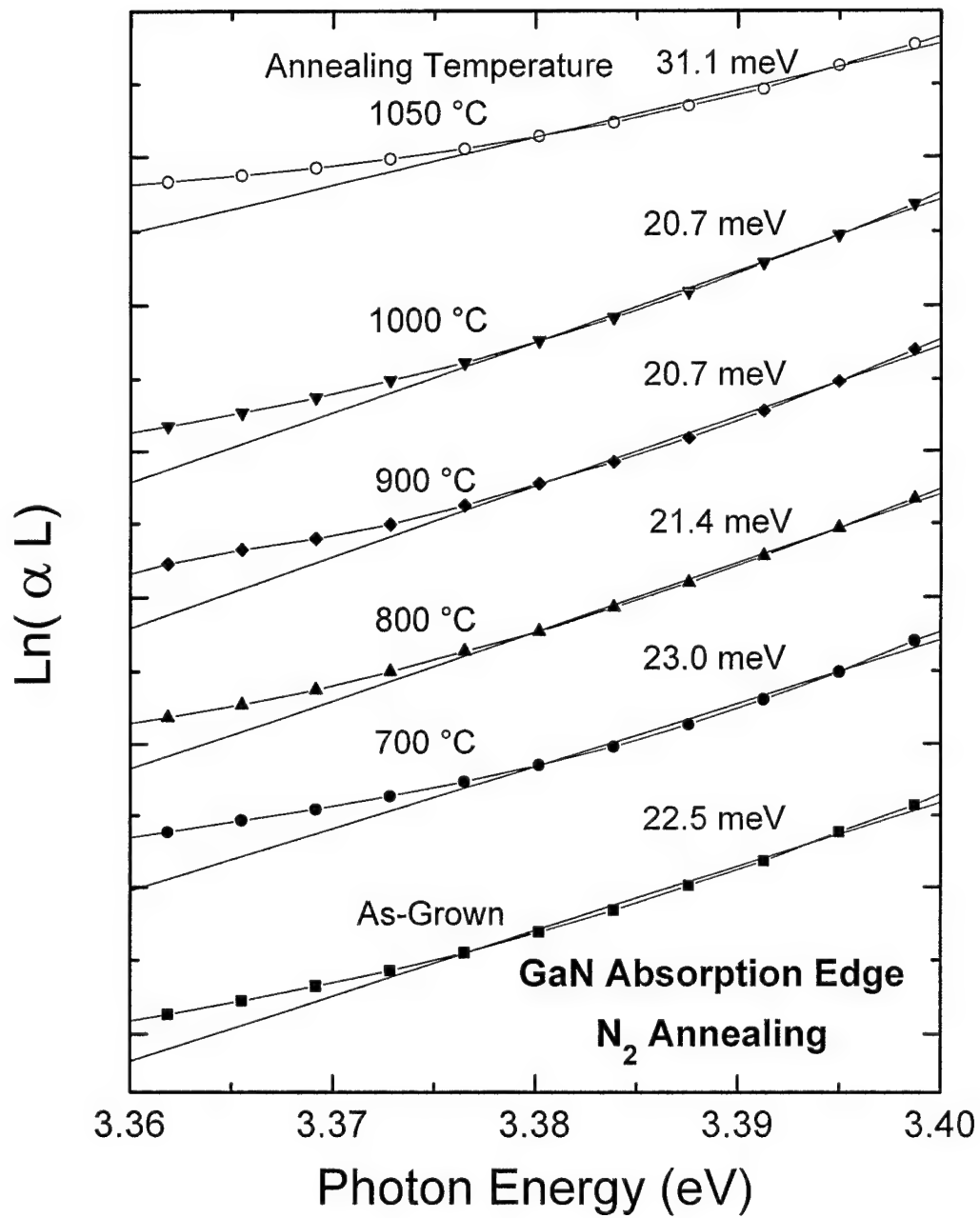
Figure 5-14. Room temperature absorption edge of as-grown GaN annealed at various temperatures in a N$_2$ environment.

can be ruled out as a cause for the D-A intensity increase with higher temperature NH_3 annealing. Other possible contaminants such as carbon and oxygen have not been linked to D-A emissions. Thus, the issue of contamination may play a minimal role in the decrease in overall luminescence in the present work.

In both cases of NH_3 and N_2 annealing, an overall decrease in exciton luminescence intensity was observed. This fact suggests the creation of non-radiative centers at the surface. The lowered intensity of the exciton emissions is consistent with other reports of annealed GaN (Pankove and Hutchby, 1976; Lin *et al.*, 1993). Lin *et al.* (1993) postulated an increase in the surface recombination velocity or a change in the carrier diffusion length due to defect formation to explain the decrease in exciton luminescence from N_2 annealed GaN. Thus, low temperature annealing may favor the formation of non-radiative defects at the GaN surface. This may explain the decreasing trend of the exciton, D-A, and yellow peak intensities after low temperature annealing

The results for the NH_3 annealed samples also showed that the luminescence intensity of the D-A emissions were not directly related to the intensity of the yellow peak. The fact that the relative intensity of the D-A and yellow peaks are not linked implies that the luminescence mechanisms of both peak mechanisms are not directly related. The growth of the D-A intensity with annealing temperature in NH_3 up to 1000 °C while the yellow peak does not grow at the same rate implies that more native defects involved in D-A luminescence were being formed during annealing but not the type of defects responsible for the yellow luminescence. Thus, since the D-A peak is thought to be related to V_N, the yellow peak is probably not related to V_N. In fact, the yellow peak

has been attributed to Ga_N or C impurities, a situation which is entirely consistent with the data in this study

The above results strongly suggest that damage occurred at the GaN surface during annealing. In order to test whether the surface was the cause of the increased D-A emissions, the samples were illuminated from the back surface. Spectra taken from the NH_3 annealed samples with laser excitation through the back sapphire side of the sample do not help resolve the issue of whether surface damage was the cause of the increase in D-A emissions. These particular samples from APA Optics were grown with a GaN buffer layer grown at low temperature. The back side illumination emissions were more broadened and are of considerably lower intensity than emissions from surface illumination. Figure 5-15 shows the comparison of front and back illumination of a sample annealed at a high temperature in an NH_3 environment. It is believed that the back side luminescence spectrum originating from the buffer layer by D-A emissions. Thus the increased D-A emissions from the NH_3 annealed samples originated in the GaN above the buffer layer. However, it could not be determined whether the increase in sharp D-A transitions occurred within a thin layer near the GaN surface.

In summary, the annealing of as-grown GaN in NH_3 or N_2 gas has been performed. Annealing at temperatures as low as 600 °C resulted in an overall reduction in exciton luminescence which was attributed to increased non-radiative recombination at the GaN surface. NH_3 annealing resulted in an increased D-A luminescence which was
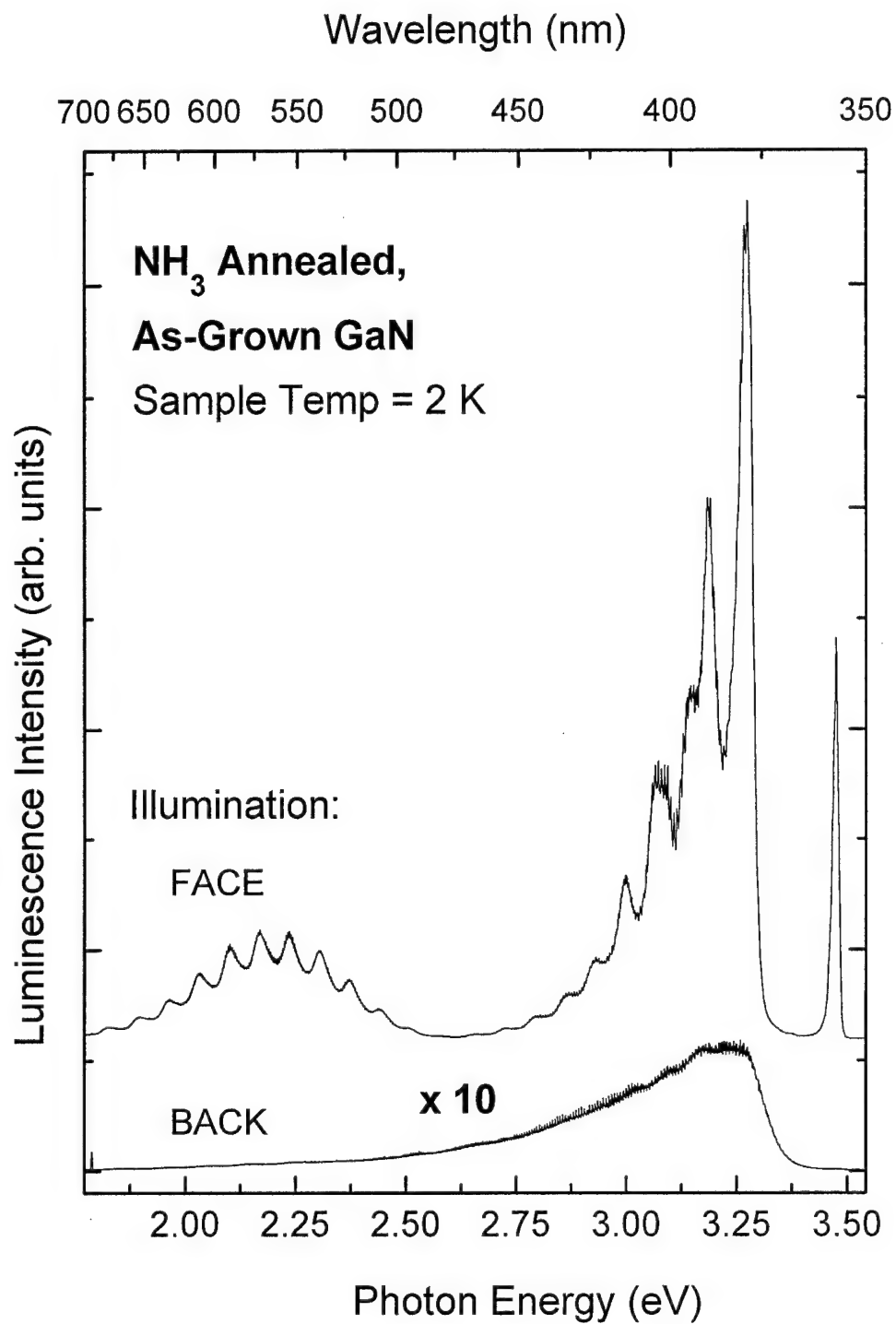
Figure 5-15. Photoluminescence spectra taken at 2 K for as-grown GaN annealed in NH_3 illuminated from the face and back.

attributed to decomposition of the GaN surface via the reaction $GaN + 3/2H_2 \rightarrow Ga + NH_3$ and increased concentration of V_N. Annealing in N_2 did not result in an increase in D-A emissions and no evidence for surface decomposition was observed even at 1000 °C. Thus, several previously unknown results have been discovered which are consistent with the literature on GaN decomposition in various atmospheres at elevated temperatures.

Argon is a chemically inert noble gas which should remain chemically inert after implantation. Thus, argon should not form chemical bonds within the GaN lattice, but should be free to outgas from the samples upon high temperature annealing. However, since implantation damage is dependent on the energy and charge of the ions in the beam and not the ion species, implantation damage created by argon ions should be very similar to implantation damage created by other ion species. Any new luminescence peaks observed after argon implantation would therefore be the result of damage.

A set of MOCVD grown samples, #873.3, obtained from APA Optics was implanted with argon at 390 keV with a dose of 5×10^{14} cm^{-2}. The maximum implantation energy, limited by the implantation apparatus, was chosen in order to produce a high degree of implantation damage. Also, the highest dose used for other implanted species was chosen to insure the highest level of disorder was created. Samples were annealed for 90 min in an NH_3 environment at 800, 900, 1000, and 1050 °C. The annealing conditions were also chosen to be similar to annealing conditions used for other implanted species. Two samples, those annealed at 900 and 1000 °C, were annealed by APA Optics under an NH_3 atmosphere at low pressure (76 Torr). Additionally, two other samples were annealed in flowing N_2 gas. One sample was annealed at 800 °C for 120 min in N_2, and the other was annealed first at 800 °C for 30 min in N_2 and then at 1000 °C for 30 min in N_2.

In order to test the extent of the damage, low temperature PL was performed on the as-implanted samples. In all cases, the low temperature PL intensity of the implanted samples before annealing was very low and showed no discernible structure. Thus, implantation had indeed caused lattice damage sufficient to quench all of the characteristic GaN luminescence peaks. Further evidence of lattice damage was found in room temperature absorption measurements of as-implanted samples. Significant absorption was found below the bandgap of all implanted, un-annealed samples.

Room temperature absorption measurements were taken below the bandedge to examine the effects of implantation and annealing. Below bandgap absorption can indicate perturbations of the bandedge caused by the random perturbations of defects. Figure 5-16 is a plot of the natural log of absorption as a function of photon energy near the bandedge for the NH_3 annealed samples. The as-grown, un-implanted sample's room temperature absorption data showed slight absorption below the bandedge. A nearly linear relationship between ln αL and photon energy just below E_g was found. The inverse slope of a linear fit gave an energy, E_0, of 22.7 meV. Following Pankove's treatment (1965), this value represents the 'length' of the exponential tail of states at the bandedge. A shallow tail in the density of states near the bandedge was expected at room temperature. This so-called Urbach tail (1953) has length $1/kT = 25$ meV at 300 K. Thus, this low value for E_0 demonstrated the high quality of the GaN used. The as-implanted sample, on the other hand, showed very significant below bandgap absorption. The data indicated the presence of a significant tail below the bandedge which was characterized
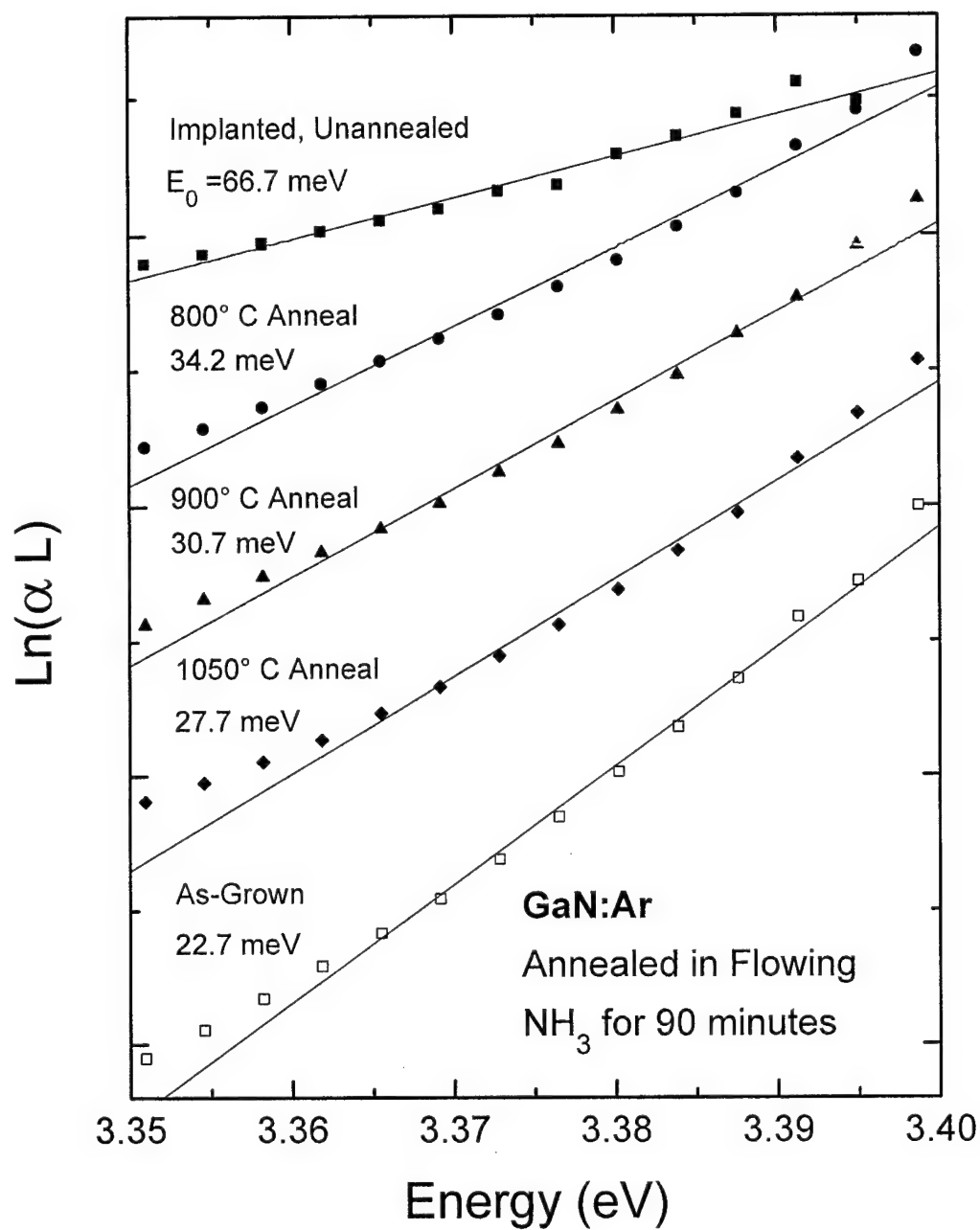
Figure 5-16. Room temperature absorption edge of GaN implanted with argon at an energy of 390 keV to a dose of 5×10^{14} cm^{-2} and annealed at various temperatures in a NH$_3$ environment.

by an E_0 value of 66.7 meV. Annealing can be expected to remove much of the below bandgap absorption. The data clearly showed an increasingly sharp absorption edge which nearly reached the as-grown level as the annealing temperature was increased. However, the sample annealed at 1000 °C fell outside this trend and the absorption measurement result of the sample is not shown in this figure. This particular sample was annealed at low pressure and therefore showed significant annealing induced surface degradation. This 1000 °C anneal showed much greater surface degradation than seen for 1000 °C, atmospheric pressure, NH_3 annealed samples. The low pressure annealed sample had an opaque, white appearance, which was most pronounced at the edges. This surface degradation resulted in significant below bandgap absorption and thus could not be expected to follow the trend of recovery seen in the other anneals. The trend for the 800, 900, and 1050 °C anneals showed a clear decrease in absorption below the bandedge indicative of successful annealing of ion implantation damage.

The room temperature absorption data from the N_2 annealed samples also showed a similar trend with increased annealing temperature as shown in Figure 5-17. The 'length' of the bandtail for the 800 °C anneal was 34.7 meV. This value was nearly identical to the 'length' of the bandtail for the 800 °C NH_3 annealed sample, which was 34.2 meV. Furthermore, the sample annealed at two stages of 1000 and 800 °C in N_2 had a band tail characterized by $E_0 = 29.4$ meV. This value was slightly larger than the value of 27.7 meV found for the 1050 °C NH_3 anneal. One would expect a slightly larger value if the trend only depended on temperature for a 90 min anneal. It should be noted that the
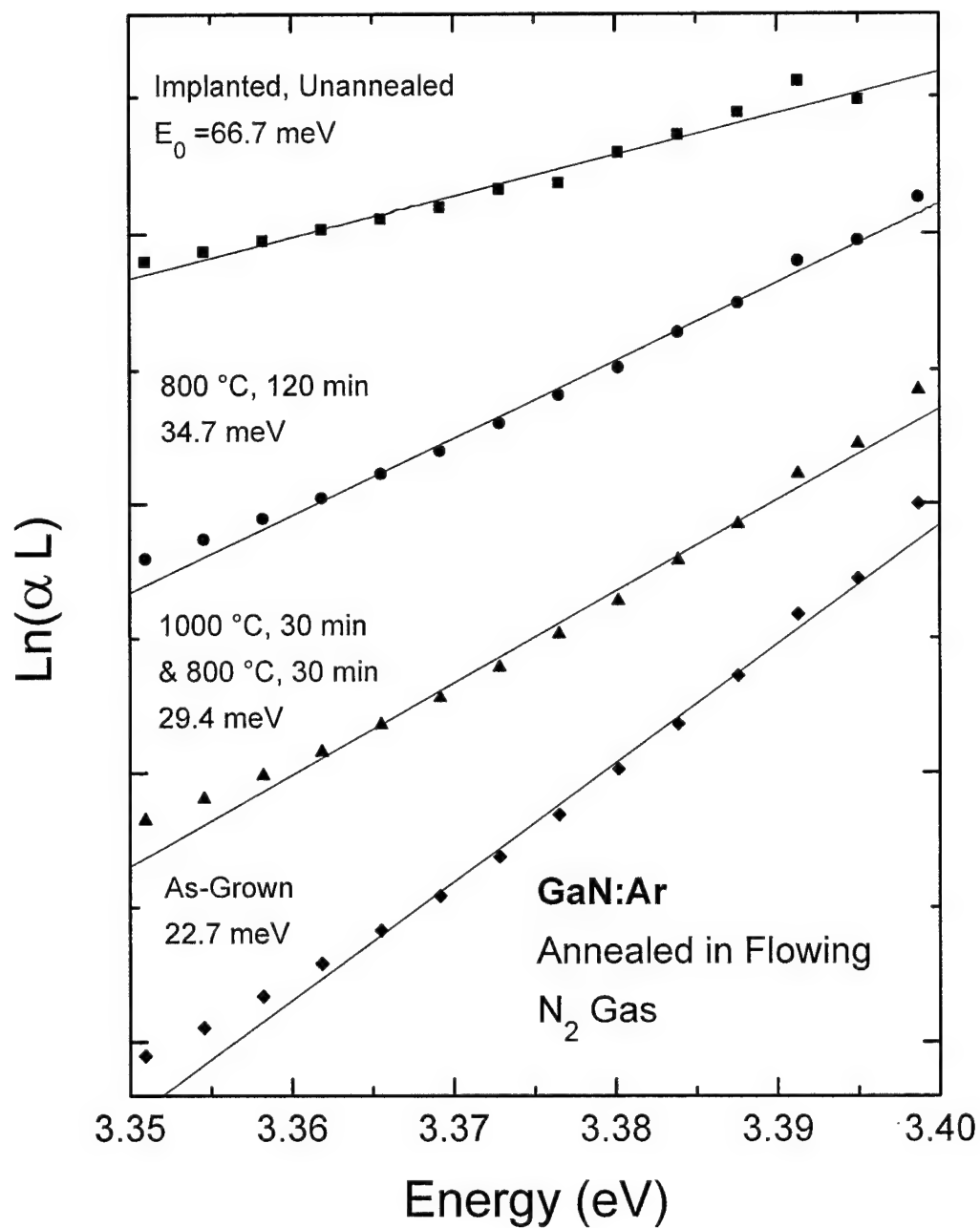
Figure 5-17. Room temperature absorption edge of GaN implanted with argon at an energy of 390 keV to a dose of 5×10^{14} cm^{-2} and annealed at various temperatures in a N$_2$ environment.

data from the low pressure 1000 °C NH_3 anneal could not be compared due to the heavy annealing related surface damage. These results demonstrated that the anneal temperature, and not the anneal gas environment, was the key factor in governing the recovery of the crystalline damage caused by implantation. Thus, virtually identical annealing behavior was observed for NH_3 and N_2 annealing. The N_2 data also suggested that anneal time was not important for lattice damage recovery above a certain minimum anneal time. The 30 min annealing time created the same recovery in N_2 as the 90 min time did in NH_3 at 800 °C. The above data led to the conclusion that high temperature furnace annealing was effective for reconstituting the implantation damaged layer. However, this result does not preclude the presence of point defects which may still be present in high concentration after annealing.

The Arhennius plot shown in Figure 5-18 was prepared from the NH_3 annealing data in order to determine whether the annealing process could be characterized by a single activation energy. The 800, 900, and 1050 °C anneals showed a clearly linear relationship. The activation energy for the annealing process determined by a linear fit was found to be 103±7 meV. It should be noted that the un-annealed, as-implanted sample, plotted at 300 K, did not fall on this line. Thus, annealing did not occur at room temperature. Therefore, a threshold temperature for the annealing process can be postulated. This threshold should occur at the temperature at which the fit line crossed the E_0 value for the un-annealed sample. Using this method, the threshold temperature was found to be 668 K or 395 °C. Again, the 1000 °C anneal did not fall on this line due
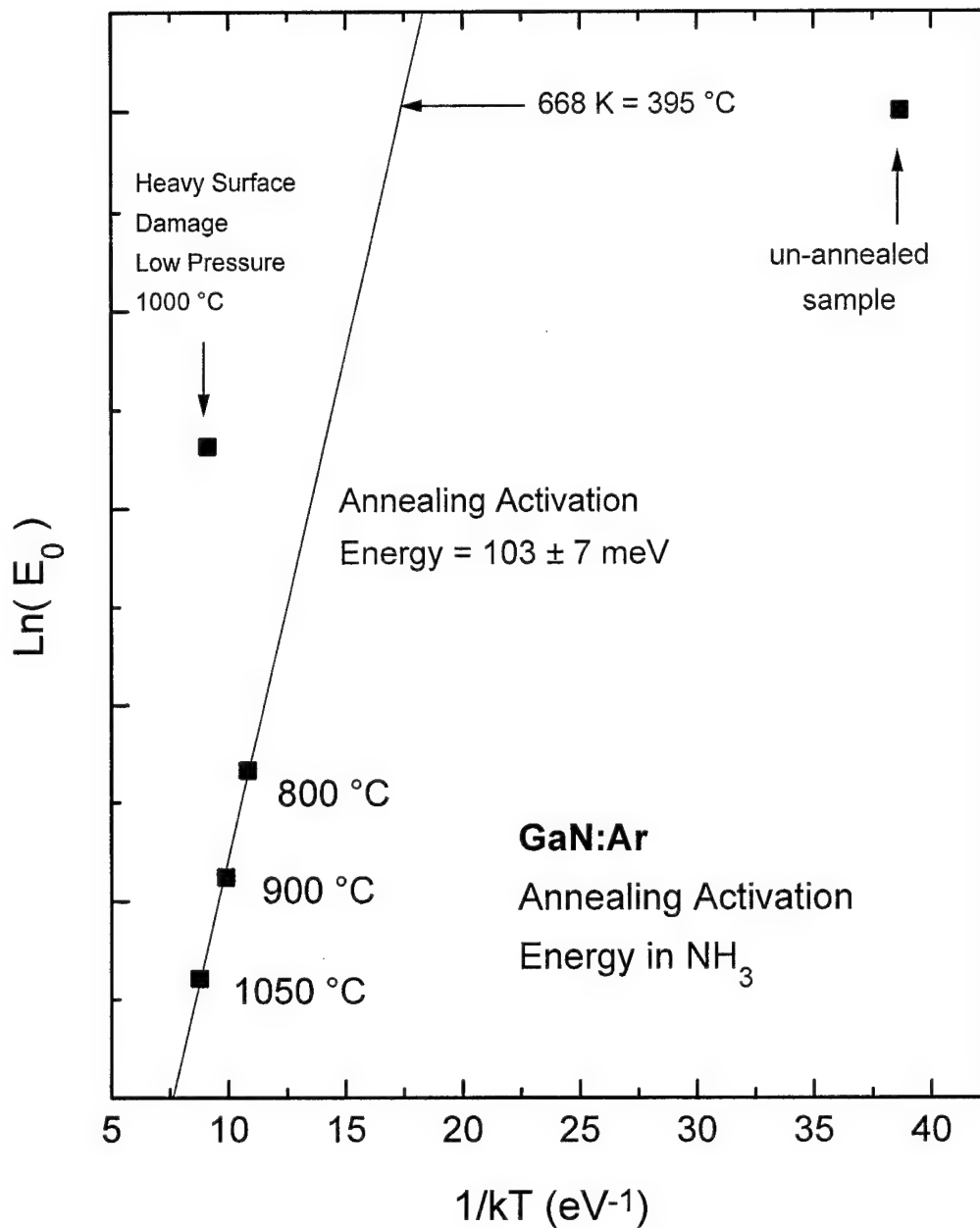
Figure 5-18. Arhennius Plot of the Bandedge Recovery of GaN implanted with argon at an energy of 390 keV to a dose of 5×10^{14} cm^{-2} and annealed at various temperatures in a NH$_3$ environment.

to the severe surface degradation of this sample. An Arrhenius plot was not made for the N_2 anneals since only two samples (non-isochronal) were tested. However, the nearly identical E_0 values for N_2 and NH_3 annealing at each temperature implied a nearly identical activation energy for N_2 and NH_3 annealing. Again, annealing temperature and not annealing gas was the determining factor for bandedge recovery.

Low temperature PL was used to characterize the post-implantation recovery of luminescence upon annealing. Prior to annealing, none of the characteristic GaN luminescence could be observed. The low temperature PL spectra of the samples annealed at various temperatures is shown in Figure 5-19. No PL peaks other than the well known, characteristic GaN peaks were observed. The native D-A peak at 3.27 eV dominated the spectrum of all argon implanted and annealed samples. As the annealing temperature was increased from 800 to 1000 °C, the integrated intensity of the D-A emissions increased by a factor of about 36. This result was very similar to the increase in the D-A emissions observed for the NH_3 annealed un-implanted samples, which were also grown by APA Optics. The major observed difference was that in the un-implanted case, the D-A peaks were clearly resolved into a no-phonon peak with several LO phonon replicas. The fact that the peaks in the argon implanted samples were not well resolved indicated that the density of implantation induced defects remained quite high even after annealing. A high density of defects would cause random fluctuations in the inter-atomic potential resulting in random shifts in the position of the individual D-A transitions. Thus, a broadened D-A spectrum would result. As discussed in the previous section on

Wavelength (nm)
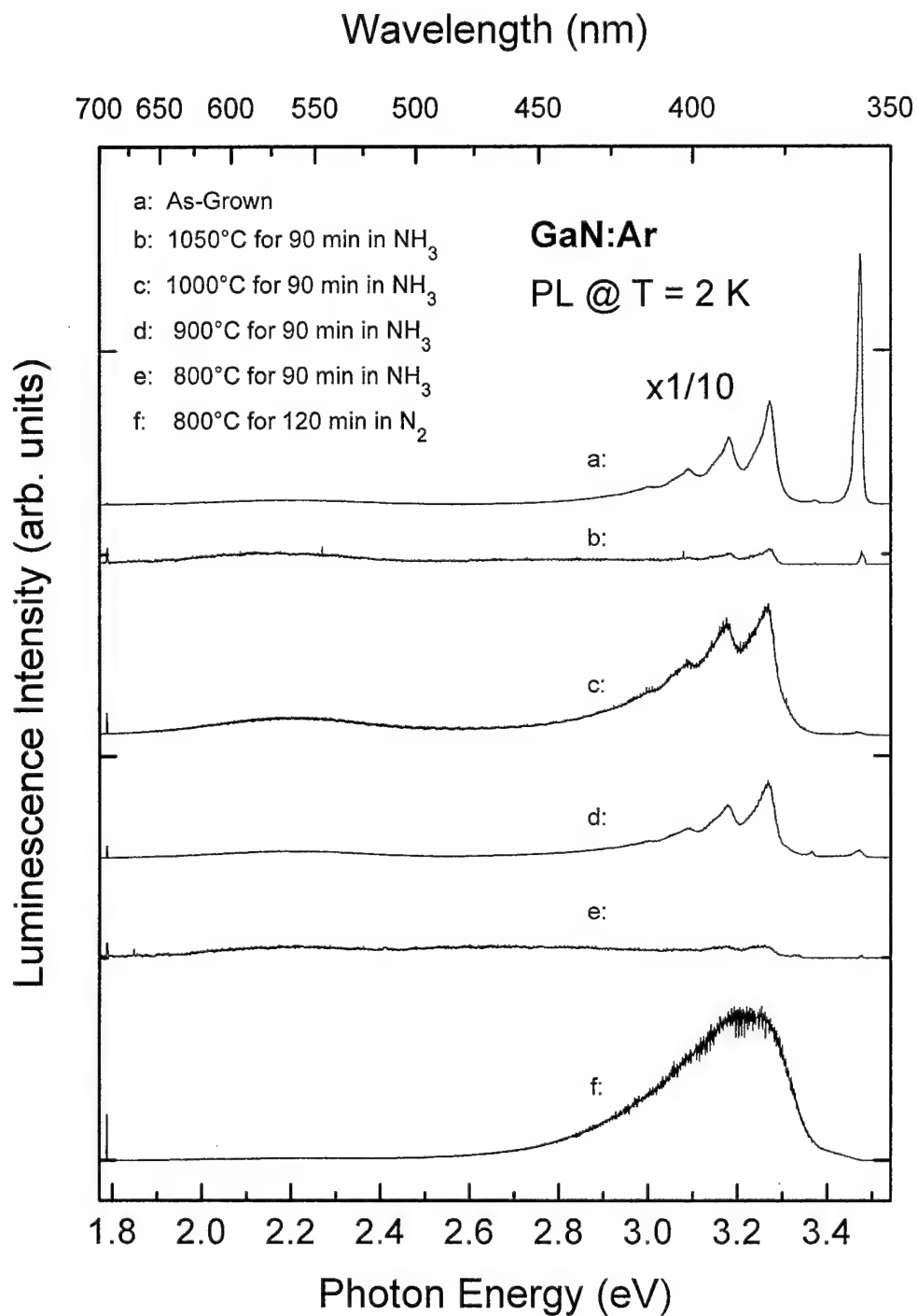
Figure 5-19. Photoluminescence at 2 K of GaN implanted with argon at an energy of 390 keV to a dose of 5×10^{14} cm^{-2} and annealed at various temperatures in a NH$_3$ and N$_2$ environment.

un-implanted annealed samples, the D-A peaks are most likely associated with the V_N native defect. The luminescence intensity of the argon implanted D-A peaks was lower than the as-grown sample's levels, indicating the radiative efficiency of the D-A transitions was suppressed after annealing. This result was further evidence of residual damage in the implanted layer.

Another indicator of native defects or common impurities is the yellow peak centered at 2.2 eV. This peak was observed to become active with the 900 °C anneal, and remained at about the same intensity for the 1000 °C anneal. It was unclear whether this peak had been changed by implantation and annealing. The luminescence intensity of the yellow peak was still below the as-grown sample's level as was the case for the D-A peaks.

The UV exciton peak was observed at low intensity in the 900, 1000, and 1050 °C NH_3 anneals. The exciton peak intensities of the annealed sample was greatly suppressed compared to that of as-grown sample. This was a clear indication of un-annealed damage defects in the implanted layer. The N_2 annealed samples showed no indication of the exciton peak.

The PL signal of the sample annealed at 1050 °C was quite poor compared to that of the 900 and 1000 °C anneals. As with the un-implanted samples annealed at 1050 °C, the argon implanted samples also showed that cap-less annealing at 1050 °C results in the creation of non-radiative de-excitation mechanisms.

The sample annealed at 800 °C for 120 min in flowing N_2 gas displayed a low temperature PL signal about as intense as the signal seen with the samples annealed at

1000 °C in an NH_3 environment. However, the D-A band was completely unresolved in the N_2 anneal, that is, the envelope of the emissions enclosed the D-A structure, but no individual peaks could be resolved. The overall structure peaked at about 3.2 eV. As stated previously, the absorption measurements showed recovery of the crystalline lattice similar to the NH_3 anneals, thus the broadening must have been related to a high density of point defects. The PL data also showed a high energy shoulder extending from the D-A peak to the exciton peak energy near the bandgap. This may be evidence that the tail of states at the bandedge merged with the defect levels which give rise to the D-A band. This shoulder was not observed in any of the samples annealed in NH_3. Thus, although bandedge recovery was nearly identical in NH_3 and N_2 annealing, the N_2 annealed samples showed poor post-implantation luminescence recovery.

In conclusion, argon implantation was used for the study of implantation damage and annealing. Samples were found to recover their sharp room temperature absorption edge upon annealing at temperatures of 1000 to 1050 °C. Nearly identical recovery was found for samples annealed in NH_3 and N_2 annealing environments. Thus, annealing temperature appeared to be the determining factor in the GaN's bandedge recovery. An activation energy of 103 ± 7 meV with a threshold temperature of 395 °C was found for the annealing process. The recovery of the as-grown GaN luminescence spectrum could not be achieved from the annealed samples in either NH_3 or N_2 atmospheres. The low temperature spectra of argon implanted and annealed GaN were dominated by the 3.27 eV D-A band. Furthermore, the D-A luminescence was less intense after implantation and annealing. The intense exciton peak of the as-grown GaN was quenched. Thus,

implantation damage remained after annealing, and resulted in non-radiative decay pathways. The NH_3 anneals displayed better resolved D-A peaks than N_2 annealed samples. Thus, NH_3 annealing resulted in better luminescence recovery. As was expected for this inert element, no unique PL peaks associated with argon were observed. These results can now serve as a baseline for the comparison of other implants.

Zn was implanted at 390 keV into MOCVD grown GaN obtained from Honeywell. Three different doses of 1×10^{13}, 1×10^{14}, and 2.25×10^{14} cm^{-2} were implanted. Optimal implantation damage recovery conditions were explored by furnace annealing in either flowing NH$_3$ or flowing N$_2$ gas over a range of annealing temperatures. Both room temperature absorption and low temperature photoluminescence were performed to characterize the degree of recovery and optical activation of Zn. Characteristic changes in luminescence efficiency were examined as a function of annealing temperature and laser excitation intensity.

Room temperature absorption measurements were performed to examine the post-implantation recovery of the GaN bandedge with annealing in NH$_3$. Figure 5-20 shows the results of an absorption study for GaN implanted with a Zn dose of 2.25×10^{14} cm^{-2}. This set of samples was annealed in flowing NH$_3$ gas for 90 min at temperatures ranging from 800 to 1050 °C. The plot shows the near bandedge region of the absorption spectra which have been offset vertically for clarity. At low temperature, a perfect semiconductor would be expected to have a vertical absorption edge. At elevated temperature, the absorption edge of a perfect semiconductor can be expected to have an Urbach (1953) edge with slope 1/kT. Thus, a slope of up to 25 meV at 300 K would not indicate significant bandtailing. As would be expected, the as-grown sample had the sharpest absorption bandedge. Since this sample had not undergone implantation and was therefore undamaged, little band tailing was expected. In contrast, the as-implanted
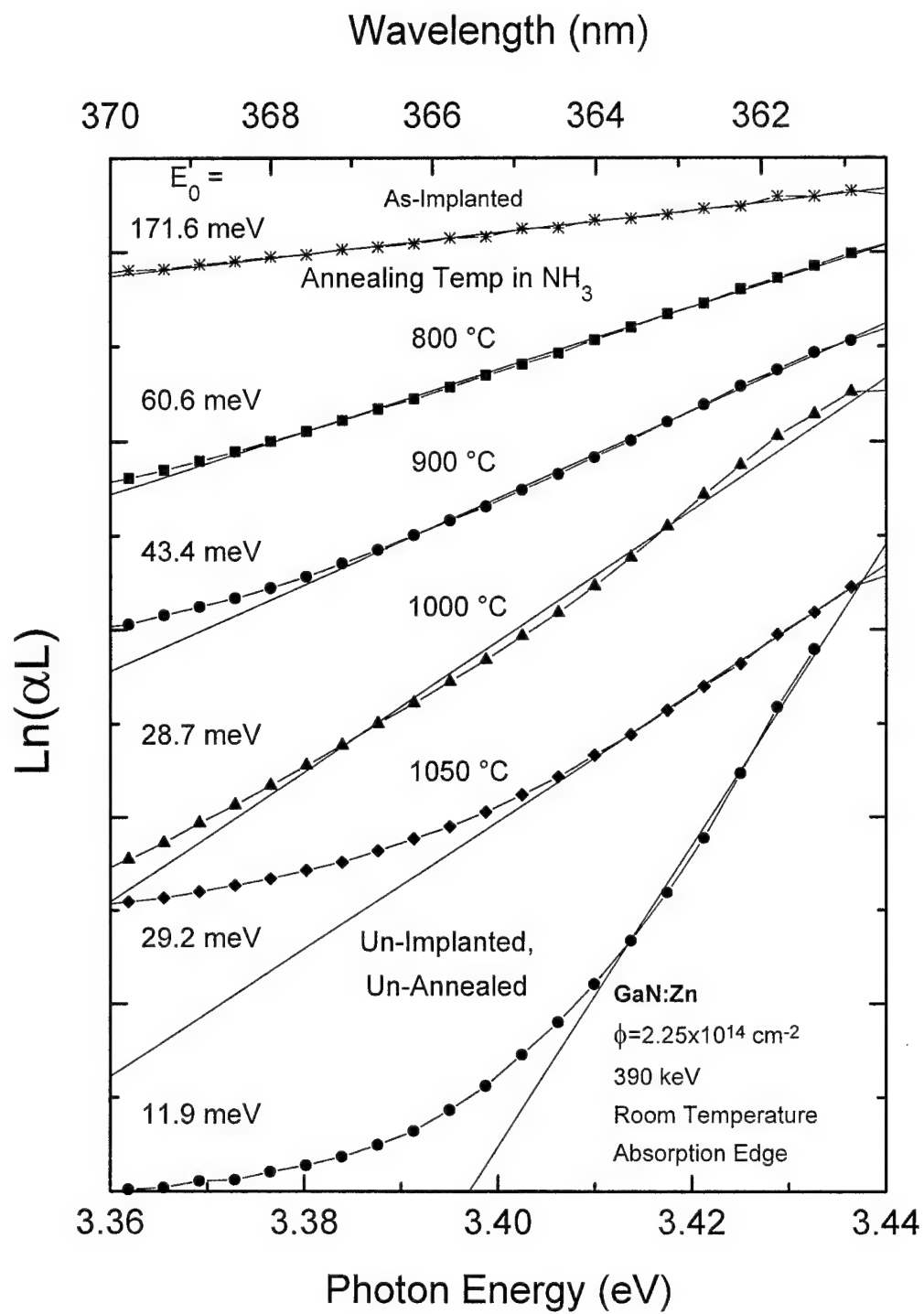
Figure 5-20. Room temperature absorption edge of GaN implanted with 2.25×10^{14} cm^{-2} Zn annealed for 90 min in NH$_3$ at various temperatures.

sample having been damaged by implantation but not yet annealed was found to have the least sharp bandedge with $E_0 = 171.6$ meV. This result was also expected since implantation is known to produce extensive lattice damage which results in numerous defect states. Defect states perturb the bandedge resulting in increased below bandgap absorption. The annealed samples showed intermediate levels of bandedge recovery. In fact, a very clear trend of recovery was found for the 800, 900, and 1000 °C anneals. Figure 5-20 lists the values of E_0 calculated from a linear fit to the absorption spectra near the bandedge. The value of E_0 observed for each annealed sample approached the as-grown sample's E_0 value as the annealing temperature was increased. However, the E_0 value measured for the 1050 °C anneal was increased relative to the 1000 °C anneal. The 1050 °C anneal displayed increased absorption at all wavelengths due to severe surface degradation. Thus, this sample's E_0 value was observed to be increased. This sample's surface also had a milky, white appearance which was particularly evident near the edges.

The visible deterioration of the 1050 °C, NH_3 annealed, Zn implanted sample was similar to that observed for un-implanted samples annealed above 1000 °C in NH_3. In the case of the un-implanted sample annealed at 1050 °C in NH_3, E_0 increased slightly, by about 4 meV, over the value for the un-annealed, un-implanted sample. This increase could be attributed to annealing alone. However, the Zn implanted and annealed sample showed a much more substantial rise in E_0 for the 1050 °C NH_3 anneal as compared to the as-grown sample of the same substrate. Furthermore, the value of E_0 for Zn implanted and annealed samples approached but never fully attained the as-grown value. This result was similar to the observations of Ar implanted GaN annealed in NH_3. Thus,

Zn implanted GaN appears to have additional residual defects which resulted in below bandgap absorption which cannot be attributed to annealing alone. However, as was the case for Ar implanted GaN, this absorption can be attributed to residual implantation damage.

To examine trends in the below bandgap absorption, E_0 was plotted as a function of annealing temperature. Figure 5-21 shows a clear linear relationship between E_0 and annealing temperature. The un-annealed sample was plotted at room temperature and a linear fit determined a slope of -0.150 ± 0.001 meV/K. According to Pankove (1965), E_0 is related to the number of responsible defect centers, N_o, by

$$ N = N_0 e^{E/E_0} . \tag{5-1} $$

where N is the number of states in the bandtail at a given energy, E, above the valance bandedge. Thus, a linear relationship between E_0 and annealing temperature would imply an exponential reduction in the number of defect states responsible for the bandtail with increasing isochronal annealing temperature. By plotting the logarithm of E_0 as a function of 1/kT, one can find the activation energy for the annealing process. The 800, 900, and 1000 °C anneals shown in Figure 5-22 maintained a linear relationship. A linear fit indicated an activation energy of 0.437 ± 0.028 eV for the annealing process. Also evident was the fact that the un-annealed sample did not fall on the same line. Thus, this
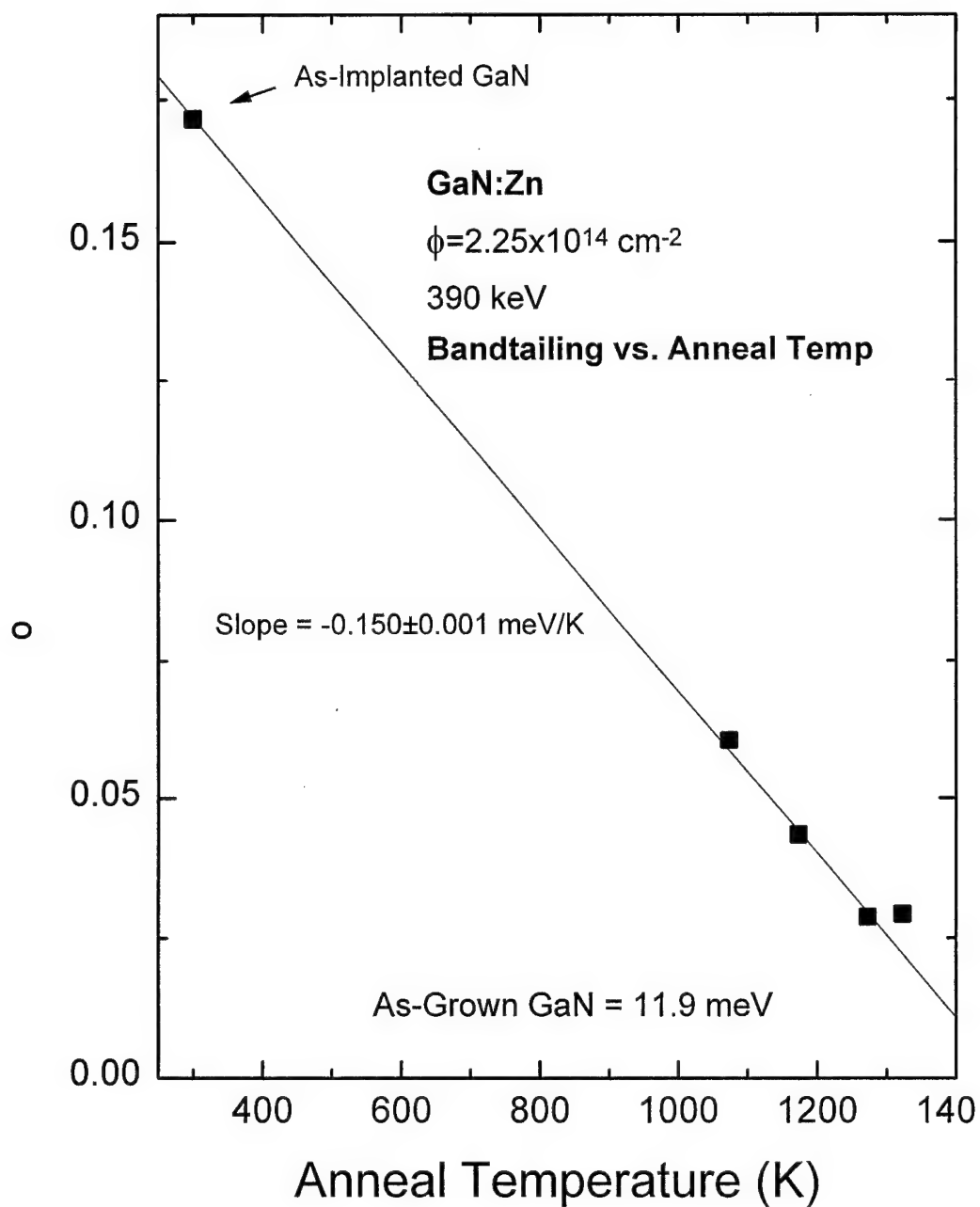
Figure 5-21. E_0 value as a function of annealing temperature for GaN implanted with Zn at a dose of 2.25×10^{14} cm^{-2} and annealed in NH$_3$ for 90 min.
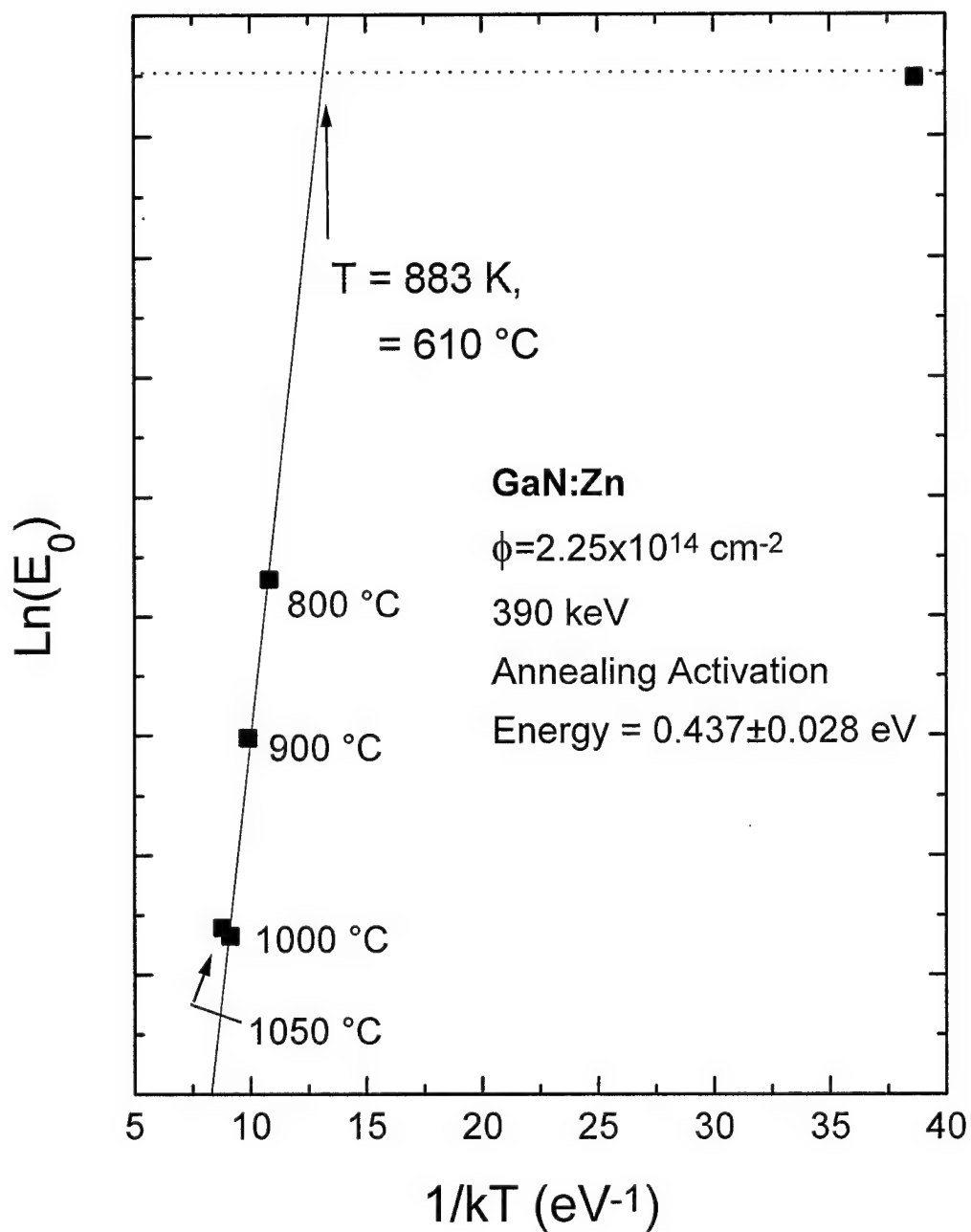
Figure 5-22. Arhennius plot of E_0 as a function of annealing temperature in NH_3 for GaN implanted with Zn at a dose of 2.25×10^{14} cm^{-2}.

annealing process was not ongoing at room temperature. If we assume that no annealing occurred until a threshold temperature was reached, then by extrapolating the line passing through the 800, 900, and 1000 °C anneals to find where it crossed the horizontal of the un-annealed, implanted sample, one can obtain a threshold temperature for the annealing process. This temperature was found to be 883 K or 610 °C. A value of ~600 °C for a threshold annealing temperature for ion implanted GaN was consistent with experimental findings for all implanted species. Samples annealed at temperatures of 600 °C and below showed virtually no luminescence recovery or activation. It can also be noted that the 1050 °C anneal deviated from the fitted line. This was further indication that bandgap recovery was nearly complete with annealing at 1000 °C and that annealing above 1000 °C resulted in additional annealing damage.

Thus, annealing of implantation damage in GaN proceeded only slowly at temperatures above 600 °C in an NH_3 environment. The best recovery of the bandedge was reached at an annealing temperature of 1000 °C for an annealing time of 90 min. The activation energy for the annealing process was found to be ~0.44 eV. However, as was previously found for un-implanted GaN, annealing at 1050 °C for 90 min in NH_3 caused severe surface degradation of the GaN film and did not result in additional bandedge recovery.

To examine the annealing conditions under which optical activation of the Zn implants occurred, a series of samples implanted with a Zn dose of 2.25×10^{14} cm^{-2} were annealed at 800, 900, 1000, and 1050 °C for 90 min in NH_3. PL was performed using the FReD laser line of 254 nm at 150 mW output by illuminating the surface of the GaN

sample and the results are shown in Figure 5-23. The as-grown samples show a strong donor bound exciton Γ_7^v line. This peak was only very weak in the zinc implanted samples. The samples annealed at 800 and 900 °C showed little or no luminescence. Annealing at 1000 and 1050 °C activated the Zn luminescence peak centered at 2.86 eV. The Zn center had approximately three times the peak intensity in the 1050 °C anneal as in the 1000 °C anneal. The FWHM remained constant at approximately 300 meV. A peak in the yellow/green centered at 2.3 to 2.35 eV was a factor of two greater in intensity in the 1050 °C anneal as compared to the 1000 °C anneal. This peak was shifted with respect to the defect peak typically observed for as-grown GaN which centered at 2.2 to 2.25 eV. Thus, an approximately 100 meV blue shift was observed. Unfortunately, no consistent shift pattern was observed with annealing temperature except to note that these shifts were always to the blue, and were only found in Zn implanted and annealed GaN. It should also be noted that no D-A emissions at 3.27 eV were observed in this sample set. Considering the demonstrated increase in D-A emissions for annealing un-implanted GaN in NH_3 at these temperatures, it was clear that the presence of Zn implants must have quenched the 3.27 eV D-A emissions. The exciton emissions were also quenched in Zn implanted samples.

We can also determine whether the activation of the Zn luminescence peak at 2.86 eV was governed by a single activation process. Figure 5-24 shows a plot of the Zn peak intensity after annealing. The activation of the Zn luminescence center increased rapidly

Figure 5-23. Face illumination photoluminescence at 2 K for GaN implanted with Zn to a dose of 2.25×10^{14} cm^{-2} and annealed in NH$_3$ for 90 min at various temperatures.

Annealing Temperature (°C)

800   900   1000   1100

Zn 2.86 eV Peak
Lumuminescence Activation
GaN:Zn
ϕ=2.25x10^{14} cm^{-2}
390 keV

Peak Intensity (Arb Units)

1000   1100   1200   1300   1400

Annealing Temperature (K)

Figure 5-24. Zn 2.86 eV peak luminescence intensity as a function of annealing temperature in NH_3 for GaN implanted with Zn to a dose of 2.25×10^{14} cm^{-2}.

as annealing temperature was increased to 1050 °C. Figure 5-25 shows an Arhennius plot of the same data. The plot showed a linear relationship between the log of luminescence intensity and 1/kT. A line was fit to this data and gave an activation energy of 1.92±0.06 eV.

Since it was known that annealing in NH_3 could result in surface damage, several experiments were conducted to examine whether such a damaged layer existed for Zn implanted and annealed GaN. First, this same series of samples was illuminated with laser intensity entering the sample at the edge. Figure 5-26 shows low temperature photoluminescence spectra taken with this edge illumination. Other than the previously noted shifts in the yellow/green peaks, identical luminescence peak locations were observed. However, the relative intensities have changed as compared to the spectra collected with face luminescence. The Zn peak at 2.86 eV now dominated in both the 1000 and 1050 °C annealed samples rather than the yellow/green peak. This increase in absolute as well as relative intensity for the Zn peak at 2.86 eV upon illuminating the sample from the edge indicated the existence of a damaged surface layer. When illuminated from the surface, a portion of the laser intensity was absorbed in this surface layer. Due to the damage, the non-radiative decay path was substantial. Since less of the laser intensity was able to penetrate and excite the bulk of the Zn luminescence centers, less Zn luminescence could be observed. It was clear that Zn luminescence centers were present below this damaged surface layer. The yellow/green absolute peak intensity showed little change in all four samples.
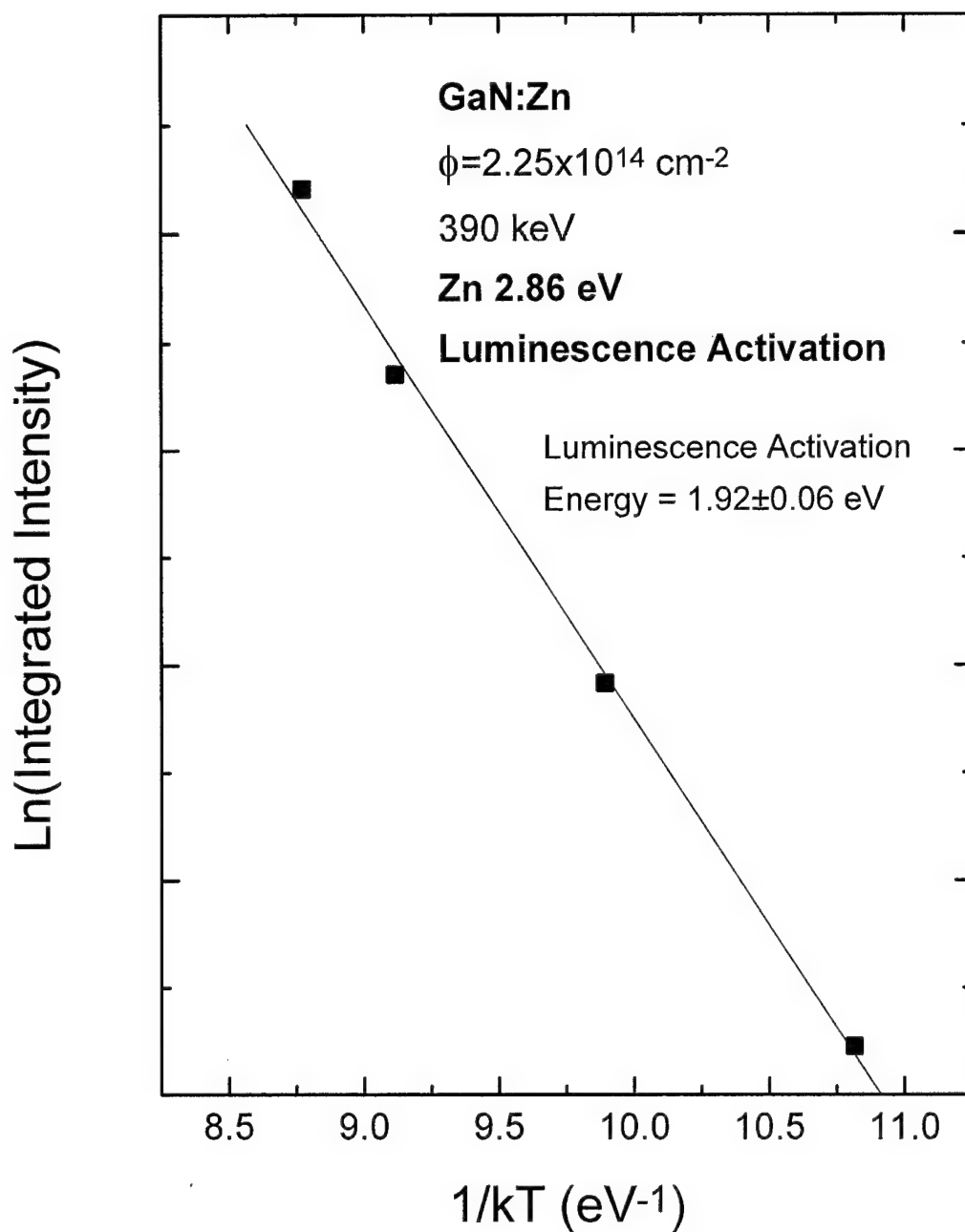
Figure 5-25. Arhennius plot of Zn 2.86 eV blue peak intensity as a function of annealing temperature for GaN implanted with Zn at a dose of 2.25×10^{14} cm^{-2}.
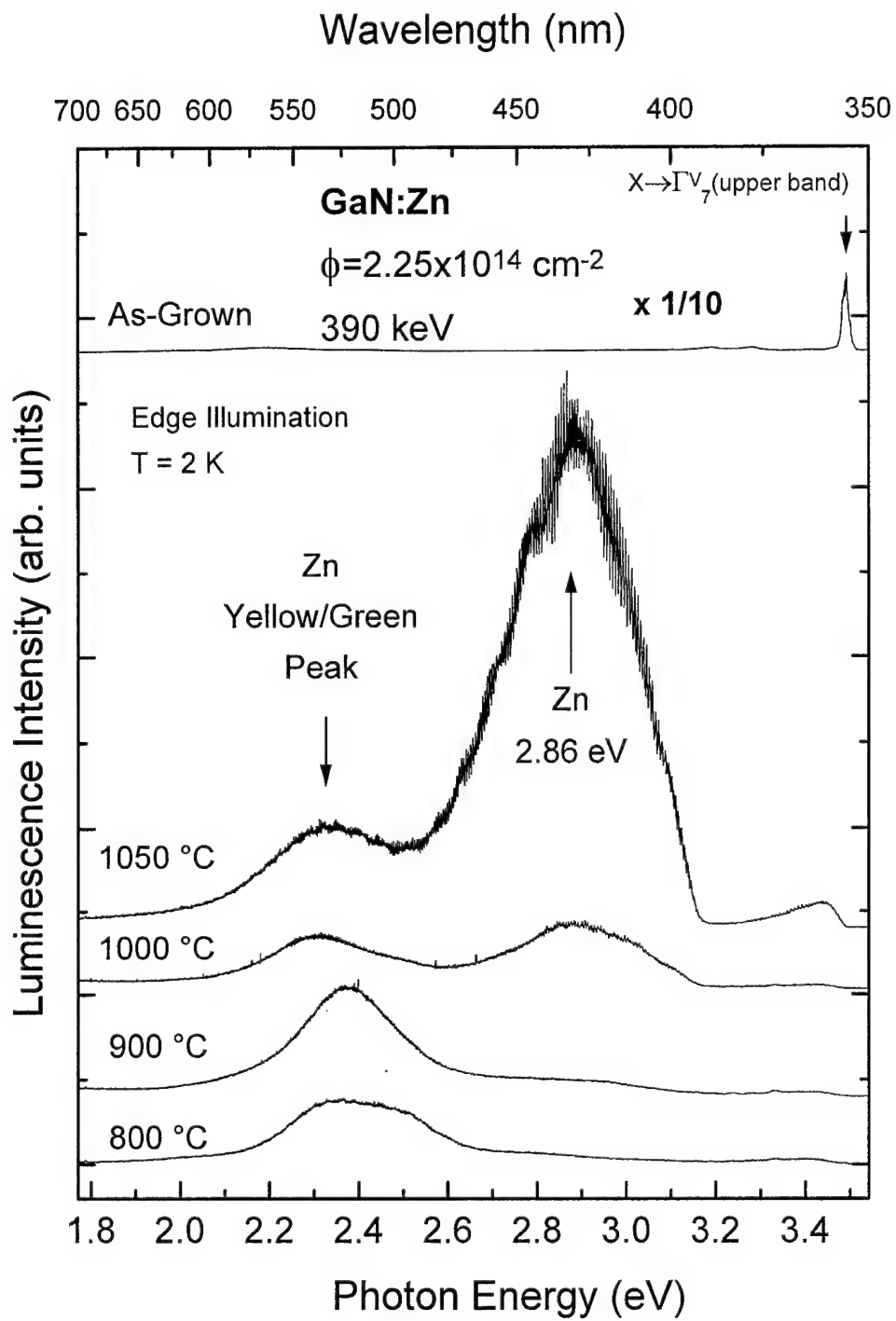
Figure 5-26. Edge illumination photoluminescence at 2 K for GaN implanted with Zn to a dose of 2.25×10^{14} cm^{-2} and annealed in NH$_3$ for 90 min at various temperatures.

Additional samples of lower Zn dose were also examined. Low temperature PL was performed on two GaN samples implanted with a Zn dose of 1×10^{14} cm^{-2} annealed in NH$_3$ at temperatures of 900 and 1000 °C for 90 min. Upon illumination from the face, the 2.86 eV Zn peak appeared only in the 1000 °C annealed sample as shown in Figure 5-27. Both the 900 and 1000 °C anneals exhibited D-A pair emissions at 3.27 eV. In contrast to the higher dose samples, the D-A peaks were not completely quenched. This effect may be related to the lower Zn dose. There was also an unresolved tail on the low energy side Zn peak from 2.00 to 2.50 eV which was clearly visible in the 1000 °C anneal sample. This tail occurred in the region of the yellow/green peak, and may simply be the result of a merging of that peak with the 2.86 eV Zn peak. Two UV peaks, labeled P$_1$ and P$_2$, were also evident in the spectrum of the 1000 °C sample. These peaks were found to occur at 3.471 (P$_1$) and 3.416 eV (P$_2$) at 2 K.

The 3.471 eV (P$_1$) peak occurred at the energetic location of the $(D,X) \rightarrow \Gamma_9^V$ peak, which is an exciton bound to donor transition. In contrast, the as-grown sample spectrum was dominated by the $X \rightarrow \Gamma_7^V$ (upper band) transition at 3.494 eV, which is a free exciton peak. Thus, lower dose implantation and annealing resulted in an increase in donors, most likely V_N. This result was consistent with the as-grown annealing studies reported earlier. The lower energy peak at 3.416 eV (P$_2$) was about 55 meV below the donor bound exciton, peak and thus cannot be an LO phonon replica of the donor bound exciton. Due to the low signal level and obvious overlaps with nearby peaks, the shape and maximum of this peak could not be reliably determined. Since the bandgap was
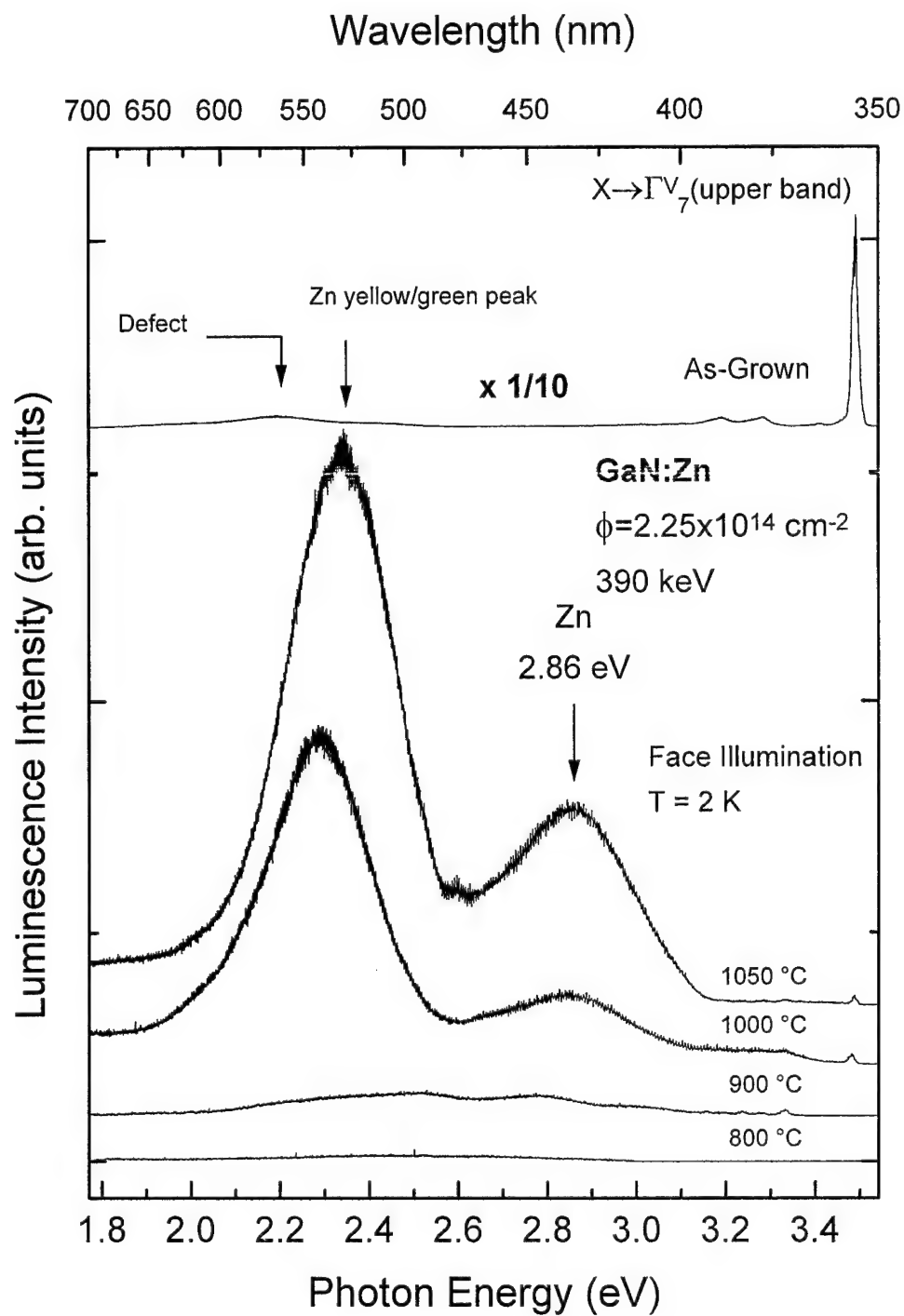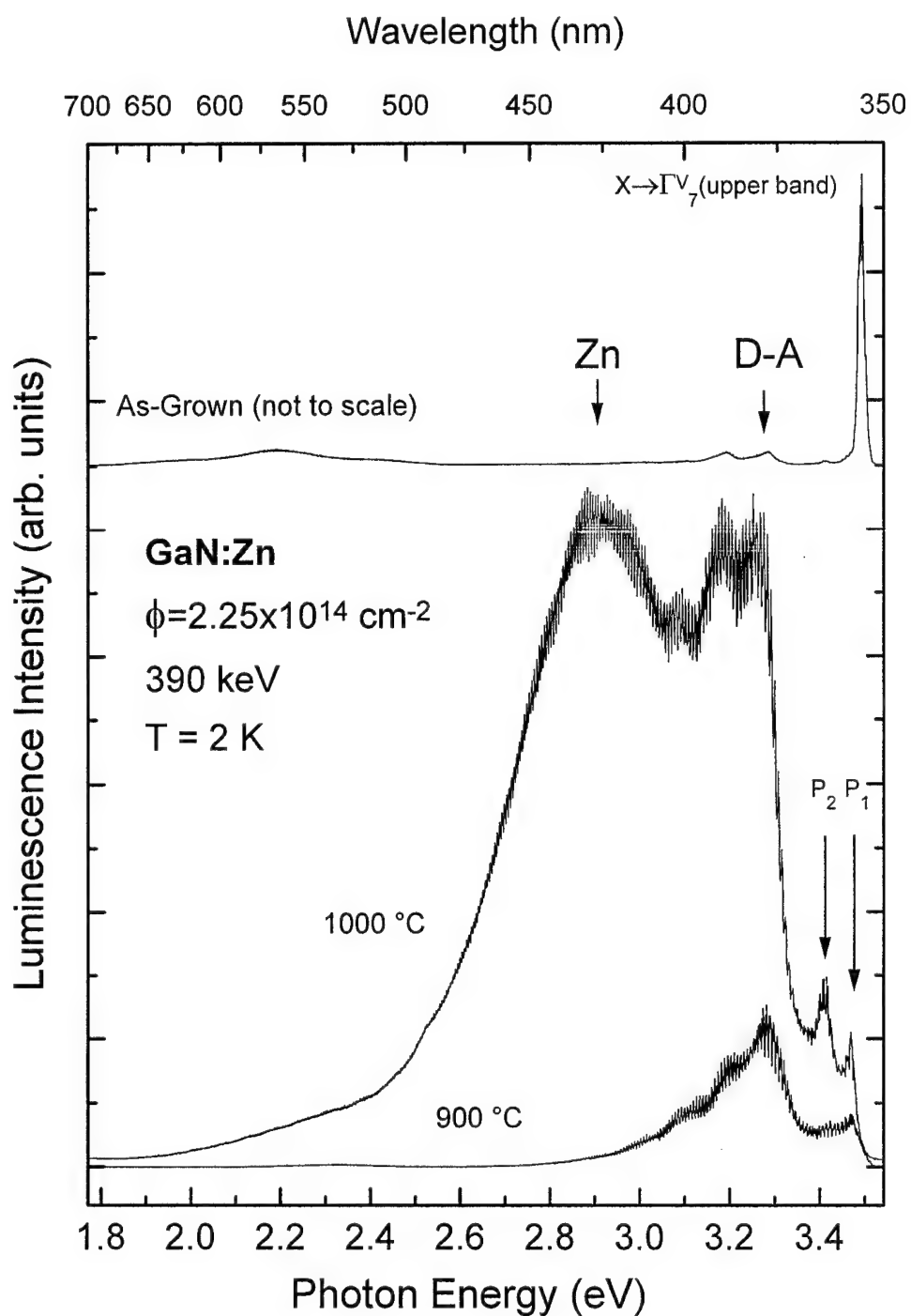
Figure 5-27. Face illumination photoluminescence at 2 K of GaN implanted with Zn to a dose of 1×10^{14} cm^{-2} and annealed in NH$_3$ for 90 min at various temperatures.

assumed to be 3.5 eV at low temperature, this peak occurred about 84 meV below the bandgap. This peak has not been identified in Zn-doped GaN before. However, since the peak was not observed in other implanted or as-grown samples, it may be associated with Zn implants. A candidate physical process to explain this peak was a radiative transition of an electron in the conduction band or a tail of states in the conduction band to the deep Zn acceptor level. This explanation would place the Zn acceptor level at only 84 meV above the valence band. This interpretation greatly differed from previous researcher's conclusions that the 2.86 eV Zn related emissions are a conduction band to acceptor transition with the Zn acceptor level at about 340 meV above the valence band edge. Another candidate process was an LO phonon replica of the $X \rightarrow \Gamma_7^V$ (upper band) transition, which would be expected at 3.494-0.090 = 3.404 eV. It was unknown why this peak should have occurred in the absence of the free exciton peak. Another possible source of the 3.416 eV peaks might be an exciton bound to Zn acceptor. With the above data, no final conclusion can be drawn as to the origin of this unique peak.

Since the 900 °C anneal did not show Zn luminescence when illuminated from the face, it was possible that only minimal activation of Zn luminescence centers occurred due at this lower annealing temperature. This result was consistent with the results of the higher dose sample set, which also had a low Zn signal for the 900 °C anneal. The second possibility was that, excessive surface damage from implantation and/or annealing could have resulted in absorption of the excitation laser beam. To gather further evidence, the sample was illuminated from the edge. This was done in order to probe the layer below the surface, a layer which would not have experienced surface damage during

annealing. The result was that the Zn related peak at 2.86 eV was indeed found. However, it was clear that activation of the 2.86 eV Zn center was much less efficient at 900 °C than at 1000 °C. Thus, evidence supporting both conclusions was found. The Zn luminescence centers were in fact present but at a lower density than the 1000 °C anneal, and the states responsible were below a damaged surface layer.

To further test the hypothesis that a damaged surface layer was absorbing a large portion of the laser light resulting in lowered Zn luminescence, the sample implanted with a dose of 2.25×10^{14} cm^{-2} dose annealed at 1050 °C sample was also illuminated from the back surface. After penetrating the sapphire substrate, the laser light entered the GaN layer from the substrate side. For comparison, Figure 5-28 shows the spectra taken with face, edge, and back laser illumination. The Zn luminescence peak was strongest when the sample was illuminated from the back. However, the intensity of the yellow/green peak was greatest with face illumination. This result suggested that the yellow/green peak was associated with the near surface damage region, whereas the blue peak was associated with a region deeper within the GaN sample. Also, the heavily damaged surface layer absorbed a large portion of the laser intensity, and de-excitation could then occur via non-radiative pathways at the surface. Also of note was the fact that this particular sample's GaN layer was only 0.8 mm thick. With the implantation parameters used, the upper half of the GaN volume was doped with Zn at concentrations over 1×10^{19} cm^{-3}. Deeper within the GaN volume, lower doping levels prevailed.
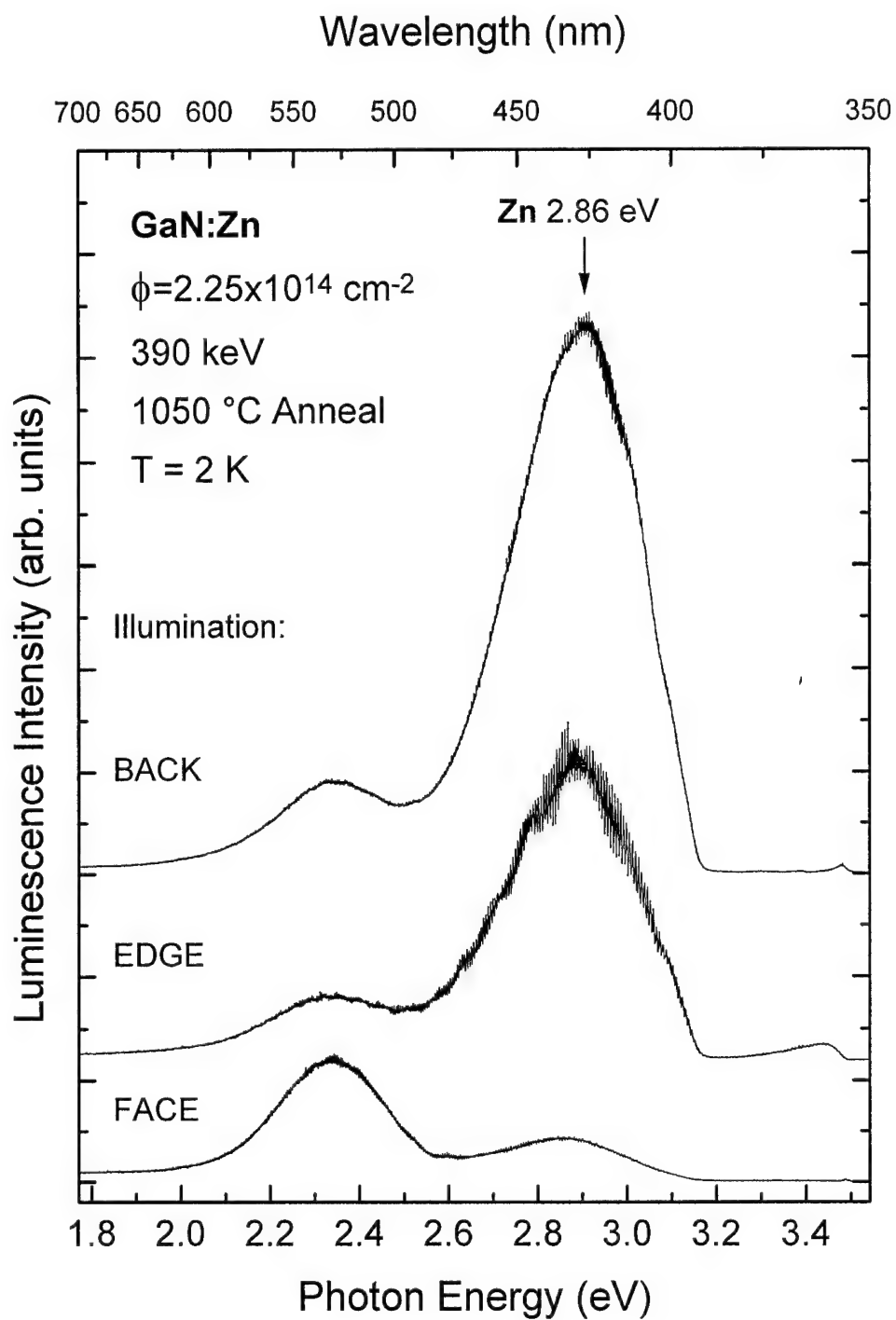
Figure 5-28. Face, edge, and back illumination Photoluminescence at 2 K for GaN implanted with Zn to a dose of 2.25×10^{14} cm^{-2} and annealed in NH$_3$ for 90 min.
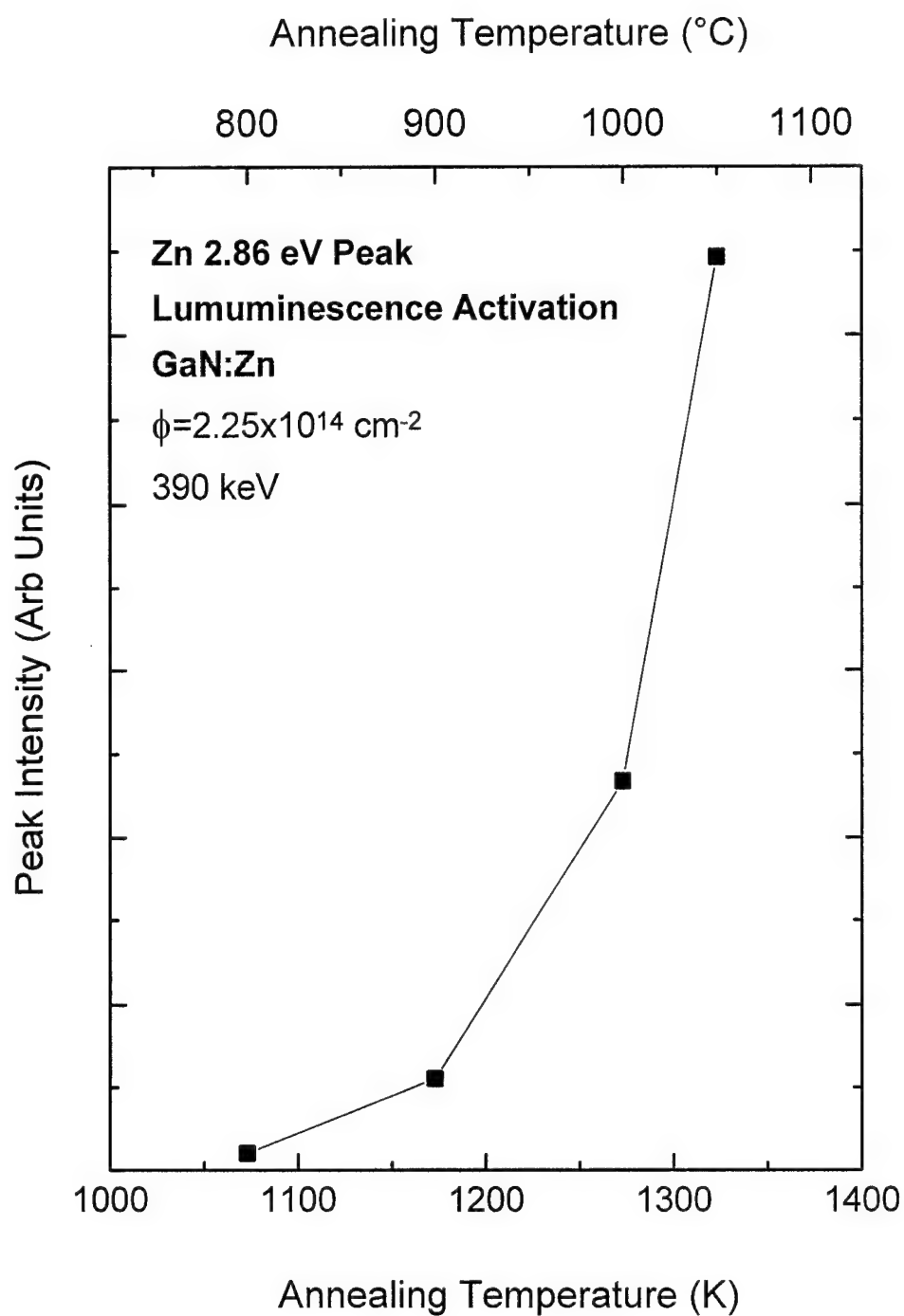
Furthermore, due to the presence of Zn, the free and donor bound exciton bands normally seen in the as-grown GaN were not observed even with back illumination.

To test whether the Zn signal would improve with further annealing time, the sample implanted with a dose of 1×10^{14} cm^{-2} and annealed at 900 °C was re-annealed at 900 °C for another 90 min in NH$_3$. The results showed that weak D-A emissions still dominated the spectrum under face illumination, but overall they were less intense than before. When illuminated from the edge, however, the Zn luminescence was evident at 2.86 eV, and was approximately a factor of two stronger after the second 90 min anneal. This experiment demonstrated that annealing in NH$_3$ at 900 °C incrementally lessened the D-A emissions from the surface of the sample while incrementally enhancing the Zn luminescence. Thus, the D-A quenching was linked to Zn activation and an annealing time of 180 min was somewhat better at activating Zn luminescence at 900 °C. Surface damage appears to have increased after the second anneal.

An experiment was conducted to explore the lower limit of annealing time necessary for activation of the Zn luminescence. A single sample from substrate E02525 implanted with a Zn at a dose of 2.25×10^{14} cm^{-2} was annealed at 1000 °C in flowing NH$_3$ gas for 15 min, and then re-annealed in 15 min increments to a total time of 75 min. After each annealing stop, low temperature PL and room temperature absorption measurements were performed. The E_0 values obtained from the near edge absorption spectra are plotted in Figure 5-29. The E_0 value dropped sharply from its as-implanted value of 123 meV to 22 meV after the first 15 minutes of annealing time. Subsequently,
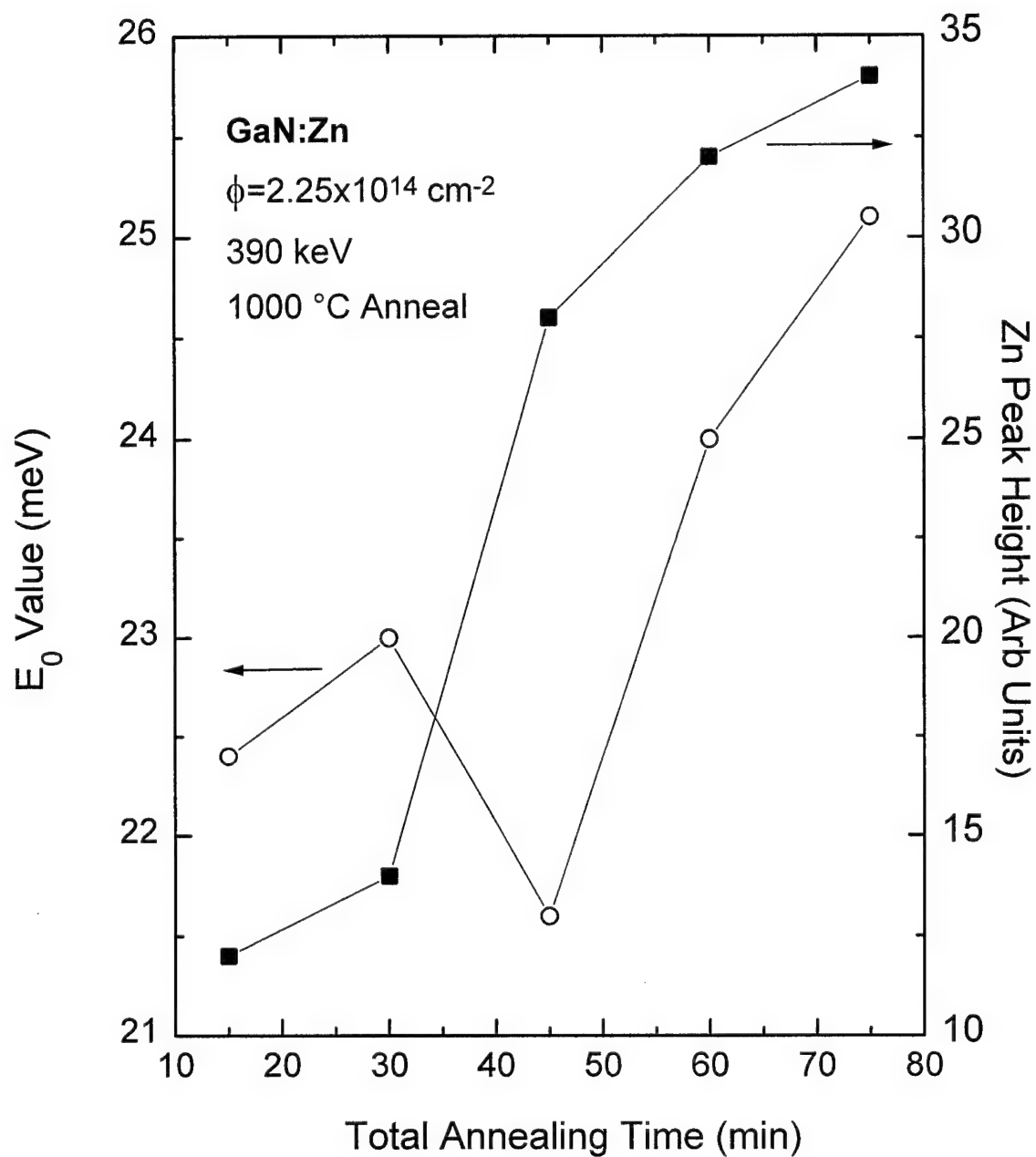
Figure 5-29. E_0 value and Zn 2.86 eV peak height as a function of annealing time in NH_3 for GaN implanted with Zn to a dose of 2.25×10^{14} cm^{-2}.

only a 12% change in the absorption edge slope was observed for annealing times above

15 min. Thus, the GaN lattice appears to recover after only a 15 min annealing time at

1000 °C. In fact, the E_0 value showed an increasing trend with annealing time which may

be indicative of further damage caused by annealing. The Zn peak intensity was also

plotted in Figure 5-29. A factor of three increase was observed as total annealing time

increased. Thus, although lattice damage repair annealed quickly, the activation of the Zn

luminescence center appeared to require longer annealing times at a temperature of 1000

°C. Furthermore, the activation rate slowed after 60 minutes of annealing time. Thus,

additional annealing time would appear to activate additional Zn centers, but at a lower

rate.

To examine the effects of annealing gas environments, two identical samples were

annealed under identical conditions except for the presence of flowing N_2 or NH_3 gas.

The results showed a striking difference. Both samples were implanted with Zn at a dose

of 1×10^{14} cm^{-2} and annealed at 1000 °C for 90 min. When the samples were illuminated

from the GaN face with 150 mW of 257 nm laser line, and examined with 1 mm slits (0.2

slit height setting) the N_2 anneal showed only very weak, broadband luminescence in the

yellow and red as shown in Figure 5-30 and no Zn luminescence was observed. On the

other hand, the NH_3 anneal, showed a strong Zn peak at 2.86 eV. Also, D-A and near-

edge luminescence was evident in the NH_3 anneal. When the samples were illuminated

from the edge, both showed Zn luminescence. However, even under edge illumination,

the NH_3 anneal had the most intense Zn peak. The NH_3 anneal did not show the distinct
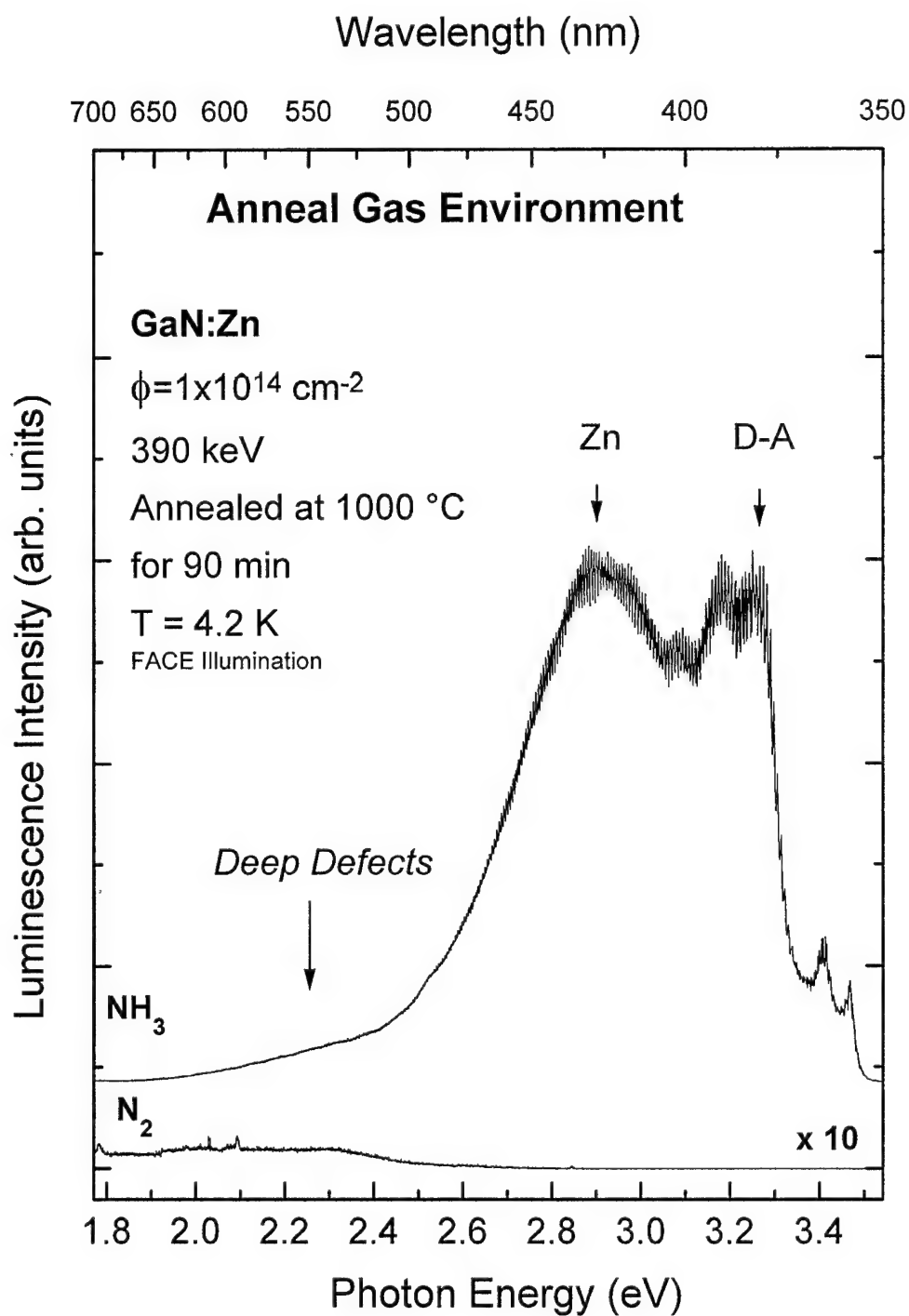
Figure 5-30. Photoluminescence at 4.2 K for GaN implanted with Zn to a dose of 1×10^{14} cm^{-2} and annealing in either NH$_3$ or N$_2$ for 90 min at 1000 °C.

3.27 eV D-A peaks under-edge illumination; however, broadband luminescence was observed from the bandedge to the Zn peak. The absence of the 3.27 eV D-A bands in the NH_3 anneal when illuminated from the edge demonstrated that the D-A peaks must have originated near the surface of the sample. This result was consistent with enhancement of D-A emissions resulting from NH_3 annealing as previously discussed for un-implanted, annealed samples. Zn luminescence was also clear from the data of sapphire side illumination of the N_2 annealed sample. This result proved that although Zn was present and forming luminescence centers in the GaN, the remaining damaged surface layer after the N_2 anneal absorbed the laser excitation resulting in non-radiative de-excitation. This reinforces previously discussed conclusions that there was residual damage in the surface layer of N_2 annealed samples resulting in absorption of the laser energy with subsequent non-radiative decay. Furthermore, these data reinforced the conclusion that the NH_3 annealing environment may enhance Zn activation.

An experiment was conducted in order to examine the damage caused by annealing in the NH_3 gas environment. Two identically implanted samples with a dose of 2.25×10^{14} cm^{-2} at 390 keV energy were annealed together at 1050 °C for 90 min; however, one sample was left with it's GaN:Zn surface exposed to the NH_3 environment, while the other was matched face-to-face with an un-implanted GaN sample. This second sample will be referred to as the proximity-cap annealed sample. Proximity-cap annealing should in theory provide some degree of additional nitrogen over-pressure during annealing. Since nitrogen has a higher over-pressure than gallium, the exposed sample should be more susceptible to surface depletion of nitrogen than the proximity-

cap annealed sample. However, gases from the NH_3 environment may still pass between the two proximity-cap annealed samples since they are only loosely covering one another. Low temperature photoluminescence was performed by illuminating both samples from the face since the surface layer was of most interest. The result shown in Figure 5-31 revealed that the proximity-cap annealed sample had a strong D-A and yellow luminescence. The presence of etalon peaks signified a smooth GaN surface. On the other hand, the exposed sample had a white, opaque appearance. The exposed sample showed only weak Zn luminescence and overall lower luminescence for the yellow/green peak. Thus, it was clear that the exposed sample had higher laser absorption at the surface which resulted in increased non-radiative decay. The D-A peaks present in the proximity-cap anneal sample were greatly enhanced compared to the as-grown sample's D-A spectrum. However, the exciton peak was quenched by Zn implantation and annealing. The results of this experiment were unclear. Although some luminescence signal was apparent in the expected Zn peak location for the proximity-cap annealed sample, the D-A signal dominated. Thus, proximity-cap annealing did appear to afford some protection of the GaN surface, but it cannot be said to be beneficial for Zn activation. The Zn signal may be enhanced relative to the open faced annealed sample, but it was very small relative to the D-A signal, and did not dominate the proximity-cap annealed sample's spectra.
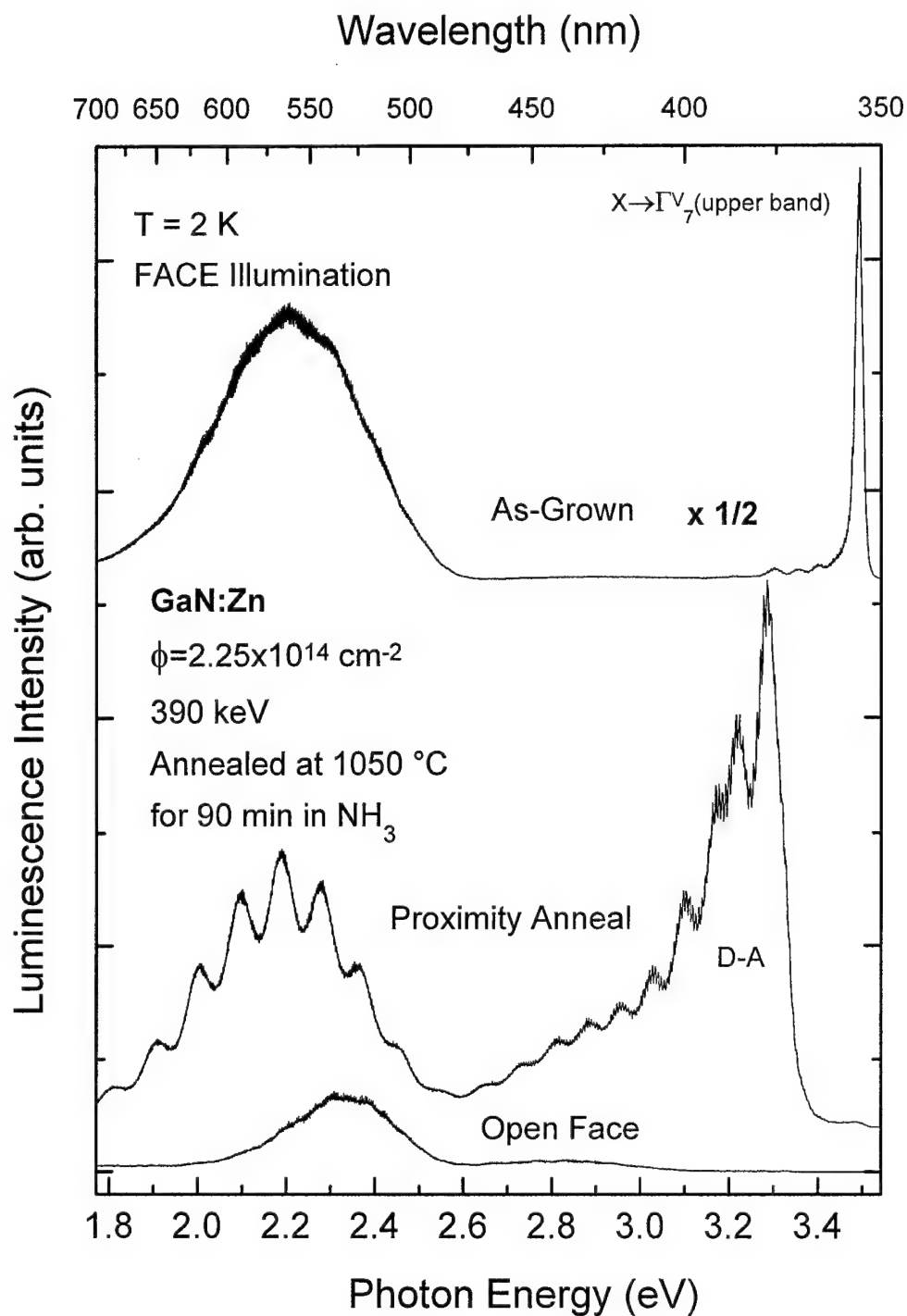
Figure 5-31. Photoluminescence at 2 K for GaN implanted with Zn to a dose of 2.25×10^{14} cm^{-2} and annealed at 1050 °C for 90 min in NH$_3$ by the proximity-cap or open face annealed method.

Since three different doses of Zn were implanted, a limited comparison of dose effects was possible. Figure 5-32 shows spectra taken with 150 mW laser power, 1000 μm slits, and the 0.2 slit height setting. All samples were annealed at 1000 °C for 90 min in NH_3, and were aligned for maximum intensity on the 355 nm luminescence line. The lowest dose sample, 1×10^{13} cm^{-2}, showed no signs of the Zn luminescence peak. In fact, the spectrum was very similar to as-grown except that the exciton peak has shifted from the $X\rightarrow\Gamma_7^V$ (upper band) to the $(D,X)\rightarrow\Gamma_7^V$ (upper band) transition. Thus, implantation damage and subsequent annealing must have resulted in the creation of V_N. For the higher dose samples implanted, at 1×10^{14} and 2.25×10^{14} cm^{-2}, both showed strong Zn luminescence and a quenching of the near edge luminescence. The Zn peak was more intense in the highest dose sample by a factor of 1.9. This value was not substantially different from the dose difference factor of 2.25. Also, the yellow/green luminescence was strongest in the highest dose sample as would be expected if this peak was Zn related.

The physical origin of the Zn related peaks is still disputed in the literature. To gain additional information about these peaks, an intensity dependence study was performed for the samples implanted at 390 keV with a dose of 2.25×10^{14} cm^{-2} and annealed at 1050 °C for 90 min in NH_3. Figure 5-33 shows the resulting spectra as laser intensity was varied by two orders of magnitude. The spectra have been normalized on the 2.8 eV Zn peak to more clearly show the relative height of the yellow/green peak. A clear change in the relative heights of the two main peaks was observed. At high
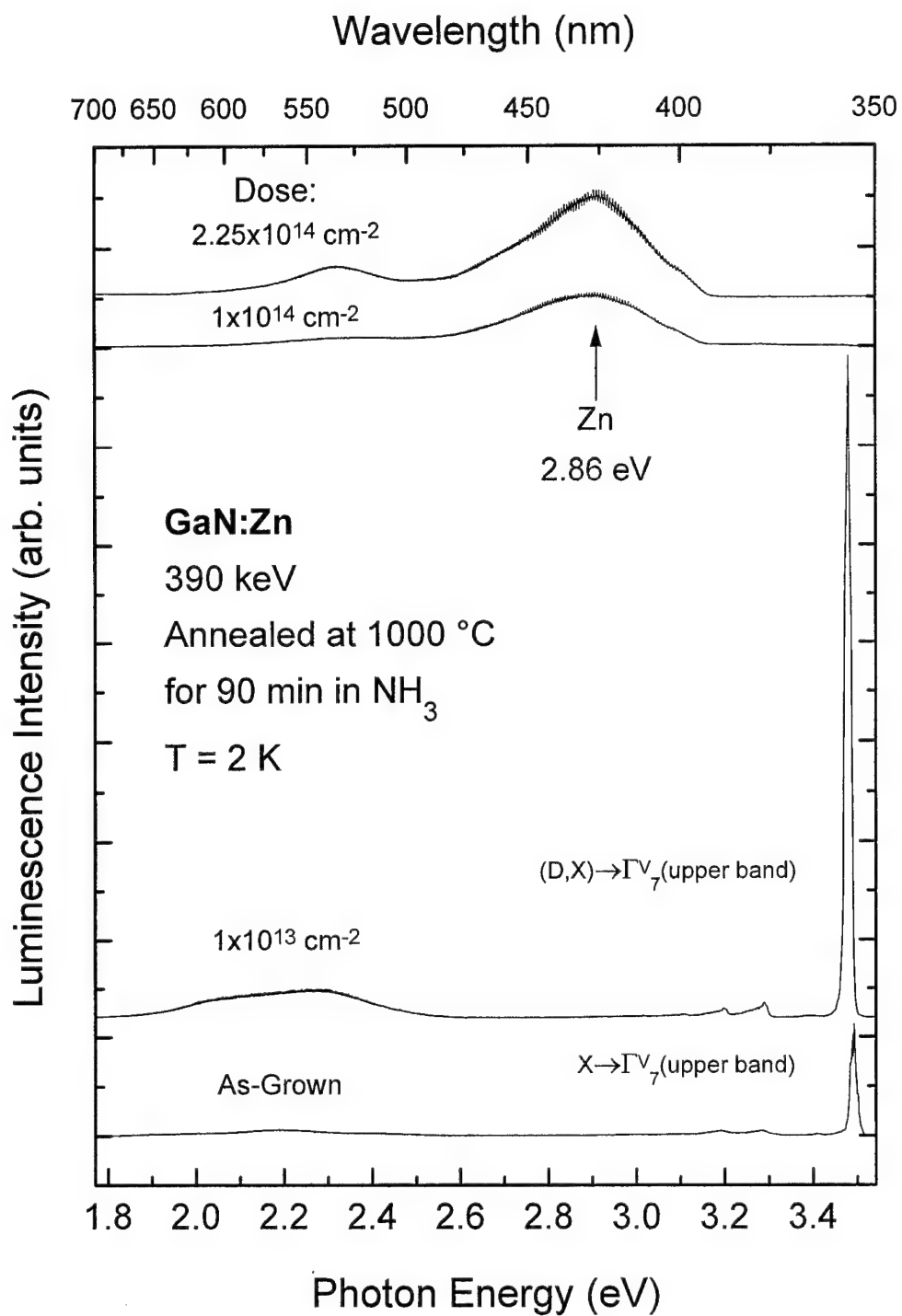
Figure 5-32. Photoluminescence at 2 K for GaN implanted with Zn to three different doses and annealed for 90 min at 1000 °C in NH₃.
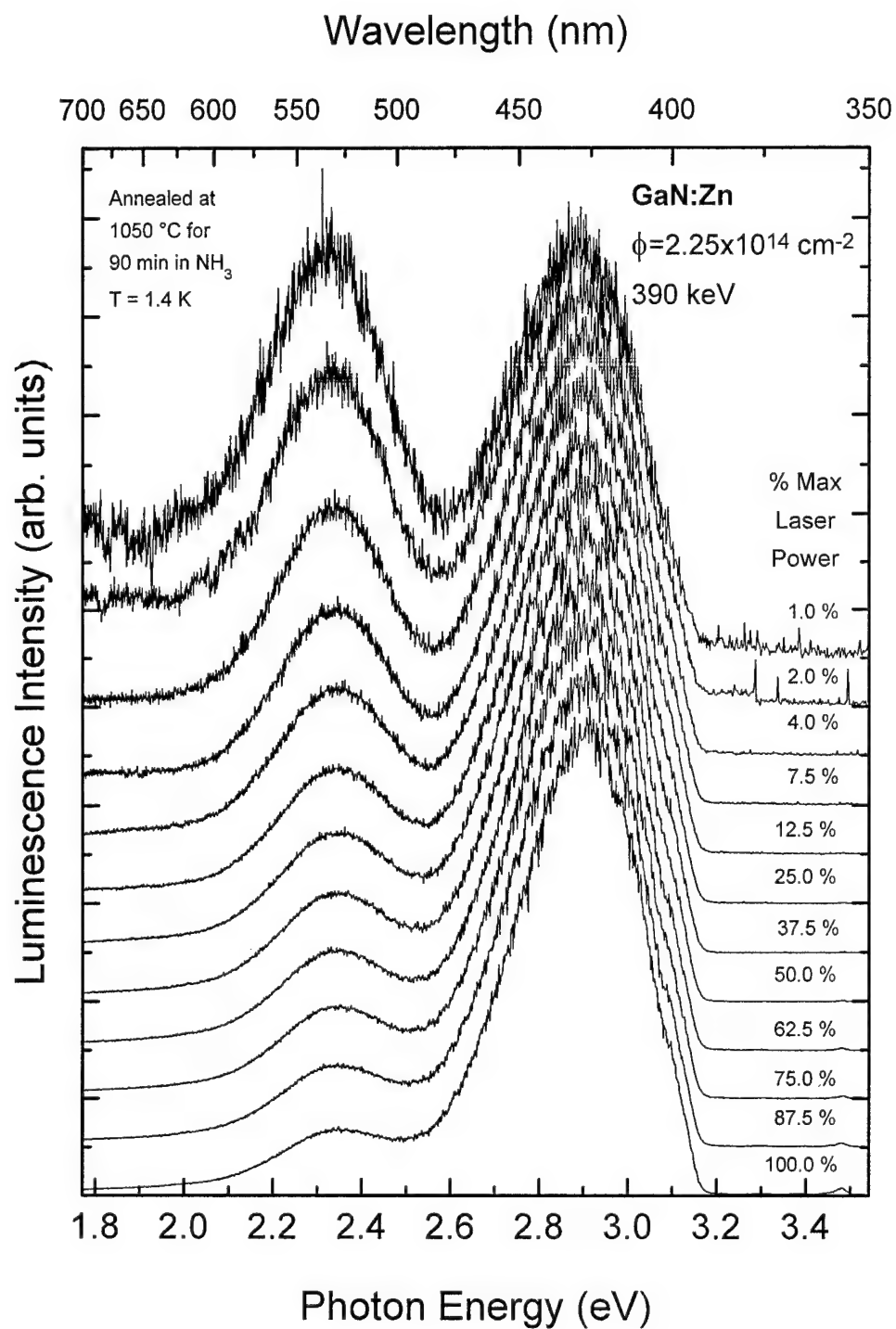
Figure 5-33. Photoluminescence spectra taken at 2 K of GaN implanted with Zn to a dose of 2.25×10^{14} cm^{-2} and annealed in NH$_3$ for 90 min at a temperature of 1050 °C with the spectra normalized on the Zn peak.

excitation intensities, the Zn peak dominated whereas at the lower excitation intensities, the two peaks were of comparable magnitude. The peaks showed no wavelength shift with excitation intensity and the FWHM of the blue peak remained constant at 300 meV. The FWHM and position of the yellow/green peak also appear to remain constant, although there is a greater uncertainty because of the overwhelming intensity of the Zn peak at higher excitation intensity. Figure 5-34 shows the peak intensities of the two peaks as a function of laser power, and Figure 5-35 shows the ratio of the blue to yellow/green peaks. The yellow/green peak experienced a region of almost linear growth after a plateau occurred in the initial more rapid growth at a low intensity. This may indicate that this yellow-green peak originated from the surface layer. The Zn peak also showed rapid initial growth at a rate higher than the yellow/green peak. The incident laser beam was mostly absorbed within the surface layers. As the laser intensity increased, gradually more laser penetrated the sample and thus the growth rates slowly increased. The blue peak increased at a much higher rate as laser power increased further as would be expected since the laser beam penetrated much deeper within the GaN. At the higher excitation intensities, a super-linear growth in the Zn luminescence occurred. The yellow/green also showed signs of super-linear growth. No narrowing of the FWHM was observed. Such a super-linear growth can often indicate the onset of stimulated emission. However, in this case, the laser power was still low and most of the laser beam was absorbed in the Zn layer below the damaged surface. This may simply be the result of a non-linear depth profile for the Zn luminescence centers.
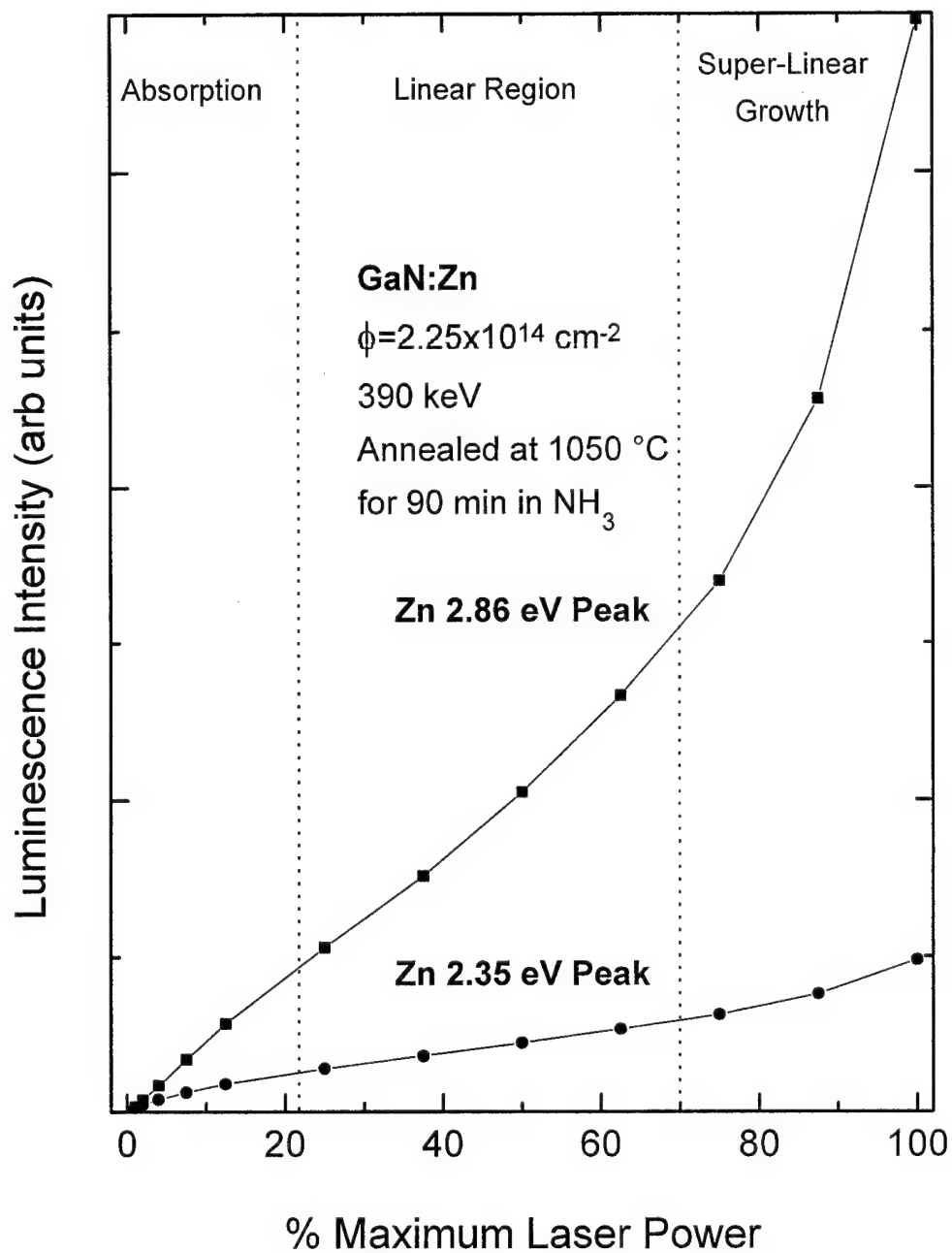
Figure 5-34. Zn 2.86 eV photoluminescence peak intensity taken at 2 K for GaN implanted with Zn to a dose of 2.25×10^{14} cm^{-2} and annealed in NH$_3$ for 90 min at a temperature of 1050 °C as a function of excitation intensity.
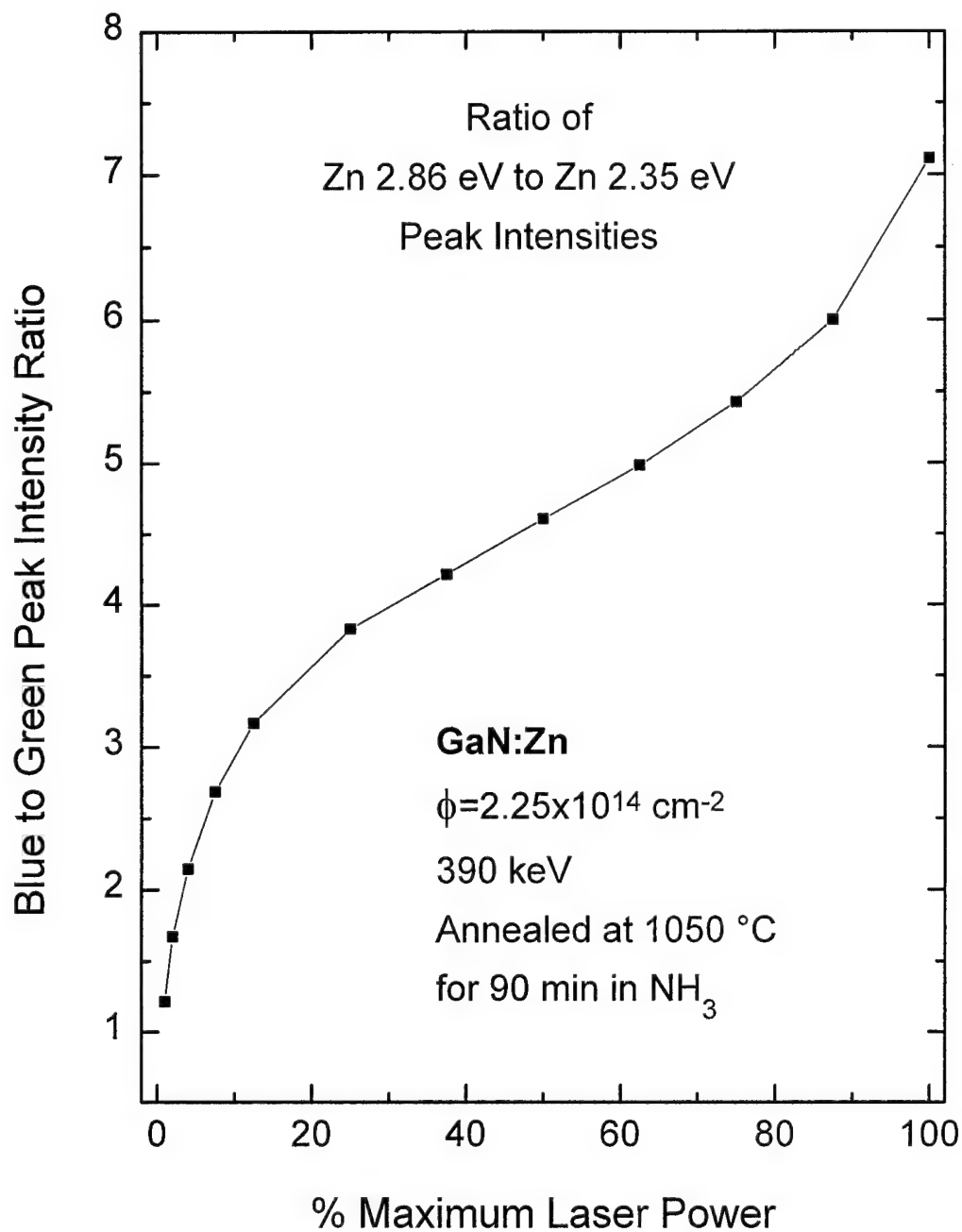
Figure 5-35. Zn 2.86 eV intensity ratio of blue to yellow/green photoluminescence peak intensities taken at 2 K for GaN implanted with Zn to a dose of 2.25×10^{14} cm^{-2} and annealed in NH$_3$ for 90 min at a temperature of 1050 °C as a function of excitation intensity.

A temperature dependence study was undertaken on the most intense Zn sample. This was the sample implanted with 390 keV Zn at a dose of 2.25×10^{14} cm^{-2} annealed at a temperature of 1050 °C for 90 min in NH$_3$. Difficulties were encountered in transmitting the laser intensity through the dewar windows as temperatures increased. It was believed that contamination on the dewar windows may have condensed forming an opaque film. This effect made it impossible to keep the laser intensity on the sample stable as temperature was changed. Efforts made to mitigate this difficulty were unsuccessful. Thus, the only valid data obtained for the temperature dependence study were the peak locations and FWHM as a function of temperature. The Zn peak was found to persist up to temperatures above 200 K with virtually no change in FWHM. The Zn peak position also showed no shift at all over the full temperature range. The yellow/green peak shift with temperature as shown in Figure 5-36. This peak was suspected to differ from the yellow 2.25 eV peak seen in as-grown GaN based on its different energetic location at low temperature. The temperature dependence confirmed this suspicion. Unlike the as-grown sample's yellow peak which was expected to shift to lower energy (red shift) with increasing temperature (Ogino and Aoki, 1980), the yellow/green peak observed for Zn implanted GaN shifted to higher energy (blue shift). The total blue shift observed was 80 meV over 225 K. In general, a red shift results from a radiative recombination pinned to a band. A blue shift results from an internal transition at a luminescence center. Thus, this data indicated an internal transition as the origin of this yellow-green peak. This result was very similar to the results of Matsumoto et al. (1974).
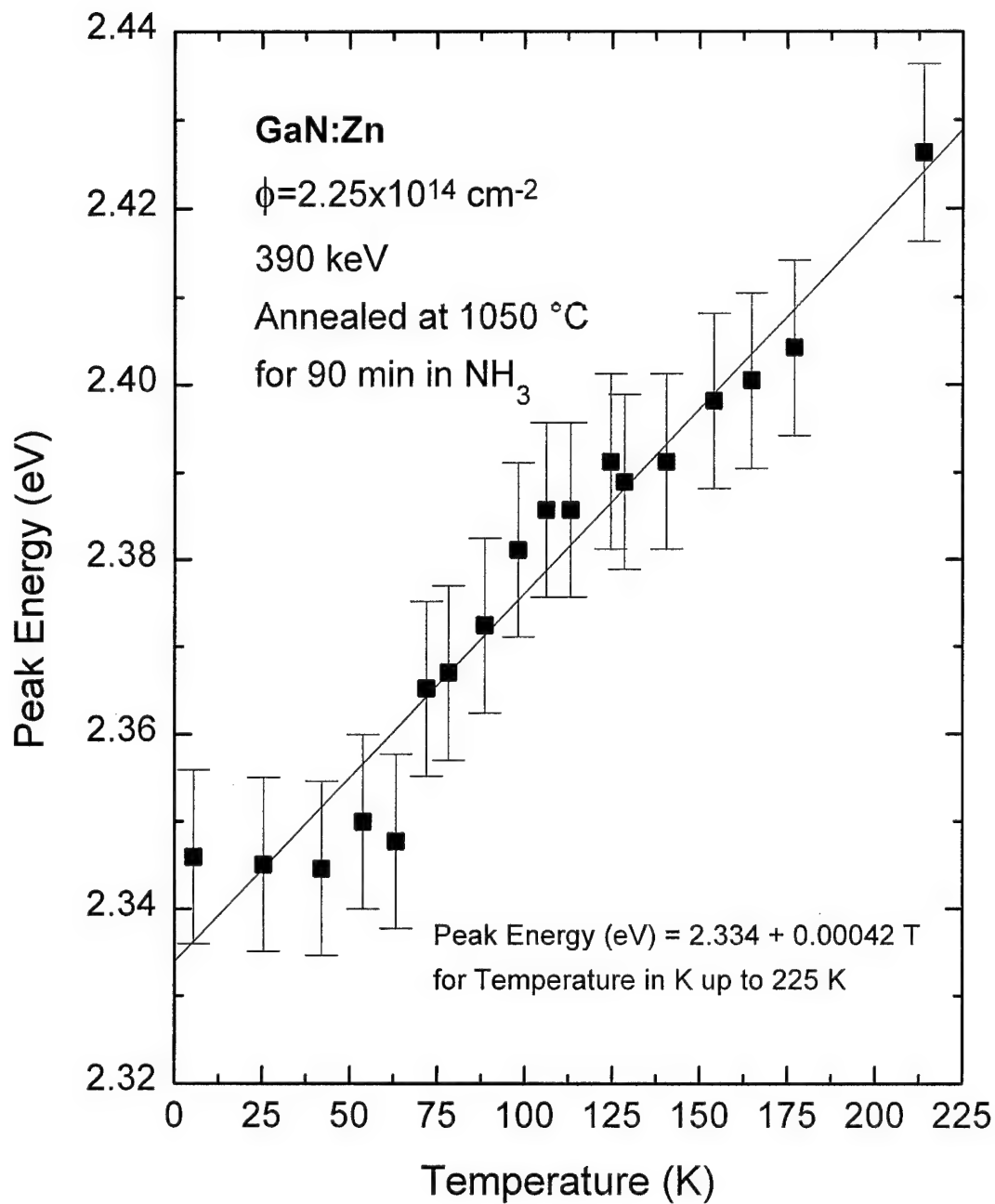
Figure 5-36. Shift in peak energy for the Zn yellow/green peak observed as a function of sample temperature for GaN implanted to a dose of 2.25×10^{14} cm^{-2} and annealed in NH$_3$ for 90 min at a temperature of 1050 °C.

In summary, the results for Zn implanted GaN can be broken down into three areas: recovery of the GaN crystalline structure from implantation damage and surface damage, the activation of the Zn luminescence centers, and the nature of the Zn luminescent transitions.

Crystalline damage in Zn implanted GaN has been shown to be largely repaired by furnace annealing in either NH_3 or N_2 at temperatures approaching 1000 °C for 90 min. A threshold temperature for the observed annealing process of 610 °C was inferred from the data. The repair was rapid at 1000 °C with nearly full recovery of the absorption edge after 15 min in NH_3. An activation energy of 0.437 eV was determined for the annealing process. However, annealing at temperatures above 1000 °C resulted in unrecoverable surface degradation of the GaN:Zn layer. Under an annealing condition of 1050 °C, NH_3 environment for 90 min, the surface turned opaque with a white color and showed increased below bandgap absorption.

The Zn luminescence at 2.86 eV with 300 meV FWHM was observed to occur only for annealing temperatures of 900 °C and above. From barely detected at 900 °C, the intensity of the Zn peak increased up to 1050 °C. However, surface damage at 1050 °C tended to mask the strength of the Zn peak. The highest Zn dose sample at 2.25×10^{14} cm^{-2} showed the strongest Zn luminescence. The fact that no luminescence was seen from the N_2 annealed samples under face illumination demonstrated that luminescence quenching was occurring at the surface. However, N_2 annealing even at 1000 °C resulted in a smooth sample surface with no visible degradation. On the other hand, the NH_3 environment clearly attacks the GaN surface. Thus, the laser quenching in the N_2 anneal

was not due to surface damage during annealing, but resulted from either residual implantation damage not annealed out or additional non-radiative decay somehow resulting from N_2 annealing.

Several interesting properties of the Zn luminescent center at 2.86 eV were observed. The 2.86 eV Zn luminescence showed no change in FWHM over two orders of magnitude of excitation intensity. The sample temperature dependence also showed no change in FWHM. The insensitivity of FWHM and lack of shifts of the Zn peak suggested an internal transition at the Zn center. The Zn peak at 2.35 eV also showed the characteristics of an internal transition not pinned to a bandedge.

Room temperature absorption measurements were performed on all implanted and annealed samples. As was the case for all other implants, the as-implanted samples always showed significantly enhanced below bandgap absorption. After annealing, the absorption was restored to a level intermediate between the as-grown and as-implanted values. Figures 5-37, 5-38, and 5-39 show the E_0 values for carbon-, oxygen-, and silicon-implanted GaN as a function of annealing temperature. The E_0 value for un-annealed, as-implanted samples was plotted at room temperature. Similar to the other implants, the E_0 values found for the annealed samples roughly approached the as-grown E_0 value as annealing temperature increased. Significant bandedge recovery was evident for the Si implanted sample annealed even at 600 °C. This result was consistent with findings of a 400 °C onset temperature for annealing in GaN:Ar and a 600 °C onset for annealing in GaN:Zn. In the case of the oxygen implanted samples, the E_0 value for the 1050 °C anneal was significantly increased relative to the 1000 °C anneal. This was not the case for the identically annealed carbon implants. Although no Si sample was annealed at 1050 °C, no significant increase was seen in E_0 for the 1000 °C anneal. Thus, oxygen showed evidence of an enhancement in the degradation of the GaN surface layer. This result was similar to Chung and Gershenzon's (1992) finding of an absorption tail for samples grown with intentionally high oxygen content.

The low temperature photoluminescence data were measured for the samples implanted with Si, C, O, and Be. Unfortunately, no luminescence peaks other than the
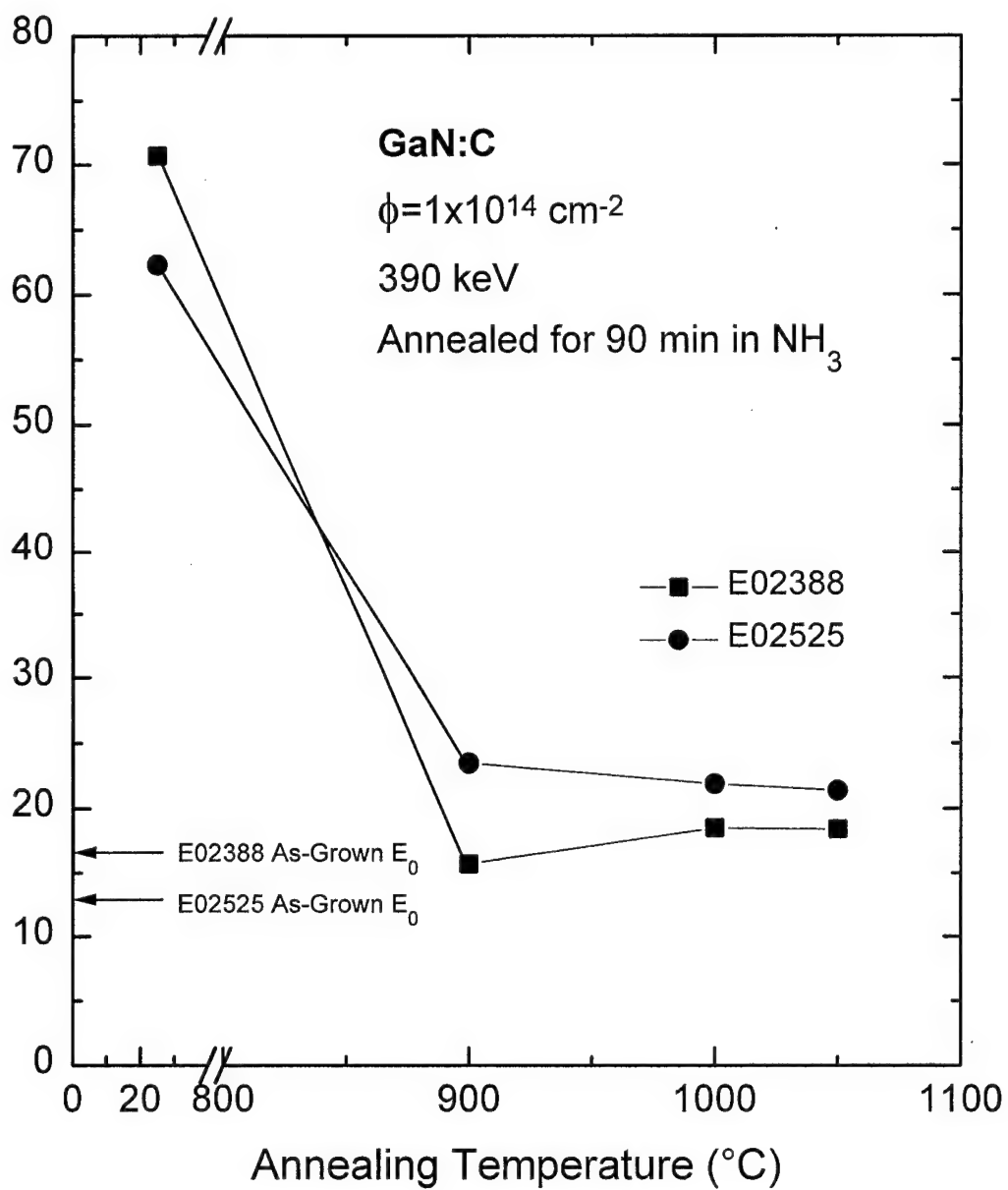
Figure 5-37. Calculated value of E_0 for carbon-implanted GaN as a function of annealing temperature in NH_3.
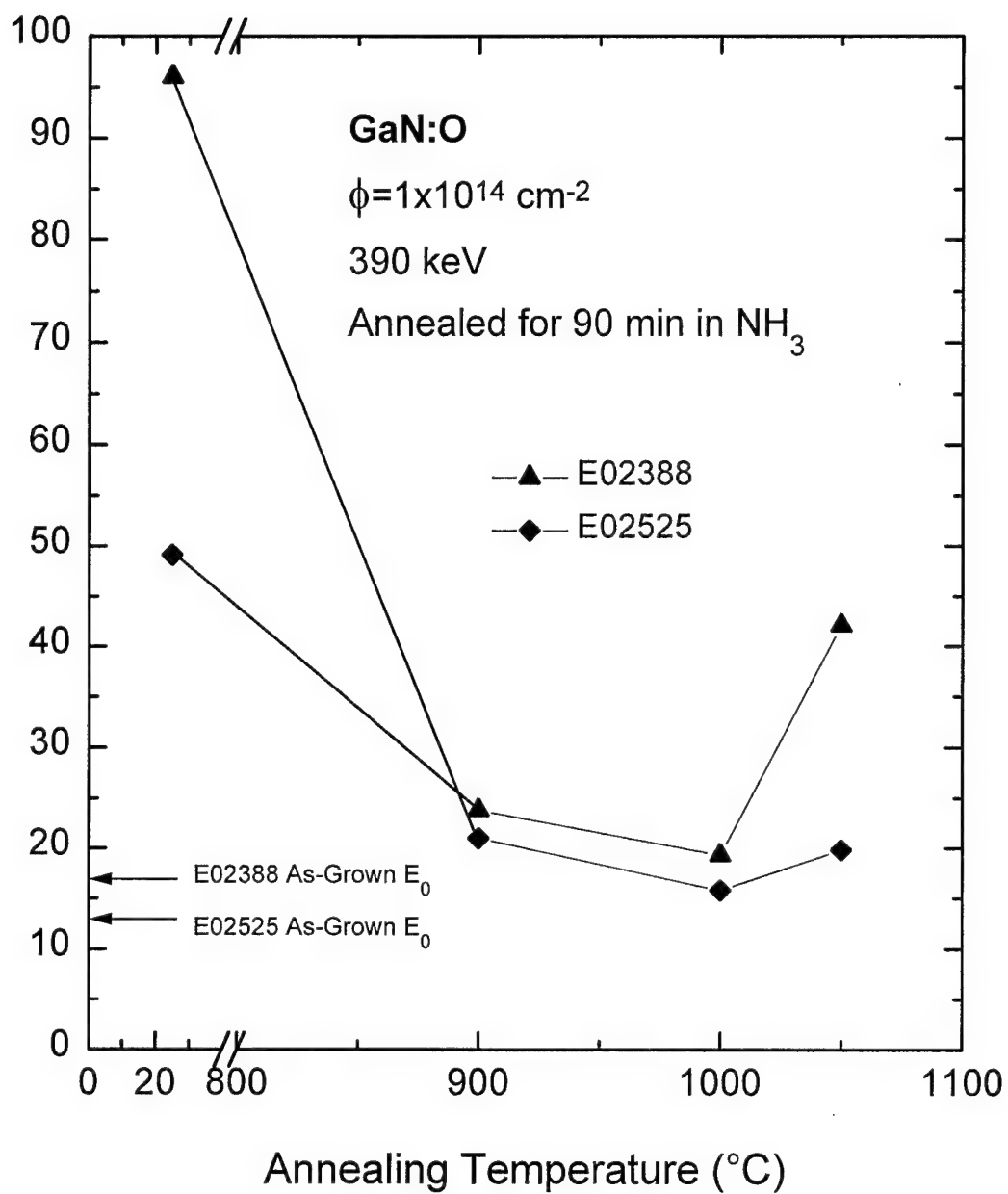
Figure 5-38. Calculated value of E_0 for oxygen-implanted GaN as a function of annealing temperature in NH_3.
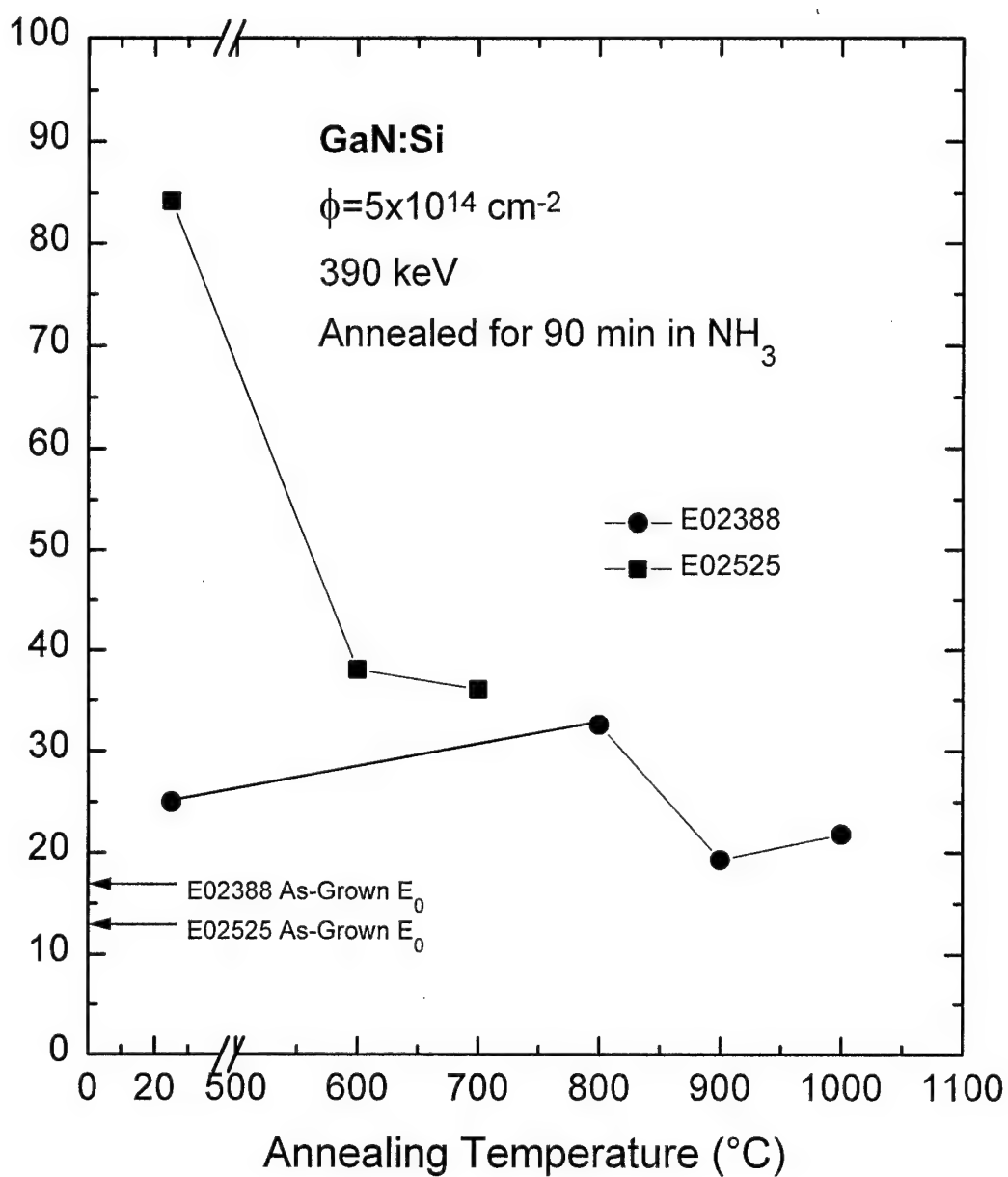
Figure 5-39. Calculated value of E_0 for silicon-implanted GaN as a function of annealing temperature in NH_3.

exciton, D-A, and yellow peak were observed. Some general observations can be made however. Luminescence from GaN implanted with Si at an energy of 390 keV to a dose of 5×10^{14} cm^{-2} was always dominated by D-A emissions with the exciton and yellow bands usually being quenched as shown in Figure 5-40. This result was similar to PL reported for MOCVD grown Si-doped GaN (Nakamura *et al.*, 1992c). The only report of luminescence from Si implanted GaN indicated only yellow band emissions (Pankove and Hutchby, 1976). The D-A peaks were broadened in relation to the well resolved D-A peaks seen in the as-grown samples. Although the D-A peaks dominated in Si implanted GaN, the peak intensity was below the as-grown sample's intensity. That is, there was decreased luminescence efficiency and a quenching of the exciton and yellow peaks.

For the GaN implanted with carbon at an energy of 390 keV with a dose of 1×10^{14} cm^{-2}, the yellow band showed a substantial increase in intensity as annealing temperature was increased to 1000 °C for the as seen in Figure 5-41. This result was not inconsistent with results suggesting carbon is linked to the yellow band (Ogino and Aoki, 1980). Again, Pankove and Hutchby (1976) observed luminescence observed in the yellow band for GaN:C.

The low temperature luminescence from GaN implanted with oxygen at an energy of 390 keV with a dose of 1×10^{14} cm^{-2} was quite unremarkable as seen in Figure 5-42. It can be noted, however, that these implants did not show a peak at 3.424 eV which was observed by Chung and Gershenzon (1992). However, the oxygen peak concentration
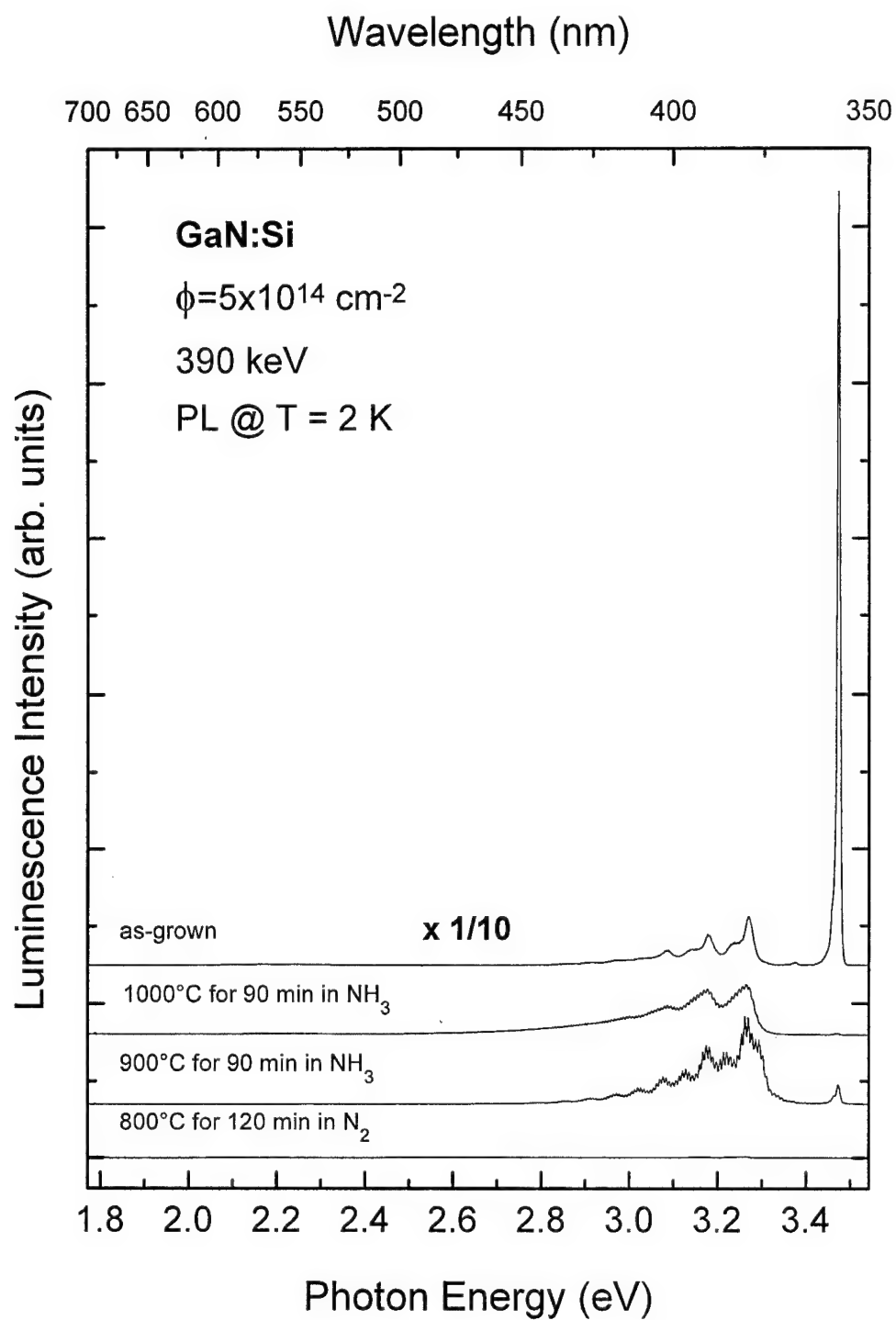
Figure 5-40. Photoluminescence spectra at 2 K of GaN implanted with silicon at 390 keV to a dose of 5×10^{14} cm^{-2} and annealed at various temperature along with as-grown GaN spectrum.
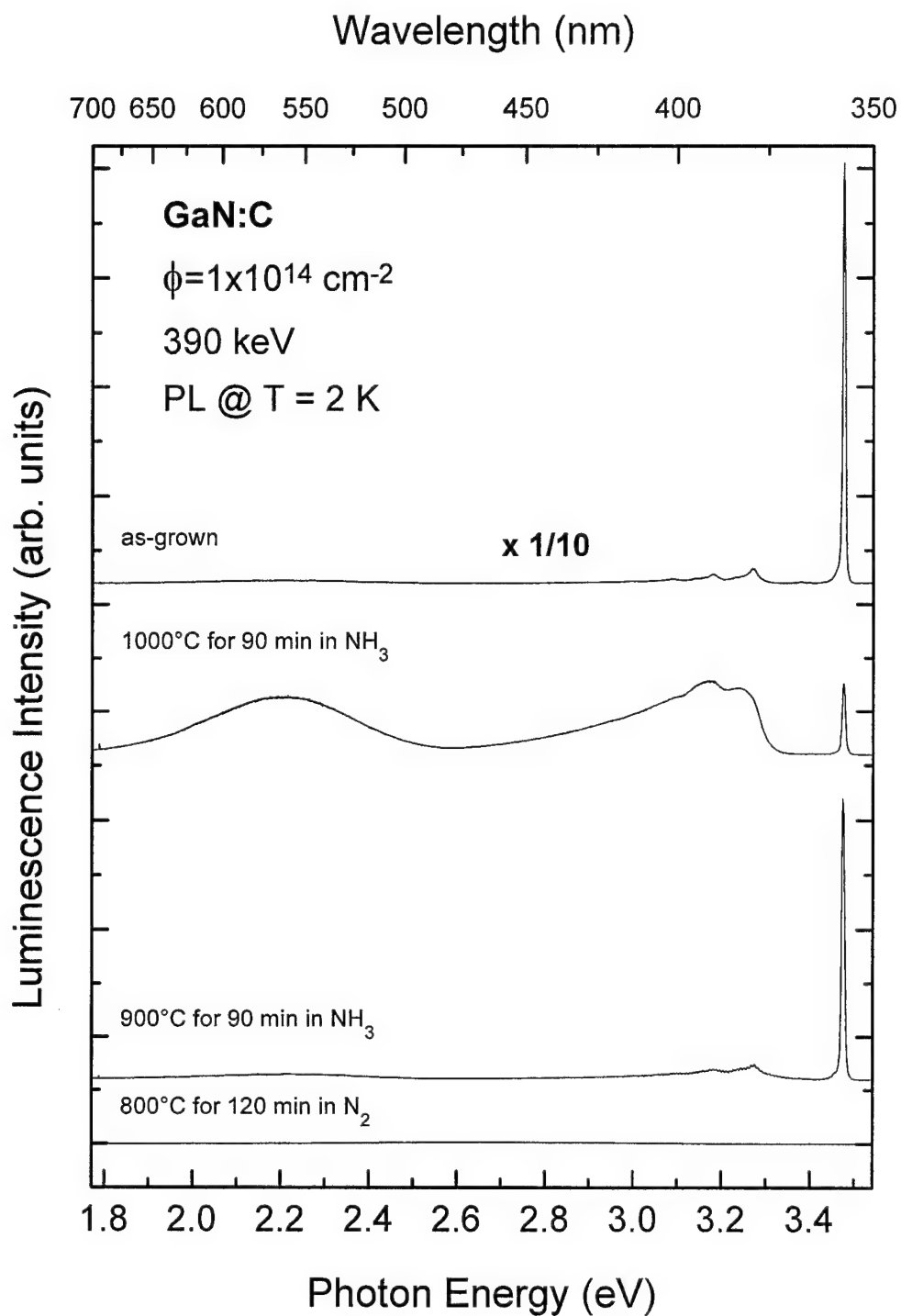
Figure 5-41. Photoluminescence spectra at 2 K of GaN implanted with carbon at 390 keV to a dose of 1×10^{14} cm^{-2} and annealed at various temperature along with as-grown GaN spectrum.
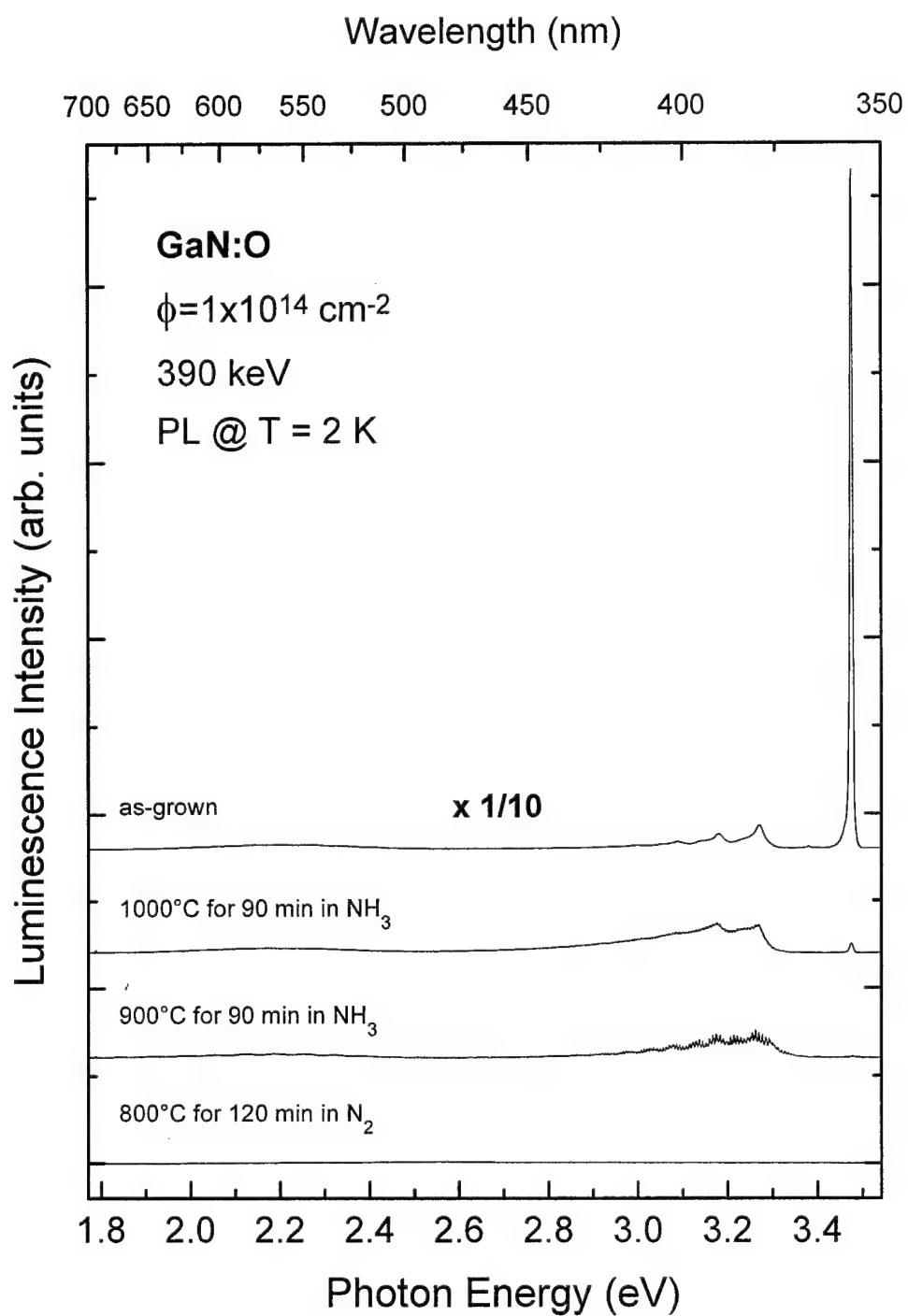
Figure 5-42. Photoluminescence spectra at 2 K of GaN implanted with oxygen at 390 keV to a dose of 1×10^{14} cm^{-2} and annealed at various temperatures along with as-grown GaN spectrum.

necessary to observe this peak was $\sim 10^{20}$ cm^{-3}, which was well above the concentration used in this study.

GaN samples implanted with beryllium and annealed in either NH$_3$ or N$_2$ also showed no new luminescence peaks. However, apart from a large overall intensity decrease, the PL spectrum of as-grown GaN was nearly completely recovered as annealing temperature was increased. Figure 5-43 shows low temperature PL for GaN:Be at an energy of 200 keV to a dose of 5×10^{13} cm^{-2} and annealed in N$_2$ for 20 min at various temperatures. The exciton peak intensity for the 900 °C anneal was about 1 % of the as-grown sample's exciton peak intensity. The intensity of the D-A peaks also decreased with annealing temperature for these samples. The yellow peak showed a slight increase in intensity as annealing temperature was increased as compared to the as-grown samples. However, the yellow peak did not show significant enhancement in contrast to a previous report on Be-implanted GaN (Pankove and Hutchby, 1976). No unique Be luminescence peaks have been reported yet in the literature.

GaN:Be samples were also annealed in NH$_3$ environment as shown in Figure 5-44. The sample annealed at 900 °C for 90 min recovered it's exciton peak intensity to a level of 12 % of the as-grown samples' value. The 1000 °C anneal produced an even better recovery to a value of 27 % of the as-grown samples peak intensity. Thus, NH$_3$ annealing resulted in more substantial post-implantation recovery of the near-edge GaN emissions than the N$_2$ annealing.
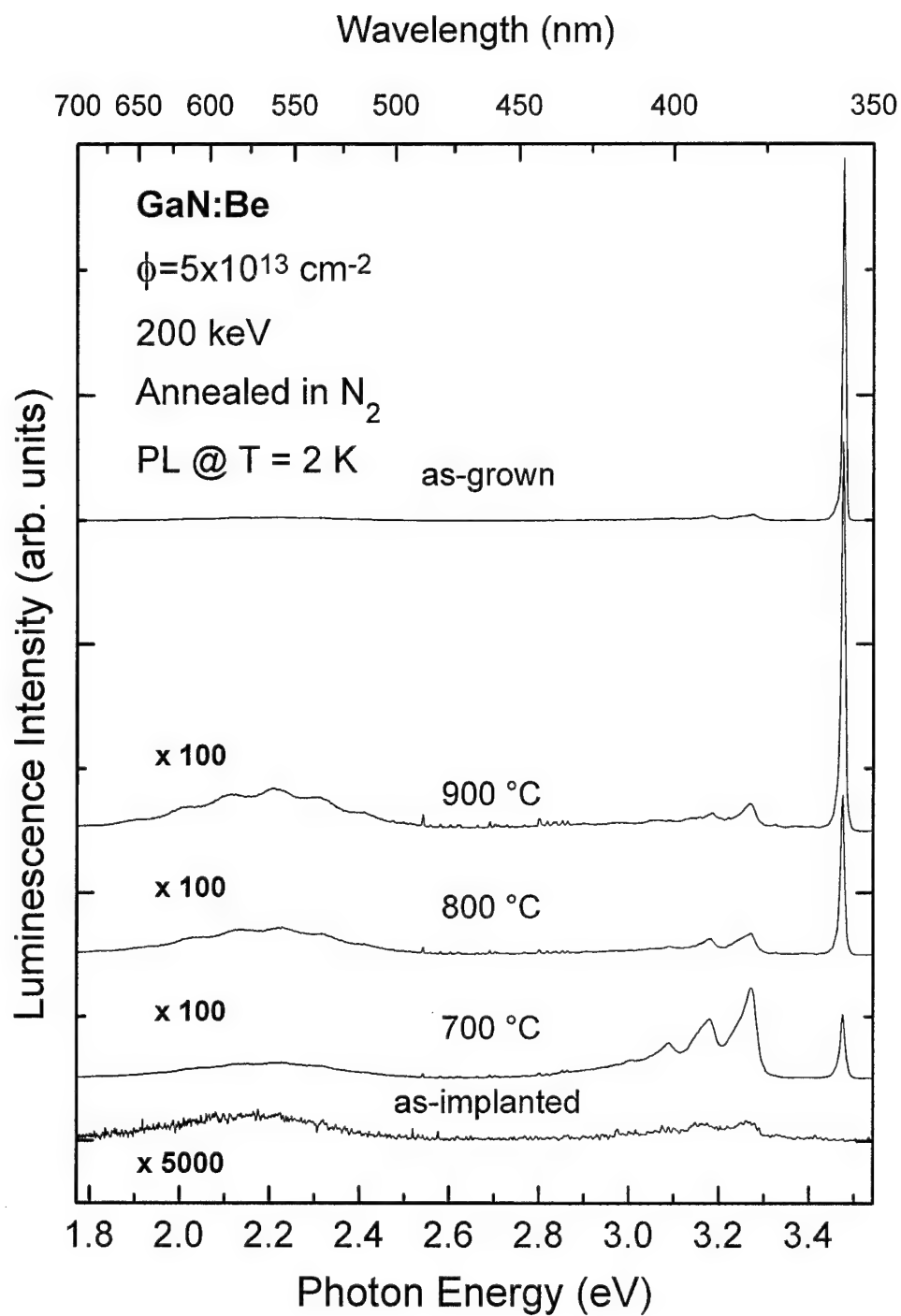
Figure 5-43. Photoluminescence spectra at 2 K of GaN implanted with beryllium at 200 keV to a dose of 5×10^{13} cm^{-2} and annealed at various temperatures in N$_2$ along with as-grown GaN spectrum.
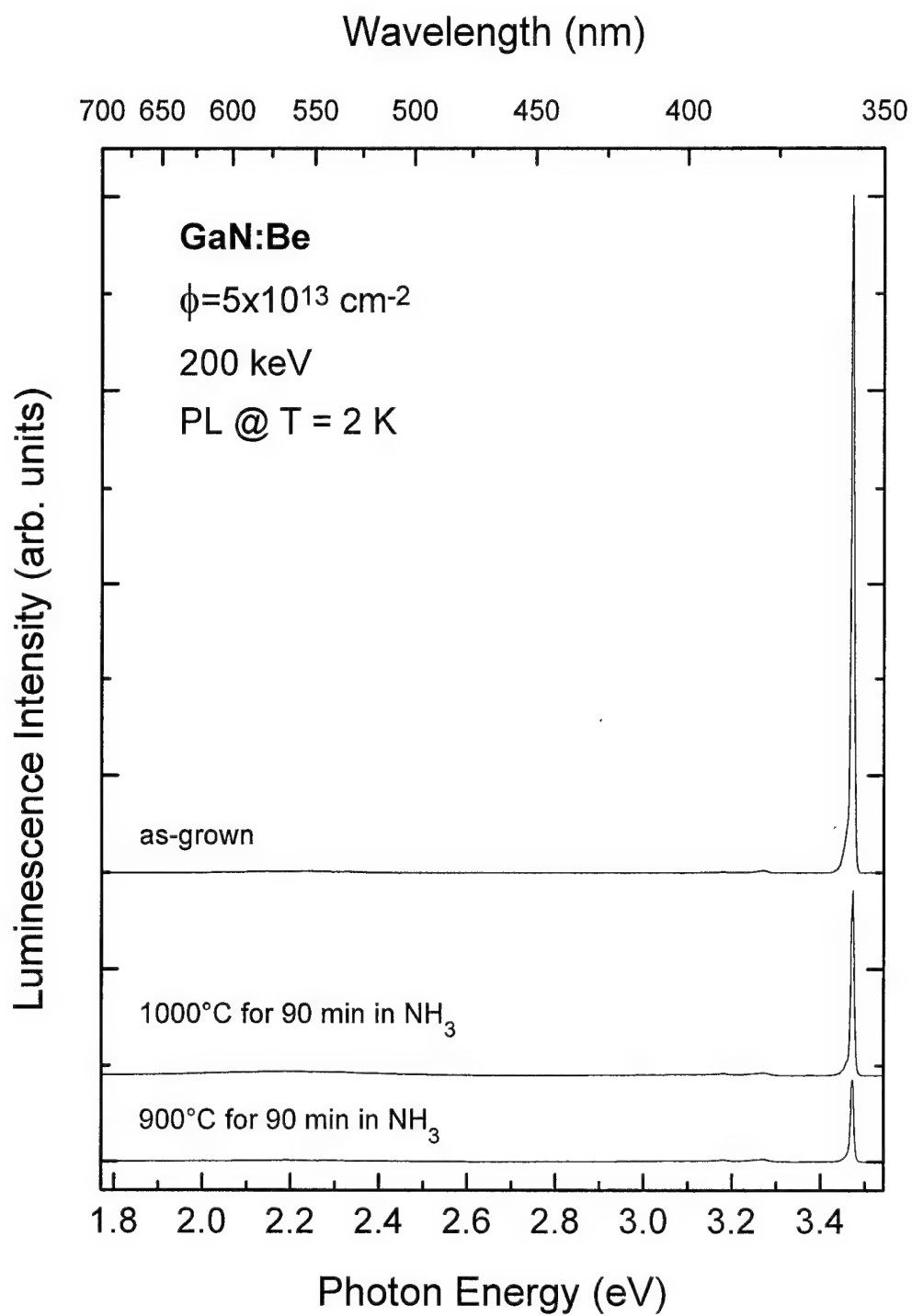
Figure 5-44. Photoluminescence spectra at 2 K of GaN implanted with beryllium at 200 keV to a dose of 5×10^{13} cm^{-2} and annealed at various temperatures in NH$_3$ along with as-grown GaN spectrum.

Since the N_2 annealing data showed a clear trend of recovery, an Arrhenius plot could be made using the natural log of the exciton peak intensity plotted against $1/kT$, where T is the annealing temperature. This analysis, shown in Figure 5-45, gave an activation energy of 880 meV. This energy represents the energy barrier which must be overcome to anneal out the implantation damage.
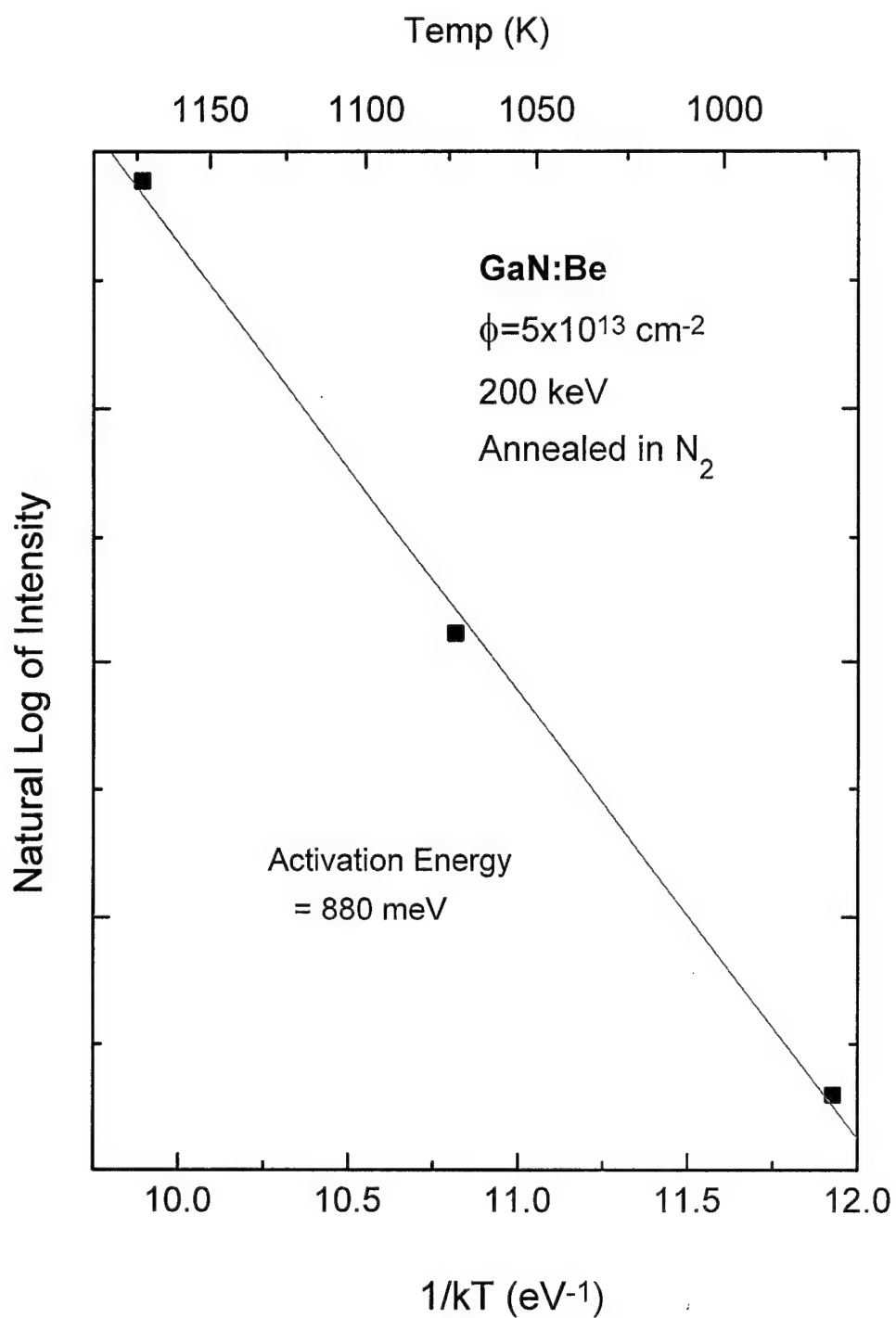
Figure 5-45. Arhennius plot of exciton peak intensity for GaN implanted with beryllium at 200 keV to a dose of 5×10^{13} cm^{-2} and annealed at various temperatures in N$_2$

GaN samples were implanted with Mg at 100 keV with a 5×10^{13} cm^{-2} dose, and 300 keV with doses of 2.2×10^{14} cm^{-2} and 8.2×10^{14} cm^{-2}. A total of five different GaN hosts were implanted with magnesium. These included both MOCVD and MBE grown GaN. The implanted samples were annealed in either NH_3 or N_2 gas environments at temperatures ranging from 700 ° to 1050 °C.

Room temperature absorption measurements were performed on the MOCVD grown samples annealed in an NH_3 environment. MBE grown samples could not be measured since the sapphire substrate side was coated with indium metal during growth. The results were similar to those found for other implants. As-implanted GaN:Mg had increased below-bandgap absorption. Table V-2 lists the implantation and annealing parameters for each sample as well as the value of E_0 calculated from the below-bandgap absorption data measured at room temperature. After annealing, the slope of the absorption edge increased, and attained a value of E_0 intermediate between the values found for as-grown and as-implanted samples. As a general rule, the slope approached the as-grown value as annealing temperature or annealing time was increased. However, the GaN:Mg sample annealed at 1050 °C for 90 min in NH_3 had extensive surface damage which was manifested in an increased E_0 value. Thus, it has been found that a temperature of 1000 °C was the optimal annealing temperature for restoration of the sharp GaN bandedge.

Table V-2. Room Temperature Absorption E_0 Values for GaN:Mg Annealed in NH_3

Substrate	Implant Parameters	Annealing Parameters	E_0 (meV)
E02524	100 keV, 5×10^{13} cm^{-2}	none (as-implanted)	36.8
E02524	100 keV, 5×10^{13} cm^{-2}	900 °C, 90 min	24.6
E02524	100 keV, 5×10^{13} cm^{-2}	1000 °C, 90 min	22.4
E02524	100 keV, 5×10^{13} cm^{-2}	1050 °C, 90 min	44.4
946.1	300 keV, 8.2×10^{14} cm^{-2}	none (as-implanted)	54.5
946.1	300 keV, 8.2×10^{14} cm^{-2}	1000 °C, 30 min	32.0
946.1	300 keV, 8.2×10^{14} cm^{-2}	1000 °C, 90 min	28.8
946.1	none (as-grown)	none	25.4

Low temperature PL was performed on the GaN:Mg implanted and annealed samples. The low energy and low dose GaN:Mg samples, implanted with 5×10^{13} cm^{-2} at 100 keV, showed weak luminescence with no change in the luminescence peaks other than a dramatic decrease in luminescence intensity. Most samples implanted with a dose of 2.2×10^{14} cm^{-2} showed strong luminescence in the D-A region near 3.27 eV or a set of peaks near the bandedge at energies above 3.3 eV.

MOCVD grown GaN:Mg samples implanted at 300 keV with a dose of 2.2×10^{14} cm^{-2} and annealed in N_2 showed an interesting progression of PL signals as annealing temperature was increased from 700 to 900 °C. Figure 5-46 shows low temperature PL spectra from this sample set which was annealed for 90 min in flowing N_2. The 700 °C anneal showed a relatively weak near edge free exciton peak at 3.483 eV. The near edge peak for the 800 °C anneal was nearly three times as intense. This peak was also slightly

Figure 5-46. Photoluminescence spectra taken at 2 K for GaN implanted with magnesium at an energy of 300 keV with a dose of 2.2×10^{14} cm^{-2} and annealed in N_2 at various temperatures for 90 min.

shifted to the red with an energy of 3.381 eV. Since the free exciton and native donor bound exciton peaks band are separated by only 6 meV (Shan *et al.*, 1995a), this shift may indicate the creation of binding centers for excitons. However, there was still no distinct indication of Mg activity. The 900 °C anneal showed a dramatic quenching of the exciton peak and the emergence of two new peaks at lower energies. One peak was centered at 3.426 eV, and the second lower energy peak was centered at 3.311 eV. The origins of these two peaks were uncertain. The position of the higher energy peak was lower than that reported for the Mg bound exciton peak at 3.455 eV (Ilegems and Dingle, 1973). However, due to differences in the GaN material growth methods and Mg concentration levels, this difference may not be taken as conclusive evidence that the Mg bound exciton was not present. The energy separation of these two peaks was 115 meV. Thus, it was unlikely that the second peak was an LO phonon replica of the higher energy peak. Both peaks were quite broad in nature having a FWHM of 40 and 70 meV, respectively. The lower energy peak occurred at an energy above what would be expected for the D-A peak at 3.27 eV. Thus, the lower energy peak may not be a D-A peak. Due to the weak nature of these peaks, only low temperature study was possible. Therefore, no more conclusive evidence as to their origins could be gathered.

Other MOCVD grown GaN samples implanted with Mg at a dose of 2.2×10^{14} cm^{-2} with an energy of 300 keV were annealed in a NH_3 environment. The sample annealed in NH_3 at 1000 °C for 90 minutes exhibited the donor-bound exciton peak at 3.478 eV as shown in Figure 5-47 which was also observed in the as-grown GaN prior to
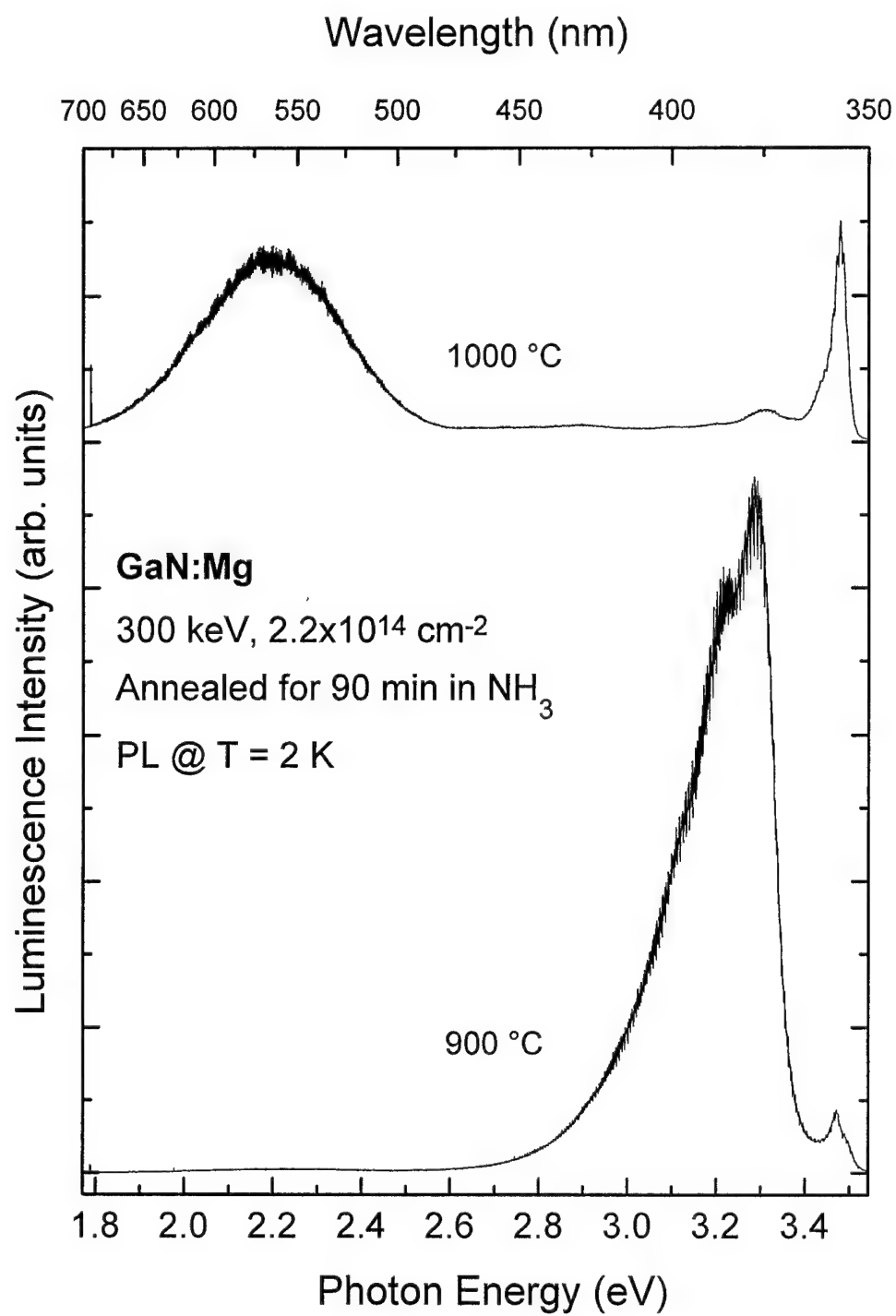
Figure 5-47. Photoluminescence spectra taken at 2 K for GaN implanted with magnesium at an energy of 300 keV with a dose of 2.2×10^{14} cm^{-2} and annealed in NH$_3$ at various temperatures for 90 min.

implantation. In addition, for this sample, a lower energy shoulder of the bound exciton peak appeared. The shoulder appeared at approximately 3.44 eV, which was near the energetic location expected for the Mg acceptor-bound exciton (Ilegems and Dingle, 1973). Also, a new peak appeared just above the energetic location of the D-A band as shown in Figure 5-48. This peak was found at 3.30 eV making it too deep to be an LO phonon replica of either exciton peak. However, this location was similar to the peak found in the 900 °C N_2 annealed sample described above. The energetic location of 3.30 eV and the presence of the Mg acceptor-bound exciton line suggested a Mg related free-to-bound transition as the origin of this peak.

The highest dose samples implanted with 8.2×10^{14} cm^{-2} of Mg at 300 keV were annealed in N_2 at a temperature of 800 °C for 90 or 120 min. Figure 5-49 shows the low temperature PL spectra observed from these samples. Both samples showed only a broad, multiply peaked structure in the D-A spectra region, and thus, the higher Mg dose resulted in a quenching of the near edge luminescence. It should also be noted that this band peaked in the spectral region of the 1 LO phonon replica of the zero phonon D-A line. Furthermore, the D-A peaks have been considerably broadened such that the distinct LO replica structure was difficult to discern. This type of effect was consistent with other reports of Mg doped GaN (Ilegems and Dingle, 1973; Liu *et al.*, 1977). However, the D-A band did not merge into a single peak nor did it shift to lower energy as Mg concentration was increased as has been reported previously (Ilegems and Dingle, 1973; Liu *et al.*, 1977).
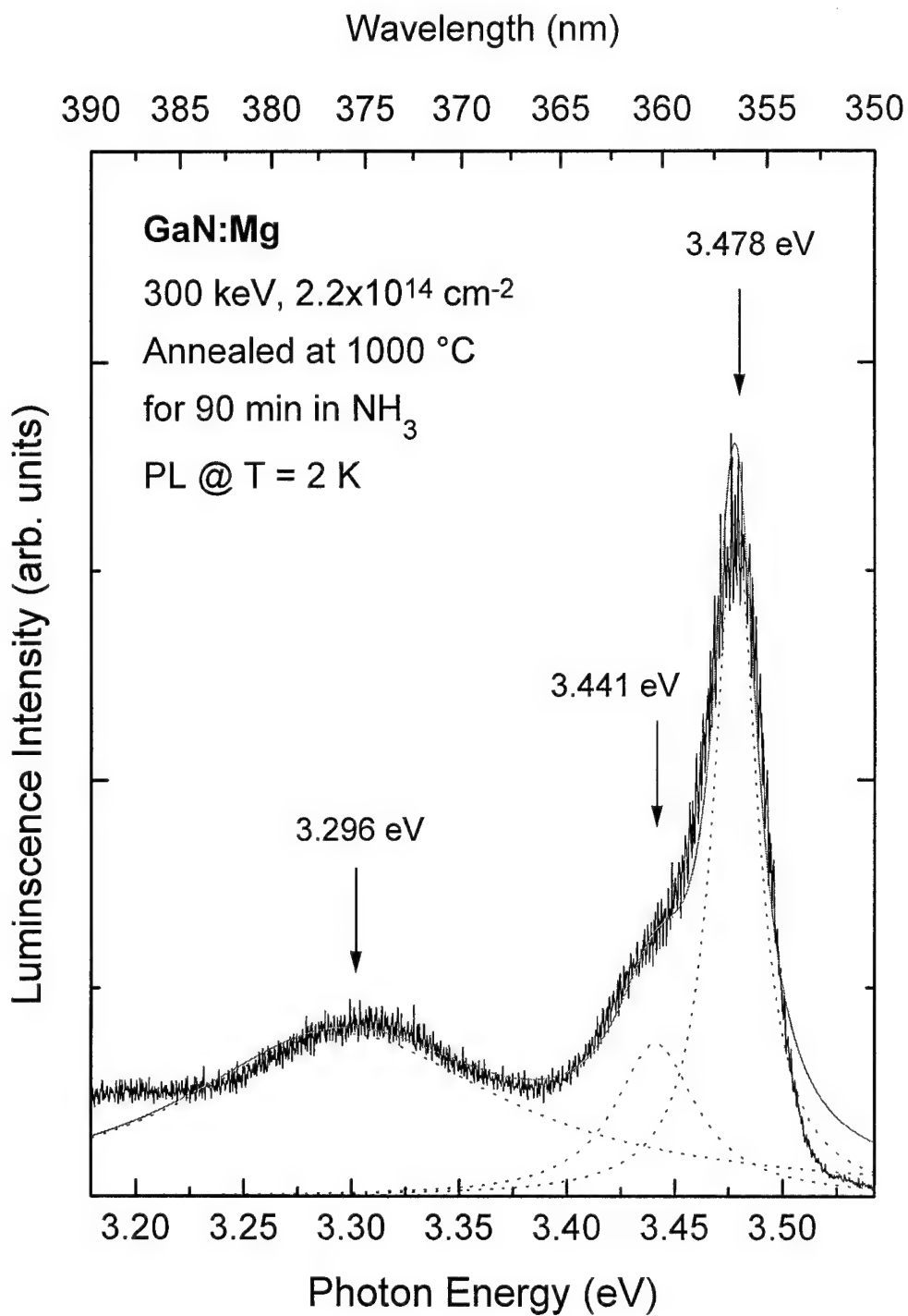
Figure 5-48. Photoluminescence spectra taken at 2 K for GaN implanted with magnesium at an energy of 300 keV with a dose of 2.2×10^{14} cm^{-2} and annealed in NH$_3$ at 100 °C for 90 minutes.
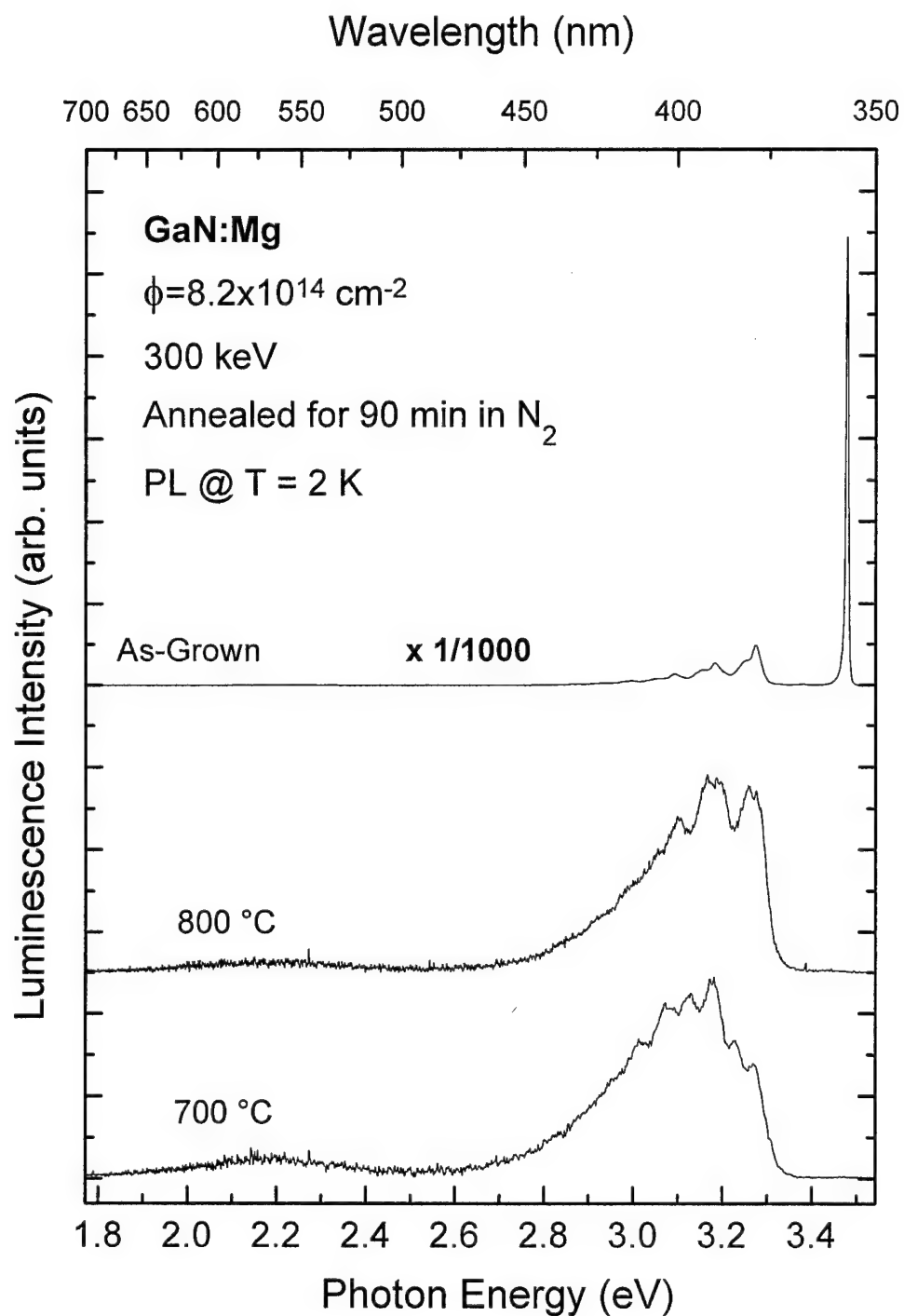
Figure 5-49. Photoluminescence spectra taken at 2 K for GaN implanted with magnesium at an energy of 300 keV with a dose of 8.3×10^{14} cm^{-2} and annealed in N$_2$ at various temperatures for 90 minutes.

MBE grown GaN was also implanted with Mg and annealed in N_2 at temperatures of 700, 800, and 900 °C, and the PL spectra for these samples are shown in Figure 5-50. A peak at 3.43 eV was observed for these samples as well as blue emissions peaking near 2.8 eV especially for the 700 °C annealed samples. Prior to implantation, this particular sample showed low temperature cathodoluminescence peaks at 3.448 and 3.402 eV. However, implantation and annealed induced broadening could have resulted in the overlapping of the original two peaks into one structure at 3.43 eV. Unfortunately, no clear peaks related to Mg have been observed.

In summary, three different dose and energy combinations were implanted in MOCVD GaN and one into MBE GaN. Annealing at a temperature of 1000 °C was found to be optimal for GaN band edge recovery by room temperature absorption. Several unique peaks were observed in the low temperature PL spectra in GaN:Mg annealed at temperatures near 1000 °C in both N_2 and NH_3 atmospheres. The shoulder near 3.44 eV may be the Mg-bound exciton transition. The observed peak near 3.426 eV was in the correct spectra region for the Mg free to bound transition.
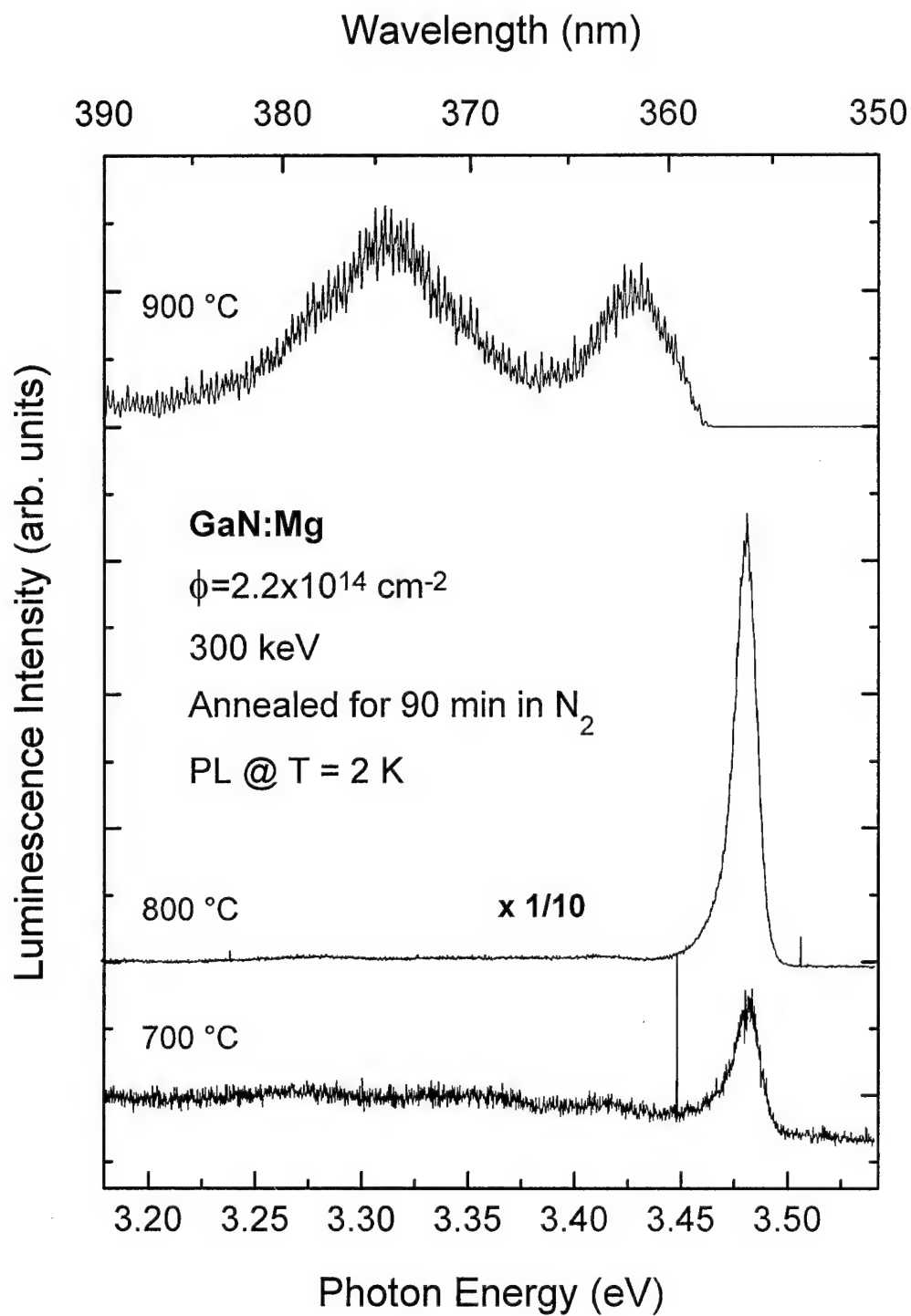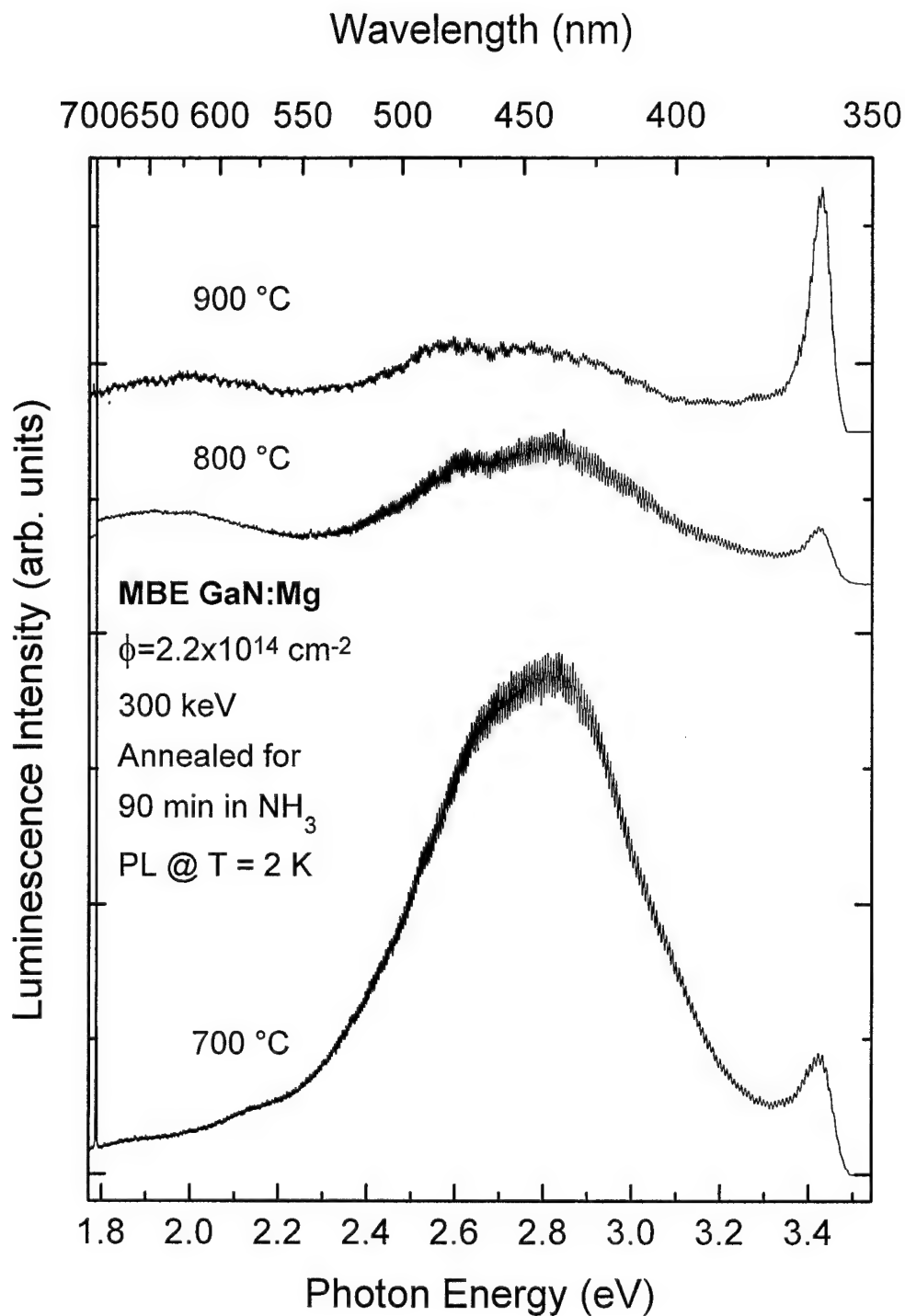
Figure 5-50. Photoluminescence spectra at 2 K for MBE grown GaN implanted with magnesium at an energy of 300 keV with a dose of 2.2×10^{14} cm^{-2} and annealed in N$_2$ at various temperatures for 90 minutes.

MOCVD grown GaN obtained from Honeywell was implanted with Nd at an energy of 910 keV with two different doses, 1×10^{13} and 5×10^{13} cm^{-2}. The samples were furnace annealed using the proximity cap method at temperatures of 700, 800, 900, and 1000 °C for a duration of 90 min. Since severe deterioration of the GaN surface at anneal temperatures above 1000 °C was found to occur for other implants, and the number of available samples was limited, no Nd implanted samples were annealed at temperatures above 1000 °C.

Low temperature PL was performed using the 514.5 nm line of the Ar$^+$ ion laser. Below bandgap excitation photons were used since the RE element Er has been found to be luminescent with laser excitation at these wavelengths (Wilson *et al.*, 1995; Qiu *et al.*, 1995). Nd implanted GaN annealed at 1000 °C revealed strong luminescence emissions from the crystal-field split intra-4f shell transitions associated with Nd^{3+} as shown in Figure 5-51. Three manifolds of lines were observed at low temperature, and were identified as originating from the $^4F_{3/2} \rightarrow {}^4I_{13/2}$ transitions at 1.46-1.57 μm, the $^4F_{3/2} \rightarrow {}^4I_{11/2}$ transitions at 1.09-1.20 μm, and the $^4F_{3/2} \rightarrow {}^4I_{9/2}$ transitions at 0.94-0.98 μm (Pappalardo, 1977).

Also present in the spectra was an intense, broad luminescence peak which was identical in both Nd and Er implanted GaN. This peak was not present in un-implanted GaN, and must therefore be associated with implantation damage. The nature of the
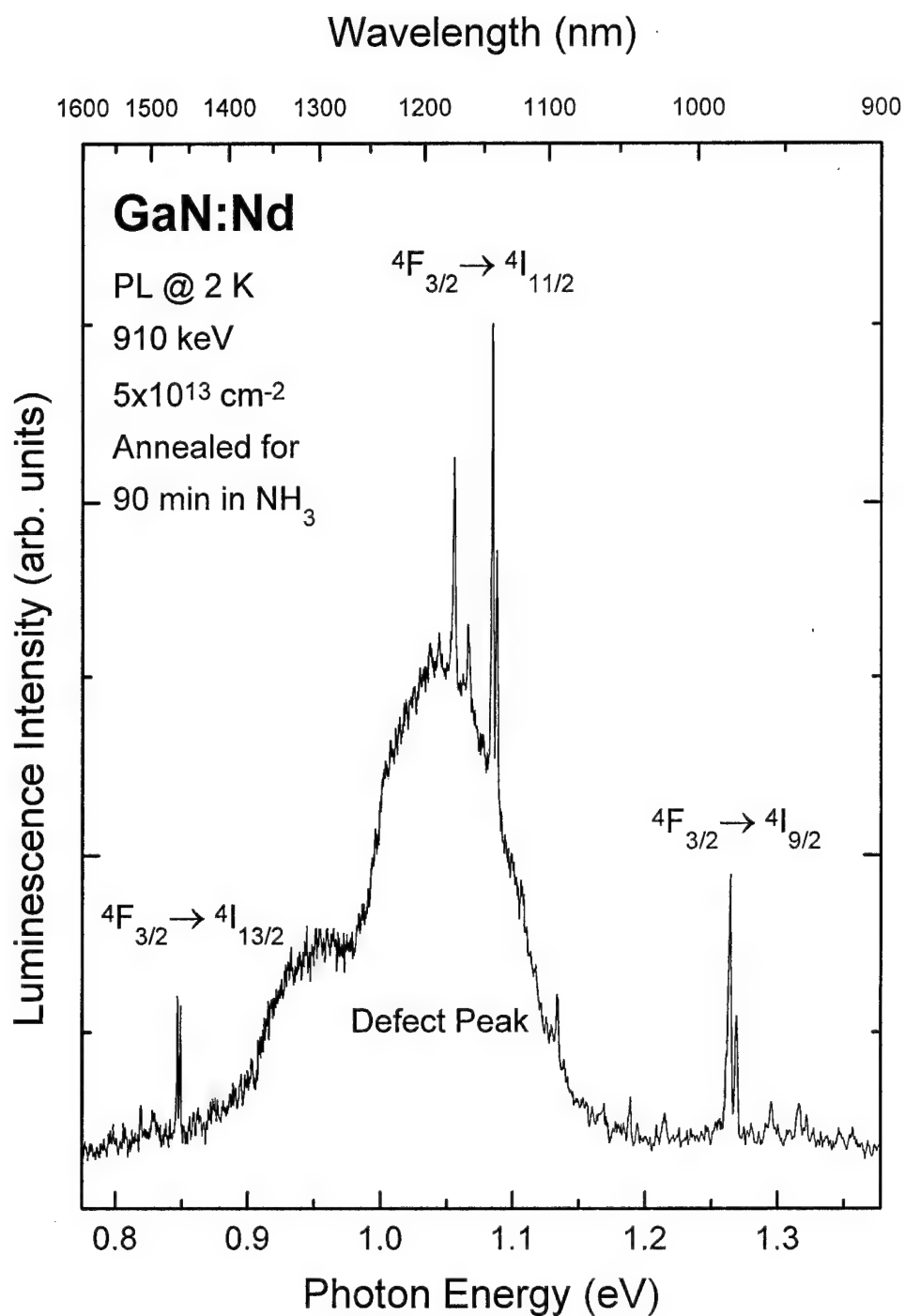
Figure 5-51. Photoluminescence spectra taken at 2 K for GaN implanted with neodymium at 910 keV to a dose of 5×10^{13} cm^{-2} and annealed at 1000 °C for 90 min in NH$_3$.

responsible implantation damage-related luminescence center for this peak was unknown. Similar damage-related peaks have been reported for other III-V materials implanted with RE ions (Elsaesser *et al.*, 1995). No luminescence could be observed from the as-implanted samples.

Annealing studies were performed to determine the optimal annealing temperature for activation of the Nd^{3+} intra-4f shell luminescence. Figures 5-52, 5-53, and 5-54 show the Nd^{3+} peaks observed at low temperature from the $^4F_{3/2} \rightarrow {}^4I_{13/2}$, $^4F_{3/2} \rightarrow {}^4I_{11/2}$, and $^4F_{3/2} \rightarrow {}^4I_{9/2}$ transitions, respectively. Although the 700 °C anneal showed no Nd^{3+} related luminescence, weak Nd^{3+} luminescence from all three sets of lines was observed from the 800 °C anneal. The intensity of all three manifolds was higher for the 900 °C anneal, and maximum intensity was attained for the 1000 °C anneal. Since annealing GaN at temperatures above 1000 °C resulted in surface deterioration, it can be concluded that 1000 °C was near the optimal annealing temperature for Nd implanted GaN using the proximity-cap method.

It is well known that the number of lines observed in each manifold can hold clues about the symmetry of the RE^{3+} luminescence center responsible (Pappalardo, 1977). In particular, it is possible to distinguish between cubic and non-cubic symmetry by the number of luminescent peaks at low temperatures from each RE^{3+} luminescence center. Table V-3 shows the expected number of Stark splittings for the given term symbols under cubic and non-cubic symmetry. In general, non-cubic symmetry splits degenerate states, resulting in a greater number of crystal-field split luminescence peaks. If the Nd

Figure 5-52. Photoluminescence spectra taken at 2 K for the $^4F_{3/2} \rightarrow {}^4I_{13/2}$ transition of Nd^{3+} for GaN implanted with neodymium at 910 keV to a dose of 5×10^{13} cm^{-2} and annealed at various temperatures for 90 min in NH_3.

Figure 5-53. Photoluminescence spectra taken at 2 K for the $^4F_{3/2} \rightarrow {}^4I_{11/2}$ transition of Nd^{3+} for GaN implanted with neodymium at 910 keV to a dose of $5 \times 10^{13} cm^{-2}$ and annealed at various temperatures for 90 min in NH_3.

Figure 5-54. Photoluminescence spectra taken at 2 K for the $^4F_{3/2} \rightarrow {}^4I_{9/2}$ transition of Nd^{3+} for GaN implanted with neodymium at 910 keV to a dose of 5×10^{13} cm^{-2} and annealed at various temperatures for 90 min in NH_3.

Table V-3. Number of Crystal-Field Split Levels for Cubic or Non-Cubic Symmetry.

Term:	No. Splittings with Cubic Sites	No. Splittings with Non-Cubic Sites
$^4F_{3/2}$	1	2
$^4I_{9/2}$	3	5
$^4I_{11/2}$	4	6
$^4I_{13/2}$	5	7
$^4I_{15/2}$	5	8
Reference:	Lea *et al.*, 1962	Walter, 1984

ions occupied one of the octahedral or tetrahedral voids of the wurtzite lattice, a cubic site symmetry would be expected. For the cubic case, the number of crystal-field split levels would be less than the number of levels for the non-cubic case. Since GaN has the wurtzite structure, and thus has underlying hexagonal symmetry, the site symmetry of an ion on a lattice site of the crystal is non-cubic. In addition, an interstitial RE^{3+} would be found on an asymmetric site. Thus, one might expect non-cubic Stark splittings for both the interstitial and substitutional cases.

At very low temperature under low excitation conditions, radiative transitions would be expected to originate from the lowest crystal-field split level of the upper manifold, in this case $^4F_{3/2}$. Thus, under the above conditions, the maximum number of luminescence peaks expected would be identical to the number of crystal-field split levels in the lower manifold. Thus if the symmetry were non-cubic, five lines could be expected from the $^4F_{3/2} \rightarrow ^4I_{9/2}$ transition, six lines from the $^4F_{3/2} \rightarrow ^4I_{11/2}$, and seven lines from the $^4F_{3/2} \rightarrow ^4I_{13/2}$ transition. In fact, the low temperature results for Nd implanted GaN give very good agreement with non-cubic Stark splittings. The $^4F_{3/2} \rightarrow ^4I_{9/2}$ transition showed exactly five lines as was expected for the non-cubic case. Only three lines would

be present if the symmetry were cubic. The $^4F_{3/2} \rightarrow {}^4I_{11/2}$ transition showed seven lines, one more than was expected for the non-cubic case. However, it was discovered that the highest energy line observed was in fact associated with a transition from the upper $^4F_{3/2}$ level as will be discussed in greater detail below. Thus, there were exactly six crystal-field split levels detected, which were associated with the $^4I_{11/2}$ manifold. Again, only four would have been expected for cubic symmetry. Only the $^4F_{3/2} \rightarrow {}^4I_{13/2}$ transition displayed less than the maximum expected number of lines for non-cubic symmetry, showing only four lines. In fact, there were less than the expected maximum number of lines for a cubic center. In summary, these results showed conclusively that the Nd ions occupied non-cubic centers within the crystal; however, no determination can yet be made as to whether these sites were substitutional or interstitial.

The number of luminescence lines and the annealing behavior observed suggested the occurrence of only one Nd^{3+} luminescence center. The likelihood of different luminescence centers having identical annealing temperature dependencies was small (Bryant et al., 1983). Thus, if more than one Nd^{3+} luminescence center were present, several distinct sets of lines with different annealing temperature dependence would be observed. This was not the case; all peaks showed identical annealing temperature dependence. This fact, coupled with the identical number of peaks expected for non-cubic luminescence centers, strongly suggests the presence of only one non-cubic Nd^{3+} luminescence center.

Photoluminescence was also taken with samples held at room temperature. After examining all manifolds, only luminescence from the $^4F_{3/2} \rightarrow {}^4I_{11/2}$ manifold of Nd^{3+} was

observed. Figure 5-55 shows the annealing temperature dependence behavior of this manifold. The other two groups of transitions quenched as temperature was raised above 50 K. No physical mechanism was evident to explain why only this manifold survived to room temperature. However, since this manifold was observed to have the most intense lines at low temperature, it's survival to room temperature may be simply a consequence of a higher transition probability.

Higher energy lines appeared in the luminescence of the $^4F_{3/2} \rightarrow ^4I_{11/2}$ manifold at room temperature as compared to the low temperature spectrum. Five discernible lines were observed at 300 K as shown in Figure 5-56. The relative intensities of these lines followed a nearly identical pattern to the five highest energy lines of the manifold observed at low temperature as shown in Figure 5-57. Also, the highest intensity line, C', occurred in the exact energetic position of the seventh line observed at low temperature. This line was therefore not the result of a blue shift of any of the low temperature lines. In fact, this result was a manifestation of the temperature independent nature of the RE^{3+} emissions. The 1.135 eV peak did not shift in energy as temperature was increased from 2 to 300 K. Furthermore, the energy spacings of the low and high temperature line groupings followed a nearly identical pattern. It should also be noted that the lines were broadened at elevated temperature and the background intensity was considerably increased. Thus, the exact energetic position of the lines at 300 K was less well
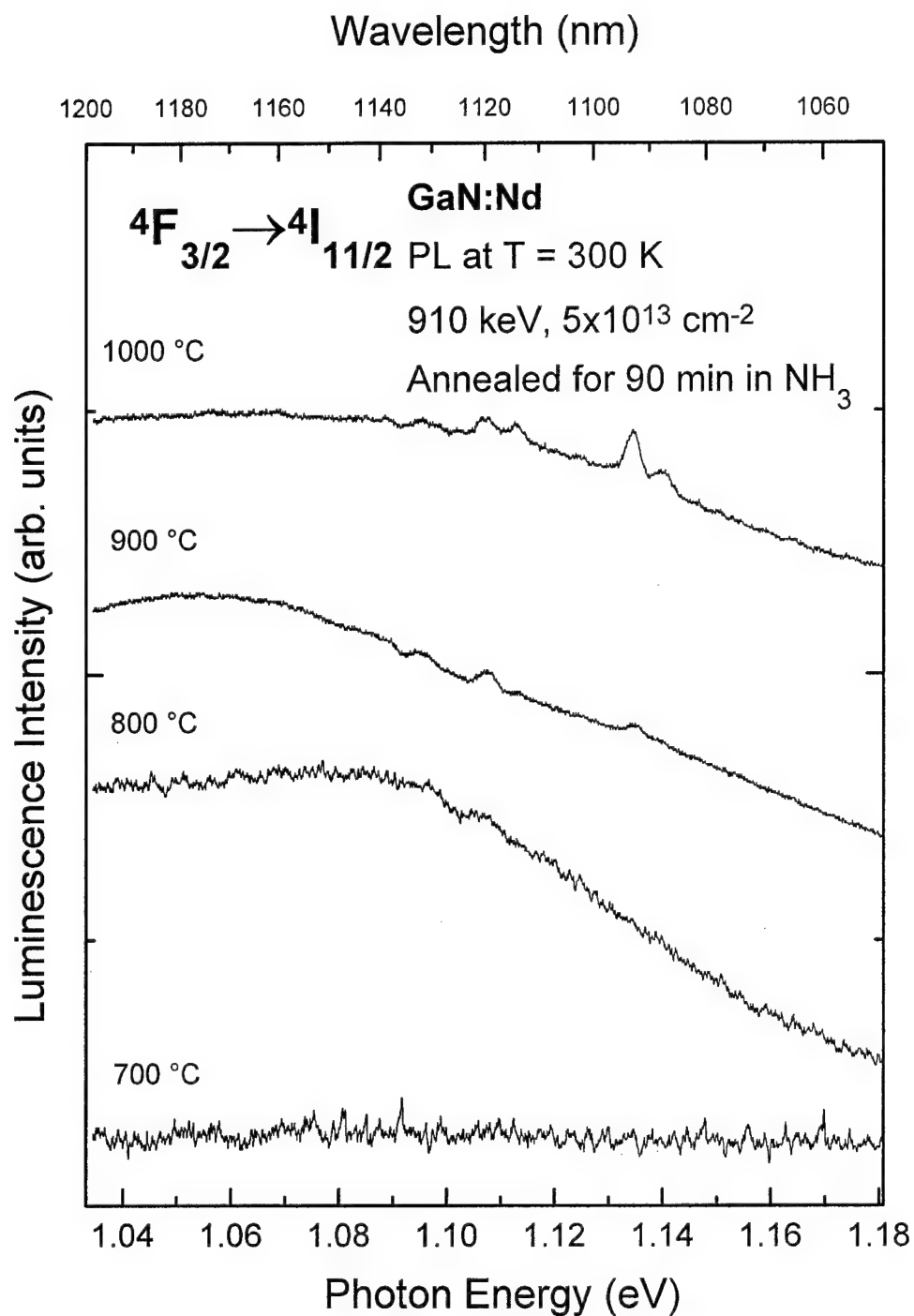
Figure 5-55. Photoluminescence spectra taken at 300 K for the $^4F_{3/2} \rightarrow {}^4I_{11/2}$ transition of Nd^{3+} for GaN implanted with neodymium at 910 keV to a dose of 5×10^{13} cm^{-2} and annealed at various temperatures for 90 min in NH$_3$.
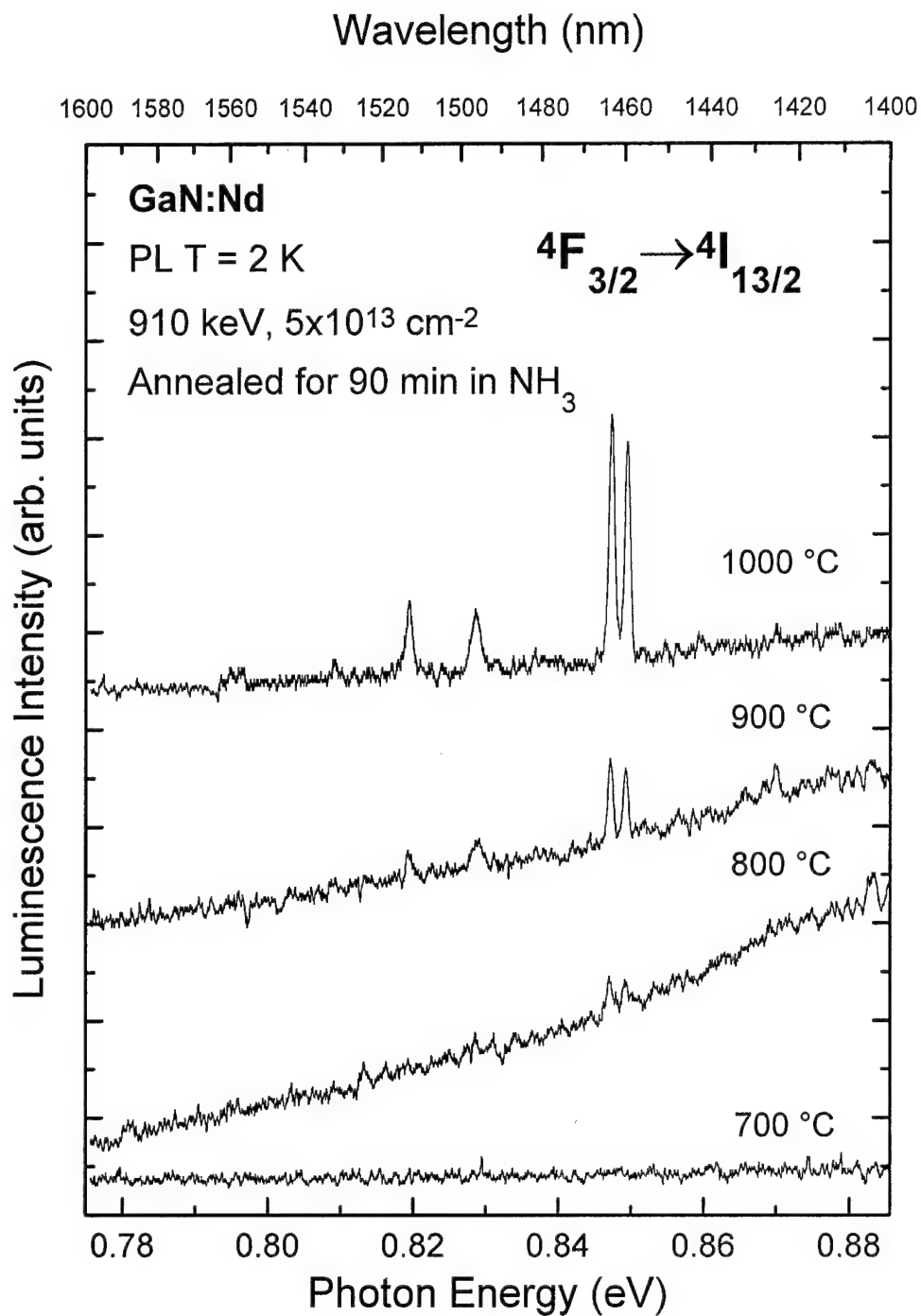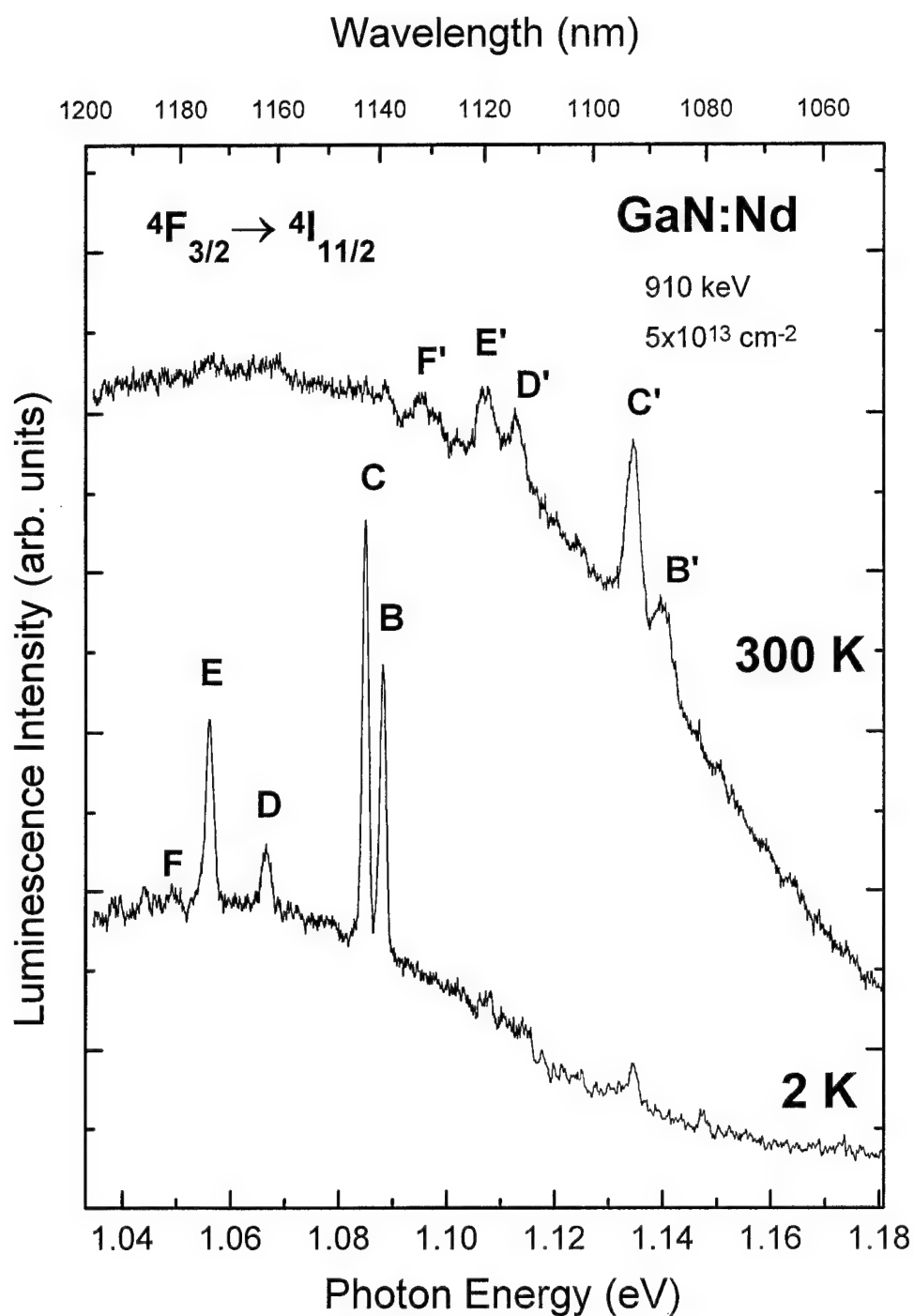
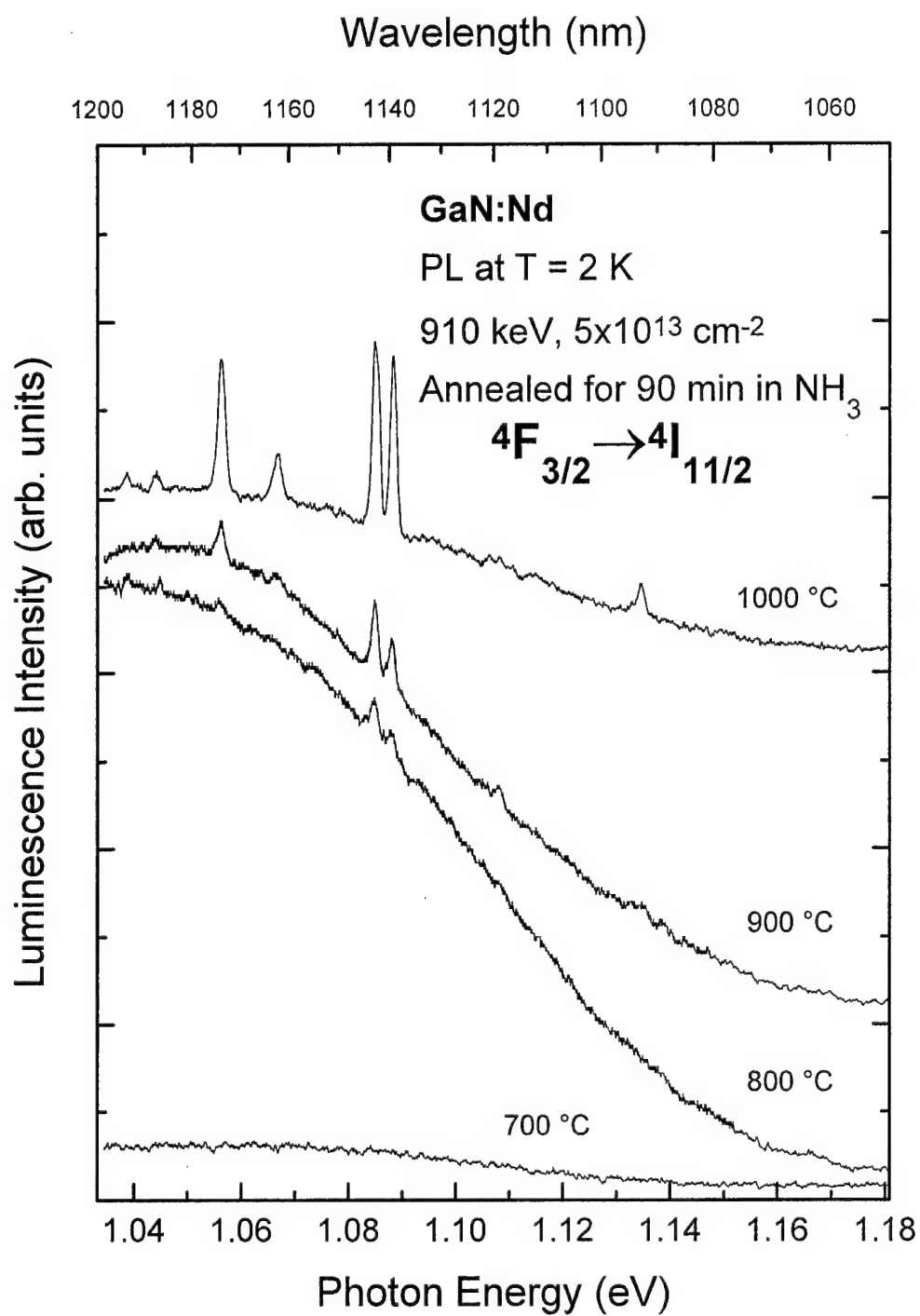**Figure 5-56.** Photoluminescence spectra taken at 2 and 300 K for the $^4F_{3/2} \rightarrow {}^4I_{11/2}$ transition of Nd^{3+} for GaN implanted with neodymium at 910 keV to a dose of 5×10^{13} cm^{-2} and annealed at 1000 °C for 90 min in NH_3.
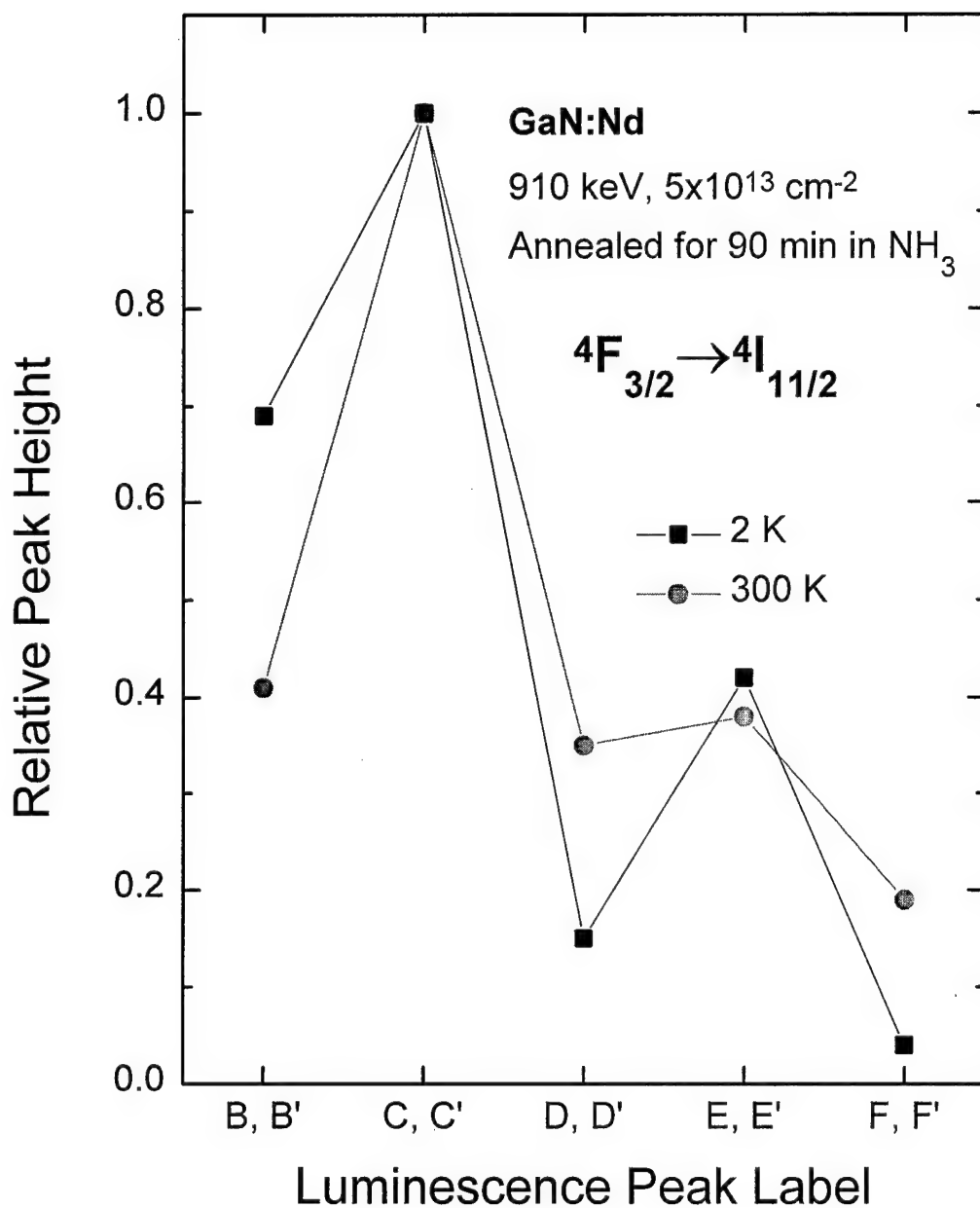
Figure 5-57. Comparison of the relative photoluminescence peak heights in the $^4F_{3/2} \rightarrow$ $^4I_{11/2}$ transition of Nd^{3+} at 2 and 300 K for GaN implanted with neodymium at 910 keV to a dose of 5×10^{13} cm^{-2} and annealed at 1000 °C for 90 min in NH$_3$

Table V-4. Temperature Dependent Shift of Nd^{3+} $^4F_{3/2} \rightarrow$ $^4I_{11/2}$ Transitions.

Energetic Location	Low Temperature (eV)	Room Temperature (eV)	Delta (meV)
B, B'	1.0443	1.0954	51.11
C, C'	1.0562	1.1076	51.14
D, D'	1.0671	1.1126	45.53
E, E'	1.0849	1.1345	49.53
F, F'	1.0884	1.1395	51.16

determined. Table V-4 shows that the low intensity line labeled D' had a somewhat smaller energy spacing compared to the spacings observed between the other lines. When all lines were considered, a relative difference of 49.7 meV was found between the low and high temperature groupings. This value may be somewhat underestimated since the position of line D' was more uncertain. The uncertainty in the position of line D' could be attributed to the lower intensity of this peak. If the relative energy spacing was recomputed without the position of peak D', the relative difference between the centers of the peak groups was 50.7 meV. Thus, the separation between the two crystal-field split levels within the $^4F_{3/2}$ manifold was approximately 50 meV. A splitting of the $^4F_{3/2}$ manifold into two levels does not occur under cubic symmetry. Thus, the observed splitting of the $^4F_{3/2}$ manifold reconfirmed the low temperature data which suggested a non-cubic site symmetry for the Nd^{3+} luminescence center.

Since two different Nd doses were implanted, limited comparisons of dose dependence were possible. All sets of lines were observed in both sample sets and showed identical annealing temperature dependence. Figures 5-58, 5-59, and 5-60 show the annealing temperature dependence for the 1×10^{13} cm^{-2} dose implanted samples, which
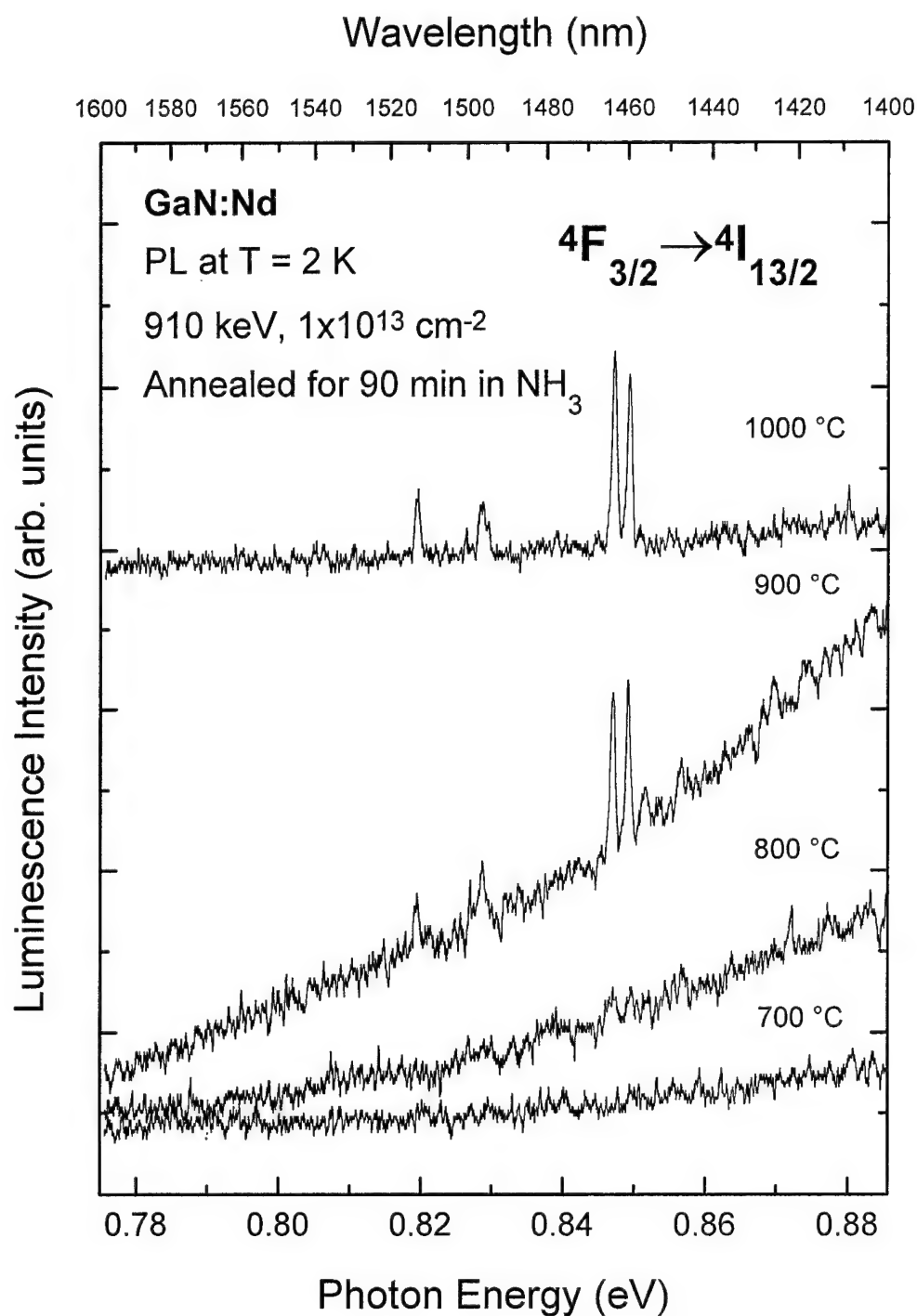
Figure 5-58. Photoluminescence spectra taken at 2 K for the $^4F_{3/2} \rightarrow {}^4I_{13/2}$ transition of Nd^{3+} for GaN implanted with neodymium at 910 keV to a dose of 1×10^{13} cm^{-2} and annealed at various temperatures for 90 min in NH$_3$.
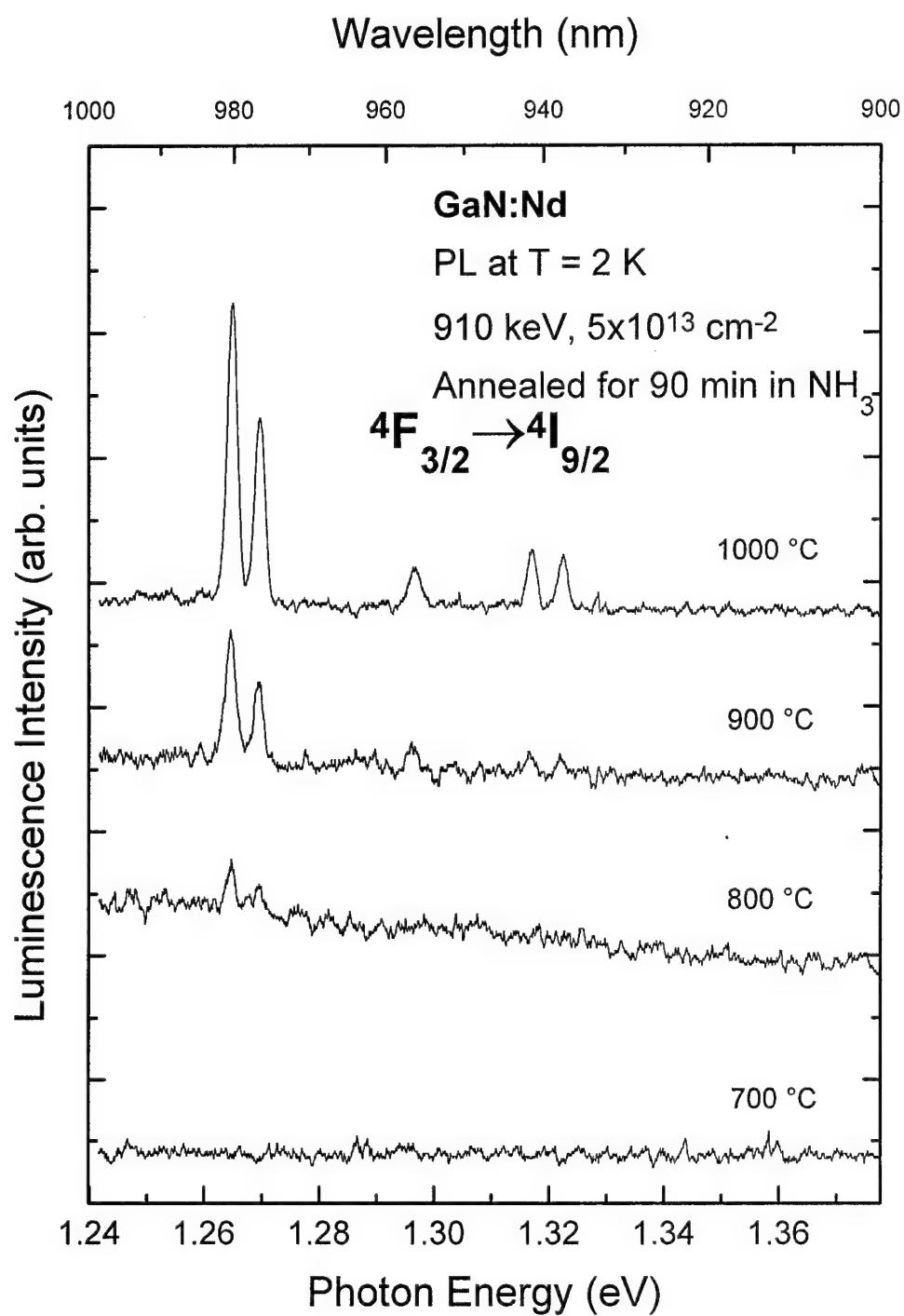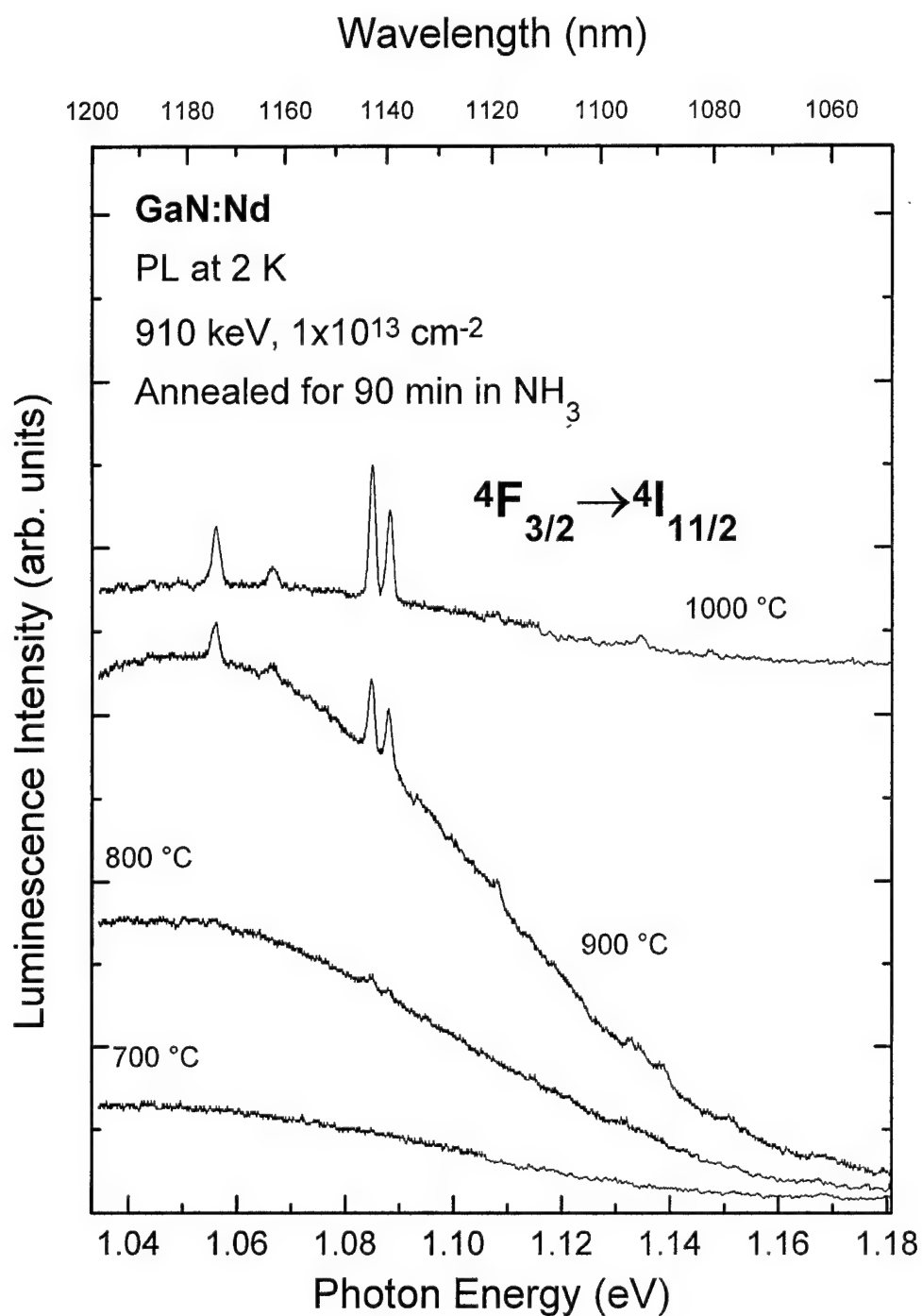
Figure 5-59. Photoluminescence spectra taken at 2 K for the $^4F_{3/2} \rightarrow {}^4I_{11/2}$ transition of Nd^{3+} for GaN implanted with neodymium at 910 keV to a dose of 1×10^{13} cm^{-2} and annealed at various temperatures for 90 min in NH_3.
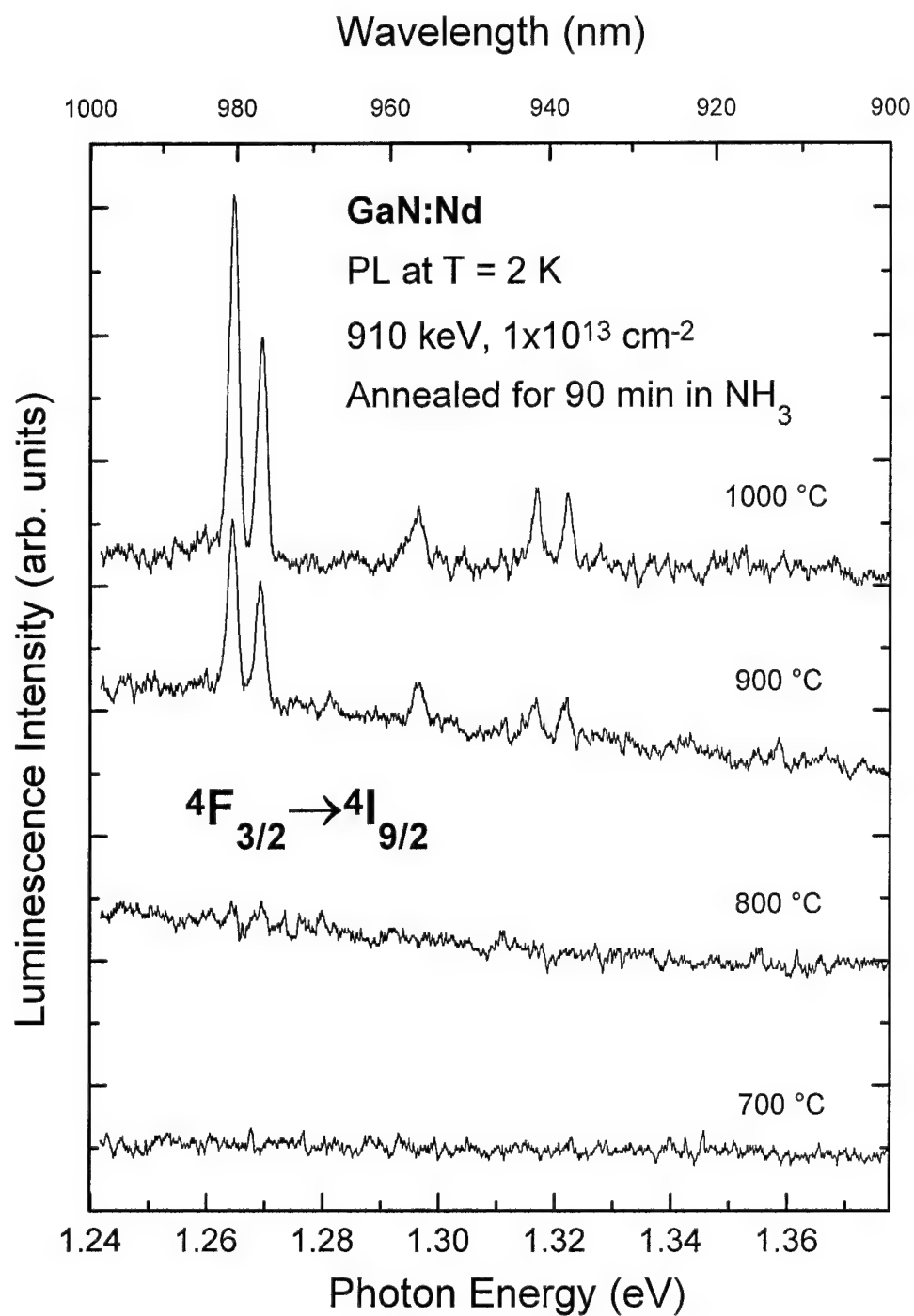
Figure 5-60. Photoluminescence spectra taken at 2 K for the $^4F_{3/2} \to {}^4I_{9/2}$ transition of Nd^{3+} for GaN implanted with neodymium at 910 keV to a dose of 1×10^{13} cm^{-2} and annealed at various temperatures for 90 min in NH_3.

can be readily compared with Figures 5-51, 5-52, and 5-53 for the 5×10^{13} cm^{-2} dose implanted samples. Apart from the total intensity of the Nd related luminescence, no significant changes in the manifolds were observed. Thus, over the limited dose range examined, no changes were observed in the type of Nd^{3+} centers formed. The intensity of the main peak in each manifold was between three and five times larger in the higher dose samples. Some uncertainty was inherent in measuring the relative intensities of different samples as discussed previously. However, the intensity difference of three to five times agreed with the difference in dose which was a factor of five. This also indicated that the doses selected had not exceeded the solubility limit of Nd in GaN.

The Nd^{3+} luminescence was also studied as a function of the exciting photon wavelength. The Ar^{+} laser was capable of lasing on a number of discrete lines using an intracavity prism. Since the efficiency of the minor laser lines was low, a laser power level of 50 mW was chosen. This power level was a factor of ten lower than the 500 mW power level typically used to obtain the high resolution spectrum reported above.

Numerous new luminescence peaks were observed as the wavelength of the excitation laser was lowered. Higher energy photons excited additional transitions between the Nd^{3+} manifolds. Figures 5-61 through 5-64 show the detailed spectra for the various transitions. The uppermost trace in each figure was taken with the argon ion laser operating multiline in the UV from 351.1 nm to 363.8 nm. Thus, the exciting photons in this case were both slightly below and above the GaN bandgap at low temperature. A
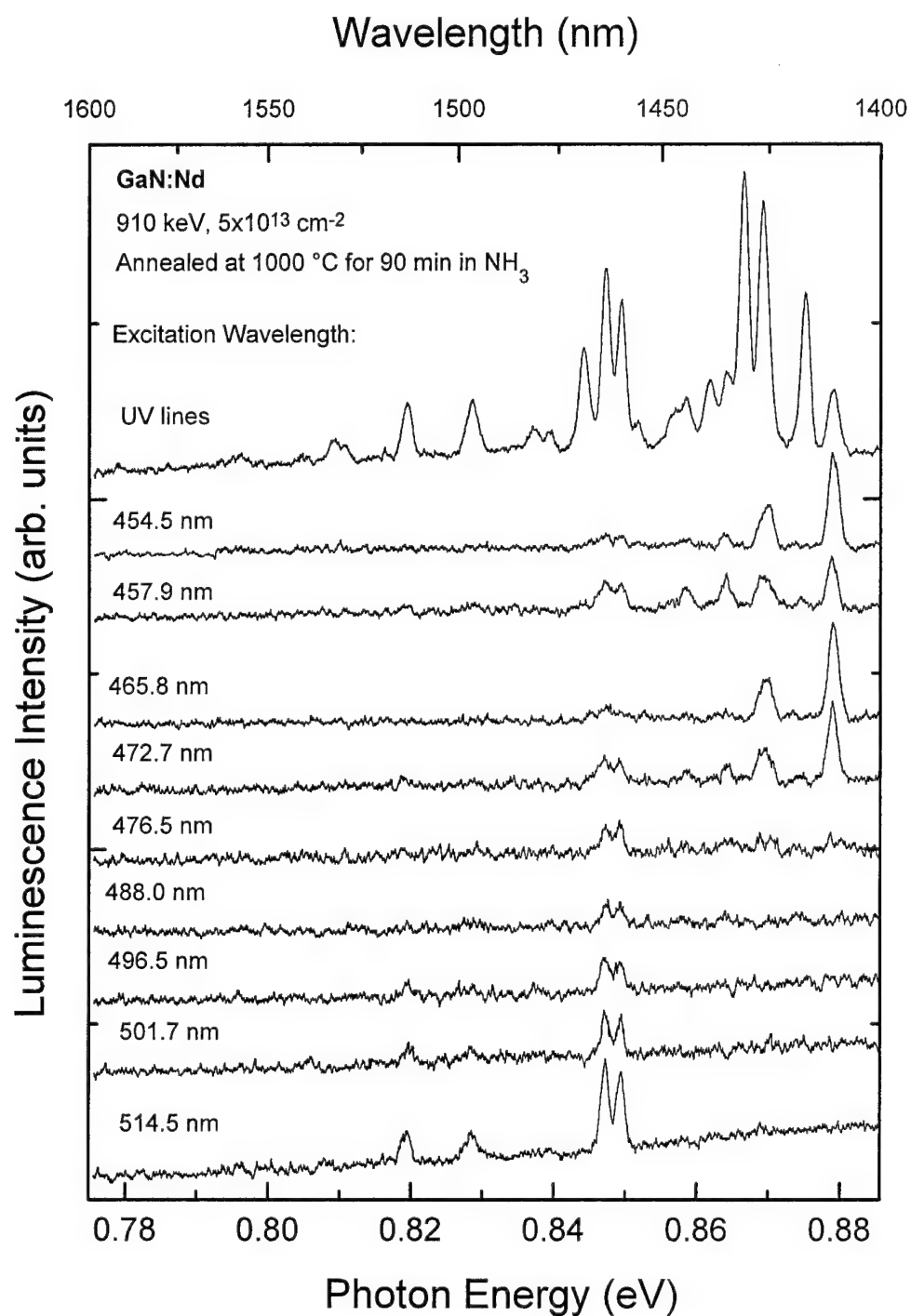
Figure 5-61. Photoluminescence spectra taken with various excitation wavelengths at a temperature of 2 K in the range from 1600-1400 nm for GaN implanted with neodymium at 910 keV to a dose of 5×10^{13} cm^{-2} and annealed at 1000 °C for 90 min in NH$_3$.
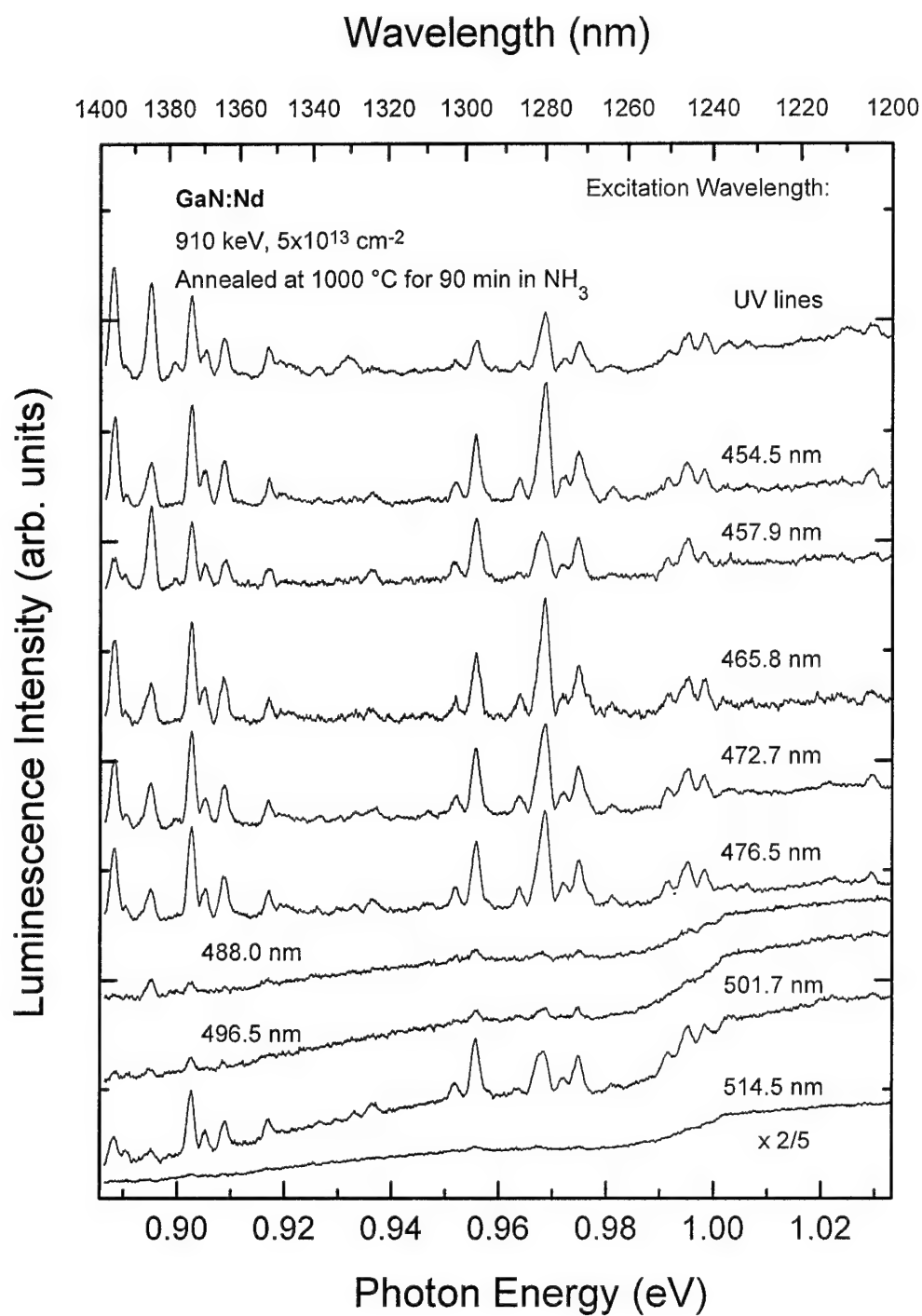
Figure 5-62. Photoluminescence spectra taken with various excitation wavelengths at a temperature of 2 K in the range from 1400-1200 nm for GaN implanted with neodymium at 910 keV to a dose of 5×10^{13} cm^{-2} and annealed at 1000 °C for 90 min in NH$_3$.
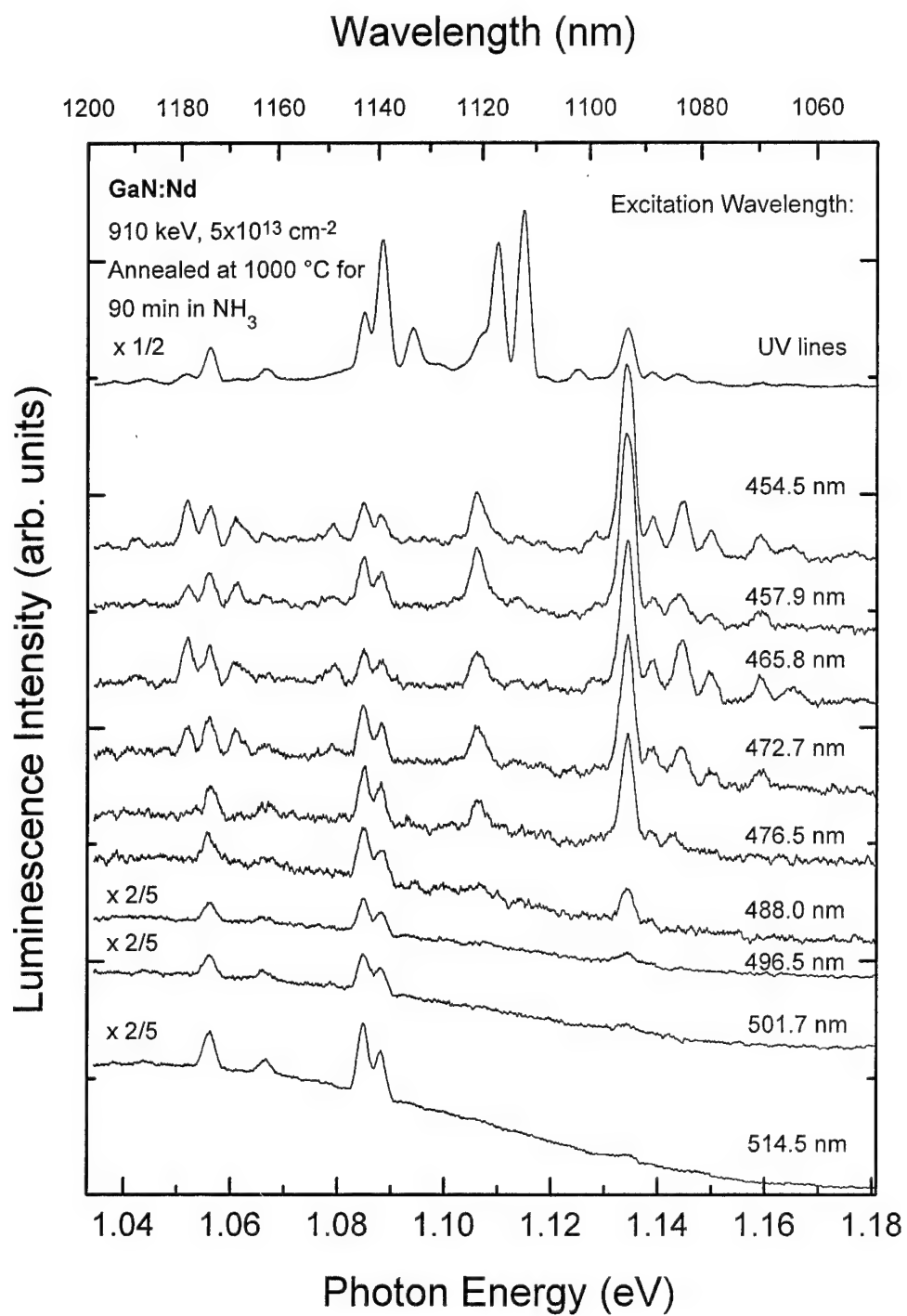
Figure 5-63. Photoluminescence spectra taken with various excitation wavelengths at a temperature of 2 K in the range from 1200-1050 nm for GaN implanted with neodymium at 910 keV to a dose of 5×10^{13} cm^{-2} and annealed at 1000 °C for 90 min in NH$_3$.
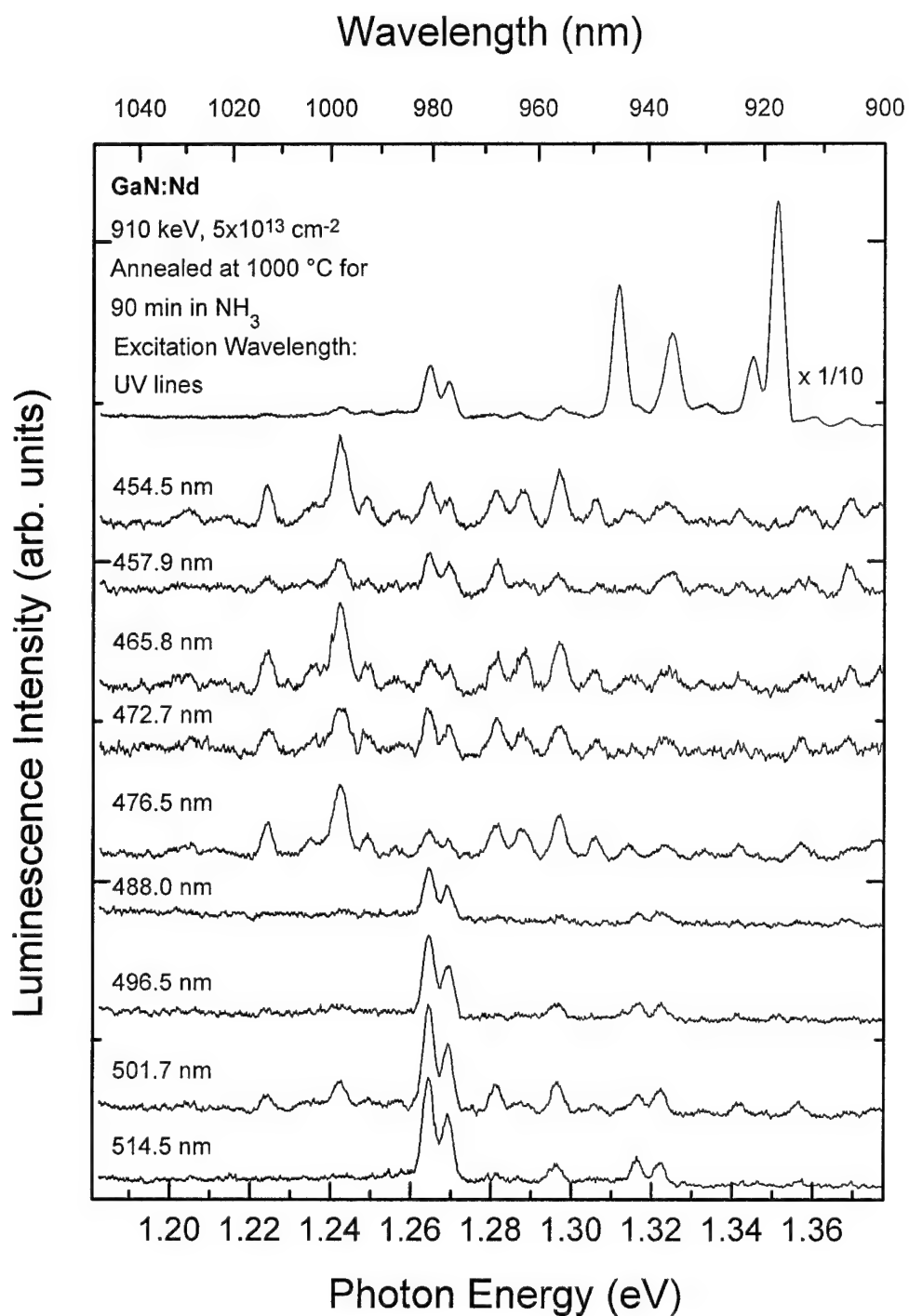
Figure 5-64. Photoluminescence spectra taken with various excitation wavelengths at a temperature of 2 K in the range from 1050-900 nm for GaN implanted with neodymium at 910 keV to a dose of 5×10^{13} cm^{-2} and annealed at 1000 °C for 90 min in NH$_3$.

significant change in the Nd^{3+} lines was observed as photon energy was increased from 454.5 nm to the UV lines.

The proliferation of transitions observed with higher energy photon excitation cannot have originated from the $^4F_{3/2} \rightarrow {}^4I_{13/2}$, $^4F_{3/2} \rightarrow {}^4I_{11/2}$, and $^4F_{3/2} \rightarrow {}^4I_{9/2}$ transitions alone. Transitions between the upper Nd^{3+} manifolds were likely to become more probable as the exciting photon energy was increased. One manifestation of this phenomenon was the occurrence of transitions from the upper $^4F_{3/2}$ energy level to the $^4I_{13/2}$, $^4I_{11/2}$, and $^4I_{9/2}$ manifolds. Transitions at an energy approximately 50 meV higher than the transitions for the lower $^4F_{3/2}$ were found for excitation with 454.5 nm and the UV lines. No other such energy spacing occurred for all of the transitions. Table V-5 lists all of the observed transitions under UV laser excitation. The lines which appeared under 514.5 laser excitation are highlighted in bold. The lines which were approximately 50 meV higher in energy are highlighted in italics. The average energy spacing of these lines was found to be 49 meV. This result offered further confirmation of the 50 meV spacing of the energy levels within the $^4F_{3/2}$ manifold. Figure 5-65 shows the full spectral range of the emissions studied with excitation by the 514.5 nm, 454.5 nm, and UV lines. The intensity of the Nd^{3+} lines observed with 514.5 nm excitation were reduced in intensity under 454.5 nm excitation while the other lines were increased. The UV excitation case showed a rise in intensity with the most intense lines being five times more intense than the 454.5 nm case. This was similar to a result reported by Wagner *et al.* (1986) for GaP:Nd. They found an approximately five times higher low temperature

Table V-5. Energetic positions of Nd^{3+} transitions under UV laser excitation of 351.1 to 363.8 nm.

Wavelength (nm)	Energy (eV)	Wavelength (nm)	Energy (eV)
1531.89	0.8094	1241.89	0.9984
1513.09	**0.8194**	1204.24	1.0296
1496.34	**0.8286**	1194.04	1.0384
1481.34	0.8370	1187.29	1.0443
1476.49	0.8397	1178.94	1.0517
1468.69	0.8442	**1173.84**	**1.0562**
1463.24	**0.8473**	1168.24	1.0613
1459.59	**0.8495**	**1162.04**	**1.0670**
1444.34	0.8584	*1142.64*	*1.0851*
1438.49	0.8619	**1139.04**	**1.0885**
1435.19	0.8639	*1133.24*	*1.0941*
1430.74	0.8666	*1116.94*	*1.1100*
1426.49	*0.8692*	*1112.04*	*1.1149*
1416.74	0.8751	1101.69	1.1254
1410.19	*0.8792*	*1092.94*	*1.1344*
1395.94	0.8882	*1088.49*	*1.1391*
1385.09	*0.8951*	1083.99	1.1438
1378.34	*0.8995*	1078.64	1.1495
1373.59	0.9026	1069.24	1.1596
1369.74	0.9052	1065.64	1.1635
1364.19	0.9089	997.34	1.2432
1351.94	0.9171	**980.29**	**1.2648**
1338.34	0.9264	**976.69**	**1.2694**
1330.69	0.9317	968.34	1.2804
1323.94	0.9365	963.29	1.2871
1302.39	0.9520	**955.79**	**1.2972**
1297.34	0.9557	*945.29*	*1.3116*
1286.39	0.9638	**942.89**	**1.3149**
1279.84	0.9688	**935.89**	**1.3248**
1275.74	0.9719	929.69	1.3336
1271.89	0.9748	*921.79*	*1.3450*
1263.64	0.9812	917.69	1.3511
1250.24	0.9917	*911.29*	*1.3605*
1246.09	0.9950	*905.79*	*1.3688*
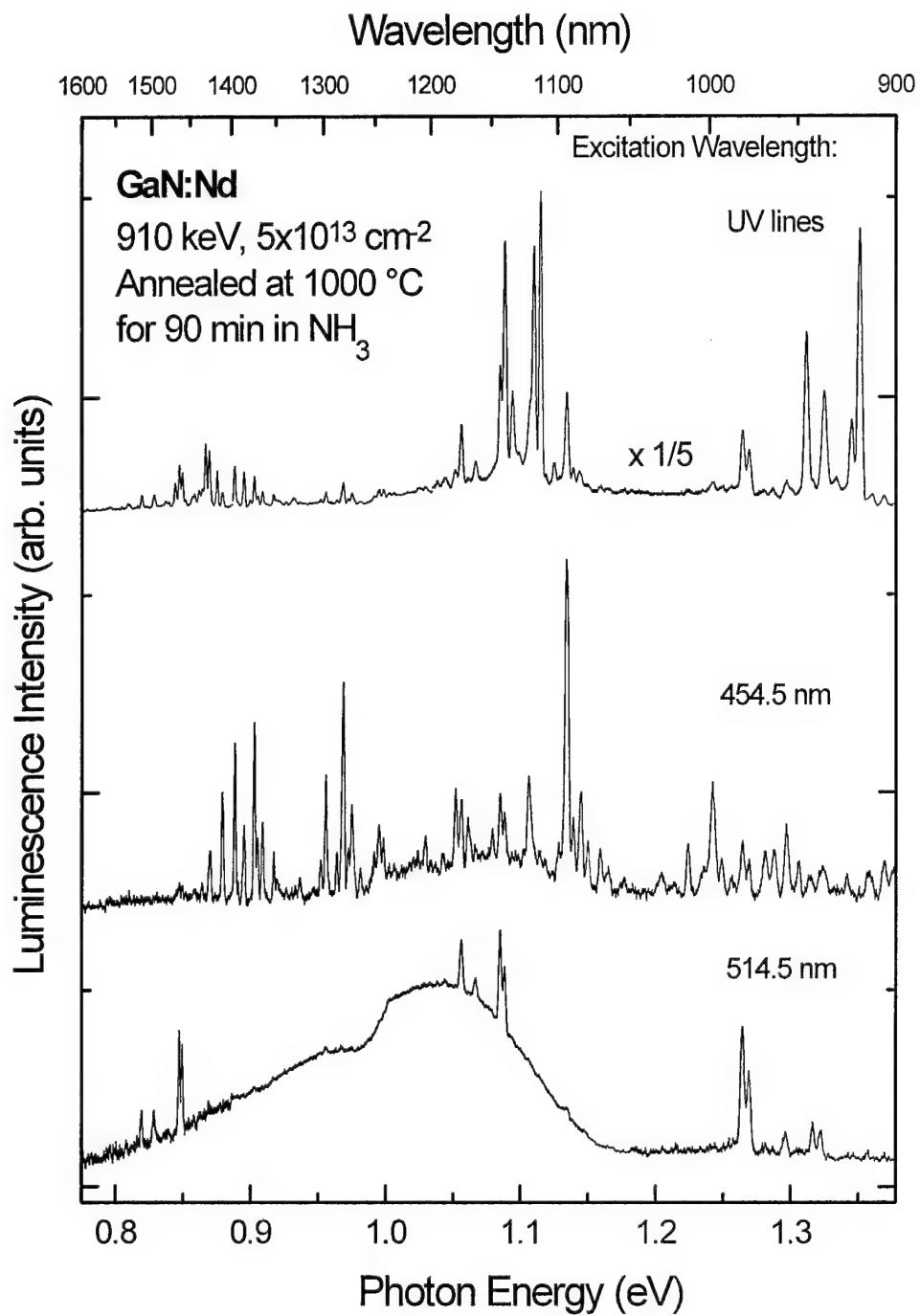
Figure 5-65. Photoluminescence spectra taken with various excitation wavelengths at a temperature of 2 K in the range from 1600-900 nm for GaN implanted with neodymium at 910 keV to a dose of 5×10^{13} cm^{-2} and annealed at 1000 °C for 90 min in NH$_3$.

PL intensity for above bandgap excitation than for resonant intra center excitation. Also of note was a decrease in intensity of the broad defect level as phonon energy was increased.

Nd-implanted GaN was oxygen co-implanted at an energy of 135 keV and a dose of 5.0×10^{14} cm^{-2}. The implantation parameters were chosen such that the oxygen peak concentration of 2.8×10^{19} cm^{-3} fell directly on the Nd implantation concentration peak. To obtain the best possible estimate of the relative intensities of the luminescence from the co-doped and non-co-doped samples, the samples were placed one above another on the sample holder. Thus, only a minor height adjustment and no rotation adjustment was necessary to collect a spectrum. This methodology insured that no other system parameters required adjustment. Using this technique, the overall intensity of the Nd^{3+} luminescence of the co-implanted sample was found to be 65% of the intensity of the non-co-implanted GaN:Nd as seen in Figures 5-66, 5-67, and 5-68. The positions and relative intensities of all luminescence lines were identical to those observed in the non-co-implanted material.

As seen in Figures 5-69, 5-70, and 5-71, the GaN:(Nd+O) co-implanted samples showed the same annealing behavior as non-co-implanted GaN:Nd. The optimal annealing temperature was 1000 °C for all three sets of lines as was the case for non-co-implanted GaN:Nd. Due to the lower luminescence efficiency, only the most intense luminescence peaks can be seen in these figures. Furthermore, the luminescence peaks in oxygen co-implanted GaN:Nd quenched when temperature was raised above 40 K.
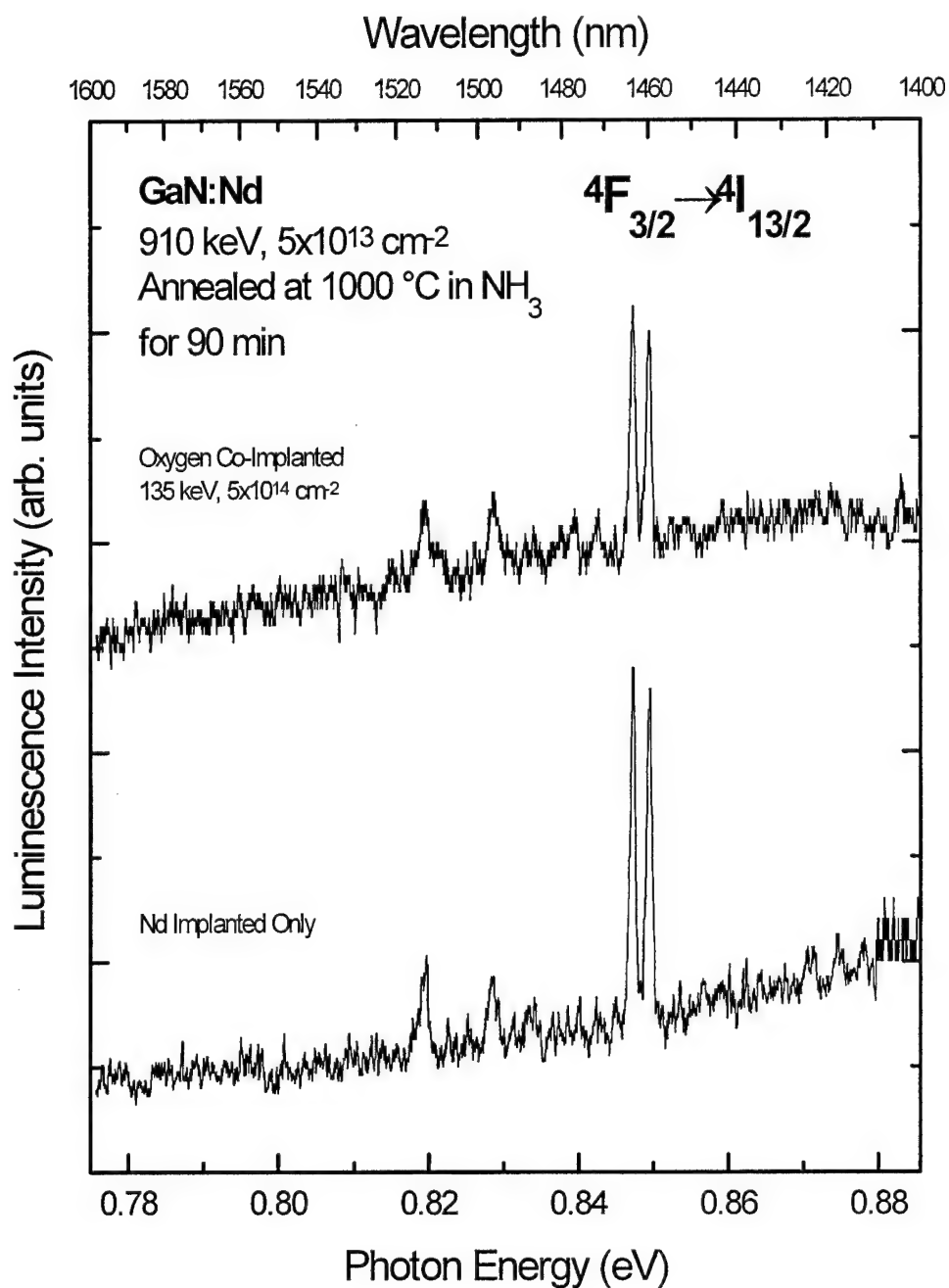
Figure 5-66. Absolute intensity comparison of photoluminescence spectra of the $^4F_{3/2} \rightarrow$ $^4I_{13/2}$ transitions of oxygen co-implanted (oxygen at 135 keV, 5×10^{14} cm^{-2}) and non-co-implanted (Nd at 910 keV, 5×10^{13} cm^{-2}) GaN annealed at 1000 °C for 90 min in NH$_3$.
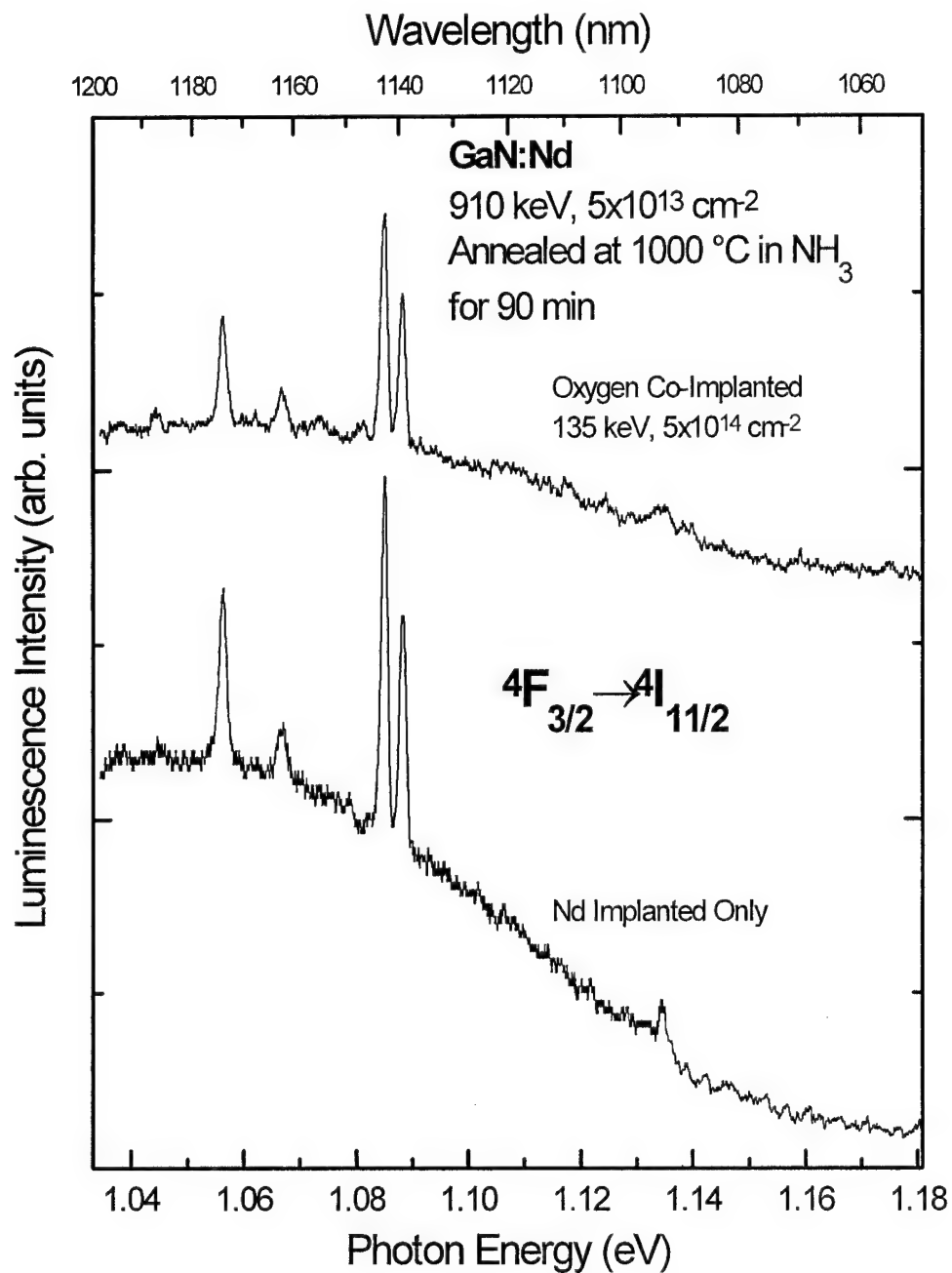
Figure 5-67. Absolute intensity comparison of photoluminescence spectra of $^4F_{3/2} \rightarrow$ $^4I_{11/2}$ transitions of oxygen co-implanted (oxygen at 135 keV, 5×10^{14} cm^{-2}) and non-co-implanted (Nd at 910 keV, 5×10^{13} cm^{-2}) GaN annealed at 1000 °C for 90 min in NH$_3$.
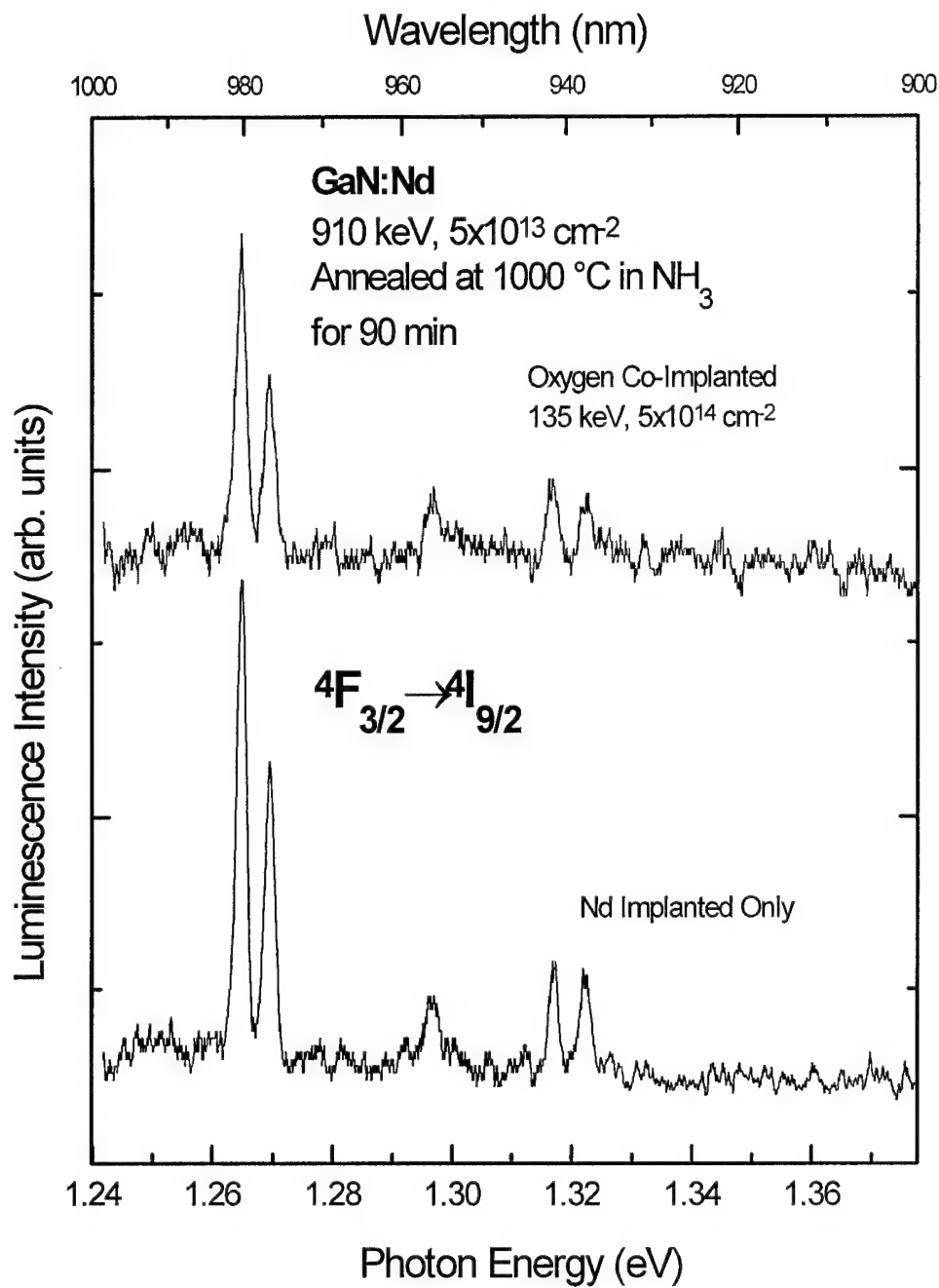
Figure 5-68. Absolute intensity comparison of photoluminescence spectra of $^4F_{3/2} \rightarrow {}^4I_{9/2}$ transitions of oxygen co-implanted (oxygen at 135 keV, 5×10^{14} cm^{-2}) and non-co-implanted (Nd at 910 keV, 5×10^{13} cm^{-2}) GaN annealed at 1000 °C for 90 min in NH$_3$.
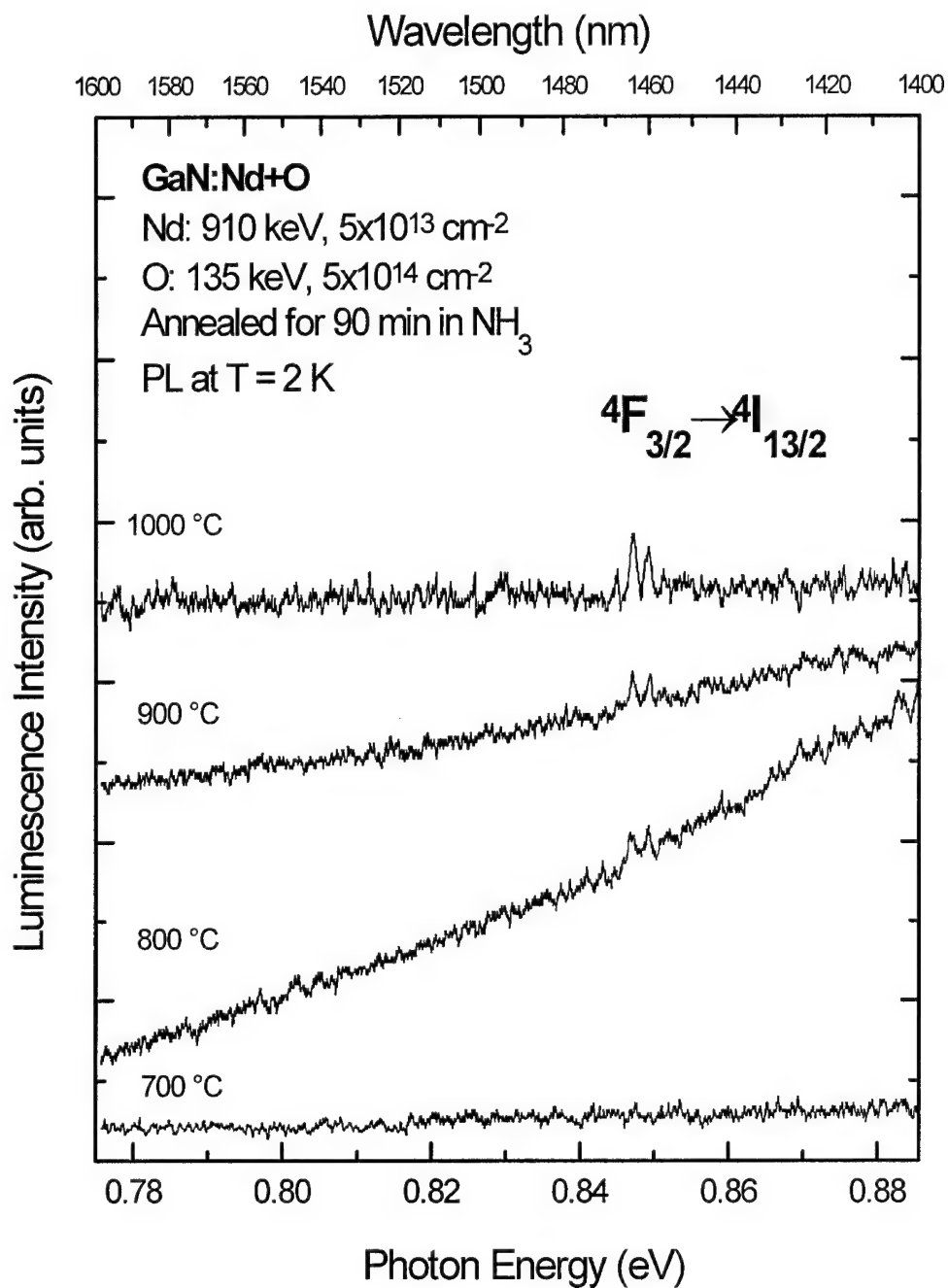
Figure 5-69. Photoluminescence spectra of $^4F_{3/2} \rightarrow {}^4I_{13/2}$ transitions of oxygen and neodymium co-implanted (oxygen at 135 keV, 5×10^{14} cm^{-2}, Nd at 910 keV, 5×10^{13} cm^{-2}) GaN annealed at various temperatures for 90 min in NH$_3$.
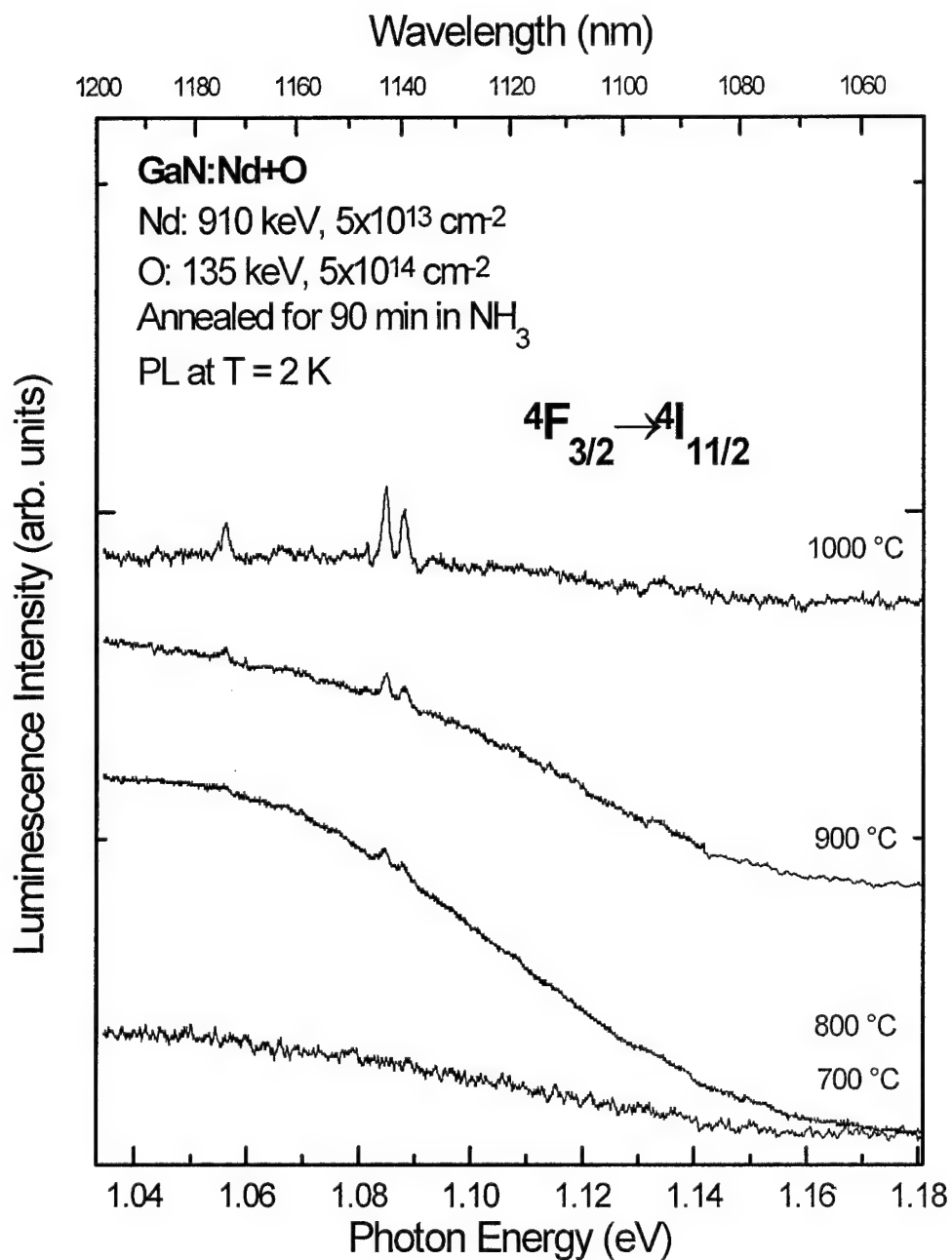
Figure 5-70. Photoluminescence spectra of $^4F_{3/2} \rightarrow {}^4I_{11/2}$ transitions of oxygen and neodymium co-implanted (oxygen at 135 keV, 5×10^{14} cm^{-2}, Nd at 910 keV, 5×10^{13} cm^{-2}) GaN annealed at various temperatures for 90 min in NH₃.
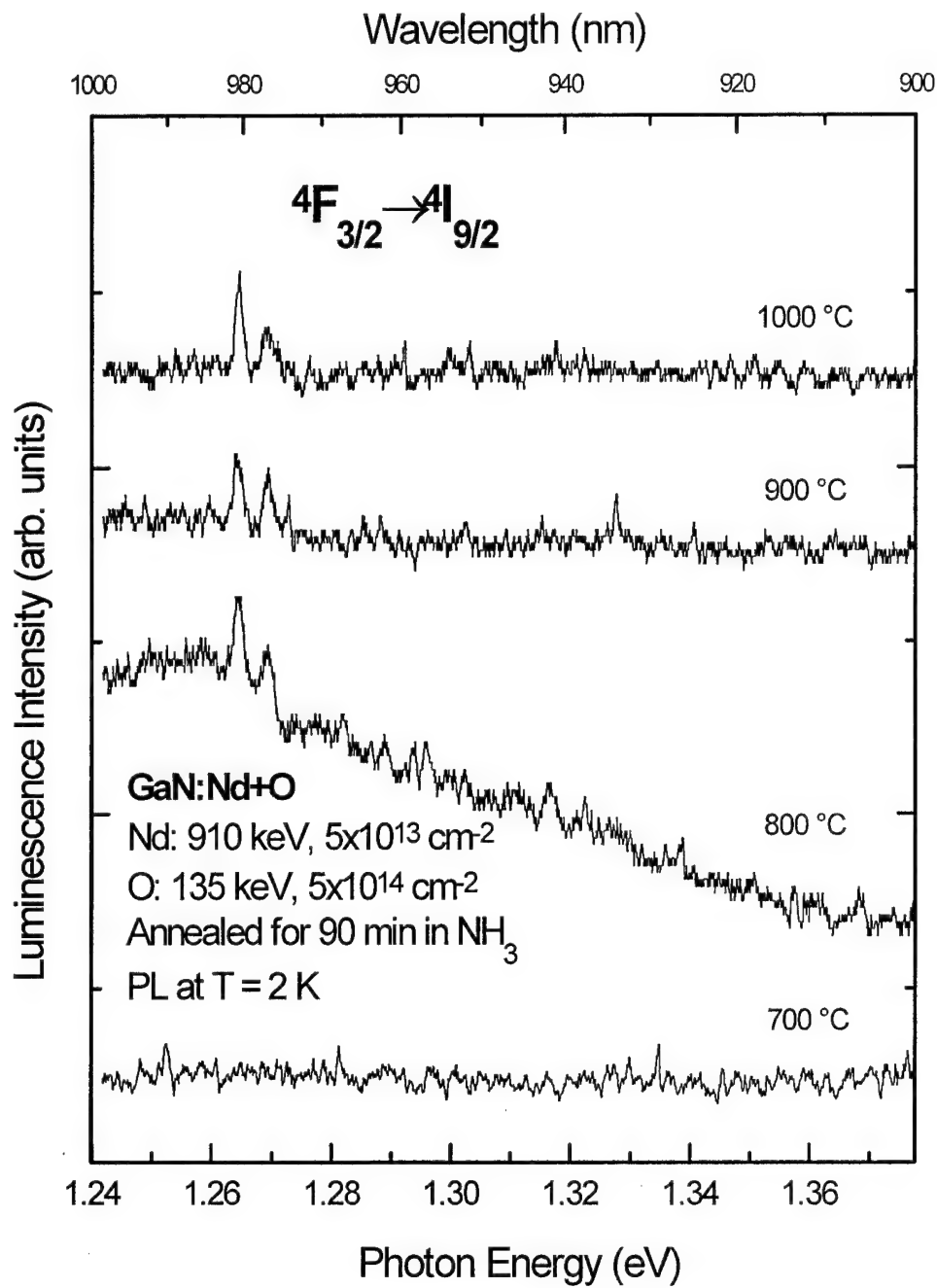
Figure 5-71. Photoluminescence spectra of $^4F_{3/2} \rightarrow \, ^4I_{9/2}$ transitions of oxygen and neodymium co-implanted (oxygen at 135 keV, 5×10^{14} cm^{-2}, Nd at 910 keV, 5×10^{13} cm^{-2}) GaN annealed at various temperatures for 90 min in NH$_3$.

Thus, oxygen co-doping did not create new types of luminescence centers. In fact, the responsible luminescence centers appeared to be identical in co-implanted material. The overall luminescence efficiency of the co-implanted GaN was lower; it was not clear whether this could be attributed to a quenching of the luminescence due to additional crystalline damage resulting from the oxygen implantation or from a reduction in the number of Nd^{3+} luminescence centers due to co-implanting with oxygen.

Using the assignments discussed above, a best fit model for the Nd^{3+} energy levels in the $^4F_{3/2}$, $^4I_{13/2}$, $^4I_{11/2}$, and $^4I_{9/2}$ manifolds was formulated. Figure 5-72 shows the proposed energy level spacings drawn to scale. The $^4I_{13/2}$ manifold was only shown to have four of the seven expected energy levels since only four were well determined. Transitions were observed from the lower $^4F_{3/2}$ energy level to all of the identified levels within the $^4I_{13/2}$, $^4I_{11/2}$, and $^4I_{9/2}$ manifolds at low temperature under 514.5 nm excitation. Under higher photon energy excitation, all transitions were observed from the upper $^4F_{3/2}$ state as well. The value obtained for the splitting of the $^4F_{3/2}$ manifold compares to values of 36.8 and 34.6 meV found for two different Nd^{3+} centers in GaP (Wagner *et al.*, 1986).

In summary, Nd was implanted into GaN, and studied for the first time. A rich luminescence spectrum was found resulting from transitions between principally three manifolds of energy levels. Annealing temperature dependence studies determined an optimal annealing temperature of 1000 °C for activation of the Nd^{3+} luminescence center. Evidence for only one, non-cubic luminescence center was found, and the energy levels

Neodymium Energy Levels

$^4F_{3/2}$ ——————————————— 50.98 meV
          ——————————————— 0.00   1.318 eV

Energy ↑

$^4I_{13/2}$ ═══════════════════ 30.00 meV
                                 20.92
                                 2.20
                                 0.00   0.470 eV

$^4I_{11/2}$ ═══════════════════ 49.37 meV
                                 43.89
                                 31.95
                                 21.51
                                 3.41
                                 0.00   0.233 eV

$^4I_{9/2}$ ═══════════════════ 57.09 meV
                                 52.46
                                 25.75
                                 5.51
                                 0.00   0.000 eV
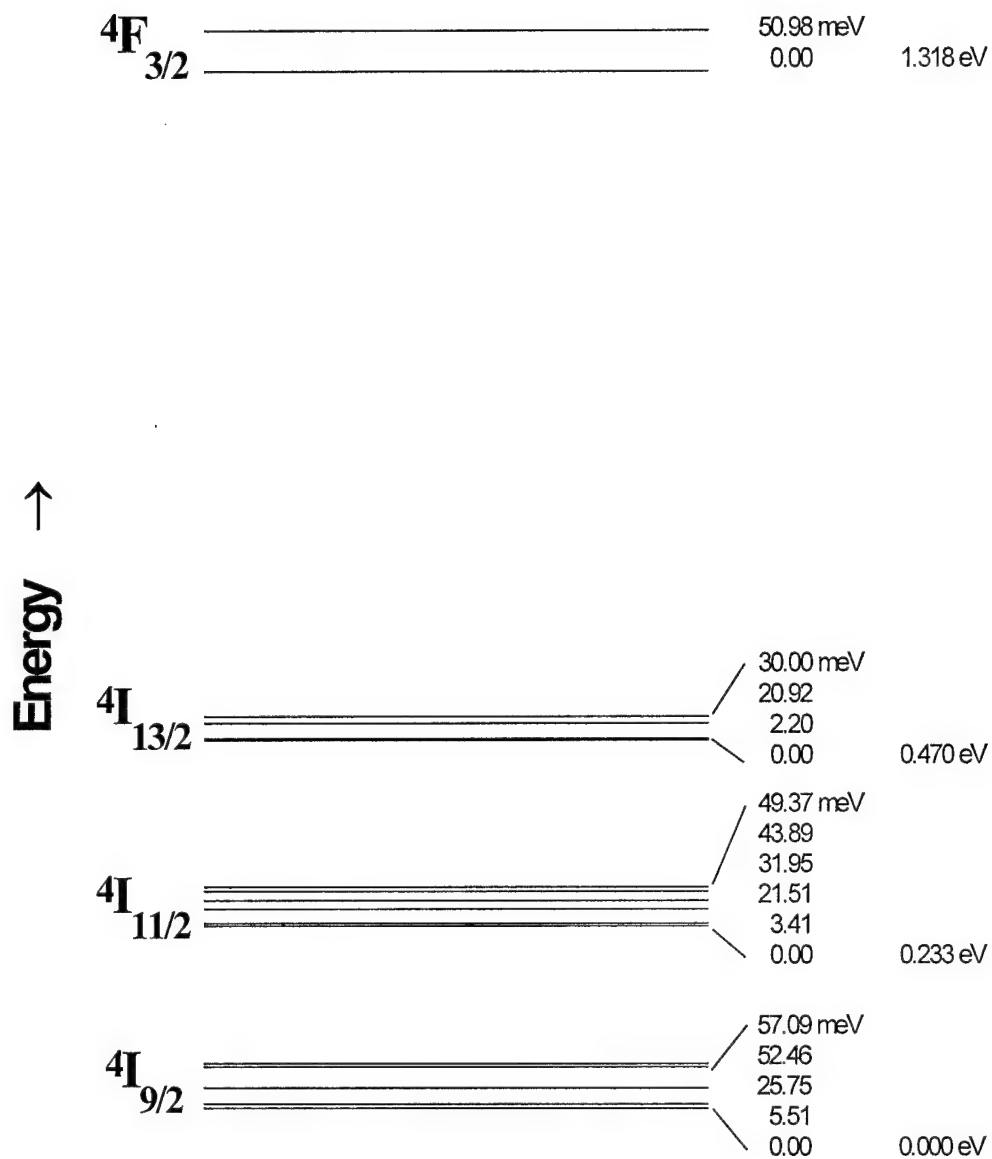
Figure 5-72. Energy level model for GaN:Nd^{3+}.

were mapped. Oxygen co-doping did not result in an increase in the Nd luminescence, and in fact may have been detrimental. Co-doping did not result in the observation of any additional Nd luminescence centers.

Two different Er doses, 1×10^{13} and 5×10^{13} cm^{-2}, were implanted at an energy of 1150 keV into MOCVD grown GaN from Honeywell. The samples were furnace annealed by the proximity cap method in an NH$_3$ environment at 700, 800, 900, or 1000 °C for 90 min. As with Nd implanted GaN, annealing above 1000 °C was not performed since previous results with other implants resulted in detrimental surface degradation. Also, to further prevent surface deterioration during annealing, the proximity cap method was used.

Low temperature PL was performed using the 514.5 nm line of the Ar$^+$ ion laser. Below bandgap excitation photons were used since Er has been found to be luminescent with laser excitation at these wavelengths (Wilson *et al.*, 1995; Qiu *et al.*, 1995). Er^{3+} luminescence was observed in photoluminescence at sample temperatures of 2 K. Figure 5-73 shows strong luminescence from the $^4I_{13/2}\rightarrow{}^4I_{15/2}$ transitions near 1.54 μm and from the $^4I_{11/2}\rightarrow{}^4I_{15/2}$ transitions near 1 μm (Pappalando, 1977). Also present was a broad defect peak centered at about 1.2 μm. This peak was identical in shape and location to the peak observed in GaN:Nd. The origin of this peak was unknown, although it was very similar to a peak observed in GaAs:Er (Elsaesser *et al.*, 1995).

The $^4I_{13/2}\rightarrow{}^4I_{15/2}$ transitions of Er^{3+} at ~1.54 μm appeared in all samples, and increased in intensity as annealing temperature was increased from 700 to 1000 °C as shown in Figure 5-74. The luminescence associated with the $^4I_{11/2}\rightarrow{}^4I_{15/2}$ transition of
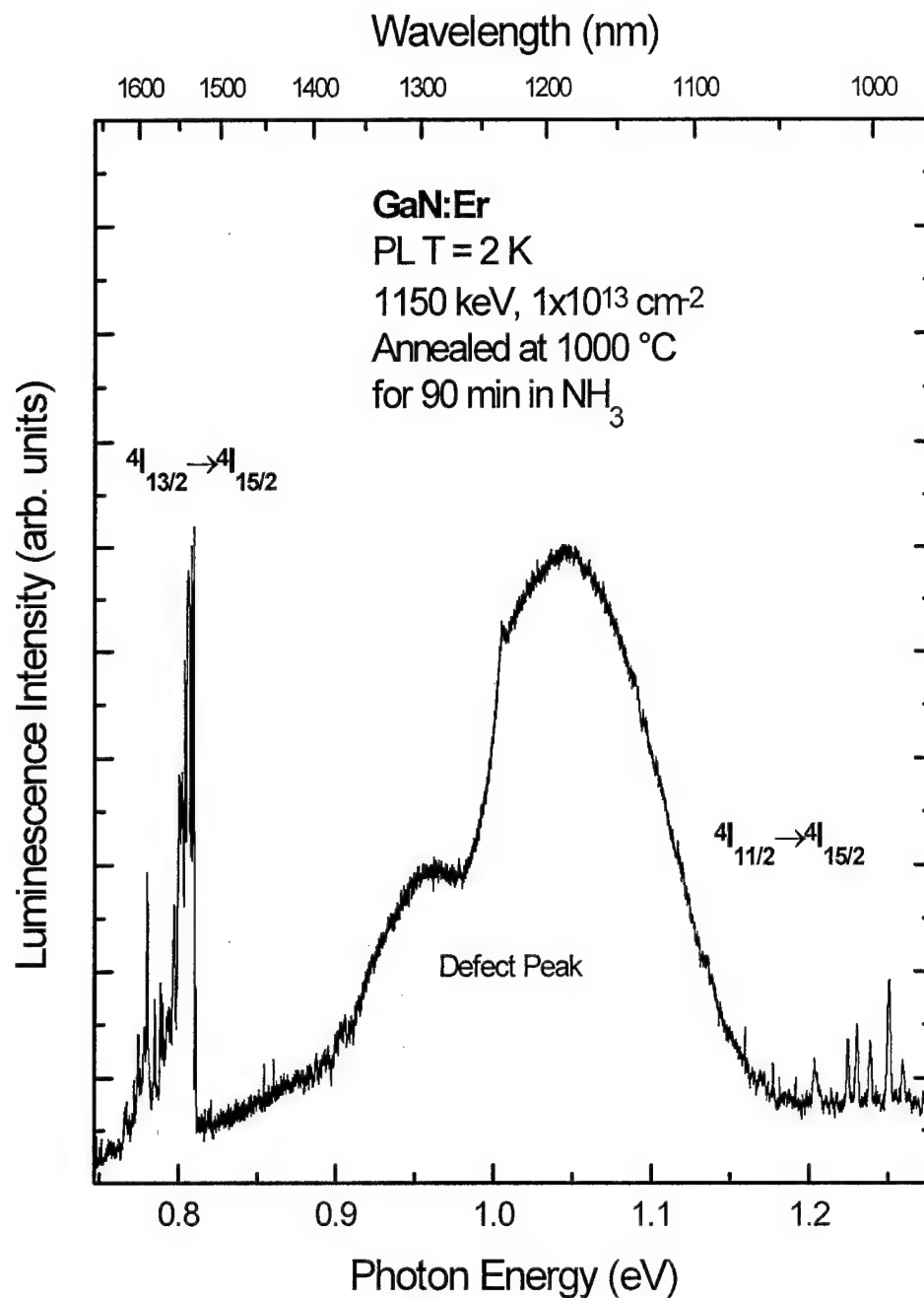
Figure 5-73. Photoluminescence spectra taken at 2 K for GaN implanted with erbium at 1150 keV to a dose of 5×10^{13} cm^{-2} and annealed at 1000 °C for 90 min in NH$_3$
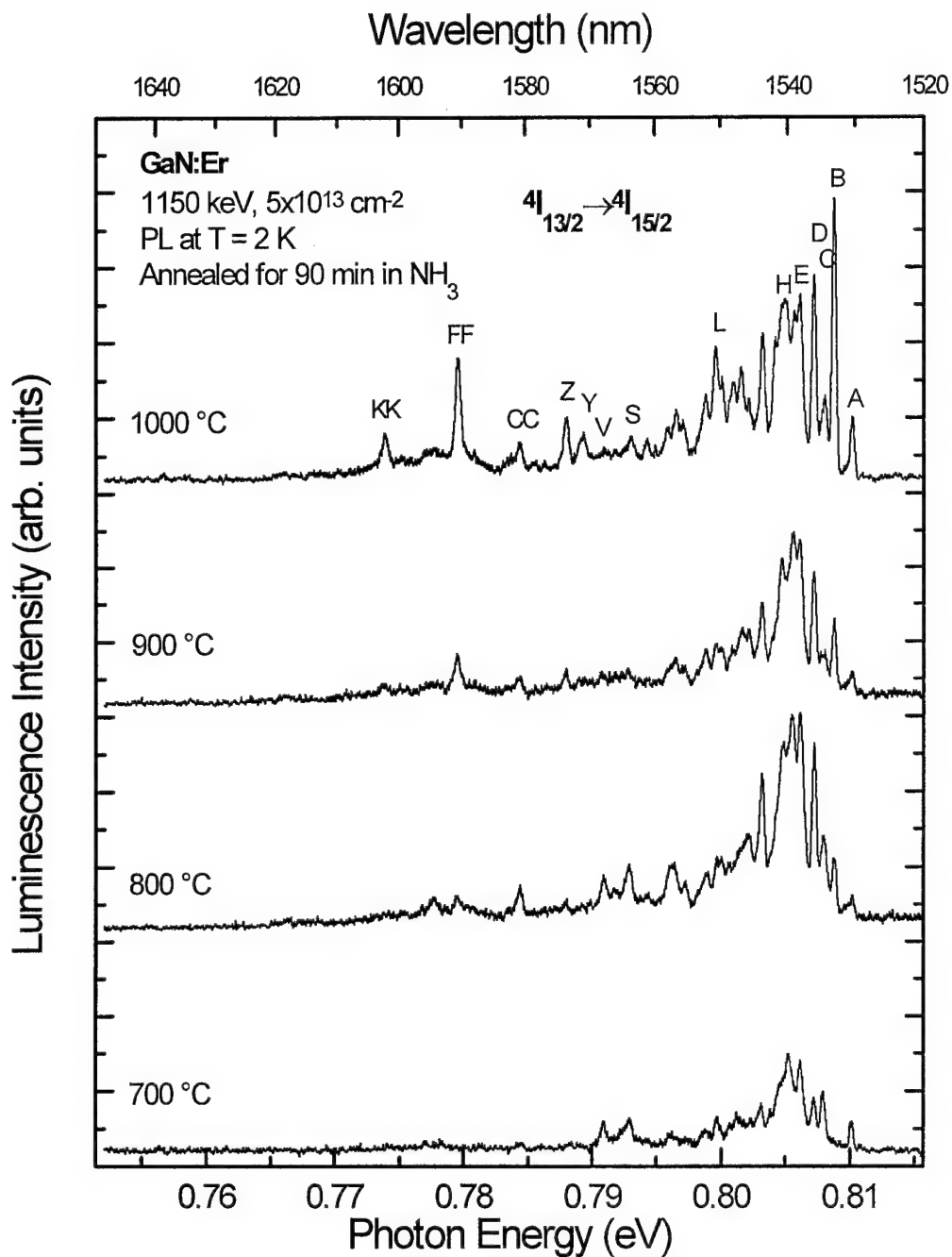
Figure 5-74. Photoluminescence spectra taken at 2 K from the $^4I_{13/2} \rightarrow {}^4I_{15/2}$ transition of Er^{3+} for GaN implanted with erbium at 1150 keV to a dose of 5×10^{13} cm^{-2} and annealed at various temperatures for 90 min in NH$_3$.

Er^{3+} at ~1.0 μm was not observed from the 700 °C annealed sample as shown in Figure 5-75. However, the ~1.0 μm transitions appeared in the 800 °C annealed sample, and increased in intensity with annealing temperature through the 1000 °C annealed sample.

The results demonstrated that a 1000 °C annealing temperature was optimal for Er optical activation of both manifolds of Er^{3+} in GaN. This result was similar to the findings for implanted Nd, Zn, and Mg in GaN, yet differed from the results of Wilson *et al.* (1995). They reported that the ~1.54 μm luminescence from GaN:Er co-implanted with oxygen decreased with annealing temperatures above 700 °C. Further investigation using oxygen co-implanted GaN was performed to explore whether co-doping was responsible for this difference. The results will be reported below. It was also interesting that the $^{4}I_{11/2} \rightarrow {}^{4}I_{15/2}$ transition was not observed for 700 °C anneals, and indeed Wilson *et al.* (1995) did not report having observed it. Qiu *et al.* (1995) also reported a negative result for the $^{4}I_{11/2} \rightarrow {}^{4}I_{15/2}$ transitions in low temperature CL for oxygen co-implanted GaN:Er. Thus, this was the first report of the $^{4}I_{11/2} \rightarrow {}^{4}I_{15/2}$ transitions occurring in GaN:Er. This was also the first report of Er luminescence for GaN not co-implanted with oxygen.

The energetic positions of the Er^{3+} lines of the $^{4}I_{11/2} \rightarrow {}^{4}I_{15/2}$ transitions were tabulated at each annealing temperature for the 5×10^{13} cm^{-2} dose samples, and are shown in Table V-6. Thirty-seven distinct lines have been tabulated. There were almost certainly more lines which could not be identified due to overlaps with the more intense
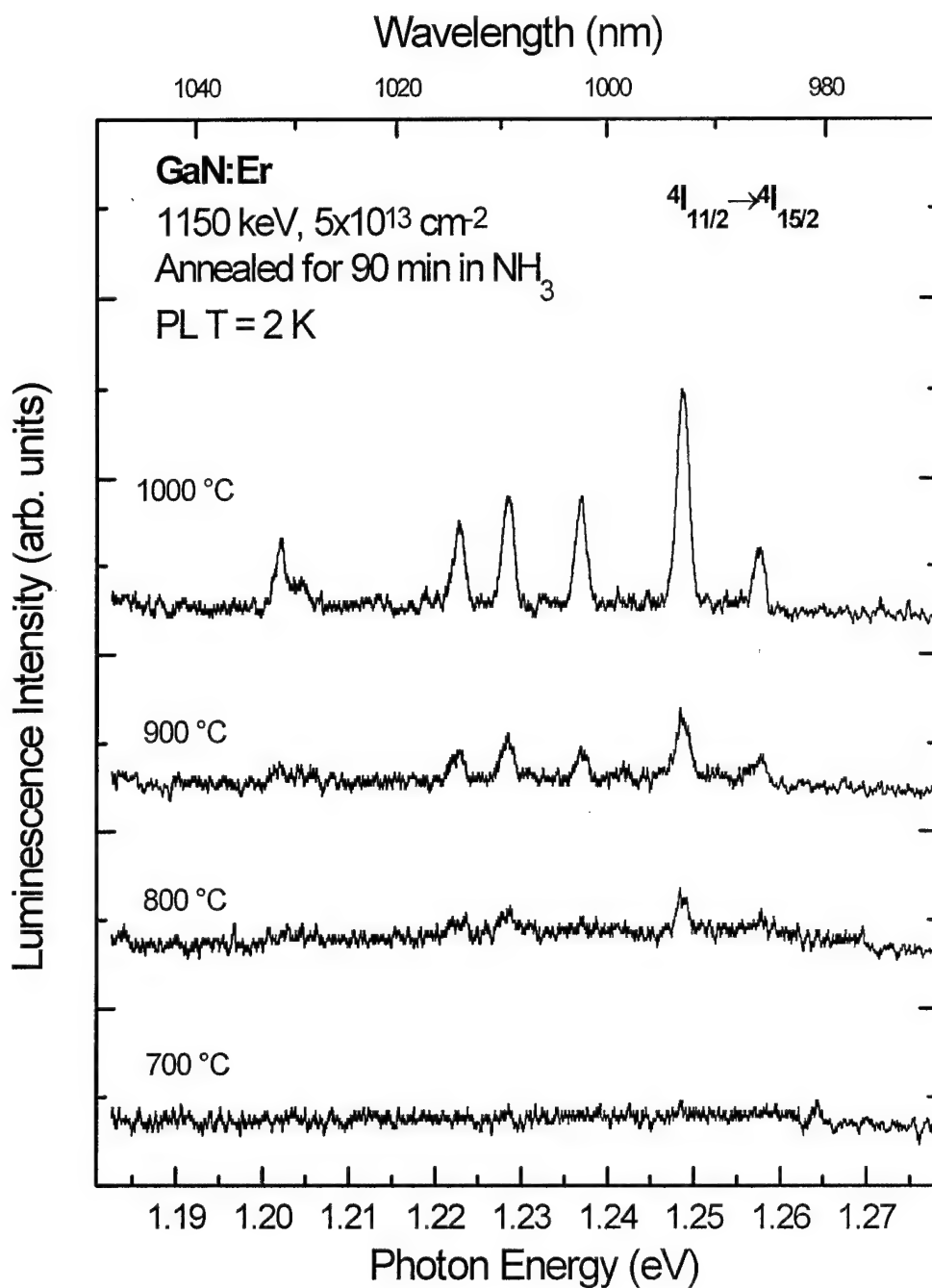
Figure 5-75. Photoluminescence spectra taken at 2 K from the $^4I_{11/2} \rightarrow {}^4I_{15/2}$ transition of Er^{3+} for GaN implanted with erbium at 1150 keV to a dose of 5×10^{13} cm^{-2} and annealed at various temperatures for 90 min in NH_3.

Table V-6. Energetic locations of observed Er^{3+} lines in GaN for samples annealed at 700, 800, 900, and 1000 °C .

Line	700°C	800°C	900°C	1000°C
	eV	eV	eV	eV
A	0.81016	0.81021	0.81012	0.81017
B		0.80873	0.80878	0.80876
C	0.80793	0.80797	0.80804	0.80803
D	0.80721	0.80722	0.80718	0.80718
E	0.80615	0.80611	0.80607	0.80611
F	0.80522	0.80550	0.80559	0.80568
G		0.80477	0.80474	0.80494
H	0.80314	0.80319	0.80320	0.80321
I		0.80215	0.80219	0.80217
J	0.80118		0.80166	0.80151
K				0.80103
L	0.79973	0.80002	0.79968	0.79957
M	0.79876	0.79896	0.79888	0.79881
N	0.79723	0.79726	0.79720	0.79703
O	0.79622	0.79639	0.79648	0.79650
P				0.79584
Q	0.79437	0.79439	0.79420	0.79487
R				0.79425
S	0.79294	0.79288	0.79364	0.79304
T			0.79277	
U		0.79173	0.79176	0.79170
V	0.79093	0.79088	0.79129	0.79088
W			0.79073	
X		0.78986	0.79001	
Y			0.78897	0.78929
Z	0.78823	0.78801	0.78796	0.78801
AA	0.78607			0.78631
BB				0.78554
CC	0.78415	0.78440	0.78440	0.78440
DD				0.78367
EE	0.78144		0.78091	0.78081
FF	0.78012	0.77951	0.77947	0.77953
GG	0.77816	0.77776		0.77780
HH	0.77711			0.77711
II				0.77582
JJ				0.77513
KK	0.77404	0.77382	0.77391	0.77385

peaks. Resolution and intensity were carefully adjusted to insure the maximum number of lines were observed. Weaker lines appeared as shoulders or as asymmetries of the distinct peaks. There were numerous lines which changed in relative intensity as annealing temperature was increased. These changes were indicative of multiple Er^{3+} luminescence centers (Colon *et al.*, 1993). Due to the sheer number of lines involved, it was difficult to determine the number of centers involved from these data alone; however, several trends in relative intensity vs. annealing temperature were observed.

Several lines showed a consistent trend of increasing intensity with annealing temperature. The lines labeled B, FF, and KK in Figure 5-74 were significantly stronger in the 1000 °C annealed sample as compared to those of the 700 °C sample. The lines labeled Y and Z also showed a distinct rise. This same set of lines increased in intensity with annealing temperature in the 1×10^{13} cm^{-2} dose samples as well, proving that this effect was not spurious. Figure 5-76 shows how the normalized intensity of these peaks increased with annealing temperature. The peak intensities have been normalized against the strongest peak within each spectrum to remove the effects of sample to sample changes in overall luminescence intensity. The trend was somewhat obscured at the lower annealing temperatures due to the difficulty in distinguishing low intensity peaks from the background. There was also a clear trend of decreasing relative intensity found among the peaks labeled C, S, and V as shown in Figure 5-77. Another group of lines was found to peak in relative intensity with the 800 °C anneal, and drop in relative intensity for higher annealing temperatures as shown in Figure 5-78. Peaks in this
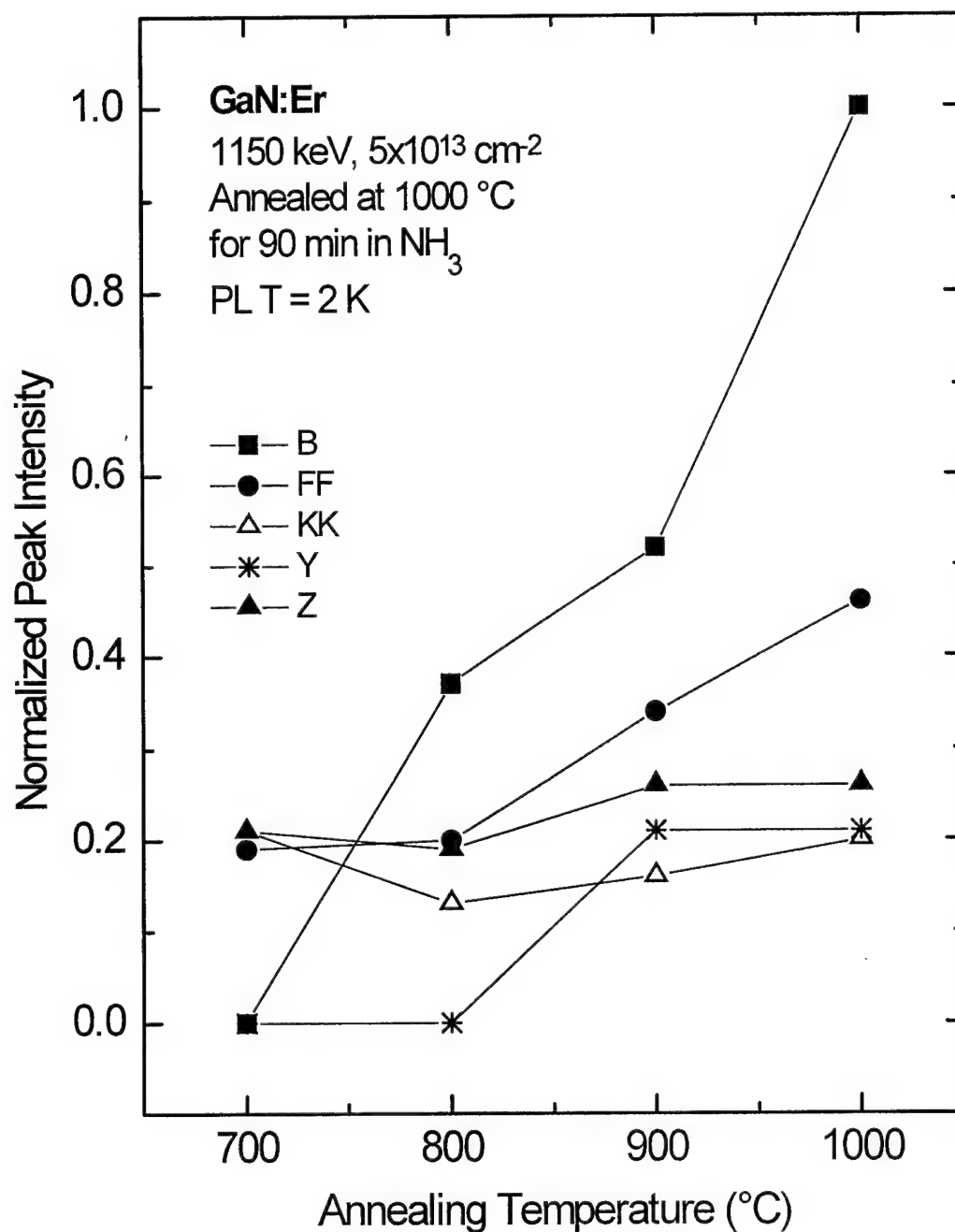
Figure 5-76. Photoluminescence peak intensity collected at 2 K plotted against annealing temperature for a set of peaks in the $^4I_{13/2} \rightarrow {}^4I_{15/2}$ group which increased in intensity with annealing temperature.
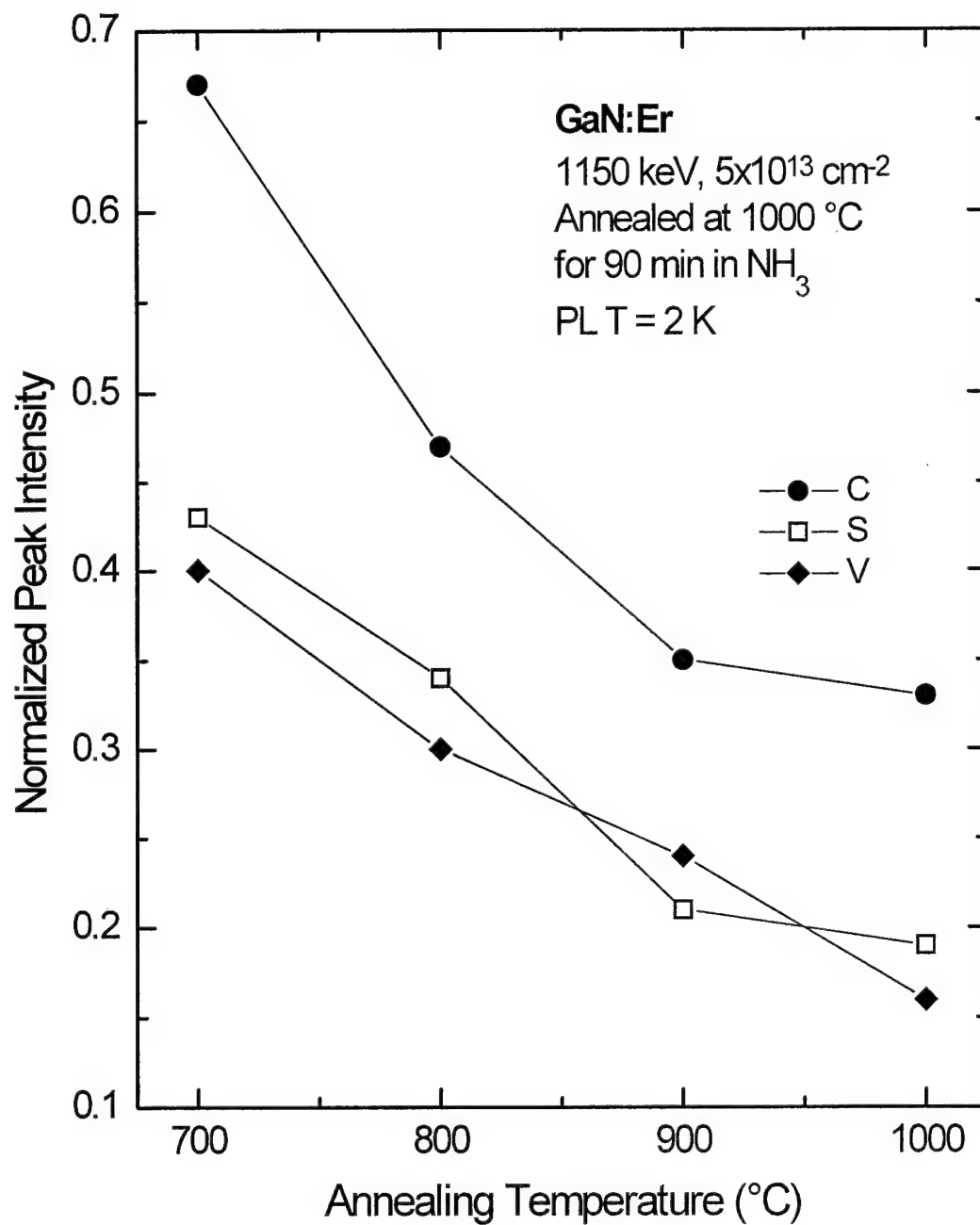
Figure 5-77. Photoluminescence peak intensity collected at 2 K plotted against annealing temperature for a set of peaks in the $^4I_{13/2} \rightarrow {}^4I_{15/2}$ group which decreased in intensity with annealing temperature.
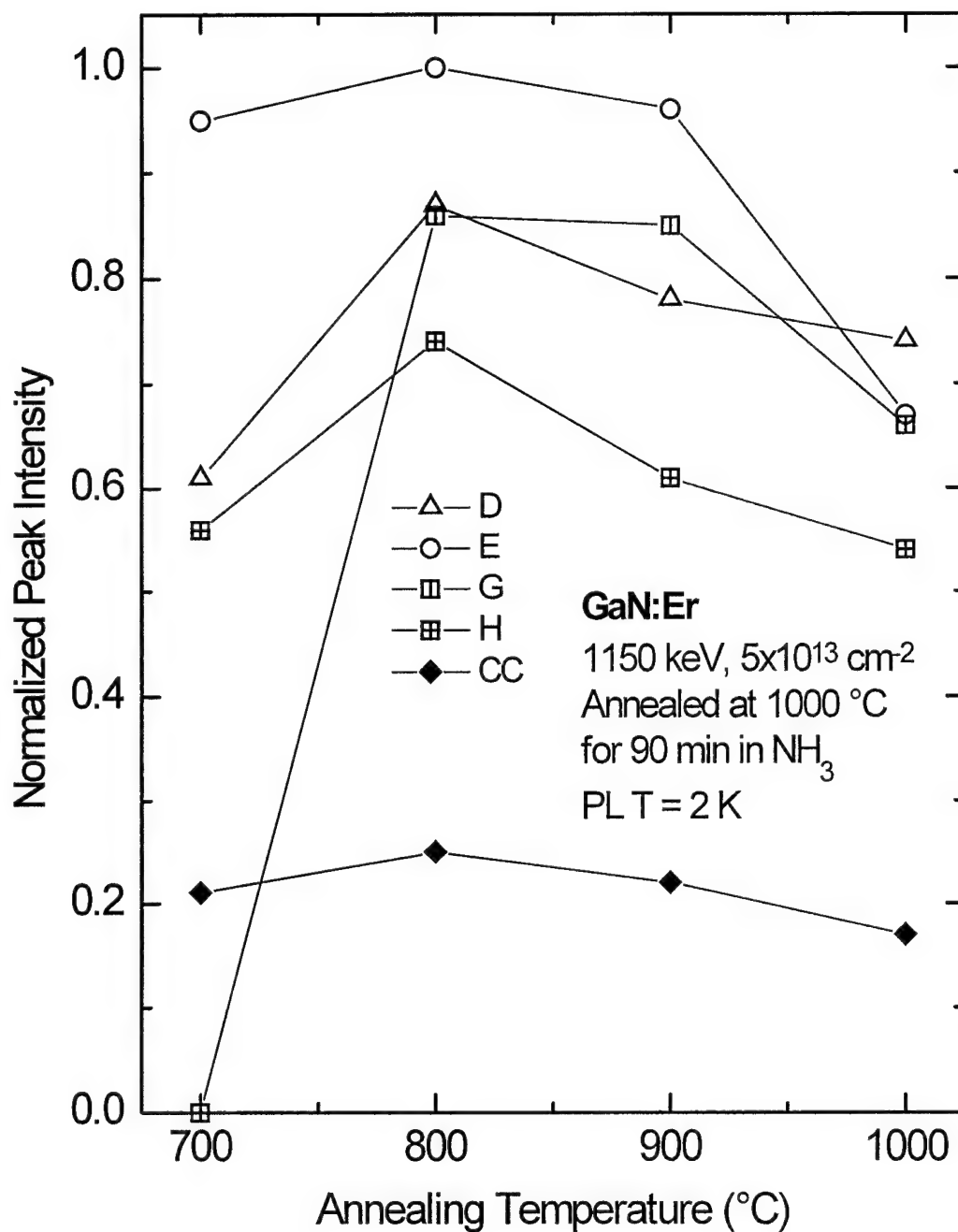
Figure 5-78. Photoluminescence peak intensity collected at 2 K plotted against annealing temperature for a set of peaks in the $^4I_{13/2} \rightarrow {}^4I_{15/2}$ group which peaked in intensity at an 800 °C annealing temperature.

category included D, E, G, H and CC. The remaining lines either were too weak in intensity to track with annealing temperature, or were too near other strong peaks which obscured any underlying trend. These groupings of peaks having distinct annealing temperature behaviors strongly suggested the presence of several distinct Er^{3+} luminescent centers with differing optimal annealing temperatures (Colon *et al.*, 1993; Bryant *et al.*, 1983). Thus, there were probably at least two, and possibly more distinct Er luminescent centers.

Observations about the energetic location of these lines gave valuable clues as to their origin. The energetic locations and spacing of those lines which increased in intensity with annealing temperature were compared to the energetic locations and spacing of those lines which were present in the 700 °C annealed sample. In order to determine whether these new lines originated or terminated on a common level with any set of lines in the 700 °C annealed sample set, the manifold was systematically shifted in energy with respect to itself to search for multiple coincidences of peak overlap. Such a coincidence would represent a case where two groups have identical energetic spacing. The greatest coincidence for the B, FF, and KK lines occurred when the manifold was shifted by +1.3 meV. This shift brought the A line into coincidence with the B line, the EE line into coincidence with the FF line, the JJ line into coincidence with the KK line, and the Y line into coincidence with the Z line. No consistent trend was found in the annealing temperature behavior of the A, EE, JJ, or Y lines; however, any such trend could have been obscured by the low intensity of these peaks. A negative shift was also explored; however, no significant coincidences were observed.

There are several possible ways to interpret these data. First, the two sets of peaks could have originated from different Er luminescent centers. In this case, the energy difference would be due to the differing crystal-field of two different Er^{3+} centers in GaN. Second, as shown in Figure 5-79a, these results could indicate that the A, Y, EE, and JJ all originated on a common level within the upper crystal-field split manifold, $^4I_{13/2}$. In which case, B, Z, FF, and KK would have also originated from a common upper crystal-field split level which was lower in energy than the level from which A, Y, EE, and JJ originated. Similarly, as shown in Figure 5-79b, these results could indicate that A, Y, EE, and JJ all terminated on a common lower level within the $^4I_{15/2}$ manifold. In which case, B, Z, FF, and KK would have all terminated on a common lower level which was higher in energy than the level which A, Y, EE, and JJ terminated on. The final possibility was that these spacings were coincidental, however, this seemed unlikely since all of the high temperature annealing lines showed the same spacing with respect to lines present at all annealing temperatures. Based on the fact that a consistent energy spacing was found, and that higher energy lines were of low intensity, the most likely origin of these peaks was that the A, EE, and JJ lines all originated from a common energy level which was 1.3 meV above the energy level from which the B, FF, and KK lines originated. This would be the case illustrated in Figure 5-79a.
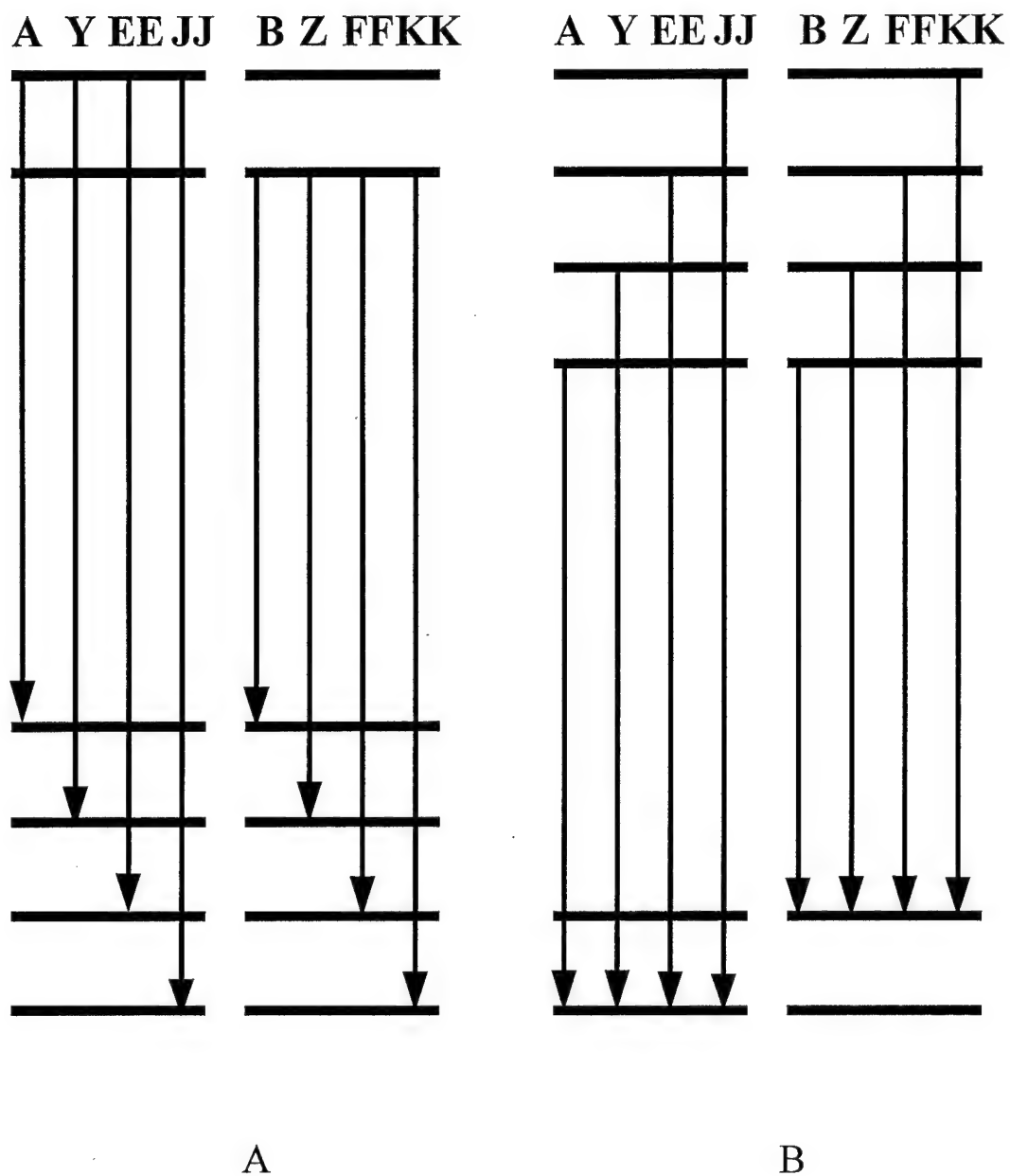
Figure 5-79. Two scenarios to account for the observed spacings of two groupings of peaks in the $^4I_{13/2} \rightarrow {}^4I_{15/2}$ transition.

The underlying cause for the changes in relative intensities among the various luminescence peaks as annealing temperature was increased cannot be determined with absolute certainty from the data in hand. However, it was clear that some change must have occurred in the nature of the Er^{3+} luminescence centers as annealing temperature was increased. First, since the total luminescence intensity does not increase substantially with annealing temperature, it was probable that the number of Er luminescence centers did not change substantially. Thus, this change must be related to the nature of the Er centers or the energy transfer mechanism. These results could indicate that a different type of Er luminescent center was formed at high annealing temperature. A second possibility was that this change could have resulted from an increase in the luminescence efficiency of the B, Z, FF, and JJ transitions within one type of Er^{3+} center due to the more ordered crystalline environment present after higher temperature annealing. However, the data was also clear in that the manifold of lines present in the 700 °C annealed sample was also present in the 1000 °C annealed sample albeit with some changes in relative line strengths. This fact argued for the conclusion that a different type of Er^{3+} center was created at the higher annealing temperature. Without further data, it remains impossible to pinpoint the cause, but it was without doubt that some change in the Er^{3+} luminescence did occur. Before further systematic study of the $^4I_{13/2} \rightarrow ^4I_{15/2}$ transitions is undertaken, it will be helpful to examine the data provided by the $^4I_{11/2} \rightarrow ^4I_{15/2}$ transitions.

The $^4I_{11/2} \rightarrow ^4I_{15/2}$ transitions observed with low temperature PL contained a relative few number of lines. Thus the assignment of these peaks to specific transitions

within the manifolds was simplified. At the lowest sample temperatures obtained, the most likely transitions were those originating from the lowest energy level within the upper manifold; in this case, the $^4I_{11/2}$. Thus, the presence of six lines in the low temperature PL spectra shown in Figure 5-74 would favor the hypothesis that these transitions originated in the lowest $^4I_{11/2}$ energy level, and terminated on the six lowest energy levels in the $^4I_{15/2}$ manifold. Thus, the first six energy spacings in the $^4I_{15/2}$ manifold would be determined by the peak spacings at a sample temperature of 2 K shown in Figure 5-74. For cubic symmetry, a maximum of only five lines would be expected (Lea *et al.,* 1962), and for non-cubic symmetry a maximum of eight lines would be expected (Walton 1984). Since six well resolved lines were observed at a sample temperature of 2 K, the lines must have come from either more than one Er^{3+} luminescence center or from a single Er^{3+} luminescence center of non-cubic symmetry. Since the annealing temperature dependence showed only a consistent increase of all luminescence lines with annealing temperature, it was unlikely more than one luminescence center was involved in these emissions. Thus, the best model was that a single Er^{3+} luminescence center of non-cubic symmetry was responsible for the ~1.0 μm luminescence. Since only six of a maximum of eight expected lines were observed, it was likely that the other two lines were either not strong enough to be observed, or were nearly degenerate with other lines.

'Hot' lines were observed in the $^4I_{11/2} \to {}^4I_{15/2}$ manifold as sample temperature was increased to 25 K, but the luminescence was almost completely quenched by 175 K. Figure 5-80 shows the sample temperature dependence behavior of this group of transitions up to 175 K. The six lines labeled a, c, d, f, h, and j were all present at a sample temperature of 2 K. As sample temperature was increased, at least five new lines labeled b, e, g, i, and k appeared with increasing relative intensity. With the exception of the g line which had the weakest intensity, all of the 'hot' lines were spaced at approximately the same distance from the low sample temperature lines immediately lower in energy. Figure 5-81 shows that the relative spacing of the 'hot' lines also followed very closely the non-equal spacing of the low sample temperature lines.

Under a shift of +4.45 meV, the lines a, d, h, and j fell almost exactly on the positions of b, e, i, and k, respectively. The c line became almost coincident with the position of the d line after the shift. Thus, due to overlap, no 'hot' line could be observed for the c peak. The data strongly fit a model wherein the low temperature lines originated from the lowest energy crystal-field split level within the $^4I_{11/2}$ manifold. Furthermore, the 'hot' lines all originated from a common, higher laying energy level within the $^4I_{11/2}$ manifold, and terminated upon the corresponding energy level within the $^4I_{15/2}$ manifold. Thus, the energy spacing of the crystal-field split levels involved could be determined. Figure 5-82 shows the best fit to the data for the $^4I_{11/2}$ and $^4I_{15/2}$ manifolds. Only six of a maximum eight expected energy levels could be mapped for the $^4I_{15/2}$ manifold, and only two of a maximum of six levels could be mapped for the $^4I_{11/2}$ manifold.
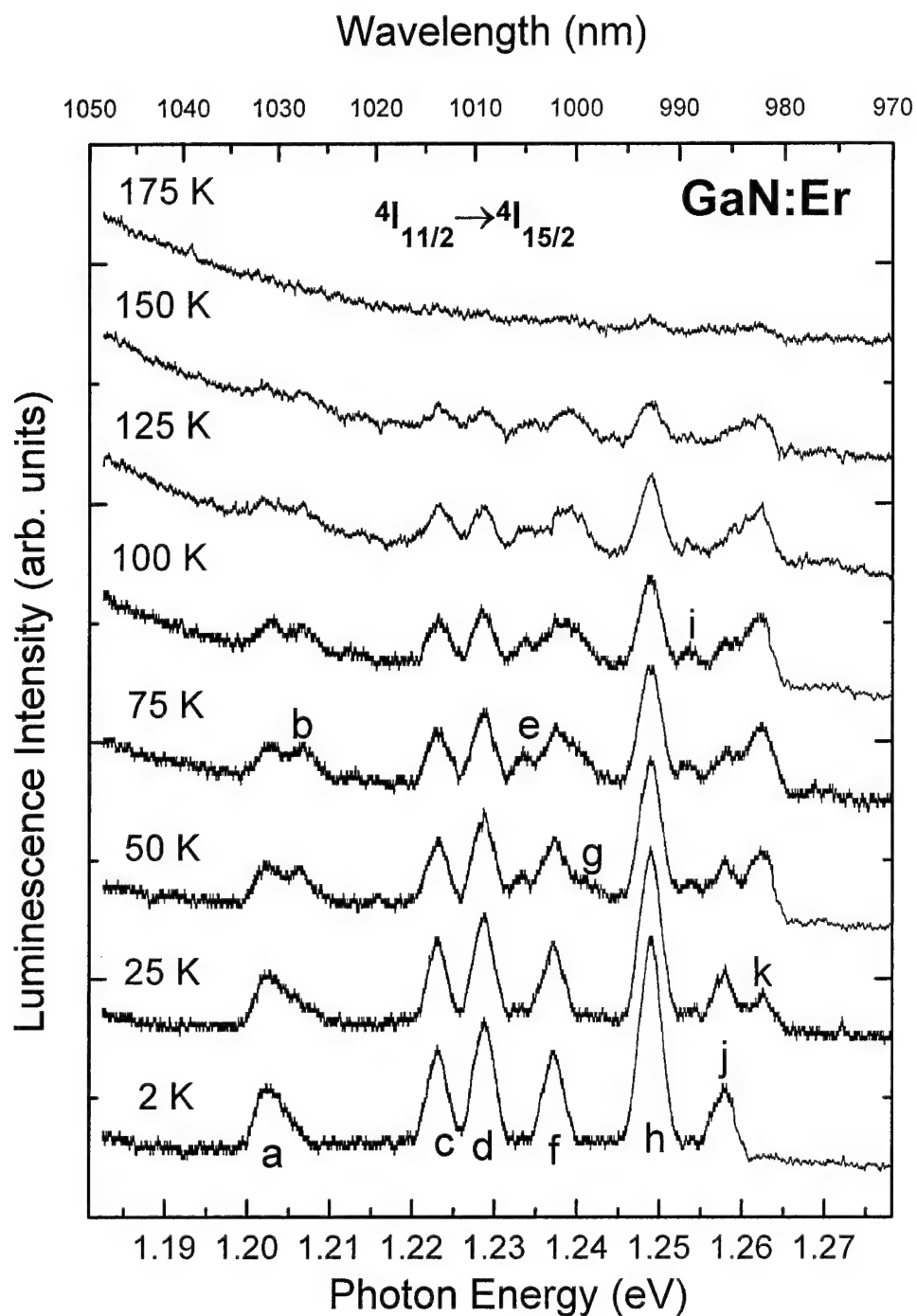
Figure 5-80. Photoluminescence spectra taken from 2 to 175 K from the $^4I_{11/2} \rightarrow {}^4I_{15/2}$ transition of Er^{3+} for GaN implanted with erbium at 1150 keV to a dose of 5×10^{13} cm^{-2} and annealed at 1000 °C for 90 min in NH_3.

Er 1 μm Peak Spacings
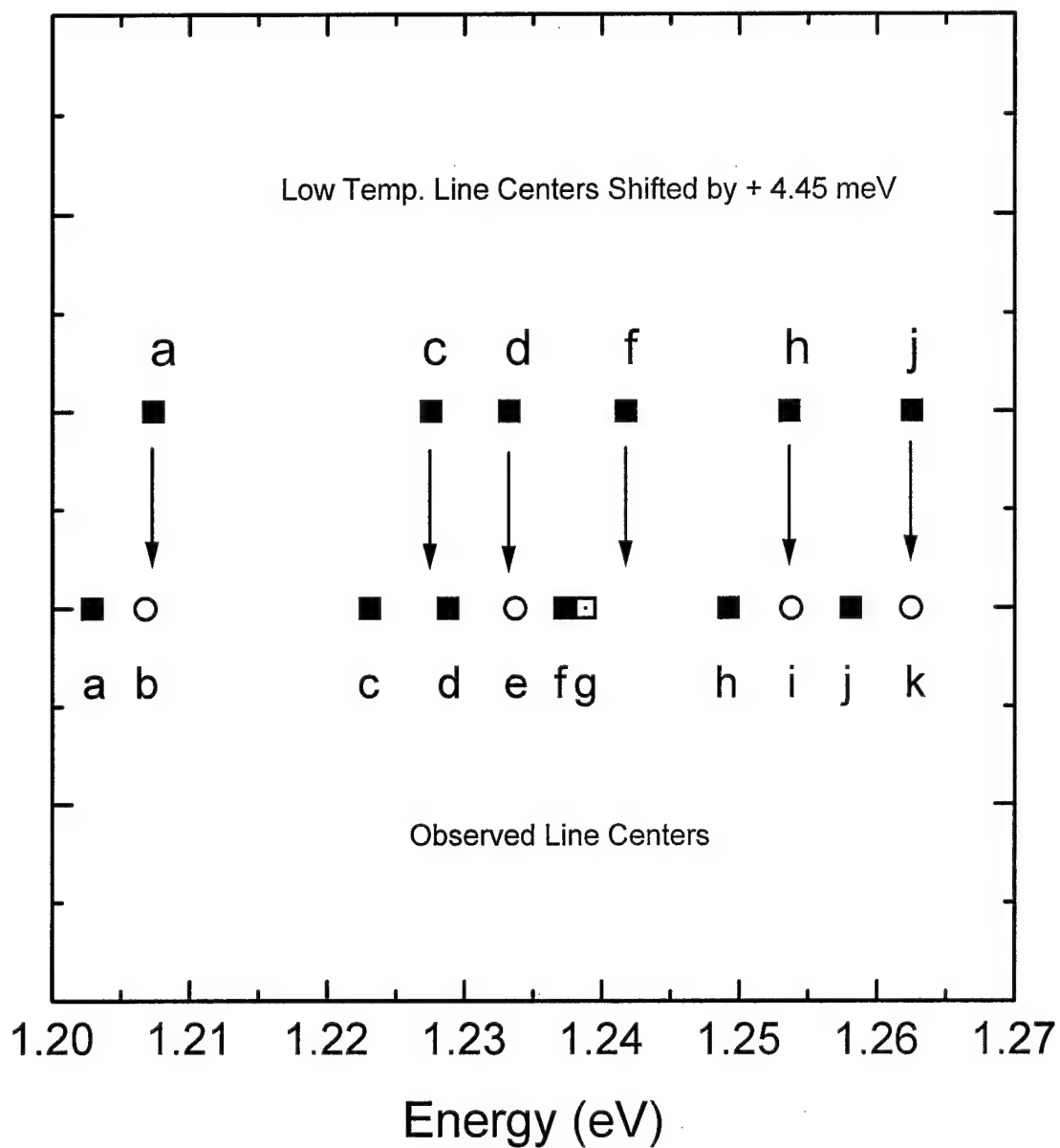
Figure 5-81. Energy spacing observed for the $^4I_{11/2} \rightarrow {}^4I_{15/2}$ transitions of Er^{3+} in GaN.

Erbium Energy Levels
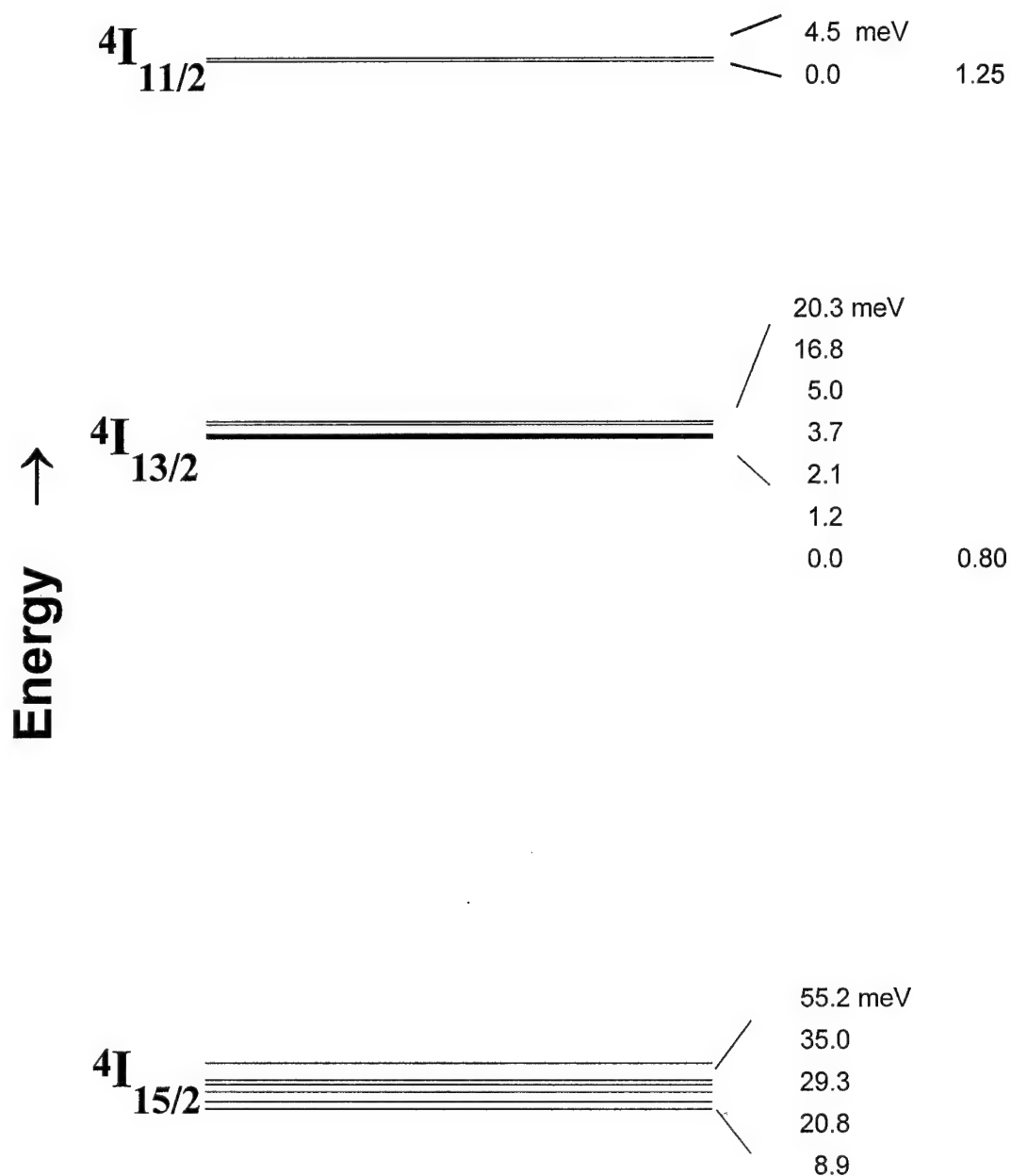
Figure 5-82. Assigned energy spacings for the first Er^{3+} luminescence center.

The $^4I_{13/2}$ manifold was mapped by examining the ~1.54 µm emissions at low temperature. The lines which increased in intensity together with annealing temperature, the B, Z, FF, and KK lines, were found to have energy spacings consistent with the spacings found from the $^4I_{15/2}$ manifold. If the B line originated for an energy level 0.8088 eV above the ground state, then the Z, FF, and KK spacings fit as shown in Figure 5-82. The other line which was found to increase in intensity with annealing temperature was the Y line. Recalling the earlier discussion, the Y line was found to be consistent with a transition originating from 1.3 meV above the Z line. In fact, the A to D, EE to FF, and JJ to KK spacings were all 1.3 meV. Thus, those lines were also consistent with the energy spacings of the $^4I_{15/2}$ manifold if they all originated from a level 1.3 meV above the other set. These transitions are also shown in Figure 5-83. It should also be noticed that the J transition was also fit by this energy diagram. The J peak also appeared to increase in intensity with annealing temperature although its increase was somewhat obscured by the other closely spaced spectral features. Also of note was the peak predicted by this energy schedule to occur predicted at 0.8002 eV, which was not labeled in the 1000 °C annealed sample's spectrum. After close examination of the spectrum, there does appear to be a peak in the region between the L (0.7996 eV) and K peaks (0.8010 eV). None of the transitions which decreased in intensity or peaked at 800 °C as annealing temperature was changed were predicted by these energy spacings. Furthermore, since the $^4I_{15/2}$ energy spacings were consistent, it was also clear that these

transitions must all be related to the same Er luminescence centers responsible for the ~1.0 μm transitions.

Additional luminescence peaks can be predicted by the model when the D, E, and G energy spacings are set as the energy level spacings in the ground state as shown in Figure 5-82. Only one transition predicted by this spacing was not observed; no peak was observed at an energy of 0.7977 eV. The D, E, G, and CC were all found to have a peak in relative intensity for the sample annealed at 800 °C. These energy levels are consistent with the $^4I_{15/2}$ energy spacing mapped earlier using data from the ~1.0 μm luminescence center. Thus, these two sets of peaks may originate from the same luminescence center.

However, in order to fit the C peak within this energy level model, a new energy level within the upper manifold was necessary. However, when this was done, none of the other unmatched peak positions were predicted through transitions to the known levels within the lower manifold. Furthermore, all of the newly predicted positions had not been observed. A similar situation was found for the other remaining unmatched peaks. To determine whether any pattern could be found, the energy spacings between the remaining unassigned peaks were examined. A new pattern was found which matched all of the remaining peaks except the C, R, and DD peaks as shown in Figure 5-83. This pattern was not consistent with the previously found energy spacings, but did explain nearly all of the remaining luminescence peaks. Thus, it was possible that these

Erbium Energy Levels

$^4I_{13/2}$ 4.6 meV
2.1
1.0
0.0   0.8

Energy →

$^4I_{15/2}$ 10.2 meV
6.2
0.0   0.000
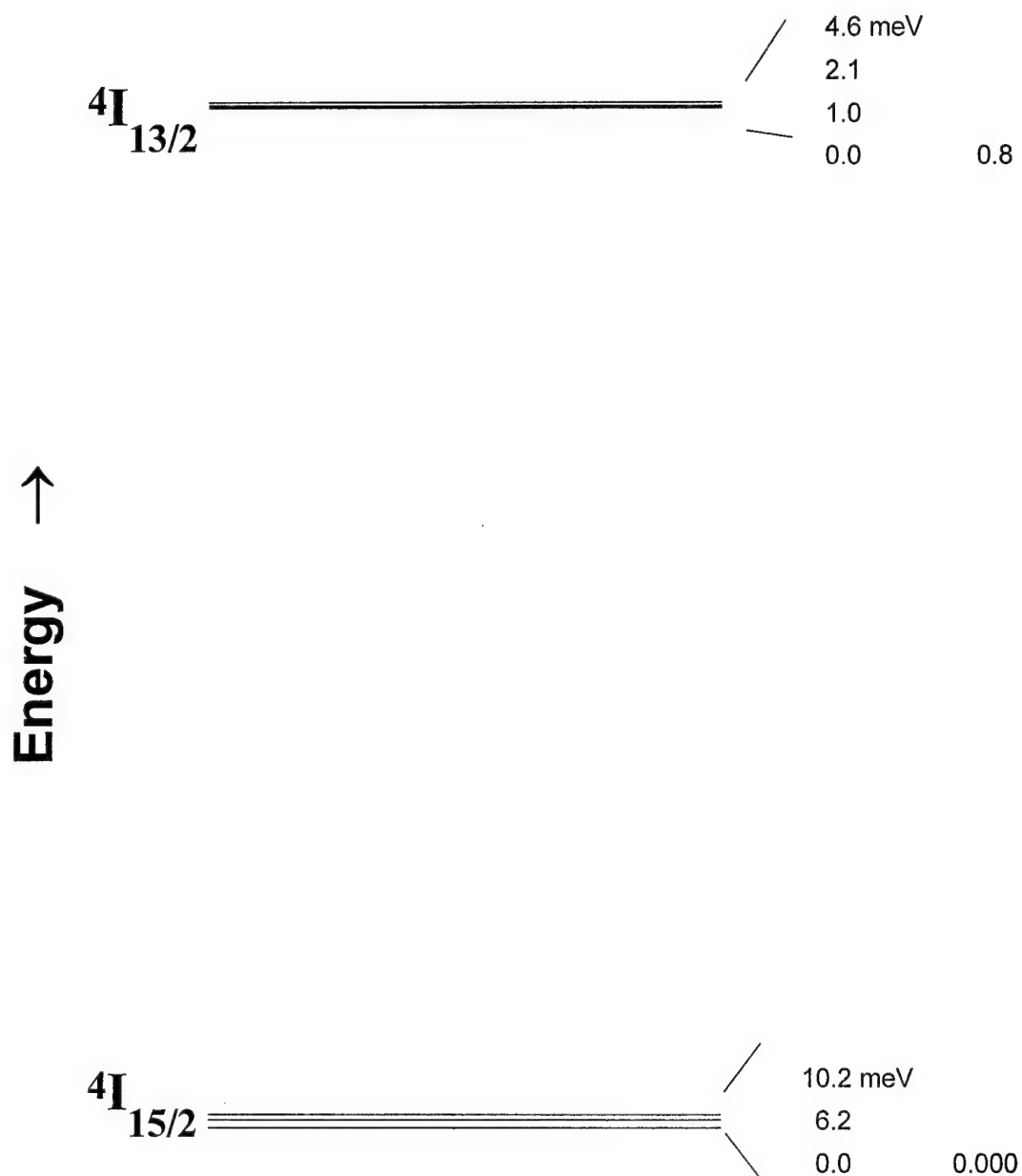
Figure 5-83. Assigned energy spacings for second Er^{3+} luminescence center.

peaks all originated from a second Er luminescence center distinct from the luminescence center responsible for the $^4I_{11/2} \rightarrow {}^4I_{15/2}$ transitions.

The appearance of 'hot' lines in the room temperature $^4I_{13/2} \rightarrow {}^4I_{15/2}$ spectrum of the 1000 °C annealed sample gave further peaks to fit. Figure 5-84 shows a high resolution spectrum taken at 300 K. Unfortunately, the lower intensity and thermal broadening of the background made it more difficult to identify the Er peaks. The peaks which occurred at energies above the A peak were of most interest. In fact, no new lower energy peaks were found. Three new peaks at 0.8254, 0.8219, and 0.8168 eV were identified. These peaks were fit with the two remaining unassigned energy levels in the $^4I_{13/2}$ manifold. Several predicted peaks resulted from this assignment ,which were not observed at low temperature. Table V-7 shows the peak positions and identifications for the energy level model developed to fit the majority of the luminescence peaks observed.

In contrast to the $^4I_{11/2} \rightarrow {}^4I_{15/2}$ luminescence at ~1.0 μm, the $^4I_{13/2} \rightarrow {}^4I_{15/2}$ luminescence of Er^{3+} at ~1.54 μm remained strong as sample temperature was raised to room temperature as seen in Figure 5-85. New, higher energy 'hot' lines also appeared in this manifold as temperature was increased, but the integrated intensity of the entire manifold of lines dropped by less than 50% as sample temperature was increased from 2 to 300 K. These results were similar to the findings of Wilson *et al.* (1995), who reported sample temperature dependence data for oxygen co-implanted GaN:Er. They observed a negligible loss of luminescence intensity for this manifold as sample temperature was increased from 6 to 77 K, and a factor of two loss in intensity from 77 to 300 K. Qiu *et*
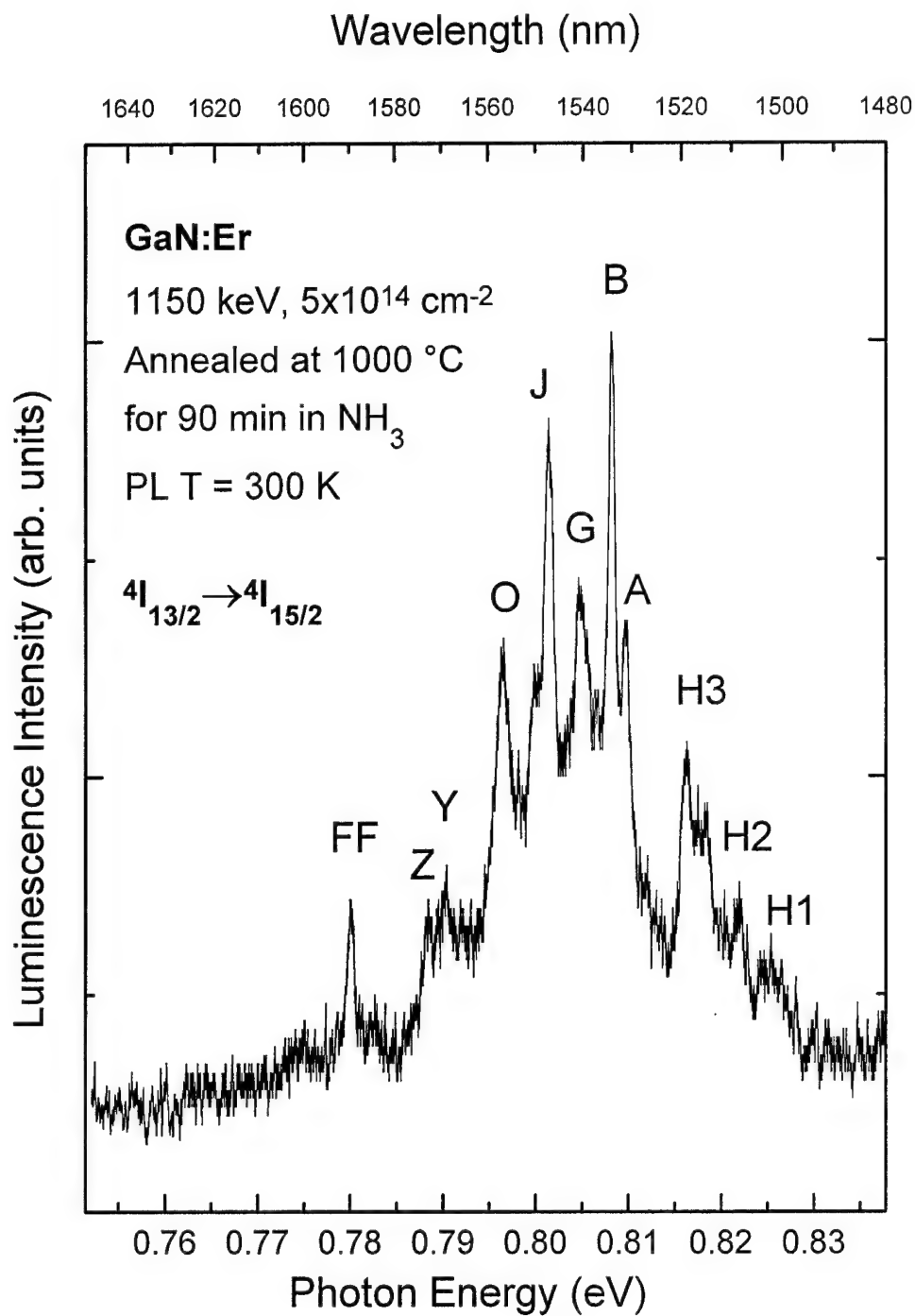
Figure 5-84. High resolution photoluminescence spectrum of the $^4I_{13/2} \rightarrow \, ^4I_{15/2}$ transitions taken at 300 K for GaN implanted with Er at 1150 keV to a dose of 5×10^{13} cm^{-2}.
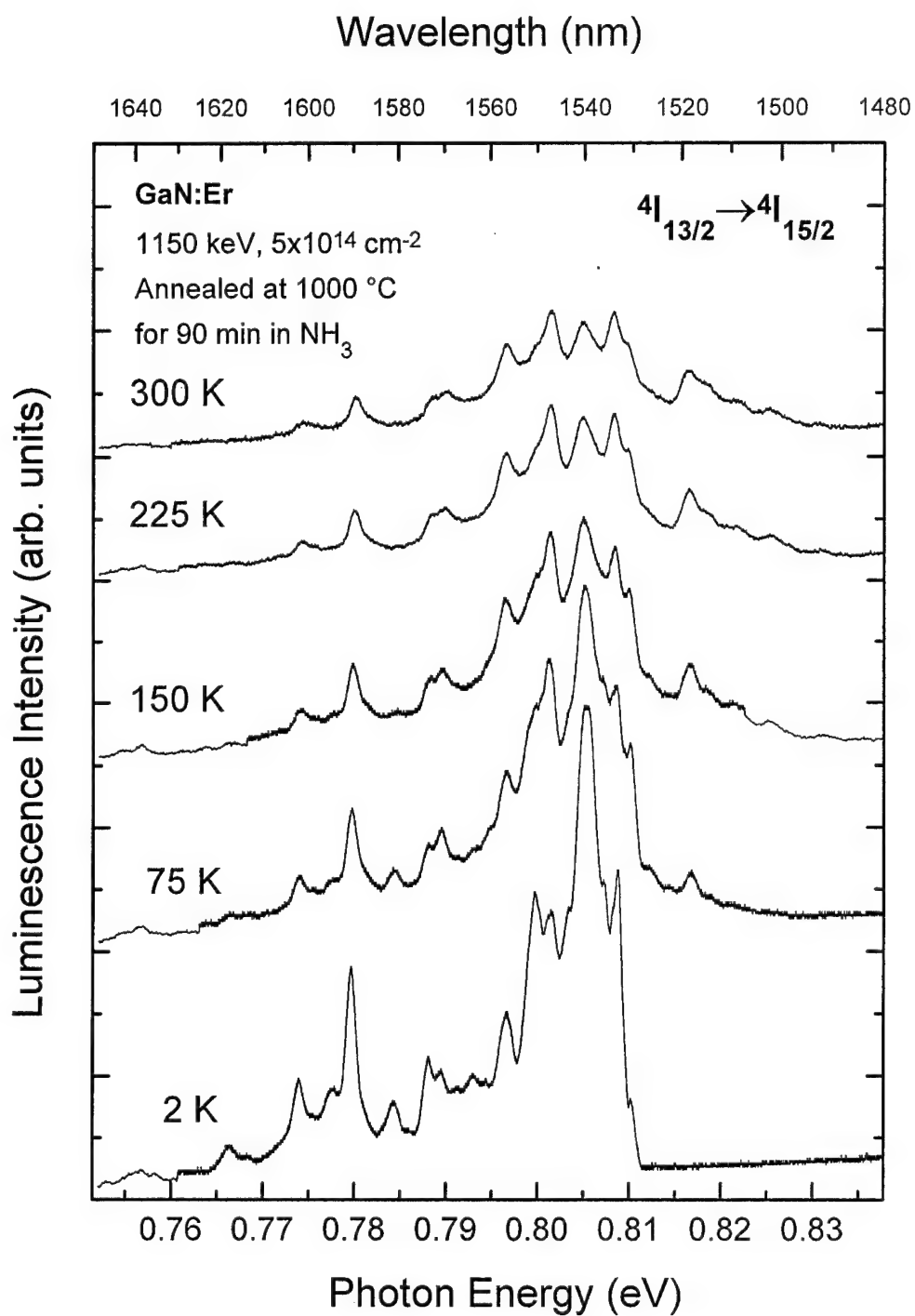
Figure 5-85. Photoluminescence spectra of the $^4I_{13/2} \rightarrow {}^4I_{15/2}$ transitions taken at various temperatures for GaN implanted with Er at 1150 keV to a dose of 5×10^{13} cm^{-2}.

Table V-7. Predicted transition energies and assignments for Er luminescence center.

Lower	Upper Energy Level (eV)						
	0.8254	0.8219	0.8101	0.8088	0.8072	0.8063	0.8051
0.0552	0.7702	0.7667	0.7549	0.7536	0.7520	0.7511	0.7499
0.0350	0.7904	0.7869	JJ 0.7751	KK 0.7738	0.7722	0.7713	0.7701
0.0293	0.7961	0.7926	EE 0.7808	FF 0.7795	GG 0.7779	HH 0.7770	II 0.7758
0.0208	0.8046	K 0.8011	Y 0.7893	Z 0.7880	AA 0.7864	BB 0.7855	CC 0.7843
0.0086	H3 0.8168	0.8133	J 0.8015	0.8002	M 0.7986	0.7977	O 0.7965
0.0000	H1 0.8254	H2 0.8219	A 0.8101	B 0.8088	D 0.8072	E 0.8063	G 0.8051

al. (1995) only observed a decrease in intensity of 18% for oxygen co-implanted GaN:Er as sample temperature was increased from 8 to 300 K. The demonstration of room temperature Er emissions in GaN was consistent with the results of Fauvenec *et al.* (1989) who found an increase in the temperature limit for quenching of Er emissions as the bandgap of the semiconductor hosts increased. Since GaN has a large bandgap, the temperature at which Er emissions should quench was expected to be above room temperature. This prediction has been borne out.

An Arhennius plot was generated from the normalized integrated area under the luminescence peaks as sample temperature was increased. Figure 5-86 shows two regions which were fit by two different activation energies. The low temperature region was fit by an activation energy of 0.11 meV, which had its onset at 2 K ($\cong$ 0.17 meV). The higher temperature region had an activation energy of 9.39 meV, and had an onset at 110 K ($\cong$ 9.48 meV). Since the onset temperatures for these activation processes were so
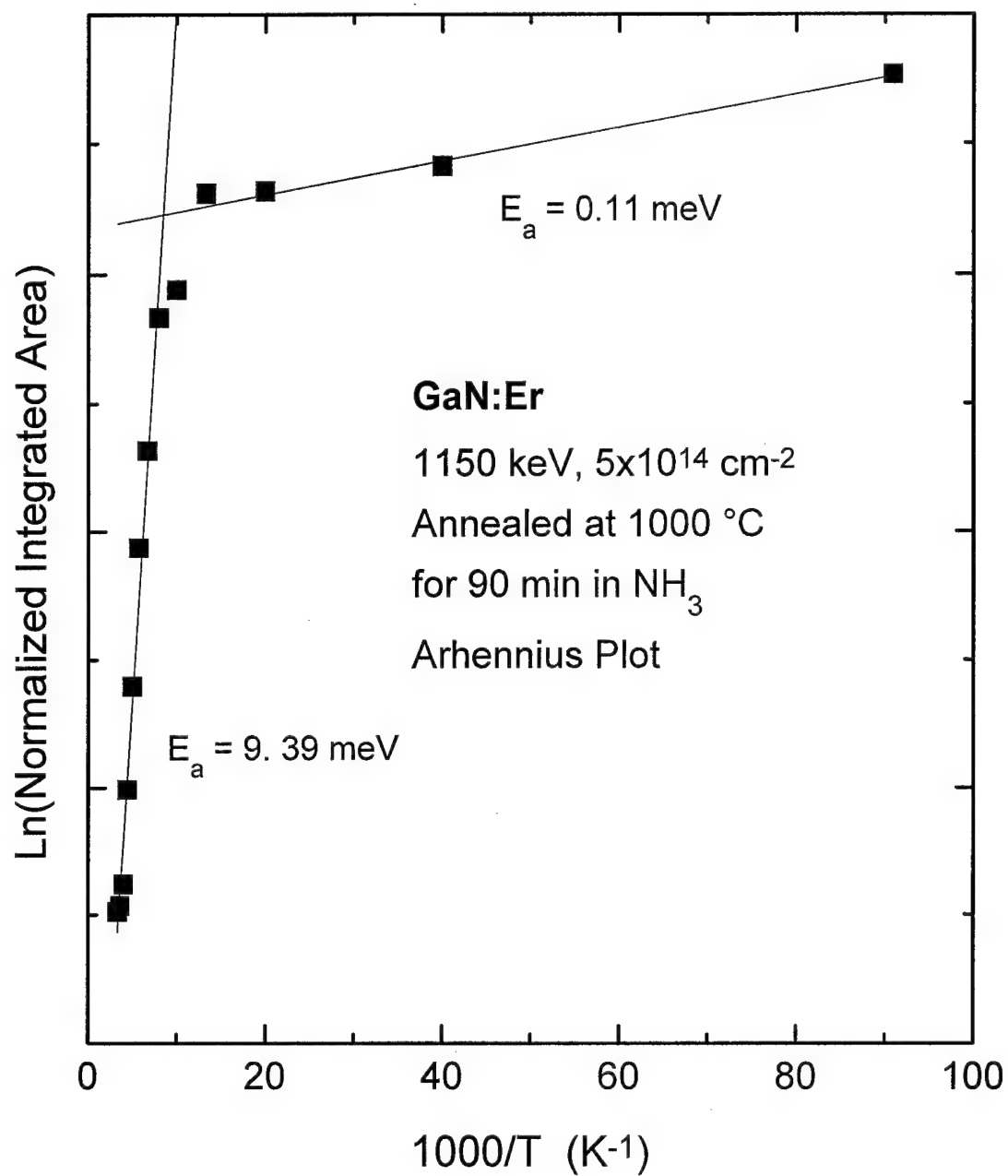
Figure 5-86. Arhennius plot of the integrated area under the $^4I_{13/2} \rightarrow {}^4I_{15/2}$ transitions of Er^{3+} as a function of temperature.

close to the thermal energy available at that temperature, it appeared that the activation processes responsible for the drop in luminescence intensity were purely thermal. Thus, as the temperature increased, the probability for non-radiative de-excitation of the Er luminescence centers increased.

As with Nd implanted GaN, limited comparisons of dose dependence were possible using the two different doses implanted. Figure 5-87 shows a comparison of low temperature PL from the $^4I_{13/2} \rightarrow {}^4I_{15/2}$ transition for the two different doses of Er implanted, 1×10^{13} and 5×10^{13} cm^{-2}. Both Er doses showed identical manifolds of lines and nearly identical annealing behavior with temperature including the relative intensities of the luminescence peaks. Thus, it could be concluded that no differentiation in the luminescence centers occurred due to dose within the limited range examined. The only change observed between the two doses was a change in the total intensity of the Er related luminescence. The intensity of the strongest peak in each manifold was between three and five times larger in the higher dose samples. Allowing for the inherent uncertainty in measuring relative intensities between different samples, and since the difference in dose was a factor of five, the evidence demonstrated that the doses selected have not exceeded the solubility limit of Er in GaN.

Photoluminescence excitation of GaN:Er was performed using the available discrete lines of the Ar$^+$ laser. A laser power level of 50 mW was used since this power level was obtainable for all lines. All wavelengths were below the low temperature GaN bandgap at ~3.5 eV with the exception of the multiline UV excitation between 351.1 and

Figure 5-87. Photoluminescence spectra taken at 2 K from the $^4I_{13/2} \rightarrow {}^4I_{15/2}$ transition of Er^{3+} for GaN implanted with erbium at 1150 keV to a dose of 1×10^{13} cm^{-2} and 5×10^{13} cm^{-2} and annealed at 1000 °C for 90 min in NH$_3$.

363.8 nm (3.408-3.531 eV). Both manifolds of transitions were observed for each excitation wavelength. Figure 5-88 shows that the $^4I_{11/2} \rightarrow ^4I_{15/2}$ transition contains all of the same lines as were observed with 514.5 nm excitation. Lower resolution was necessary since the laser power levels were lower. However, it was apparent that all of the same lines were present. No new Er^{3+} lines were observed in this manifold under higher energy photon excitation; however, with the exception of the k line, all of the previously observed 'hot' lines were apparent in the UV excited sample even at low temperatures. The appearance of these lines may indicate surface heating of the GaN:Er by the UV laser radiation. However, the temperature dependent data showed that the low temperature lines quenched upon heating. Thus, it was more likely that this indicated some change in the energy transfer to these lines. It was also notable that the total intensity of the luminescence did not change substantially with the change in excitation wavelength except for the case of UV excitation. Since the number of available photons decreased with decreasing wavelength (at constant laser power), one might expect a decrease in luminescence intensity with decreasing wavelength. Figure 5-89 shows the peak height of the h peak relative to it's value for the 514.5 nm spectrum as a function of the relative number of photons in the laser beam. We can define an external quantum efficiency for the RE luminescence as the ratio of RE 4f shell photons generated divided by the number of excitation photons absorbed. Thus, if we assume a constant external quantum efficiency, the RE luminescence intensity should decrease proportionally with the decreasing number of photons in the exciting laser beam. The data were quite noisy
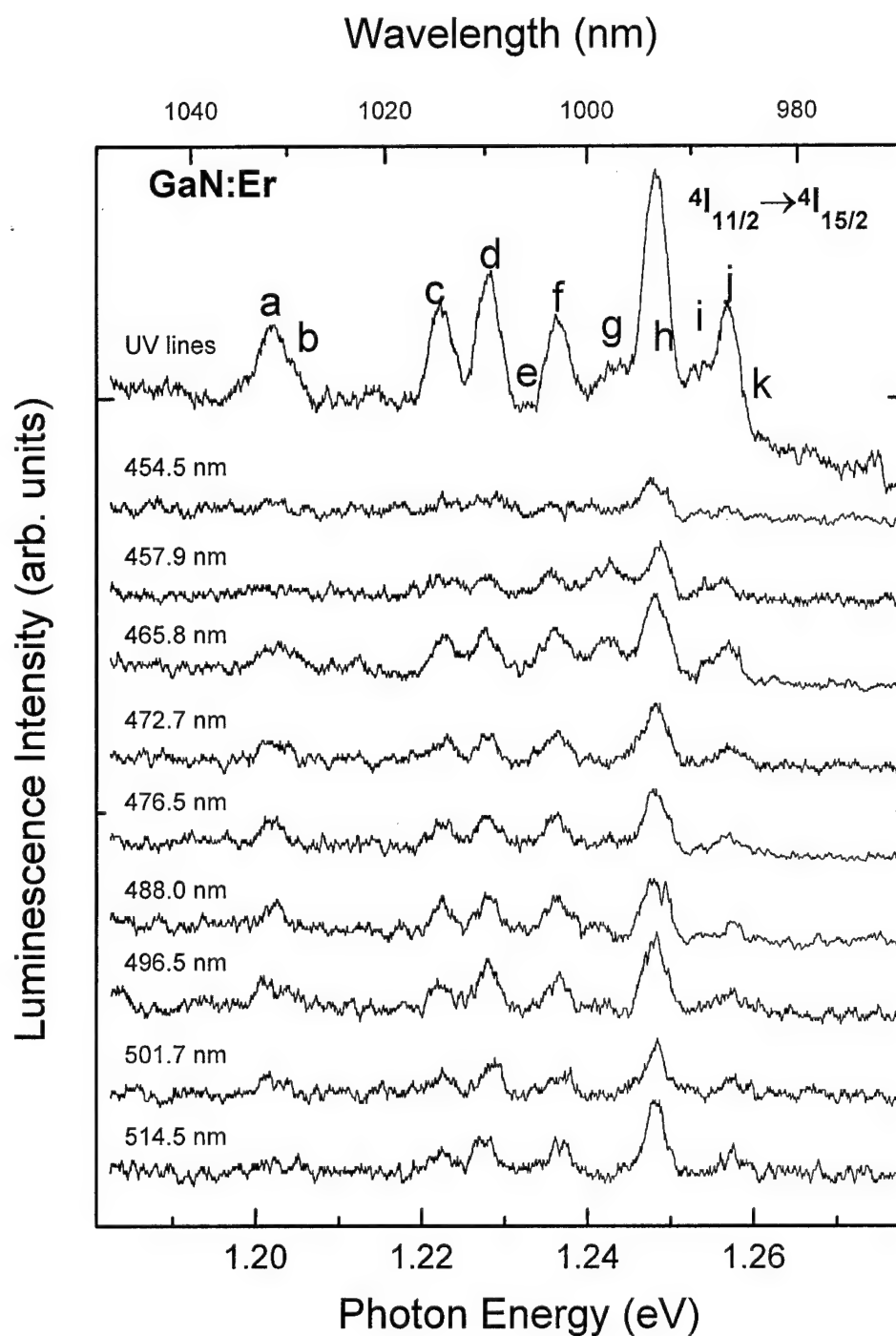
Figure 5-88. Photoluminescence spectra excited with various wavelengths taken at 2 K from the $^4I_{11/2} \rightarrow {}^4I_{15/2}$ transition of Er^{3+} for GaN implanted with erbium at 1150 keV to a dose of 5×10^{13} cm^{-2} and annealed at 1000 °C for 90 min in NH_3.
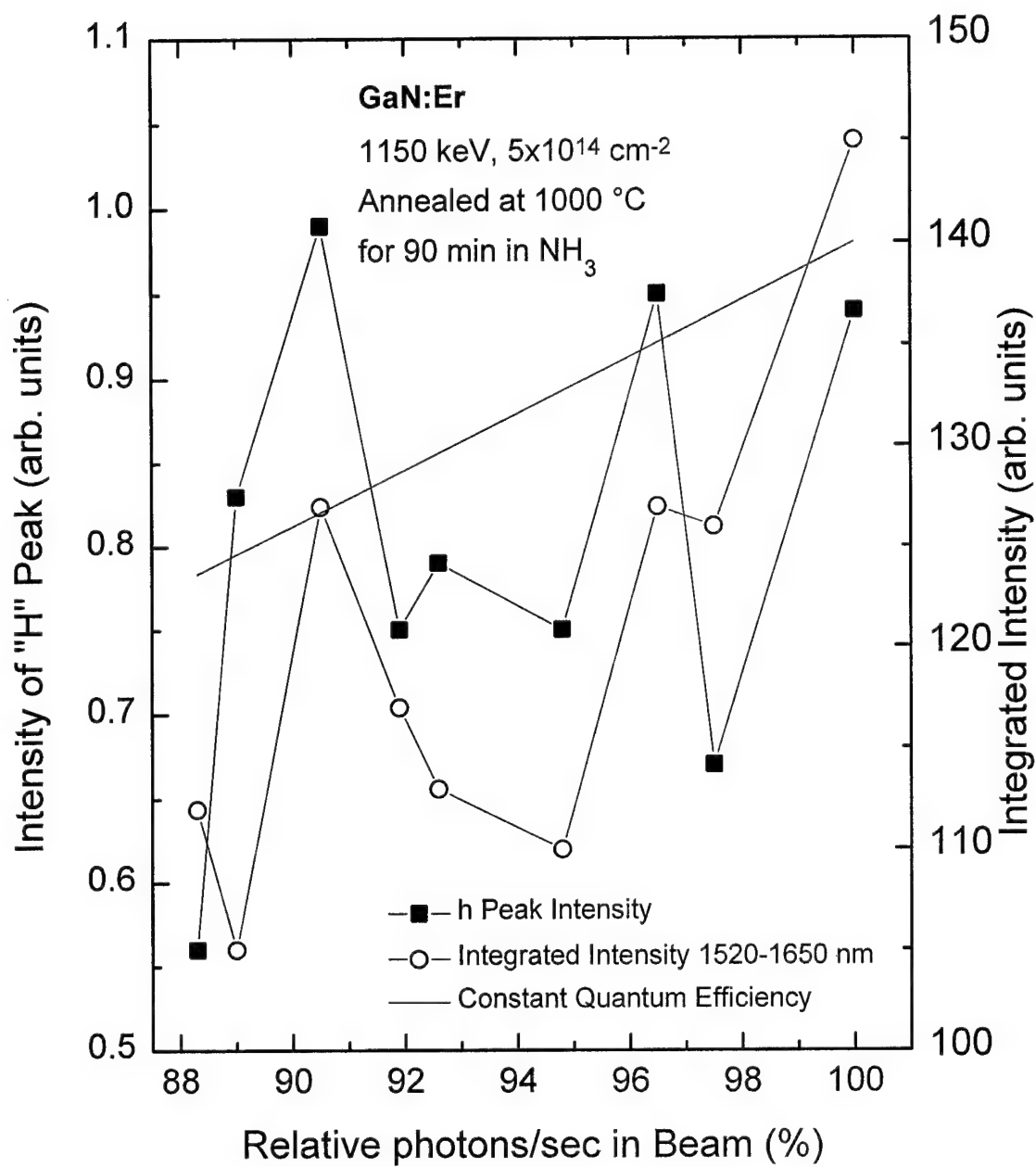
Figure 5-89. Photoluminescence intensity at a temperature of 2 K from the 'H' peak in the $^4I_{11/2} \rightarrow {}^4I_{15/2}$ transition of Er^{3+} as a function of the number of exciting photons.

due to the lower laser power, but a weak increasing trend was not ruled out. As a guide for the eye, Figure 5-89 has a line plotted which is proportional to the number of photons in the beam. Although a relationship could not be drawn with certainty, the excitation of this manifold was consistent with a constant quantum efficiency.

The $^4I_{13/2} \rightarrow {}^4I_{15/2}$ transitions at $\sim 1.54\mu m$ showed only a few, but notable changes with excitation photon energy as seen in Figure 5-90. The integrated intensity showed a weak decreasing trend as the excitation photon wavelength decreased from 514.5 to 454.5 nm. In contrast to GaN:Nd, no new luminescence peaks were observed. However, it should be noted that the peaks B, FF, and KK all decreased in concert while the relative intensities of the remaining peaks stayed essentially constant as exciting wavelength changed from 514.5 to 454.5 nm. This result provided further evidence that this set of peaks was of a common origin.

Oxygen co-doping has been reported to enhance Er emissions in other semiconductors (Colon et al., 1993; Michel et al., 1991). To study the effects of oxygen co-implantation of GaN, a set of samples was co-implanted with oxygen at an energy of 135 keV and dose of 5.0×10^{14} cm^{-2}. These parameters were chosen in order to place the oxygen peak concentration of 2.8×10^{19} cm^{-3} at the same depth as the implanted Er peak concentration. An annealing study was undertaken using conditions identical to those used for the non-co-implanted GaN:Er, thus allowing direct comparison of co-implanted and non-co-implanted GaN:Er.
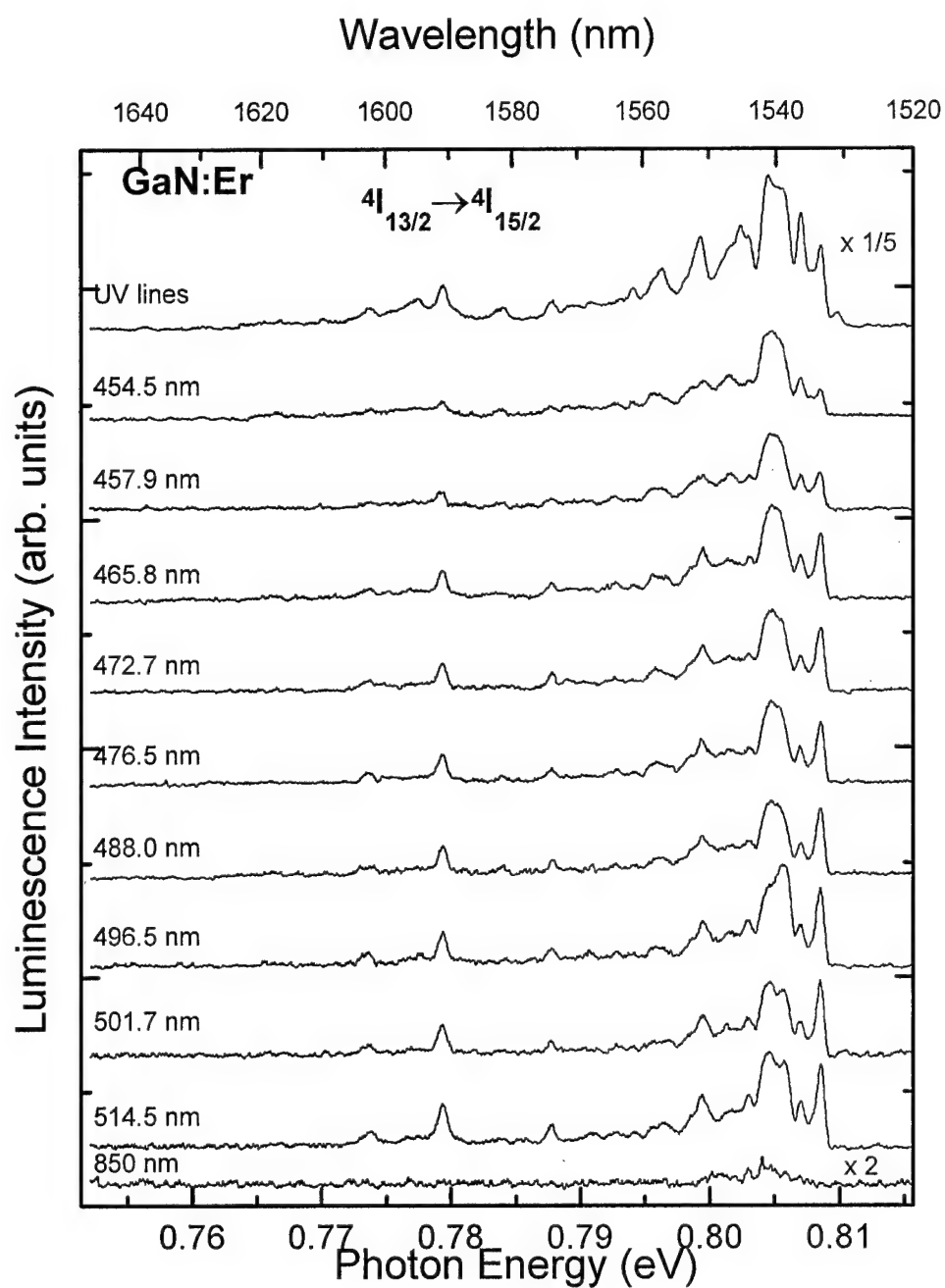
Figure 5-90. Photoluminescence spectra excited with various wavelengths taken at 2 K from the $^4I_{13/2} \to {}^4I_{15/2}$ transition of Er^{3+} for GaN implanted with erbium at 1150 keV to a dose of 5×10^{13} cm^{-2} and annealed at 1000 °C for 90 min in NH_3.

Figure 5-91 shows the low temperature PL from the $^4I_{13/2} \rightarrow ^4I_{15/2}$ transitions of 700, 800, 900, and 1000 °C annealed samples of oxygen co-implanted GaN:Er. It was clear that the strongest Er^{3+} luminescence was obtained from the 800 °C annealed sample. The 700 °C annealed sample showed no Er related luminescence. The luminescence intensity dropped at temperatures above 800 °C. Thus, a temperature between 700 and 800 °C was necessary for optimal activation of the co-implanted GaN:Er. Recalling that non-co-implanted GaN:Er had strong 4f luminescence for 1000 °C anneals, this result indicated that the luminescence centers responsible had been modified by co-implantation. A similar optimal annealing temperature was found by Wilson *et al.* (1995) for oxygen co-implanted GaN:Er. They reported a drop in Er luminescence for annealing above 700 °C.

The peak locations were nearly identical for the co-doped and non-co-doped material. Also evident was the fact that for co-implanted GaN:Er, the relative intensities of the $^4I_{13/2} \rightarrow ^4I_{15/2}$ lines remained about constant with annealing temperature. There were no lines which grew in intensity as was the case for non-co-implanted GaN:Er. Furthermore, the energetic locations of the individual lines were the same as for non-co-doped GaN:Er. Thus, the optimal annealing temperature for activating Er^{3+} luminescence for non-co-implanted and oxygen co-implanted GaN were found to be different. The mechanism responsible for this difference in annealing temperature was not known; however, one proposed mechanism for an increase in Er luminescence for co-implanted GaAs:Er was an interaction between oxygen and erbium to form a complex luminescent
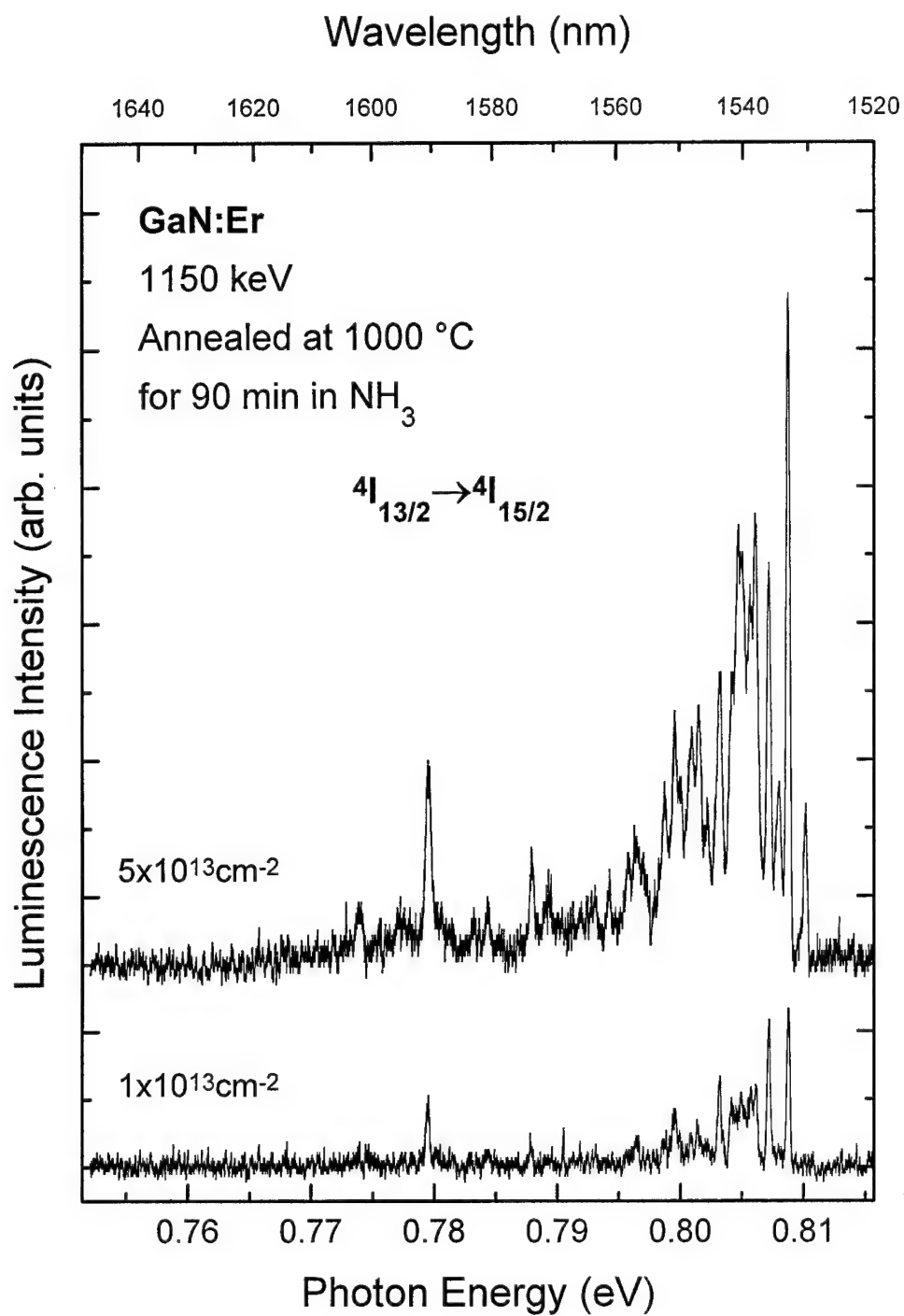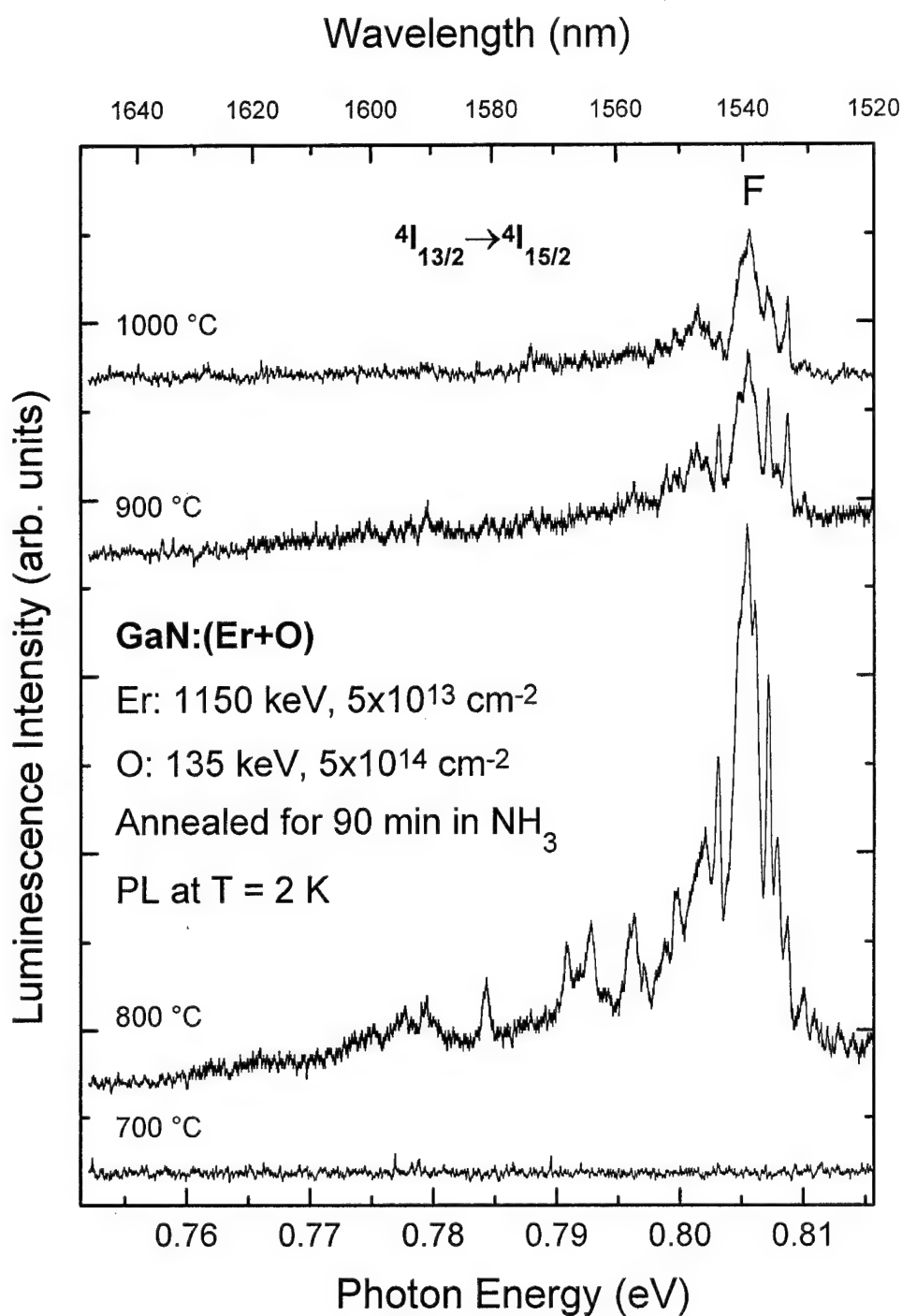
Figure 5-91. Photoluminescence spectra taken at 2 K from the $^4I_{13/2} \to {}^4I_{15/2}$ transition of Er^{3+} for GaN co-implanted with oxygen at 135 keV a dose of 5×10^{14} cm^{-2} and erbium at 1150 keV to a dose of 5×10^{13} cm^{-2} and annealed at 1000 °C for 90 min in NH$_3$.

center (Colon *et al.*, 1993). Such a mechanism could well have occurred in this case, too. The $^4I_{11/2} \rightarrow {}^4I_{15/2}$ transitions also showed this same optimal annealing temperature as seen in Figure 5-92. The 800 °C annealed sample had the highest luminescence intensity.

Figures 5-93 and 5-94 show a comparison of the low temperature PL from co-implanted and non-co-implanted GaN:Er for the $^4I_{13/2} \rightarrow {}^4I_{15/2}$ transitions and $^4I_{11/2} \rightarrow {}^4I_{15/2}$ transitions. Both samples were annealed at 1000 °C, and thus the co-implanted sample in these figures was not annealed at the optimal temperature. The co-doped sample had a slightly higher intensity for the $^4I_{13/2} \rightarrow {}^4I_{15/2}$ transitions, being more intense by a factor of 1.23. The 800 °C anneal co-implanted sample was 3.48 times more intense than the 1000 °C annealed co-implanted sample. Thus, the total difference between the optimally annealed co-implanted sample and non-co-implanted sample was a factor of about 4.3. This enhancement was similar to that found in a GaAs host (Colon *et al.*, 1993). The $^4I_{11/2} \rightarrow {}^4I_{15/2}$ transitions at ~1.0 μm were nearly identical in intensity for the 1000 °C anneals. The optimally annealed oxygen co-implanted sample also had nearly identical intensity to the 1000 °C anneal. Therefore, the $^4I_{11/2} \rightarrow {}^4I_{15/2}$ transitions were not enhanced by co-implantation.

The most intense peak for the oxygen co-implanted GaN:Er was the F peak. It reached maximum intensity for samples annealed at 800 °C. This peak was identified in the non-co-implanted GaN:Er as being the highest energy peak in the second proposed Er luminescence center. The next highest energy line, the H peak, also appeared to be enhanced in the 800 °C annealed oxygen co-implanted sample. It was more difficult to
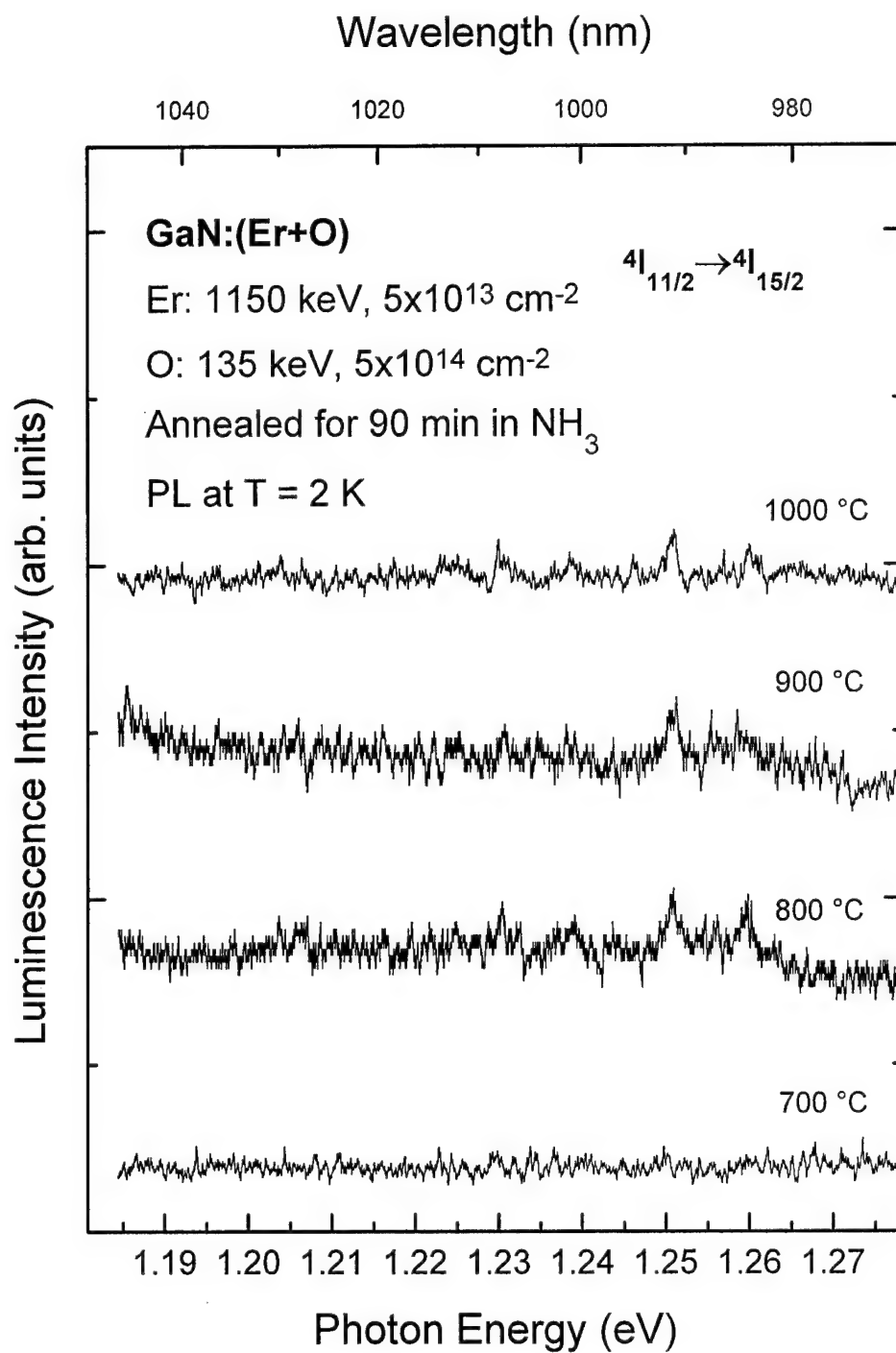
Figure 5-92. Photoluminescence spectra taken at 2 K from the $^4I_{11/2} \rightarrow {}^4I_{15/2}$ transition of Er^{3+} for GaN co-implanted with oxygen at 135 keV a dose of 5×10^{14} cm^{-2} and erbium at 1150 keV to a dose of 5×10^{13} cm^{-2} and annealed at various temperatures for 90 min in NH$_3$.
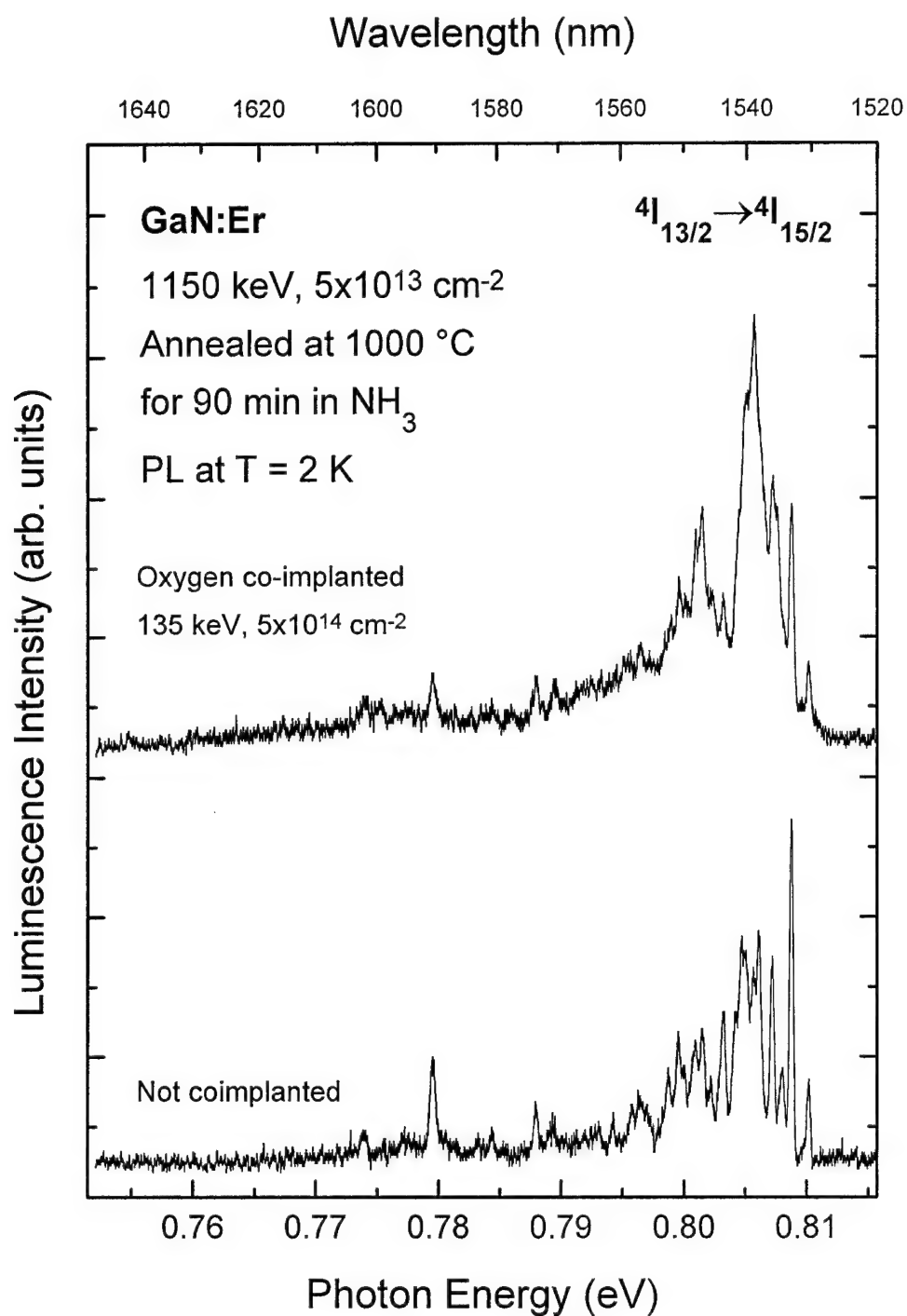
Figure 5-93. Absolute intensity comparison of photoluminescence spectra taken at 2 K from the $^4I_{13/2} \to {}^4I_{15/2}$ transition of Er^{3+} for GaN:Er co-implanted with oxygen at 135 keV to a dose of 5×10^{14} cm^{-2}, and non-co-implanted GaN:Er with erbium at 1150 keV to a dose of 5×10^{13} cm^{-2} and annealed at 1000 °C for 90 min in NH$_3$.
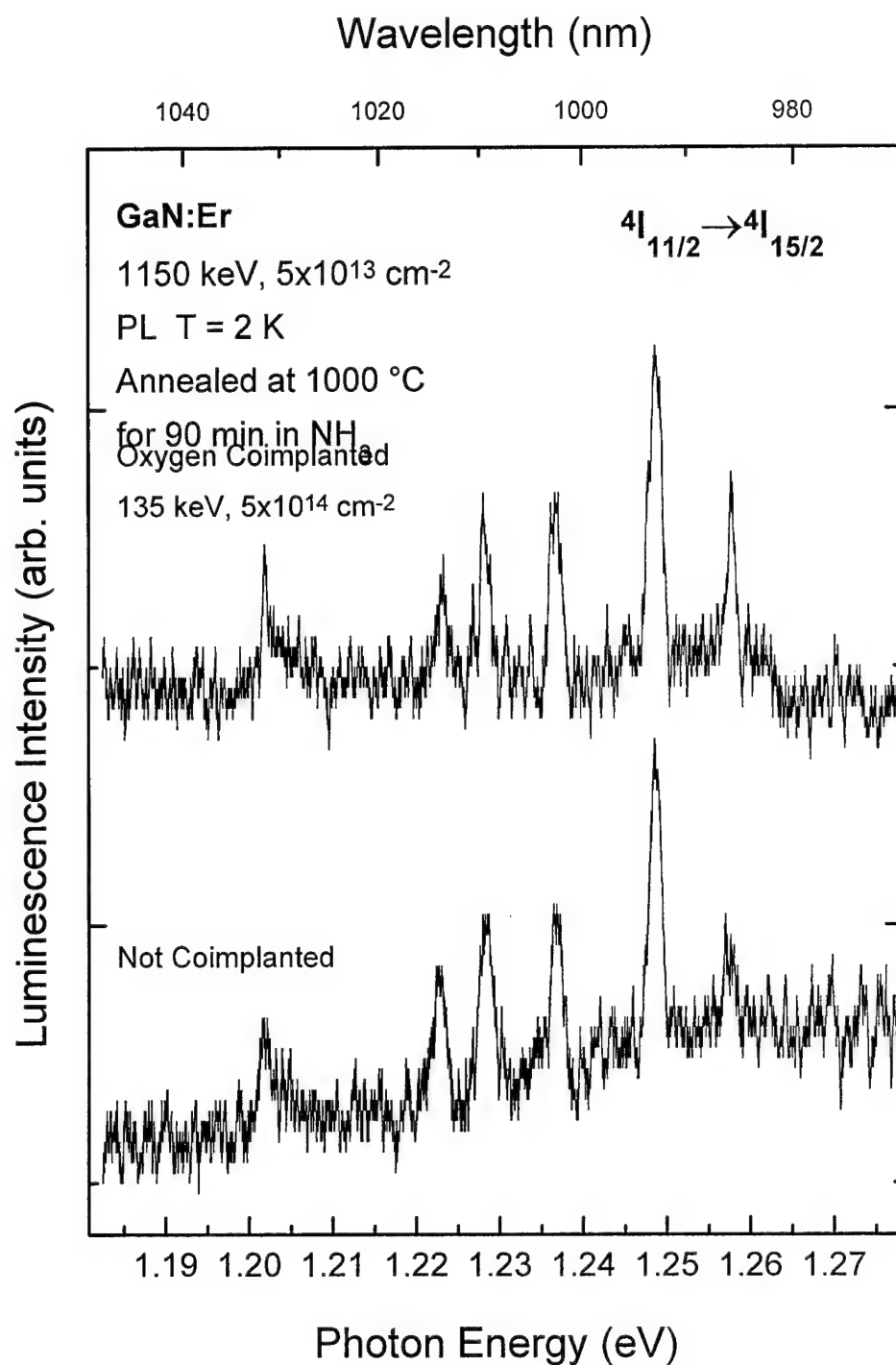
Figure 5-94. Absolute intensity comparison of photoluminescence spectra taken at 2 K from the $^4I_{11/2} \rightarrow {}^4I_{15/2}$ transition of Er^{3+} for GaN:Er co-implanted with oxygen at 135 keV to a dose of 5×10^{14} cm^{-2}, and non-co-implanted GaN:Er with erbium at 1150 keV to a dose of 5×10^{13} cm^{-2} and annealed at 1000 °C for 90 min in NH$_3$.

make any firm conclusions about the other, lower intensity peaks. This evidence supported the hypothesis of multiple Er^{3+} luminescence centers in GaN.

Some discussion about the excitation mechanism responsible for the Er luminescence center(s) is warranted. It was very clear from the results above that excitation well below the GaN bandgap could excite the Er luminescence. Thus, an excitation mechanism based on transfer from excitons as in the model proposed by Korber & Hangleiter (1988) for GaAs:Er cannot be applied. However, the 514.5 nm (2.41 eV) photon excitation source used was sufficient to excite the GaN yellow deep D-A transitions centered at 2.2 eV. These yellow emissions were always evident when the GaN:Er samples were excited by the laser. A candidate process could be the excitation of the Er luminescence center by the non-radiative decay of an excited D-A center. A similar mechanism was proposed for GaP:Yb (Kasatkin & Savel'ev, 1984).

In summary, strong 4f luminescence was detected for GaN:Er. In addition to the 1.54 μm luminescence from the $^4I_{13/2} \rightarrow ^4I_{15/2}$ transition reported by other researchers for oxygen co-implanted GaN, strong low temperature luminescence was detected from the $^4I_{11/2} \rightarrow ^4I_{15/2}$ transitions at 1.0 μm. This was the first report of luminescence from this manifold for GaN:Er. Furthermore, this was the first report of luminescence from GaN which was not co-implanted with oxygen. Annealing temperature dependence studies showed that the optimal annealing temperature for GaN:Er was 1000 °C for no-co-implanted material, but was 800 °C for oxygen co-implanted material. This result must be attributed to the formation of Er-O complexes of unknown structure. The number of luminescence peaks detected for the $^4I_{11/2} \rightarrow ^4I_{15/2}$ manifold at low temperature indicated a

non-cubic site symmetry for the Er centers. 'Hot' lines were detected in this spectrum which allowed the assignment of six energy levels in the $^4I_{15/2}$ manifold and two energy levels in the $^4I_{11/2}$ manifold. Excitation with higher energy photons confirmed the locations of the 'hot' lines in the $^4I_{11/2} \rightarrow {}^4I_{15/2}$ group. The annealing temperature dependence of the $^4I_{13/2} \rightarrow {}^4I_{15/2}$ transitions indicated the presence of multiple Er centers with different optimal annealing temperatures. 'Hot' lines were also observed for this manifold. The $^4I_{13/2} \rightarrow {}^4I_{15/2}$ transitions also showed shifts in relative peak intensity as excitation wavelength was varied. An attempt was made to fit the observed luminescence peaks with an energy level scheme. The only way found to accommodate nearly all of the observed lines was to postulate two separate Er luminescence centers. Co-implantation with oxygen was found to enhance the $^4I_{13/2} \rightarrow {}^4I_{15/2}$ peaks.

VI. Conclusion

Summary of Contributions

This study undertook three goals: to achieve successful optical activation of ion-implanted dopants in GaN, to systematically study the annealing conditions necessary for optimal dopant optical activation, and to study the optical properties of ion-implanted dopants. Each of these objectives was met. Successful means of optically activating implanted Zn, Mg, Er, and Nd were found. A larger group of dopants was examined including the potential p-type dopants: zinc, magnesium, carbon, and beryllium; the n-type dopants: silicon and oxygen, and the rare-earth elements: neodymium and erbium. A wide range of implantation and annealing conditions were examined in order to broaden the base of knowledge in this area. The implantation energies studied ranged from 100 to 1150 keV, and the doses implanted ranged from 1×10^{13} to 1×10^{15} cm^{-2}. Two different annealing gas environments were tested, NH_3 and N_2, over a range of temperatures from 600 to 1150 °C. Both uncapped and proximity-capped annealing methods were tested. These tests gave several new insights which will be reviewed below. Finally, several new discoveries were made regarding the properties of specific implanted species in GaN which have implications for future optoelectronic devices. Highlights will also be discussed below.

Through the study of this wide range of implantation and annealing parameters it was possible to reach several general conclusions. First, GaN began to decompose in an

NH$_3$ gas environment at temperatures as low as 600 °C. This decomposition was manifested as a degradation of the smooth, mirror-like surface of the GaN epilayer. The effect became more pronounced at higher temperatures. Annealing as-grown GaN samples in an NH$_3$ gas environment at these temperatures resulted in an increased D-A luminescence. This effect was attributed to decomposition of the GaN surface via the reaction GaN + 3/2H$_2$ → Ga + NH$_3$ resulting in an increased concentration of V$_N$. Annealing in an N$_2$ gas environment at elevated temperatures did not result in an increase in D-A emissions, and no evidence for surface decomposition was observed even at an annealing temperature of 1000 °C.

Furthermore, annealing as-grown GaN samples in an NH$_3$ environment at temperatures as low as 600 °C resulted in an overall reduction in exciton luminescence. This result was attributed to increased non-radiative recombination at the GaN surface. Zn implanted GaN annealed at temperatures above 1000 °C in an NH$_3$ environment resulted in an unrecoverable surface degradation of the GaN:Zn layer. Under an NH$_3$ annealing environment at a temperature of 1050 °C for 90 min, the GaN:Zn surface turned opaque, white in color, and showed increased below bandgap absorption. Oxygen-implanted GaN showed a much higher level of surface degradation as compared to GaN implanted with carbon and processed under nearly identical conditions. This result suggested that the presence of oxygen lead to an enhancement of GaN surface degradation when annealing took place in an NH$_3$ environment. Thus, a method of

protecting the GaN surface must be found if high temperature processing steps will be necessary for future optoelectronic devices.

Second, for GaN samples damaged by ion-implantation, annealing temperature was found to be the determining factor in the recovery of sharp bandedge absorption. Argon-implanted samples were found to recover their sharp room temperature absorption edge upon annealing at temperatures of 1000 to 1050 °C. Nearly identical recovery was found for GaN:Ar samples annealed in NH_3 and N_2 annealing environments. An activation energy of 103 meV with a threshold temperature of 395 °C was found for the annealing process in argon-implanted GaN. The recovery of the as-grown GaN luminescence spectrum could not be achieved for argon-implanted samples annealed in either NH_3 or N_2 atmospheres. The low temperature photoluminescence spectra of argon-implanted and annealed GaN samples were dominated by the 3.27 eV D-A band. Furthermore, the D-A luminescence was less intense after implantation and annealing. The intense exciton peak of the as-grown GaN was quenched. Thus, implantation damage remained after annealing, and resulted in non-radiative decay pathways. The argon-implanted GaN annealed in an NH_3 environment displayed better resolved D-A peaks than argon-implanted samples annealed in an N_2 environment. Thus, NH_3 annealing resulted in better luminescence recovery.

The results for Zn-implanted GaN supported the above conclusion. Crystalline damage in Zn-implanted GaN has been shown by absorption measurements to be largely repaired by furnace annealing in either NH_3 or N_2 at temperatures approaching 1000 °C

for 90 min. A threshold temperature for the observed annealing process of 610 °C was discovered. The lattice damage repair was rapid at 1000 °C with nearly full recovery of the absorption edge after annealing the implanted samples for 15 min in an NH_3 environment. An activation energy of 437 meV was determined for the annealing process. Thus, the activation energy necessary for recovery of Zn-implanted GaN was several times higher than that required for GaN:Ar. The threshold temperature for annealing was also found to be higher. The same energy was used for implantation of both Zn and Ar; thus, the GaN:Ar activation value was more indicative of the annealing of native defects in the GaN lattice. This result may be attributed to a greater interaction between the lattice and the Zn atoms than should occur with the inert element Ar.

The other implanted species showed very similar bandedge recovery results. Annealing at a temperature of 1000 °C was found to be preferred for GaN bandedge recovery for GaN:Mg. Although carbon-, oxygen-, silicon-, and beryllium-implanted GaN did not show any unique luminescence peaks, the luminescence from the 1000 °C annealed samples tended to be the strongest which was consistent with the previously stated results. Thus, the crystalline damage to GaN can be repaired with the relatively simple processing step of annealing in a conventional furnace. This simple step can be easily accomplished during optoelectronic device fabrication.

Third, in most cases, annealing ion implanted GaN in an NH_3 gas environment produced a stronger luminescence signal than annealing in an N_2 gas environment. In some cases, almost no luminescence was recovered from samples annealed in an N_2 gas

environment even at a temperature of 1000 °C. Identical samples annealed at the same temperature in an NH_3 environment showed strong low temperature luminescence. Thus, annealing ion-implanted GaN at temperatures at or below 1000 °C in an NH_3 gas environment was preferable to annealing at the same temperature in an N_2 gas environment. The mechanism responsible for this difference was unknown. The data from as-grown samples annealed in an N_2 environment suggested that it may be related to the formation of non-radiative centers rather than the loss of nitrogen stoichiometry from the GaN surface under an N_2 atmosphere. In fact, annealing under an NH_3 atmosphere at temperatures above 1000 °C was found to result in an increase in V_N, presumably attributable to loss of nitrogen stoichiometry from the GaN surface. Thus, device makers should be aware that detrimental non-radiative centers can be easily created by annealing under an N_2 atmosphere. Means to mitigate the creation of these centers should be explored in future work.

Fourth, the proximity-cap annealing method was found to afford some protection against surface degradation for GaN implanted with zinc. However, proximity-cap annealing seemed to lessen the activation of the 2.86 eV luminescence peak of Zn. Thus, some luminescence peaks associated with implanted species may require high levels of defects for optical activity. This result was not understood and requires further examination. Capping GaN during annealing should be studied in greater detail.

Among many findings of good optical activity in GaN for the various implanted species of zinc, magnesium, neodymium, and erbium, only the more significant findings

are described below. Zn-implanted GaN was found to have a strong luminescence peak

in the blue at 2.86 eV. However, this peak was observed to occur only after annealing at

temperatures of 900 °C and above. The peak was barely detected at 900 °C, but increased

substantially in intensity with annealing temperature up to 1050 °C. However, surface

damage at 1050 °C tended to mask the strength of the Zn peak. The Zn implanted sample

with the highest dose showed the strongest Zn luminescence. The fact that no

luminescence was seen from the N_2 annealed samples under face illumination

demonstrated that luminescence quenching was occurring at the surface. However, N_2

annealing even at 1000 °C resulted in a smooth sample surface with no visible

degradation. On the other hand, the NH_3 annealing environment clearly attacks the GaN

surface. Thus, the luminescence quenching in the N_2 anneal was not due to surface

damage during annealing, but resulted from either unannealed residual implantation

damage or additional non-radiative centers resulting from N_2 annealing.

Several interesting properties of the Zn luminescence center at 2.86 eV were

observed. The 2.86 eV Zn luminescence showed no change in FWHM over two orders of

magnitude of excitation intensity. The sample temperature dependence also showed no

change in FWHM. The insensitivity of FWHM and lack of shifts of the Zn peak

suggested an internal transition at the Zn center. The Zn peak at 2.35 eV also showed the

characteristics of an internal transition not pinned to the bandedge. Thus, the Zn 2.86 eV

peak offers a broad blue peak which is temperature insensitive over a wide temperature

range. This peak may be exploited to advantage for the fabrication of optoelectronic devices.

The Mg-implanted GaN sample annealed at temperatures near 1000 °C in both N_2 and NH_3 atmospheres showed several unique low temperature PL peaks. A shoulder was found to occur near 3.44 eV which may be the Mg-bound exciton transition. The observed peak near 3.426 eV was in the correct spectral region for the Mg free-to-bound transition. Too little is known about these peaks at this point to draw any definite conclusions as to their usefulness for optoelectronic devices. However, they do lie in the blue. In conjunction with magnesium's increasingly common use as a p-type dopant for GaN, they may become very attractive candidate peaks for optoelectronic device fabrication.

The rare earth elements, neodymium and erbium, showed a wealth of luminescence peaks which were studied quite extensively. It is believed that the study of Nd-implanted GaN is reported here for the first time. A rich luminescence spectrum was found resulting from transitions principally between three manifolds of energy levels. Annealing temperature dependence studies determined an optimal annealing temperature of 1000 °C for the activation of the Nd^{3+} luminescence center. Evidence for only one, non-cubic luminescence center was found, and the energy levels were mapped. Oxygen co-implantation did not result in an increase in the Nd luminescence, and in fact may have been detrimental. Co-implantation did not result in the observation of any additional Nd luminescence centers, and did not change the annealing temperature behavior. Excitation wavelength dependence studies were performed which resulted in a

very large number of additional luminescence peaks. And, an energy level model for the Nd manifolds was proposed from the results of this study.

Strong 4f luminescence was detected for GaN:Er. In addition to the 1.54 μm luminescence from the $^4I_{13/2} \rightarrow ^4I_{15/2}$ transition reported by other researchers for oxygen co-implanted GaN, strong low temperature luminescence was detected from the $^4I_{11/2} \rightarrow ^4I_{15/2}$ transitions at 1.0 μm. This was the first report of luminescence from this manifold for GaN:Er. Furthermore, this was the first report of luminescence from GaN which was not co-implanted with oxygen. Annealing temperature dependence studies showed that the optimal annealing temperature for GaN:Er was 1000 °C for non-co-implanted material, but was 800 °C for oxygen co-implanted material. This result must be attributed to the formation of Er-O complexes of unknown structure. The number of luminescence peaks detected for the $^4I_{11/2} \rightarrow ^4I_{15/2}$ manifold at low temperature indicated a non-cubic site symmetry for the Er centers. 'Hot' lines were detected in this spectrum which allowed the assignment of six energy levels in the $^4I_{15/2}$ manifold and two energy levels in the $^4I_{11/2}$ manifold. Excitation with higher energy photons confirmed the locations of the 'hot' lines in the $^4I_{11/2} \rightarrow ^4I_{15/2}$ group. The annealing temperature dependence of the $^4I_{13/2} \rightarrow ^4I_{15/2}$ transitions indicated the presence of multiple Er centers with different optimal annealing temperatures. 'Hot' lines were also observed for this manifold. The $^4I_{13/2} \rightarrow ^4I_{15/2}$ transitions also showed shifts in relative peak intensity as excitation wavelength was varied. An attempt was made to fit the observed luminescence peaks with an energy level scheme. The only way found to accommodate nearly all of

the observed lines was to postulate two separate Er luminescence centers. The resulting energy level diagrams predicted nearly all of the observed luminescence peaks. Furthermore, the second luminescence center was found to contain the most intense peaks found for the oxygen co-implanted GaN:Er. Thus, the second Er center may be associated with an Er-O complex. Co-implantation with oxygen was found to enhance the $^4I_{13/2} \rightarrow {}^4I_{15/2}$ peaks.

Thus, both Nd and Er showed the characteristic temperature independent behavior expected for rare earth elements in a semiconductor host. With GaN's wide bandgap and their demonstrated luminescence at room temperature, these species hold great promise for the creation of high temperature, stable, optoelectronic devices.

As with any experimental study, many new questions arise during the course of the work. Thus, several new avenues of research relating to ion-implantation and annealing of GaN can be formulated. Since there are countless possible research directions, only those areas directly connected with this particular work will be addressed.

Recommendations for Further Study

Since surface degradation of GaN played a large part in the determination of the optimal annealing temperature of all of the implanted species, a serious effort should be made to characterize the surface degradation mechanism. Both the NH_3 and N_2 gas environments should be examined as well as the role of hydrogen in this process.

Room temperature absorption data proved very useful in this work to characterize the degree of recovery of the GaN after post-implantation annealing. Another, more direct way to examine the recovery of ion-implantation damage is to use the Rutherford backscattering technique. This method would give a direct measure of the degree of disorder introduced in the GaN by ion-implantation. Studies could be done based on implantation energy, dose, and ion species. Annealing recovery could be characterized by this method with a larger sample set as a function of temperature and time. A more complete understanding of the annealing mechanism would be gained in this fashion.

The result that Zn implanted GaN showed the best luminescence activation when surface damage was evident leads to many unanswered questions. The Zn luminescence mechanism could be more fully explored by photoluminescence excitation spectroscopy and by measuring the time decay of the Zn luminescence peaks for Zn implanted GaN.

Other areas for study are possible. The implantation of carbon, oxygen, silicon, and beryllium could be explored in greater detail to determine what caused the poor luminescence observed in this study. Rapid thermal annealing could be explored for the same set of dopants examined here. The electrical activation of implanted dopants could also be examined, although difficulties in preparing ohmic contacts should be considered very carefully. All implantations performed for this study were accomplished while holding the GaN at room temperature. Heating or cooling of the GaN during implantation may hold great benefits when used in conjunction with the correct annealing procedure.

The rare earth elements are a rich topic for research. Lifetime studies of the luminescence peaks observed for Nd- and Er-implanted samples should provide additional evidence for assigning the energy level spacings within the various manifolds. Another technique which would be useful in this regard is photoluminescence excitation spectroscopy. Using PLE, the question of two different Er centers may be more satisfactorily resolved. Finally, rare earth elements other than Nd and Er should prove as interesting in GaN, and other co-implants could also be explored. Thus, this work has opened the door to a number of interesting topics which merit further study.

Appendix : Annealing Conditions of Implanted Samples

Tables A-1 through A-15 below list the annealing temperature, time, gas environment, and technique for all implanted and annealed samples used in this study. The two techniques used were open face annealing (OF) and the proximity-cap method (PCA).

Table A-1

Argon (390 keV, 5×10^{14} cm^{-2}) implanted sample annealing conditions.

Ar 390 keV, 5×10^{14} cm^{-2}				
Sample ID #	Temp (°C)	Time (min)	Gas	Technique
873.3	800	30	N_2	OF
	1000	30	N_2	OF
873.3	800	120	N_2	OF
873.3	800	90	NH_3	OF
873.3	900	90	NH_3	OF
873.3	1000	90	NH_3	OF
873.3	1050	90	NH_3	OF

Table A-2

Magnesium (100 keV, 5×10^{13} cm^{-2}) implanted sample annealing conditions.

Mg, 100 keV, 5×10^{13} cm^{-2}				
Sample ID #	Temp (°C)	Time (min)	Gas	Technique
890.3	700	20	N_2	OF
890.3	800	20	N_2	OF
890.3	900	20	N_2	OF
E02524	800	120	N_2	OF
E02524	900	90	NH_3	OF
E02524	1000	90	NH_3	OF
E02524	1050	90	NH_3	OF

Table A-3

Magnesium (300 keV, 2.2×10^{14} cm^{-2}) implanted sample annealing conditions.

Mg, 300 keV, 2.2×10^{14} cm^{-2}				
Sample ID #	Temp (°C)	Time (min)	Gas	Technique
283 009 c	700	20	N_2	OF
283 009 c	800	20	N_2	OF
283 009 c	900	20	N_2	OF
	900	20	N_2	OF
946.1	700	20	N_2	OF
946.1	800	20	N_2	OF
	800	90	N_2	OF
946.1	900	20	N_2	OF
	900	90	N_2	OF
946.1	800	120	N_2	OF
946.1	1000	90	N_2	OF
946.1	900	90	NH_3	OF
946.1	1000	90	NH_3	OF
946.1	1000	30	NH_3	OF
	1000	30	NH_3	OF
946.1	1000	90	NH_3	PCA

Table A-4

Magnesium (300 keV, 8.2×10^{14} cm^{-2}) implanted sample annealing conditions.

Mg, 300 keV, 8.2×10^{14} cm^{-2}				
Sample ID #	Temp (°C)	Time (min)	Gas	Technique
248.3	800	20	N_2	OF
	800	70	N_2	OF
248.3	800	120	N_2	OF

Table A-5

Beryllium (200 keV, 5×10^{13} cm^{-2}) implanted sample annealing conditions.

Be, 200 keV, 5×10^{13} cm^{-2}				
Sample ID #	Temp (°C)	Time (min)	Gas	Technique
701.3	700	20	N_2	OF
701.3	800	20	N_2	OF
701.3	900	20	N_2	OF
701.3	800	120	N_2	OF
701.3	900	90	NH_3	OF
701.3	1000	90	NH_3	OF

Table A-6

Zinc (390 keV, 1×10^{13} cm^{-2}) implanted sample annealing conditions.

Zn, 390 keV, 1×10^{13} cm^{-2}				
Sample ID #	Temp (°C)	Time (min)	Gas	Technique
E02388	600	30	N_2	OF
E02388	1000	90	NH_3	PCA
E02525	600	30	N_2	OF
	1000	30	N_2	OF
E02525	700	60	N_2	OF
	1010	120	N_2	OF
E02525	800	120	N_2	OF

Table A-7

Zinc (390 keV, 1×10^{14} cm^{-2}) implanted sample annealing conditions.

Zn, 390 keV, 1×10^{14} cm^{-2}				
Sample ID #	Temp (°C)	Time (min)	Gas	Technique
E02388	850	30	N_2	OF
	900	30	N_2	OF
	1000	90	NH_3	OF
E02388	900	90	NH_3	OF
	900	90	NH_3	OF
E02388	1000	90	NH_3	OF
E02525	700	60	N_2	OF
	1010	120	N_2	OF
E02525	850	30	N_2	OF
	900	30	N_2	OF
	1000	30	N_2	OF
E02525	1000	30	N_2	OF

Table A-8

Zinc (390 keV, 2.25×10^{14} cm^{-2}) implanted sample annealing conditions.

Zn, 390 keV, 2.25×10^{14} cm^{-2}				
Sample ID #	Temp (°C)	Time (min)	Gas	Technique
E02388	800	90	NH_3	OF
E02388	900	90	NH_3	OF
	900	90	NH_3	OF
	900	90	NH_3	OF
E02388	1000	90	NH_3	OF
E02388	1050	90	NH_3	OF
E02525	1000	90	NH_3	PCA
	1000	90	NH_3	PCA
E02525	1000	15	NH_3	PCA
	1000	15	NH_3	PCA
	1000	15	NH_3	PCA
E02525	1050	90	NH_3	OF
E02525	1050	90	NH_3	PCA

Table A-9

Silicon (390 keV, 5×10^{14} cm^{-2}) implanted sample annealing conditions.

Si, 390 keV, 5×10^{14} cm^{-2}				
Sample ID #	Temp (°C)	Time (min)	Gas	Technique
248.3	800	30	N_2	OF
	1000	30	N_2	OF
248.3	800	120	N_2	OF
248.3	900	90	NH_3	OF
248.3	1000	90	NH_3	OF
E02525	600	90	NH_3	OF
E02525	700	90	NH_3	OF
E02525	800	90	NH_3	OF
E02388	900	90	NH_3	OF
E02388	1000	90	NH_3	OF

Table A-10

Carbon (390 keV, 1×10^{14} cm^{-2}) implanted sample annealing conditions.

C, 390 keV, 1×10^{14} cm^{-2}				
Sample ID #	Temp (°C)	Time (min)	Gas	Technique
1462.1	800	30	N_2	OF
	1000	30	N_2	OF
1462.1	800	120	N_2	OF
1462.1	900	90	NH_3	OF
1462.1	1000	90	NH_3	OF
E02388	900	90	NH_3	OF
E02388	1000	90	NH_3	OF
E02388	1050	90	NH_3	OF
E02525	900	90	NH_3	OF
E02525	1000	90	NH_3	OF
E02525	1050	90	NH_3	OF

Table A-11

Oxygen (390 keV, 1×10^{14} cm^{-2}) implanted sample annealing conditions.

O, 390 keV, 1×10^{14} cm^{-2}				
Sample ID #	Temp (°C)	Time (min)	Gas	Technique
1462.1	800	30	N_2	OF
	1000	30	N_2	OF
1462.1	800	120	N_2	OF
1462.1	900	90	NH_3	OF
1462.1	1000	90	NH_3	OF
E02388	900	90	NH_3	OF
E02388	1000	90	NH_3	OF
E02388	1050	90	NH_3	OF
E02525	900	90	NH_3	OF
E02525	1000	90	NH_3	OF
E02525	1050	90	NH_3	OF

Table A-12

Erbium (1150 keV, 1×10^{13} cm^{-2}) implanted sample annealing conditions.

Er, 1150 keV, 1×10^{13} cm^{-2}				
Sample ID #	Temp (°C)	Time (min)	Gas	Technique
E02524	700	90	NH$_3$	PCA
E02524	800	90	NH$_3$	PCA
E02524	900	90	NH$_3$	PCA
E02524	1000	90	NH$_3$	PCA

Table A-13

Erbium (1150 keV, 5×10^{13} cm^{-2}) implanted sample annealing conditions.

Er, 1150 keV, 5×10^{13} cm^{-2}				
Sample ID #	Temp (°C)	Time (min)	Gas	Technique
E02524	700	90	NH$_3$	PCA
E02524	800	90	NH$_3$	PCA
E02524	900	90	NH$_3$	PCA
E02524	1000	90	NH$_3$	PCA

Table A-14

Neodymium (910 keV, 1×10^{13} cm^{-2}) implanted sample annealing conditions.

Nd, 910 keV, 1×10^{13} cm^{-2}				
Sample ID #	Temp (°C)	Time (min)	Gas	Technique
E02524	700	90	NH$_3$	PCA
E02524	800	90	NH$_3$	PCA
E02524	900	90	NH$_3$	PCA
E02524	1000	90	NH$_3$	PCA

Table A-15

Neodymium (910 keV, 5×10^{13} cm^{-2}) implanted sample annealing conditions.

Nd, 910 keV, 5×10^{13} cm^{-2}				
Sample ID #	Temp (°C)	Time (min)	Gas	Technique
E02524	700	90	NH$_3$	PCA
E02524	800	90	NH$_3$	PCA
E02524	900	90	NH$_3$	PCA
E02524	1000	90	NH$_3$	PCA

Bibliography

Abernathy, C. R. *et al.* "CCl₄ Doping of GaN Grown by Metalorganic Molecular Beam Epitaxy," *Appl Phys Lett*, 66: 1969-1971 (10 April 1995).

Akasaki, I *et al.* "Photoluminescence of Mg-doped p-type GaN and Electroluminescence of GaN p-n Junction LED," *J of Luminescence*, 48 & 49: 666-670 (1991).

Akasaki, I *et al.* "Conductivity Control of GaN and Fabrication of UV/Blue GaN Light Emitting Devices," *Physica B*, 185: 428-432 (1993).

Amano, H. *et al.* "Electron Beam Effects on Blue Luminescence of Zinc-Doped GaN," *J of Luminescence*, 40&41: 121-122 (1988).

Amano, H. *et al.* "Zn Related Electroluminescent Properties in MOVPE Grown GaN," *J Cryst Growth*, 93: 79-82 (1988).

Amano, H. *et al.* "UV and Blue Electroluminescence from Al/GaN:Mg/GaN LED Treated with Low-Energy Electron Beam Irradiation (LEEBI) ," *Inst Phys Conf Series*, 106: 725-730 (1989).

Amano, H. *et al.* "P-type Conduction in Mg-Doped GaN Treated with Low Energy Electron Beam Irradiation (LEEBI)," *Jpn J Appl Phys*, 28: L2112-2114 (December 1989).

Amano, H. *et al.* "Growth and Luminescence Properties of Mg-Doped GaN Prepared by MOVPE," *J Electrochem Soc*, 137: 1639-1641 (May 1990).

Bergman, P. *et al.* "Time-Resolved Spectroscopy of Zn- and Cd-Doped GaN," *J Appl Phys*, 61: 4589-4592 (1 May 1987).

Boulou, Michel *et al.* "Recombination Mechanisms in GaN:Zn," *J of Luminescence*, 18/19: 767-770 (1979).

Bourgoin, J. and M. Lannoo. *Point Defects in Semiconductors II: Experimental Aspects.* Berlin: Springer-Verlag, 1983.

Boyd, Robert W. *Radiometry and the Detection of Optical Radiation.* New York: John Wiley and Sons, 1983.

Brandt, M. S. *et al.* "Hydrogenation of p-Type Gallium Nitride," *Appl Phys Lett*, 64: 2264-2266 (25 April 1994).

Bryant, F. J. *et al.* "Characterization of Luminescence Centres in Neodymium Implanted Zinc Sulphide," *J Phys Chem Solids*, 44: 595-600 (1983).

Bu, Y. *et al.* "Optical Properties of GaN Epitaxial Films Grown by Low-Pressure Chemical Vapor Epitaxy using a New Nitrogen Source: Hydrazoic Acid (HN_3)," *Appl Phys Lett*, 66: 2433 (1 May 1995).

Chemical Rubber Company. *Handbook of Chemistry and Physics* (75th Edition). Edited by David R. Lide. Boca Raton: CRC Press, 1994.

Chung, B-C. and M. Gershenzon. "The Influence of Oxygen on the Electrical and Optical Properties of GaN Crystals Grown by Metalorganic Vapor Phase Epitaxy," *J Appl Phys*, 72: 651-659 (15 July 1992).

Colon, J. E. *et al.* "Enhancement of the Er^{3+} Emissions from AlGaAs:Er Codoped with Oxygen," *Appl Phys Lett*, 63: 216-218 (12 July 1993).

Cunningham, R. D. *et al.* "Variation of Photoluminescence with Carrier Concentration in GaN," *J of Luminescence*, 5: 21-31 (1972).

Dai, R *et al.* "Photoluminescence of GaN Epitaxial Layers," *J Phys C:Solid St Phys*, 15: 393-400 (1982).

Dean, P. J. "Photoluminescence as a Diagnostic of Semiconductors," *Prog Crystal Growth Charact*, 5: 89-174 (1982).

Dingle, R. and M. Ilegems. "Donor-Acceptor Pair Recombination in GaN," *Solid St Comm*, 9: 175-180 (1971).

Dingle, R. *et al.* "Absorption, Reflectance, and Luminescence of GaN Epitaxial Layers," *Phys Rev B*, 4: 1211-1218 (15 August 1971).

Ejder, E. and P. O. Fagerstrom. "Photoconductivity of Zn-Doped GaN," *J Phys Chem Solids*, 36: 289-292 (1975).

Ejder, E. and H. G. Grimmeiss. "Optical Investigations of Zn, Hg and Li Doped GaN," *Appl Phys*, 5: 275-279 (1974).

Elsaesser, D. W. *et al.* "Er-Related Deep Centers in GaAs Doped with Er by Ion Implantation and Molecular Beam Epitaxy," *J Appl Phys*, 77: 3919-3926 (15 April 1995).

Favennec, P. N. *et al.* "Luminescence of Erbium Implanted in Various Semiconductors: IV, III-V and II-VI Materials," *Electron Lett*, 25: 718-719 (25 May 1989).

Frederikse, Hans P. R. "Solid State Physics," *A Physicist's Desk Reference* (Second Edition). edited by H. L. Anderson. New York: AIP Press, 1989.

Gibbons, James F. "Ion Implantation in Semiconductors-Part I: Range Distribution Theory and Experiments," *Proceedings of the IEEE*, 56: 295-319 (March 1968).

Glaser, E. R. *et al.* "Optically Detected Magnetic Resonance of GaN Films Grown by Organometallic Chemical-Vapor Depositon," *Phys Rev B*, 51: 13326-13336 (15 May 1995).

Gotz, W. *et al.* "Deep Level Defects in n-type GaN," *Appl Phys Lett*, 65: 463-465 (25 July 1994).

Grimmeiss, H. G. and B. Monemar. "Low-temperature Luminescence of GaN," *J Appl Phys*, 41: 4054-4058 (September 1970).

Hacke, Peter. *et al.* "Characterization of the Shallow and Deep Levels in Si Doped GaN Grown by Metal-Organic Vapor Phase Epitaxy," *Jpn J Appl Phys*, 33: 6443-6447 (December 1994).

Hecht, Eugene. *Optics (Second Edition)*. Reading,MA: Addison-Wesley, 1987.

Hunsperger, R. G. *Integrated Optics: Theory and Technology, 3ed*. Berlin: Springer-Verlag, 1991.

Ilegems, M. and R. Dingle. "Luminescence of Be- and Mg-Doped GaN," *J Appl Phys*, 44: 4234-4235 (September 1973).

Ilegems, M. and H. C. Montgomery. "Electrical Properties of n-Type Vapor-Grown Gallium Nitride," *J Phys Chem Solids*, 34: 885-895 (1973).

Ilegems, M. *et al.* "Luminescence of Zn- and Cd-Doped GaN," *J Appl Phys*, 43: 3797-3800 (September 1972).

Instruments SA. *The Optics of Spectroscopy, A Tutorial, V2.0*. Part Number 22-900-075 Edison, NJ: Instruments SA, 1988.

Jacob, G. *et al.* "Effect of Growth Parameters on the Properties of GaN:Zn Epilayers," *J Cryst Growth*, 42: 136-143 (1977).

Karpinski, J. and S. Porowski. "High Pressure Thermodynamics of GaN," *J Cryst Growth*, 66: 11-20 (1984).

Karpinski, J. *et al.* "Equilibrium Pressure of N_2 Over GaN and High Pressure Solution Growth of GaN," *J Cryst Growth*, 66: 1-10 (1984).

Kasatkin, V. A. and V. P. Savel'ev. "Excitation of Ytterbium Luminescence in Gallium and Indium Phosphides," *Sov Phys Semicond*, 18: 1022-1023 (September 1984).

Khan, M. A. *et al.* "Electrical Properties and Ion Implantation of Epitaxial GaN, Grown by Low Pressure Metalorganic Chemical Vapor Deposition," *Appl Phys Lett*, 42: 430-432 (1 March 1983).

Khan, M. A. *et al.* "Properties and Ion Implantation of $Al_xGa_{1-x}N$ Epitaxial Single Crystal Films Prepared by Low Pressure Metalorganic Chemical Vapor Deposition," *Appl Phys Lett*, 43: 492-494 (1 September 1983).

Khan, M. A. *et al.* "Deposition and Surface Characterization of High Quality Single Crystal GaN Layers," *J Appl Phys*, 73: 3108-3110 (15 March 1993).

Khan, M. R. H. *et al.* "Effect of Si on Photoluminescence of GaN," *Sol St Comm*, 57: 405-409 (1986).

Khan, M. R. H. *et al.* "Study of Zn-Associated Levels in GaN," *Semicond Sci Technol*, 7: 472-477 (1992).

Koide, N. *et al.* "Doping of GaN with Si and Properties of Blue m/i/n/n^+ GaN LED with Si-Doped n^+-layer by MOVPE," *J Cryst Growth*, 115: 639-642 (1991).

Korber, W. and A. Hangleiter. "Excitation and Decay Mechanisms of the Intra-4f Luminescence of Yb^{3+} in Epitaxial InP:Yb Layers," *Appl Phys Lett*, 52: 114-116 (11 January 1988).

Lagerstedt, O. and B. Monemar. "Luminescence in Epitaxial GaN:Cd," *J Appl Phys*, 45, 2266-2272 (May 1974).

Lea, K. R. *et al.* "The Raising of Angular Momentum Degeneracy of f-Electron Terms by Cubic Crystal Fields," *J Phys Chem Solids*, 23: 1381-1405 (1962).

Lei, T. *et al.* "Gas-Source Molecular Beam Epitaxy of Gallium Nitride," *MRS Abstracts*, E3.6 (Spring, 1995).

Lester, S. D. *et al.* "High Dislocation Densities in High Efficiency GaN-Based Light-Emitting Diodes," *Appl Phys Lett*, 66: 1249-1251 (6 March 1995).

Lin, M. E. *et al.* "Thermal Stability of GaN Investigated by Low-Temperature Photoluminescence Spectroscopy," *Appl Phys Lett*, 63: 3625-3627 (27 December 1993).

Liu, S. S. *et al.* "Characterization of GaN Epitaxial Layers Using Cathodoluminescence," *J Electron Mat*, 6: 237-252 (1977).

Madelung, O. (Editor). *Semiconductors: Group IV Elements and III-V Compounds.* Berlin: Springer-Verlag, 1991.

Malinovskii, V. V. *et al.* "Characteristics of the Kinetics of Radiative Recombination in Zinc-Doped Gallium Nitride," *Sov Phys Semicond*, 14: 919-921 (1980).

Marasina, L. A. *et al.* "Cathodoluminescence of Undoped Epitaxial Gallium Nitride Films," *Sov Phys Semicond*, 9: 1162-1164 (1976).

Maruska, H. P. and D. A. Stevenson. "Mechanism of Light Production in Metal-Insulator-Semiconductor Diodes; GaN:Mg Violet Light-Emitting Diodes," *Solid State Elect*, 17: 1171-1179 (1974).

Maruska, H. P. *et al.* "Preparation of Mg-Doped GaN Diodes Exhibiting Violet Electroluminescence," *Mat Res Bull*, 7: 777-782 (1972).

Maruska, H. P. *et al.* "Violet Luminescence of Mg-Doped GaN," *Appl Phys Lett*, 22: 303-305 (15 Mar 1973).

Matsumoto, T. and M. Aoki. "Effects of Built-In Strain on Luminescence and Absorption Spectra of GaN Epitaxial Crystals," *Jpn J Appl Phys*, 13: 1583-1588 (October 1974).

Matsumoto, T. and M. Aoki. "Temperature Dependence of Photoluminescence from GaN," *Jpn J Appl Phys*, 13: 1804-1807 (November 1974).

Matsumoto, T. *et al.* "Pair Luminescence from Zn-Doped GaN," *Jpn J Appl Phys*, 13: 373-374 (1974).

Metcalfe, R. D. *et al.* "Cathodoluminescence from Gallium Nitride Implanted with Arsenic and Phosphorous," *J of Luminescence*, 16: 405-415 (1978).

Michel, J. *et al.* "Impurity Enhancement of the 1.54-μm Er^{3+} Luminescence in Silicon," *J Appl Phys*, 70: 2672-2678 (1 September 1991).

Monemar, B. "Fundamental Energy Gap of GaN from Photoluminescence Excitation Spectra," *Phys Rev B*, 10: 676-681 (15 July 1974).

Monemar, B. *et al.* "Properties of Zn-Doped VPE-Grown GaN.I. Luminescence Data in Relation to Doping Conditions," *J Appl Phys*, 51: 625-639 (January 1980).

Monemar, B. *et al.* "Properties of Zn-Doped VPE-Grown GaN.II. Optical Cross Sections," *J Appl Phys*, 51: 640-649 (January 1980).

Morimoto, Y. "Few Characteristics of Epitaxial GaN-Etching and Thermal Decomposition," *J ElectroChem Soc*, 121: 1383-1384 (October 1974).

Morkoc, H. and S. N. Mohammad. "High-Luminosity Blue and Blue-Green Gallium Nitride Light-Emitting Diodes," *Science*, 267: 51-55 (6 January 1995).

Morkoc, H. *et al.* *Current Status of Silicon Carbide and the III-V Nitrides for High Temperature Devices in Japan and USA.* Report prepared for Air Force Office of Scientific Research, Bolling AFB: DC (1993).

Nakamura, S. *et al.* "Highly p-Type Mg-Doped GaN Films Grown with GaN Buffer Layers," *Jpn J Appl Phys*, 30: L1708-1711 (October 1991).

Nakamura, S. *et al.* "Thermal Annealing Effects on P-type Mg-Doped GaN Films," *Jpn J Appl Phys*, 31: L139-142 (15 February 1992).

Nakamura, S. *et al.* "Hole Compensation Mechanism of p-Type GaN Films," *Jpn J Appl Phys*, 31: 1258-1266 (May 1992).

Nakamura, S. *et al.* "Si- and Ge-Doped GaN Films Grown on GaN Buffer Layers," *Jpn J Appl Phys*, 31: 2883-2888 (September 1992).

Ogino, T. and M. Aoki. "Photoluminescence of P-doped GaN," *Jpn J Appl Phys*, 18: 1049-1052 (June 1979).

Ogino, T. and M. Aoki. "Mechanism of Yellow Luminescence in GaN," *Jpn J Appl Phys*, 19: 2395-2405 (December 1980).

Ohba, Y. and A. Hatano. "H-Atom Incorporation in Mg-Doped GaN Grown by Metalorganic Chemical Vapor Deposition," *Jpn J Appl Phys*, 33: L1367-L1369 (1 October 1994).

Pankove, J. I. "Absorption Edge of Impure Gallium Arsenide," *Phys Rev*, 140: A2059-A2065 (13 December 1965).

Pankove, J. I. *Optical Processes in Semiconductors*. New York: Dover, 1971.

Pankove, J. I. and J. E. Berkeyheiser. "Properties of Zn-doped GaN.II. Photoconductivity,*" J Appl Phys*, 45: 3892-3895 (September 1974).

Pankove, J. I. and J. A. Hutchby. "Photoluminescence of Zn-Implanted GaN," *Appl Phys Lett*, 24: 281-283 (15 March 1974).

Pankove, J. I. and J. A. Hutchby. "Photoluminescence of Ion-Implanted GaN," *J Appl Phys*, 47: 5387-5390 (December 1976).

Pankove, J. I. *et al.* "Luminescence of Insulating Be-Doped and Li-Doped GaN," *J of Luminescence*, 8: 89-93 (1973).

Pankove, J. I. *et al.* "Properties of Zn-doped GaN.I. Photoluminescence," *J Appl Phys*, 45: 1280-1286 (March 1974).

Pappalardo, R. G. "Spectroscopy and Luminescence of Lanthanides and Actinides," *Luminescence of Inorganic Solids.* edited by B. DiBartolo. New York: Plenum Press, 1977.

Pikhtin, A. N. *et al.* "Cathodoluminescence of Gallium Nitride Single Crystals," *Sov Phys Semicond*, 8: 134-136 (July 1974).

Qui, C. H. *et al.* "Cathodoluminescence Study of Erbium and Oxygen Coimplanted Gallium Nitride Thin Films on Sapphire Substrates," *Appl Phys Lett*, 66: 562-564 (30 January 1995).

Rubin, M. *et al.* "p-Type Gallium Nitride by Reactive Ion-Beam Molecular Beam Epitaxy with Ion Implantation, Diffusion, or Coevaporation of Mg," *Appl Phys Lett*, 64: 64-66 (3 January 1994).

Ryssel, H. and I. Ruge. *Ion Implantation*. Chichester: John Wiley and Sons, 1986.

Saxena, A. N. *et al.* "Implantation of $^{14}N^+$ into Monocrystalline GaN Films," *International J of Appl Radiation and Isotopes*, 26: 33-35 (1975).

Schoonmaker, Richard C. *et al.* "Vaporization Catalysis. The Decomposition of Gallium Nitride," *J Phys Chem*, 69: 3455-3460 (October 1965).

Shan, W. *et al.* "Temperature Dependence of Interband Transitions in GaN Grown by Metalorganic Chemical Vapor Deposition," *Appl Phys Lett*, 66: 985-987 (20 February 1995).

Shan, W. *et al.* "Pressure-Dependent Photoluminescence Study of Wurtzite GaN," *Appl Phys Lett*, 66: 3492-3494 (19 June 1995).

Strite, S. and H. Morkoc. "GaN, AlN, and InN: A Review" *J Vac Sci Technol*, B10: 1237-1266 (July/August 1992).

Sun, C. J. *et al.* "Thermal Stability of GaN Thin Films Grown on (0001) Al_2O_3, (011bar2) Al_2O_3 and (0001)$_{Si}$ 6H-SiC Substrates," *J Appl Phys*, 76: 236-241 (1 July 1994).

Sze, S. M. *Physics of Semiconductor Devices*. New York: Wiley, 1981.

Teisseyre, H. *et al.* "Photoluminescence in Doped GaN Bulk Crystal," *J Phys Chem Solids*, 56: 353-355 (1995).

Thurmond, C. D. and R. A. Logan. "The Equilibrium Pressure of N_2 Over GaN" *J ElectroChem Soc*, 119: 622-626 (May 1972).

Urbach, F. "The Long-Wavelength Edge of Photographic Sensitivity and of the Electronic Absorption of Solids," *Phys Rev*, 92: 1324 (1953).

Vavilov, V. S. *et al.* "Cathodoluminescence of Undoped Gallium Nitride," *Sov Phys Semicond*, 13: 1259-1262 (November 1979).

Wagner, J. *et al.* "Neodymium Complexes in GaP Separated by Photoluminescence Excitation Spectroscopy," *J Appl Phys*, 59: 1202-1204 (15 February 1986).

Walter, U. "Treating Crystal Field Parameters in Lower than Cubic Symmetries," *J Phys Chem Solids*, 45: 401-408 (1984).

Wang, C. and R. F. Davis. "Deposition of Highly Resistive, Undoped, and p-Type, Magnesium-Doped Gallium Nitride Films by Modified Gas Source Molecular Beam Epitaxy," *Appl Phys Lett*, 63: 990-992 (16 August 1993).

Wickenden, A. E. *et al.* "The Effect of Thermal Annealing on GaN Nucleation Layers Deposited on (0001) Sapphire by Metalorganic Chemical Vapor Deposition," *J Appl Phys*, 75: 5367-5371 (15 May 1994).

Wilson, R. G. and G. R. Brewer. *Ion Beams with Applications to Ion Implantation*. Malabar FL: Robert E. Krieger Publishing Company, 1979.

Wilson, R. G. *et al.* "1.54-µm Photoluminescence from Er-Implanted GaN and AlN," *Appl Phys Lett*, 65: 992-994 (22 August 1994).

Wilson, R. G. *et al.* "Thermal Stability of Implanted Dopants in GaN," *Appl Phys Lett*, 66: 2238-2240 (24 April 1995).

Yacobi, B. G. and D. B. Holt. *Cathodoluminescence Microscopy of Inorganic Solids.* New York: Plenum Press, 1990.

Yang, X. H. *et al.* "Above Room Temperature Near Ultraviolet Lasing from an Optically Pumped GaN Film Grown on Sapphire," *Appl Phys Lett*, 66: 1-3 (2 January 1995).

Zavada, J. M. *et al.* "Hydrogenation of GaN, AlN, and InN," *Appl Phys Lett*, 64: 2724-2726 (16 May 1994).

VITA

Captain Eric Silkowski graduated from Clifton Senior High School in Clifton, New Jersey in 1982. He then studied at the University of Chicago, earning a B.A. in Physics with Honors in 1986. After graduation, he attended Officer Training School, Lackland AFB, Texas and was commissioned a Second Lieutenant in the United States Air Force on 12 May 1987. He was first assigned as a Project Officer in the Directed Energy Weapons System Program Office at Los Angeles AFB, California. There he applied his knowledge as a physicist to the conceptual design of "Star Wars" anti-ballistic missile neutral particle beam weapons systems. In May 1989 he enrolled at the Air Force Institute of Technology. He was honored as a Distinguished Graduate while earning an M.S. in engineering physics (specialty: solid state physics) in December 1990. He was subsequently assigned to the Small Intercontinental Ballistic Missile System Program Office at Norton AFB, California. Again, he applied his skills as a physicist, this time, as the Program Manager for the MK21/W87 re-entry vehicle. In 1992 Captain Silkowski enrolled in the AFIT doctoral program within the Department of Engineering Physics. His next assignment will be to McClellan Central Laboratory, AFTAC Technical Operations Division, McClellan AFB, California.

Permanent Address: 7804 Seneca Way
Antelope, CA 95843

REPORT DOCUMENTATION PAGE

Form Approved
OMB No. 0704-0188

1. AGENCY USE ONLY (Leave blank)	2. REPORT DATE	3. REPORT TYPE AND DATES COVERED
	November 1996	Doctoral Dissertation

4. TITLE AND SUBTITLE

Luminescence Study of Ion-Implanted Gallium Nitride

5. FUNDING NUMBERS

6. AUTHOR(S)

Eric Silkowski, Capt, USAF

7. PERFORMING ORGANIZATION NAME(S) AND ADDRESS(ES)

Air Force Institute of Technology
2950 P. Street
Wright-Patterson AFB, OH 45433-7765

8. PERFORMING ORGANIZATION REPORT NUMBER

AFIT/DS/ENP/96-09

9. SPONSORING / MONITORING AGENCY NAME(S) AND ADDRESS(ES)

AFOSR/NE
Physics and Electronics Directorate
Air Force Office of Scientific Research
Bolling AFB, DC 20332-0001

10. SPONSORING / MONITORING AGENCY REPORT NUMBER

11. SUPPLEMENTARY NOTES

12a. DISTRIBUTION / AVAILABILITY STATEMENT

Approved for public release; distribution unlimited

12b. DISTRIBUTION CODE

13. ABSTRACT *(Maximum 200 words)*

A successful method for achieving optical activation of ion-implanted dopants in GaN was demonstrated, and the luminescence spectra of Ar, Zn, C, O, Si, Be, Mg, Nd, and Er implanted GaN was characterized. MOCVD and MBE grown GaN was implanted at room temperature with ion energies of 100 to 1150 keV and ion doses of 1×10^{13} to 1×10^{15} cm^{-2}. Optical absorption measurements demonstrated good implantation damage recovery after annealing in flowing NH_3 or N_2 at 1000 °C for 90 min. Surface degradation occurred for annealing in NH_3 above 1000 °C. A preferred annealing environment of 1000 °C in an NH_3 atmosphere was found for the optical activation of Zn, Mg, Nd, and Er. Several new luminescence features were observed for Zn and Mg. Nd was implanted into GaN for the first time and its rich luminescence spectrum was studied. Strong evidence was obtained for the existence of only one non-cubic Nd^{3+} center and an energy level model was proposed. Er implanted GaN was found to be strongly luminescent at room temperature. Evidence indicated multiple, non-cubic Er luminescence centers and an energy level model was proposed. Oxygen co-implantation enhanced Er emissions and lowered the optimal annealing temperature to 800 °C.

14. SUBJECT TERMS

Gallium Nitride, GaN, Photoluminescence, Cathodoluminescence, Wide Bandgap, High Temperature Semiconductors, Rare Earth

15. NUMBER OF PAGES
328

16. PRICE CODE

17. SECURITY CLASSIFICATION OF REPORT	18. SECURITY CLASSIFICATION OF THIS PAGE	19. SECURITY CLASSIFICATION OF ABSTRACT	20. LIMITATION OF ABSTRACT
Unclassified	Unclassified	Unclassified	UL